Electronic Thesis and Dissertation Repository

2-17-2012 12:00 AM

Ozone Measurements and Transport

Mohammed Kedir Osman
The University of Western Ontario

Supervisor
Dr. Wayne Hocking
The University of Western Ontario Joint Supervisor
Dr. David Tarasick
The University of Western Ontario

Ozone Measurements and Transport

(Spine title: Ozone Measurements and Transport)

(Thesis format: Monograph)

by

Mohammed Kedir <u>Osman</u>

Department of Physics and Astronomy
Graduate Program in Physics

A thesis submitted in partial fulfillment
of the requirements for the degree of
Doctor of Philosophy

The School of Graduate and Postdoctoral Studies
The University of Western Ontario
London, Ontario, Canada

THE UNIVERSITY OF WESTERN ONTARIO
School of Graduate and Postdoctoral Studies

CERTIFICATE OF EXAMINATION

Supervisor:

_____
Dr. Wayne Hocking

Co-Supervisor:

_____
Dr. David Tarasick

Supervisory Committee

_____
Dr. Peter Simpson

_____
Dr. Lyudmila Goncharova

Examiners

_____
Dr. Peter Taylor

_____
Dr. Robert Mercer

_____
Dr. Robert Sica

_____
Dr. Sree Ram Valluri

The thesis by

Mohammed Kedir Osman

entitled:

Ozone Measurements and Transport

is accepted in partial fulfillment of the
requirements for the degree of
Doctor of Philosophy

_____   _____
            Date   Chair of the Thesis Examination Board

ii

Abstract

Ozone intrusions from the stratosphere to the troposphere occur as part of the Brewer-Dobson circulation, but the details of the microphysics of the process are unresolved. This research mainly focuses on near-tropopause regions, and examines stratospheric ozone intrusions into the troposphere across this stable zone. My research objective is to identify the small-scale atmospheric dynamical features responsible for the intrusion of stratospheric ozone into the troposphere, and to determine their relative importance from case to case.

Windprofiler radars, together with frequent ozonesonde launches, have been used to detect stratospheric ozone intrusions. This work has been supplemented by numerical simulation via GEM-FLEXPART to unambiguously confirm the leakage. We have identified stratospheric ozone intrusion occurrence at the measurement site, and/or in some cases at some distance from the measurement site. In the latter case, ozone reaches the radar site after being blown horizontally with the wind. We have diagnosed radar measurements of the standard deviation of the vertical wind, vertical shear of the horizontal wind, and turbulence strengths, as possible indicators of small-scale atmospheric activity. Increases in the standard deviation of the vertical wind are considered to indicate enhanced gravity wave activity, and enhancements in wind shear are taken to indicate increases in small-scale dynamics (including gravity wave activity).

The study shows frequent strong correlation between intrusion events and strong atmospheric activity. The atmospheric dynamics responsible for the intrusion of stratospheric ozone varies from case to case. On the one hand, we see that all parameters can act simultaneously, which clearly amplifies the intrusions. On the other hand, we see either one or any combination of the parameters acting to cause intrusions. However, the Eureka 2008 and Montreal 2005 (on 9th May) campaigns are exceptional cases where we do not see any strong atmospheric activity.

We have also modeled atmospheric diffusion and examined the differences due to homogeneous turbulence compared with turbulence that is spatially and temporally intermittent.

This unique combination of observational and numerical modeling helps detect the sources and sinks of ozone-related atmospheric pollutants that have negative impact on air quality, climate change and ozone depletion.

Keywords

Radar, ozonesonde, computer modeling (GEM-FLEXPART), stratospheric ozone intrusion, ozone transport, stratosphere-troposphere exchange, diffusion, tropopause, ozone

To my late father

Kedir Osman

Acknowledgments

First and foremost I would like to thank my supervisor, Prof. Wayne Hocking, for his unreserved and endless support, follow up, guidance, and detailed and constructive comments from the initial stages and up until completion of the thesis. His scientific excitement, integral view on the research, enthusiasm and everlasting energy, has made a deep impression on me. Without his effort this work would have never come to completion. I am heartily thankful to my other supervisor, Prof. David Tarasick, for his valuable advice, support and guidance during my GEM-FLEXPART training at Environment Canada. He gave me an opportunity to explore and understand it, which has been of a great value.

I wish to thank Dr. Nimalan Swarnalingam for his help in providing some of the necessary materials for our research. My thanks go to Dr. Huixia He for her essential assistance during my training at Environment Canada. I am grateful to Jonathan Davies for providing me with training in ozonesonde preparation. I warmly thank Dr. Armin Dehghan, Dr. Tushar Das, Dr. Yves Rochon, Jonathan Davies, Dr. Argall and Dr. Trevor Carey-Smith and Andrew Elford for their help at times of need. I wish to express my warm and sincere thanks to my advisory committee, Prof. Peter Simpson and Dr. Lyudmila Goncharova, for their constructive remarks and excellent advice.

I am especially thankful to Clara, Jackie, Jodi, Dr. Henry Leparskas, Phin and Peter, for their support in many respects during my studies. I am deeply indebted to Dr. Kaluarachchi, and Dr. Valluri, for their countless encouragement and support. My special thanks also go to all my friends, particularly Wondesen, Dawit R, Anteneh, Zahara, Blessing, Selam, Taher, Den, Abiye, Eba, Alee, Dawit S, Samson G and Tekleab, for their time and support in any regard.

On a more personal note, I would like to thank my family, especially my mother Bogalech Teky and my brother Shemsu, for their encouragement and support from the very beginning up until this stage. I must also acknowledge my fiancée and best friend, Zulfa Sali, for her tender care, love, patience and understanding during my study.

Table of Contents

List of Tables

List of Figures

Chapter 1

1   Introduction

One atmospheric phenomenon that needs to be better understood, and brings about change in the atmosphere, is stratospheric-tropospheric exchange. Stratosphere-troposphere exchange is a naturally occurring dynamical process that, among other things, gives rise to the transport of stratospheric ozone to the troposphere across the stable tropopause, and conversely. This study examines the detection of stratospheric ozone leakage from the stratosphere to the troposphere, as revealed by several continuous ozonesonde campaigns. We employed windprofiler radars simultaneously with ozonesonde launches in order to investigate the ozone intrusions thoroughly and determine the atmospheric dynamics that cause the intrusions. Moreover, this work was supported by the GEM-FLEXPART model to simulate ozone transport.

In this first chapter, the composition and structure of the atmosphere is discussed. The primary focus is on the upper troposphere and lower stratosphere region. Both local and global scale circulation of air are mentioned to describe stratosphere-troposphere exchange and its impact on the troposphere. Different measurement techniques of atmospheric parameters are summarized. Simultaneous observations of the atmosphere via radar and ozonesonde are discussed. Current understanding, a literature review, motivation and objective of the thesis are introduced to provide a perspective. The chapter is concluded with a brief description of the approach used to achieve our objectives, as well as campaign site locations and the types of instruments used (discussed further within the thesis).

1.1   Composition and structure of atmosphere

The atmosphere is divided into four layers based on the variation of the vertical profile of the temperature [see Figure 1.1]. Moreover, the layers, denoted troposphere, stratosphere, mesosphere and thermosphere in ascending order of height, are different in their air density, moisture, cloudiness, and chemical constituents. The troposphere is the lowest and the densest layer of the atmosphere. It contains approximately 80% of the mass of the

atmosphere. It extends from Earth's surface up to around 8 km at the poles and 15 km at the equator [Harrison, 1999]. The depth of the troposphere also varies with weather systems and seasons. In the troposphere, temperature decreases with altitude [see Figure 1.1] as a result of declining backscatter radiation coming from the surface of the Earth [Harrison, 1999]. The troposphere is statically unstable (i.e., warm air rises and cold air sinks) therefore the gases are well mixed vertically.
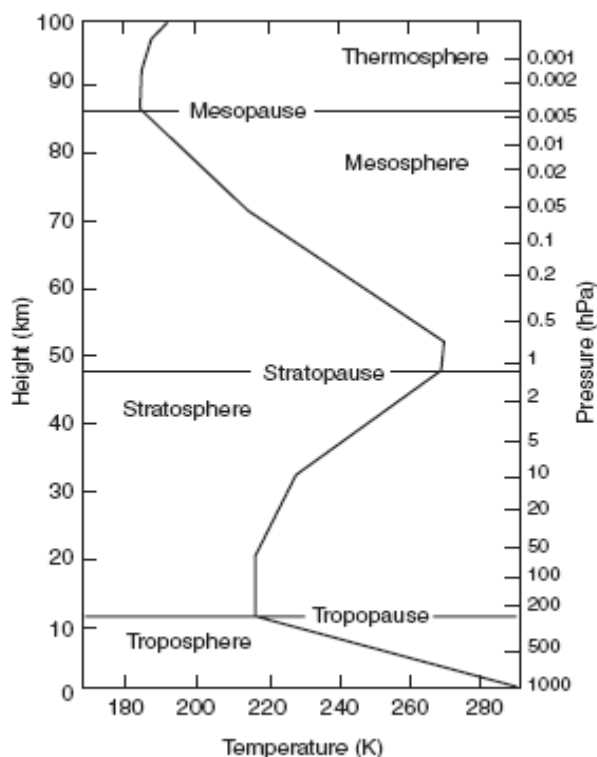
Figure 1.1. Mean temperature profile at midlatitude based on the U.S. Standard Atmosphere (1976), adapted from Holton [2004] Figure 12.1.

The stratosphere is located between the troposphere and the mesosphere [see Figure 1.1]. It resides above the tropopause and stretches up to nearly 50 km. In this layer the temperature increases with altitude due to the existence of ozone which absorbs ultraviolet radiation from the Sun and acts as a source of heat for the atmosphere. Hence, in the stratosphere the air is generally stable and turbulence is generally weak. The tropopause, whose altitude variation is tied to the weather, seasons and latitude, separates the troposphere and the stratosphere, which have different characteristics both in

chemical composition and static stability. The moisture content of the tropospheric air is very high while stratospheric air is extremely dry and ozone rich. On the other hand, decreasing temperature with altitude in the troposphere enhances mixing of air vertically, resulting in instability in the layer. In contrast, increasing temperature with height in the stratosphere inhibits vertical mixing and creates a strong, statically stable layer. The tropopause thus represents a boundary between the troposphere, where chemical constituents tend to be well mixed, and the stratosphere, where chemical diffusion is weak so that the constituents can have strong vertical gradients [Holton et al., 1995].

The boundary that separates the stratosphere from the region above (the mesosphere) is called the stratopause. The air in the mesosphere is less dense and the atmospheric pressure is quite low, averaging nearly 1 mb, which means that only 0.1% of all mass of the atmosphere is above this level, while 99.9% of the mass of the atmosphere is found below it [Ahrens, 2003]. In the mesosphere, the relative percentage of nitrogen and oxygen is nearly the same as at sea level. However, a human would not survive very long breathing in this region, since each breath would contain far fewer oxygen molecules than it would at sea level. Exposure to UV solar radiation that could cause severe burns is the other effect faced in the mesosphere. Moreover, the blood in ones veins would begin to boil at normal body temperature, given the low air pressure. Partly due to the presence of little ozone in the air that absorbs solar radiation, and also the radiation of infrared radiations to space by carbon dioxide, the air temperature in the mesosphere decreases with altitude. As a result, molecules near the top of the mesosphere can lose more energy than they absorb, which leads to an energy deficit and cooling.

The thermosphere is the hot layer just above the mesosphere [as shown in Figure 1.1]. The mesopause is the boundary layer that separates the lower, colder mesosphere from the warmer thermosphere. Oxygen molecules in the thermosphere absorb energetic solar radiation to warm the region [Ahrens, 2003]. The absorption of a small amount of energetic solar intensity can lead to a large increase in air temperature since there are relatively few atoms and molecules in the region. Moreover, in the thermosphere the temperature varies from day to day, since the amount of solar energy affecting this region depends on solar activity. The air density in the thermosphere is so low that an air

molecule will move an average distance of more than 1 km before colliding with another molecule. At the Earth's surface a similar molecule will move an average distance of less than 10 nm before colliding with another molecule. At the top of the thermosphere, nearly 500 km above the surface of the Earth, molecules can move as far as 10 km before colliding with another molecule. In this region, many of the lighter and fast moving molecules escape the gravitational attraction of the Earth. The upper limit of the atmosphere where atoms and molecules shoot off into the space is known as the exosphere [Ahrens, 2003].

The atmosphere up to this point has been divided based on the vertical profile of temperature. Nevertheless, the atmosphere may also be divided based on its composition. For instance, the atmospheric composition starts to change slightly in the lower part of the thermosphere. The composition of the air below the thermosphere is comparatively uniform, 78% nitrogen and 21% oxygen, maintained through turbulent mixing. This uniformly mixed region is called the homosphere. In the thermosphere, collisions between atoms and molecules are so infrequent that the air is incapable of keeping itself stirred. Consequently, heavier atoms and molecules such as oxygen and nitrogen tend to settle to the bottom of the layer via molecular diffusion while lighter gases such as hydrogen and helium float to the top. The region from approximately the base of the thermosphere to the top of the atmosphere is usually known as the heterosphere [Ahrens, 2003].

The ionosphere is not actually a layer but it is an electrified region within the upper atmosphere where quite large relative concentrations of ions and free electrons can be found [e.g., Ahrens, 2003]. Atoms lose electrons and become positively charged when they cannot absorb all of the energy transferred to them by a colliding energetic particle or the solar energy. The ionosphere extends from 60 km up to the top of the atmosphere and hence most of it lies in the thermosphere. The ionosphere plays a crucial role in radio communications. The lower part of the ionosphere, known as the D region, reflects standard amplitude modulation (AM) radio waves back to the Earth but simultaneously it gravely weakens them through absorption. Since the D region gradually disappears at night, AM radio waves can penetrate into the ionosphere where the waves are reflected

back to Earth. Hence at night AM radio waves can travel many thousands of kilometers since there is little absorption of radio waves in the higher ionosphere. The result is that such waves bounce repeatedly from the ionosphere to the surface of the Earth and back to the ionosphere again, allowing round-the-world communication.

Nitrogen and oxygen, which vary very insignificantly with time, are the two major components of the atmosphere with their combined proportions approximately being 99% by volume [Saha, 2008]. The atmosphere is composed of 78% N_2, 21% O_2 and 1% trace gases by volume. H_2O, CO_2 and O_3 are among trace gases that occur in small proportions but play very important roles in atmospheric processes because of their radiative and thermodynamic properties. The existence of water in the three phases in the atmosphere is very important because a phase change results either in release or absorption of heat which affects the characteristics of the atmosphere [Saha, 2008].

About 90% of atmospheric ozone is found in the stratosphere while approximately 10% resides in the troposphere. Stratospheric ozone is produced as a result of the decomposition of an oxygen molecule, O_2, into two oxygen atoms, O. Then ozone, O_3, is created via the reaction of molecular oxygen with the vigorously reactive oxygen atoms. Similarly, the destruction of ozone also takes place as ultraviolet radiation strikes ozone and breaks it into an oxygen molecule and an oxygen atom. This atomic oxygen in turn reacts with molecular ozone to create two molecules of oxygen. In the stratosphere, the temperature increases with height due to the absorption of ultraviolet radiation coming from the Sun by stratospheric ozone. Due to its vertically increasing temperature the stratosphere is vertically stable [e.g., Holton, 2004]; therefore there is no formation of convection on large scales.

Ozone is one of the most important minor constituents that play a central role in controlling the temperature of the surface of Earth and sustaining life [Marshall and Plumb, 2007]. The amount of ozone in the atmosphere varies both with time and space (altitude, latitude and longitude). It is also one of the most interesting trace gases, with contradictory properties depending where it is located and in what amount. Ozone is the major radiative heat input for the stratosphere via absorption of solar ultraviolet

insolation. Ozone in the stratosphere is vital for the existence of life on Earth as it protects us from damaging ultraviolet radiation from the Sun. On the other hand, high ozone concentration is harmful in the troposphere since it causes health problems for humans as well as animals and it also leads to low crop productions. Tropospheric ozone, which is a greenhouse gas, causes global warming if it is found in high concentration. Thus, the atmospheric ozone budget, which involves photochemical cycles and ozone transport, is a major environmental issue. The spatial and temporal variability of species that have to do with ozone photochemistry implies that the dynamics of the atmosphere that results in transporting and mixing is a critical feature of the ozone study. Photochemical, radiative and dynamical processes that are coupled to regulate the ozone distribution offer a key challenge for stratosphere-troposphere exchange research [Andrews et al., 1987].

The tropopause, the boundary between troposphere and stratosphere, plays a vital role in stratosphere-troposphere exchange studies as the transport occurs across a thin and stable layer. Thus, the identification of the tropopause is of importance for describing climate change and for understanding the stratosphere-troposphere exchange [Holton et al., 1995; Sausen and Santer, 2003]. There are different kinds of definitions of the tropopause, corresponding to various aspects such as thermal structure, dynamical process and chemical composition. The thermal tropopause, according to the World Meteorological Organization (WMO, 1995), is defined as the lowest level in the atmosphere at which the lapse rate of temperature (i.e., the rate of decrease of temperature with height) decreases to 2 K km^{-1}, and provided also that the average lapse rate between this level and any level within the next 2 km does not exceed 2 K km^{-1}. The thickness of this layer must be no less than 2 km [Reiter, 1975]. The dynamical tropopause which is calculated depending on potential vorticity (i.e., the absolute circulation of an air parcel that is enclosed between two isentropic surfaces), PV, separates the stratosphere with higher PV values from the troposphere with lower PV values [Bethan et al., 1996]. This means that the dynamical tropopause is the position of the tropopause described by the critical value of potential vorticity. There is no globally used threshold value of PV but the most frequently potential vorticity used to define the dynamical tropopause lies in the range from 1 to 3 PVU where PVU is potential vorticity unit (1 PVU = 10^{-6} K m^2 kg^{-1} s^{-1})

[Holton et al., 1995; Danielsen et al.; 1987, WMO 1986; Mohanakumar, 2008]. Besides the thermal and dynamical tropopauses, there is a different characterization of the tropopause which is based on ozone mixing ratio and vertical gradient of ozone mixing ratio. This alternate description is known as the ozone tropopause [Bethan et al., 1996]. The ozone tropopause is especially important for determining a transition in concentration of trace chemical species that exist between the troposphere and the stratosphere.

Windprofiler radars are one of several devices capable of determining the tropopause height. The radar method is based on the examination of backscattered radar power. Backscattered radar power depends on the vertical gradient of the refractive index, which is also a function of humidity, temperature and electron density. Their relative contributions depend on altitude. In the troposphere, this depends on humidity and temperature, while in the stratosphere it depends on temperature and in the mesosphere on electron density. Above the tropopause the static stability remains constant as the temperature increases with altitude, and this results in reduction of the received radar power. Just above the tropopause we observe a secondary maximum backscattered radar power and the lower edge of this maximum is known as the radar estimated tropopause height [Hocking et al., 2007; Vaughan et al., 1995].

A better estimation and understanding of the variation of tropopause heights, both spatially and temporally, is to precisely measure and quantify the mass exchange between the troposphere and the stratosphere [Allen et al., 2008; Stohl et al., 2003]. Tropopause height change has become another climate change indicator, since as a result of troposphere warming and stratosphere cooling, the tropopause height increases. Tropopause height also decreases as a result of massive volcanic eruptions that lead to stratospheric warming and tropospheric cooling [Varotsos et al., 2008]. Hocking et al. [2007] also indicated the variations of tropopause heights association with the intrusions of stratospheric ozone events.

The exchange of mass between the upper troposphere and lower stratosphere across the tropopause plays a significant role in ascertaining the chemical composition and climate

of the region. This bidirectional process is known as stratosphere-troposphere exchange (STE). On a global scale, it is mainly in the tropics that tropospheric air ascends into the stratosphere, while the descent of the stratospheric air into the troposphere frequently happens in the extratropics [see Figure 1.2]. The upward movement results in the transport of water vapor and other stratospheric ozone-depleting chemicals into the stratosphere, whereas the downward movement leads to an influx of chemical substances and stratospheric ozone into the upper and lower troposphere [Holton, 2003]. This global scale mass circulation is partially a result of zonal forces in the stratosphere which are an indirect response of breaking of propagating of large scale waves from the troposphere [Holton, 2003]. This process is called the Brewer-Dobson circulation. The STE study mainly focuses on precisely quantifying the amount of the circulation of stratospheric mass, the atmospheric dynamics that causes it and the effect on the chemistry and physics of the atmosphere.
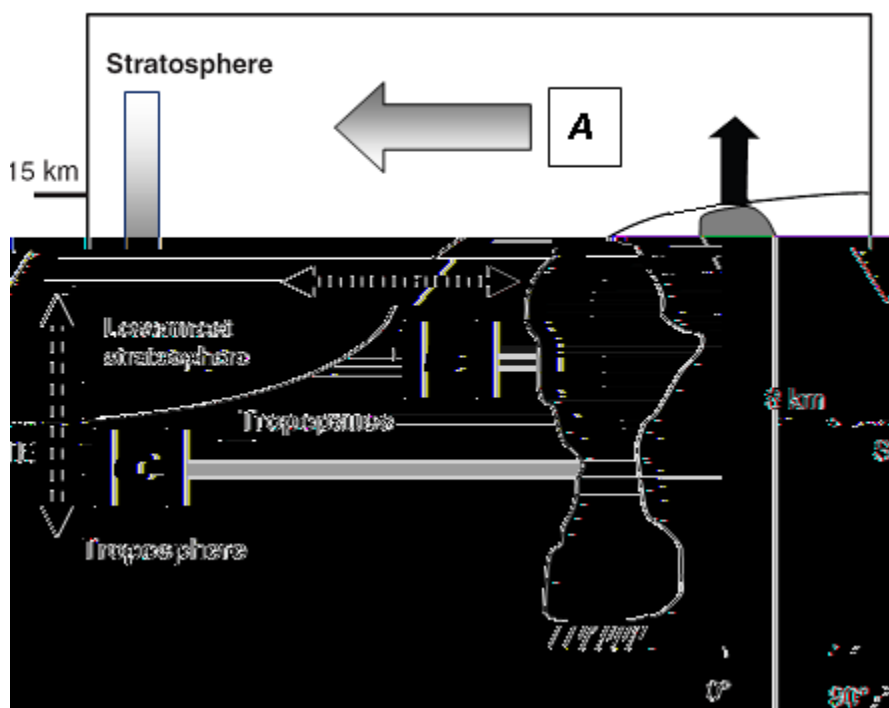
Figure 1.2. The direction of global circulation and stratosphere troposphere exchange (both hemispheres), adapted from Holton et al. [1995].

Ozone in the lower troposphere is harmful for vegetation if it is found in high concentration [Janach, 1989]. The author suggested the association of the reduction of forest coverage with an increase in ozone concentration in the troposphere that has raised a grave concern. Even if photochemistry is believed to be the major source of tropospheric ozone [Altshuller et al., 1996; Hogrefe et al., 2006], stratosphere-troposphere exchange of ozone also contributes a significant amount of ozone in the lower atmosphere [Roelofs and Lelieveld, 1997; Davies and Schuepbach, 1994]. Therefore, for quantifying the stratospheric source a precise knowledge of atmospheric dynamics that leads to stratosphere–troposphere exchange of ozone is required. The episodic transport of the stratospheric ozone to the troposphere is through the Brewer-Dobson circulation. However, the intrusion of stratospheric air into the troposphere is poorly understood both in terms of the atmospheric dynamics that cause the intrusion and the effect of intrusion on nonlinear dynamics in atmospheric chemistry and physics. Since STE plays a key role in the distribution of long-lived chemical species such as ozone and water vapor in the troposphere, understanding the cause of intrusion helps both in understanding current dynamics and in prediction of future atmospheric changes. Consequently, stratosphere-troposphere exchange has become a major research topic in the community of atmospheric scientists.

STE occurs across the tropopause, which is characterized by a growth in the static stability in going from the troposphere to the stratosphere. In the tropics, the tropopause corresponds nearly to an isentropic surface, whose annual mean potential temperature is 380 K, while in the extratropics it corresponds approximately to a surface of constant potential vorticity [Holton et al., 1995]. It is found from observation that the extratropical tropopause is noticeably close to a potential vorticity of 2 PVU. The tropopause slopes downward in moving from the equator to the poles, as can be seen from Figure 1.3.

In STE the term "exchange" means a two-way transport. In order to unambiguously differentiate the upward and downward transport cross-tropopause, Troposphere-to-Stratosphere Transport (TST) will be used to refer to the upward transport, while Stratosphere-to-Troposphere Transport (STT) to refer downward transport. The distribution of long lived atmospheric gases such as ozone and water vapor is mainly

determined by atmospheric air transport. Hence, a better understanding of the atmospheric dynamics that cause it helps not only our perception of the observed variability in these gases, but also helps to predict future atmospheric changes.
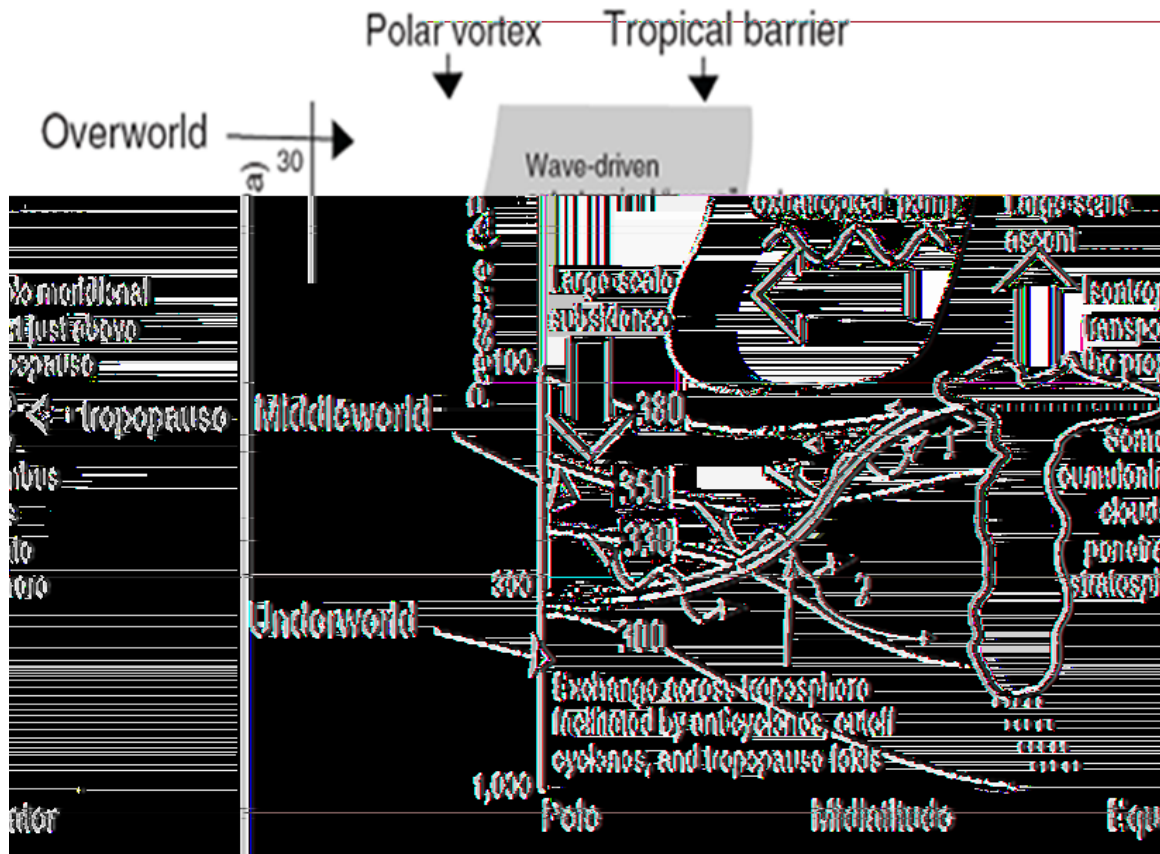
Figure 1.3. **Stratosphere–troposphere exchange through the tropopause (both hemispheres); schematic representation adapted from Holton et al. [1995]. 1 and 2 indicate shallow exchange and deep stratospheric intrusions, respectively.**

It is believed that stratospheric ozone depletion is mainly initiated by tropospheric anthropogenic sources of chemicals that are transported into the stratosphere [WMO, 1995]. On the other hand, the descent of stratospheric air is a major means of removal of stratospheric chemicals, while at the same time it contributes a considerable source of ozone and other reactive chemicals in to the troposphere [Levy et al., 1980; Holton et al., 1995]. Therefore, the mass and chemical exchange between the upper troposphere and

lower stratosphere should be known quantitatively so as to better understand the physics and chemistry of the region [Kumar et al., 2009].

Observational evidence of ozone enhancement in the middle and upper troposphere via convective processes over the tropical Atlantic was shown by Jenkins et al. [2008]. The same authors associated the enhanced ozone in the middle and upper troposphere with lightning via the formation of nitrogen oxides ($NO_x = NO + NO_2$). Sauvage et al. [2007a], Martin et al. [2007] and Thompson et al. [1997] also linked lightning with the enhancement of ozone in the upper troposphere. Although in midlatitudes there have been far-reaching stratosphere-troposphere exchange studies [Rao et al, 2008], there is only limited observational evidence in the tropics that show the intrusion of stratospheric air into the troposphere [Kumar et al., 2009; Kumar, 2006]. Kumar et al. [2009] suggested the latter to be associated with scarcity of direct measurements of vertical wind velocity around the tropopause. Nevertheless, the atmospheric dynamics responsible for the enhancement of ozone in the middle and upper troposphere has drawn great attention in the realms of atmospheric science.

On a global scale, stratosphere-troposphere exchange occurs as part of the Brewer-Dobson circulation [Holton et al., 2005]. The Brewer-Dobson circulation, which is driven by extratropical wave forcing in the middle atmosphere, comprises ascent of tropospheric air into stratosphere in the tropics, and descending stratospheric air into the troposphere in the extratropics in both hemispheres [Holton et al., 1995]. However, the details of the process on local spatial scales is not well understood. It is believed that better understanding of the dynamics of the atmosphere close to the tropopause during the stratosphere-troposphere exchange is very significant.

Windprofiler radar is one of the few instruments which can monitor the atmospheric dynamics around the tropopause. Windprofiler radars are ground-based radars that can help study the atmosphere from regions close to ground-level up to altitudes of 16 km (depending on power output) with good time and height resolution [Roettger and Larsen, 1990]. A radar transmitter sends out successive signals of radio waves into the atmosphere and receives the backscattered signals, which will then be recorded for

further analysis [Hocking et al., 2007]. The wind and turbulence strengths are among the information gathered and deduced from the returned signals [Hocking et al., 2007]. With this, Hocking et al. [2007] successfully demonstrated the detection of stratospheric ozone intrusions using a combination of frequent ozonesonde launches and windprofilers by hourly monitoring of the tropopause heights. This method shows the windprofiler's capacity to measure stratospheric ozone intrusions unquestionably. VHF radars were also employed in studying the climatology of tropopause folds over a European Arctic station [Rao et al., 2008].

Kumar [2006] observed an enhanced stratospheric air influx into the troposphere that is related to a weakening tropopause, and the variation of vertical wind velocity which is associated with gravity wave activity. Kumar et al. [2009] also showed radar echoes and strong vertical downward wind velocity around the tropopause as evidence for stratospheric ozone intrusion into the upper troposphere. The same authors explained that the downdraft as being caused by the excitation of high frequency gravity waves that resulted in the intrusion event. Sigmond et al. [2000] showed, using Lagrangian techniques, that stratosphere-troposphere exchange occurs as a result of potential vorticity mixing, with the largest downward fluxes being in tropopause folds in regions with maximum wind shear.

Even though the parameters which affect tropopause height are not fully understood, it is one of the essential features of the Earth's temperature structure. The tropopause height was found to be strongly sensitive to the temperature at the Earth's surface through changes in the moisture distribution and its resulting radiative effects. Egger [1995] demonstrated the variation of tropopause height with baroclinic wave activity. Thuburn and Craig [1997] showed the sensitivity of tropopause height to the surface temperature of the Earth using a global circulation model. Steinbrecht et al. [1998] showed the ascent of the tropopause at Hohenpeissenbergh, Germany by about 150 m per decade during the last 30 years. The same authors observed this increase to be related with an increase in temperature trend around 5 km which might be due to greenhouse gas-warming.

An important region of concern in STE studies is the upper troposphere (UT) and lower stratosphere (LS) region. The lower stratosphere is further divided into three regions, i.e., overworld, middleworld and underworld as referred by Hoskins [1991] (Figure 1.3). The region where the isentropic surfaces completely lie in the stratosphere is called the overworld. The air in this region slowly descends into the troposphere across the isentropic surfaces before it reaches the troposphere, diabatic cooling [Mullendore et al., 2005]. In the region referred to as middleworld, the isentropic surfaces partly lie in the lowermost stratosphere in the extratropics and partly in the upper troposphere in the tropics. In this region, air exchange along the isentropic surfaces takes place between the lowermost stratosphere and the troposphere in both directions [Chen, 1995]. Air in the underworld, where the isentropic surfaces lie entirely in the troposphere, ascends into the stratosphere across the isentropic surfaces before it reaches the stratosphere that result in diabatic heating [Mullendore et al., 2005].

Given the difference in transport between the overworld and the middleworld; the mass transport across the tropopause is not necessarily the best surface on which to quantify stratosphere–troposphere exchange [Holton et al., 1995]. The transport across the 380 K potential temperature surface is more suitable due to the fact that the downward control principle can be employed to describe the transport across this surface on the largest scale [Rosenlof, 1995]. This does not require understanding the details of the small-scale and mesoscale processes at the tropopause. This method can be employed to calculate the net mass transport into the troposphere across the tropopause if the seasonal fluctuation of the mass of the middleworld and the seasonal variation of the global-scale meridional circulation are estimated [Appenzeller et al., 1996b]. The same authors showed this net mass flux in the Northern Hemisphere to be maximum in late spring and minimum in early autumn.

The global estimates of the cross-tropopause net air mass flux in the extratropics have limitations due to averaging over the hemisphere (mostly Northern Hemisphere) and monthly, and consideration only for the net flux [Stohl et al., 2003b]. The diagnosis of spatial and temporal variability of the stratosphere-troposphere exchange will be undetectable in the presence of averaging. The noteworthy variation of the life time of

stratospheric ozone which can be transported to the troposphere, as a function of latitude and season is a clear example. Thus, knowledge of where and when stratospheric air masses are transported into the troposphere is required in order to study the impact of stratosphere-troposphere exchange [Stohl et al., 2003b]. The calculation of only net fluxes causes global estimates which are totally insufficient for trace gases that have sources or sinks in the lowermost stratosphere [Stohl et al., 2003b]. The same authors explained the importance of considering both the cross tropopause fluxes and the tropospheric and lower stratospheric transport preceding or following the crossing of the tropopause to show the effects of STE more entirely.

1.2   Impact of STE on the Troposphere

Due to the long lifetime of stratospheric ozone in the free troposphere [Liu et al., 1987], STE significantly contributes to the tropospheric ozone budget [Fabian and Pruchniewicz, 1977]. The transport of stratospheric ozone into the troposphere not only contributes ozone to the troposphere, but also it plays a significant role in the chemical and thermal balance of the troposphere because it controls the oxidizing capacity of tropospheric air through the formation of hydroxyl radicals and removal of other pollutants [WMO, 1999]. Even if tropospheric ozone is mainly created as a result of photochemistry [Fabian et al., 1977; Hogrefe et al., 2004; Hirsch et al., 1996], the transport of stratospheric ozone into the troposphere is vital for the overall climatology, budget and long-run trends of ozone in the region [Stevenson et al., 2006; Tarasick et al., 2005; Lin et al., 2000].

Even though in the current consensus the major contributor of the observed ozone levels in the troposphere is photochemistry [Penkett and Brice, 1986], there is still an ongoing controversy concerning the relative contribution of ozone which originates in the stratosphere on tropospheric ozone [Austin and Follows, 1991; Follows and Austin, 1992; Davies and Schuepbach, 1994; Appenzeller et al., 1996; Roelofs and Lelieveld, 1997; Schuepbach et al., 1999; Stohl et al., 2000]. However, the impact of the stratosphere to troposphere transport on tropospheric chemistry has been talked about in the last three decades [Stohl et al., 2003b]. One phenomenal interest is that there is still no consensus in the process that results in the observation of the maximum ozone in late

spring in the Northern Hemisphere [Derwent et al., 1998; Harris et al., 1998; Monks, 2000]. The association of the net cross-tropopause fluxes of ozone and surface ozone frequently led to a strong positive correlation between ozone and stratosphere to troposphere transport. However, trace gases which are not stratospheric in origin are also observed in high concentrations in spring [Derwent et al., 1998], and this may suggest that ozone may be formed from the winter time accumulated precursors because of less efficient removal processes. Moreover, in summer there is approximately a balance between ozone production and destruction, while there is a net formation in winter and spring. This is due to the fact that the climatic conditions in winter require less NO_x than in the summer for net production of ozone [Yienger et al., 1999].

Pierrehumbert and Yang [1993] indicate the presence of a partial barrier to mixing of air masses of different origins in the stratosphere-troposphere exchange process. Moreover, high level anthropogenic pollution can be seen in close proximity to stratospheric ozone and mix with each other [Parrish et al., 2000]. Accordingly, Esler et al. [2001] showed the presence of an increase in hydroxyl (OH) radical as a result of the mixing of ozone originated in the stratosphere and water vapor from the troposphere. The hydroxyl (OH) radical is produced from photo dissociation of O_3 and subsequent reaction of the resulting $O(^1D)$ (excited state of oxygen atom) with water vapor. This in turn results in determining the rate of oxidation of carbon monoxide and hydrocarbons. Therefore, inadequate model resolution or excessive numerical diffusion in Eulerian models, or insufficient parameterization of mixing processes, may result in systematic errors in chemistry model prediction.

Enhancements in the concentration of greenhouse gases are expected to cause a warming of the troposphere and a cooling of the stratosphere [Pawson et al., 1998]. The predictions of climate models suggest that warming at low latitudes and cooling at high latitudes occur above the tropopause [Rind et al., 1998]. This enhances the gradient of temperature between the low latitudes and high latitudes, thereby enhancing westerly winds around the jet stream. In addition to these effects, the cooling in the middle and upper stratosphere would lead to instability in the lowermost stratosphere. Butchart and Scaife [2001] predicted a 3% increase in mass fluxes between the stratosphere and

troposphere in climate model integration into the year 2051 that was due to increased extratropical planetary-wave driving. Through downward control, this resulted in increased extratropical downward mass flux that was balanced by the tropical upwelling in the model. The downward control principle states that under steady state conditions the extratropical mass flux across a given isentropic surface is controlled solely by the momentum forcing distribution above that surface. Possible stratosphere-troposphere future changes have to be seen against the background of these effects which are raising the heights of tropopause [Steinbrecht et al., 1998].

The quantitative contribution of STE to the tropospheric ozone budget remains relatively uncertain, even if the important mechanisms associated with it have been understood. Global chemistry transport models have been developed to explicitly take into consideration both the meteorological and photochemical processes [Roelofs and Lelieveld, 1997; Hauglustaine et al., 1998; Wang et al., 1998; Crutzen and Lawrence, 1999; Lelieveld and Dentener, 2000; Kentarchos et al., 2001]. The model results indicate that the transport from the stratosphere accounts for 619 ± 228 Tg ozone per year, while the photochemical ozone production and destruction account for 3560 ± 541 and 3288 ± 777 Tg ozone per year, respectively.

The possible impact of STE relies in the background state of the chemical in which it takes place. Its impact on tropical OH is the largest, while in the Southern Hemisphere OH is more sensitive to STE than in the Northern Hemisphere [Lamarque et al., 1999]. Moreover, the same authors showed that in the Southern Hemisphere ozone budget is more sensitive to STE than the Northern Hemisphere. Employing 3-D tropospheric chemistry model, Lamarque et al. [1999] showed that in the Northern Hemisphere, STE enhances the tropospheric ozone column by nearly 6 Dobson Units ($1DU=2.687 \times 10^{16}$ molecules cm^{-2}) and in the Southern Hemisphere by around 4.5 DU, which globally represents nearly an 11.5% increase in the tropospheric ozone column. A 5% decrease of the global OH resulted due to disregarding the tropospheric ozone originated in the stratosphere. Using a coupled tropospheric chemistry-climate model, Kentarchos et al. [2003] indicated OH formation as a result of the ozone destruction pathway, which is

photodissociation followed by $O(^1D) + H_2O$. This leads to a total ozone destruction of around 60%, while the rest is mainly caused by hydroxyl and peroxy radicals.

The annual cycle of STE of ozone reveals a maximum in winter/early spring and a secondary maximum in early summer [Kentarchos et al., 2003]. The chemical lifetime of ozone is relatively long in the extratropical troposphere in winter and spring, so that before it is photochemically destroyed in the subtropical lower troposphere, it can be transported over large distances. The OH abundance due to this destruction is approximately 15% in the Northern Hemisphere with the largest relative contribution being nearly 30% in winter. Water vapor concentrations have impact on the abundance of OH in the upper troposphere. Lower concentration in OH is observed in areas where the STE dominance is downward. Oxidation capacity is susceptible to atmospheric dynamical consequences of climate change, for it is directly related to the global-scale circulation. Other effects associated with global warming, i.e., increasing anthropogenic emissions and water vapor concentrations, may be added to or counteracted as a result [Kentarchos et al., 2003].

Particularly in the Northern Hemisphere, analysis of surface ozone data has shown many episodes of high ozone concentration which can result from local or long-range transport processes, or have origins in the stratosphere. Stratospheric air can be irreversibly mixed into the troposphere after isentropic transport across the tropopause. Such transport is usually followed by non-conservative processes such as diabatic cooling or heating and small-scale turbulent mixing in along the surface of the intruded stratospheric filaments [Holton et al., 1995].

1.3   Scientific Background

On a global scale, the circulation in the upper troposphere and the stratosphere is explained by an organized upwelling from the troposphere to the stratosphere in the tropics [Plumb, 1996; Mote et al., 1996], transport to the extratropics [Waugh, 1996], and a downward stratospheric mass flux to the troposphere in middle and high latitudes [Holton et al., 1995]. In the zonally averaged sense, this corresponds to the Brewer-Dobson circulation [Brewer, 1949] that is driven nonlocally by breaking of the Rossby

and gravity waves in the extratropical middle atmosphere. This serves as a ''suction pump,'' taking away air from the tropical upper troposphere to the stratosphere, pushing it poleward and finally downward in middle and high latitudes. This results in the so-called downward control principle in the stationary limit [Haynes et al., 1991]. Plumb and Eluszkiewicz [1999] have recently made clear that the wavebreaking must extend into the subtropics to account for the tropical upwelling.

STE in the extratropics results in the transport of dry and ozone-rich air masses from the stratosphere to troposphere. Mixing of stratospheric and tropospheric air masses modifies tropospheric distributions of ozone, water vapor and hydroxyl (OH) radicals, which in turn regulate the lifetimes of many gases [Levy, 1971]. The distribution of these species become climate-change issues in the long-term and large-scale, as well as air quality issue on episodic and regional scale. Reiter [1975] suggests mean tropopause height seasonal adjustments, organized large-scale vertical and quasi-horizontal motions defined by the mean meridional circulation, large-scale eddy transport in the jet stream and mesoscale and small-scale eddy transport across the tropopause to be the processes responsible for STE of air masses. Therefore, understanding of observed variability in these gases as well as future prediction of changes depends on our knowledge of the atmospheric dynamics involved in the processes. This dissertation discusses atmospheric dynamical processes involved in the upper troposphere and lowermost stratosphere which result in stratospheric ozone intrusions and affect the distribution of ozone in the lower atmosphere.

1.4 Literature Review

In the atmosphere, ozone is found at all levels in different concentrations. Stratospheric ozone is good for many reasons. It screens potentially dangerous ultraviolet radiation to protect the living organisms at the Earth's surface. It plays a significant role in climate change since it affects the radiative heat budget in both the ultraviolet and the infrared, as it is a radiatively active gas [Butchart and Scaife, 2001]. Thus, any change in stratospheric ozone could lead to serious environmental concerns.

If on the other hand, tropospheric ozone is found in high concentration, especially at the surface of the Earth, it is harmful to human and animal health and also negatively affects crop production. It generates reactive free radicals such as OH, which oxidize and remove pollutants from the lower atmosphere [Lelieveld and Dentener, 2000]. It is also known to be a significant greenhouse gas. Ozone transport from low-latitude sources to higher latitude sinks is one naturally occurring atmospheric dynamical process that affects ozone distribution in the atmosphere. It exclusively accounts for polar ozone in polar winter.

Stratospheric ozone intrusions into the troposphere are known to remarkably force the chemistry and consequently the radiation [Roelofs and Lelieveld, 1997] and the ozone concentration in the boundary layer can be enhanced [Wernli and Bourqui, 2002]. Upward transport of tropospheric air into the stratosphere perturbs the chemistry of the lower stratosphere and can inject a large amount of water vapor into the stratosphere [Dessler and Sherwood, 2004]. Recent works have demonstrated that due to climate change the cross-tropopause mass transport may increase in this century [Sudo et al., 2003; Collins et al., 2003]. These authors have proposed that the tropospheric ozone budget would change appreciably as a result of the long term enhancement of stratospheric-originated ozone. Therefore, STE plays an important role in transporting chemical species including ozone from the lowermost stratosphere and brings about change in chemical composition of the region. The dynamical processes accountable for STT have been examined in numerous studies and different kinds of mechanisms are known. STT depends considerably on the relative importance of these parameters from case to case.

STE occurs episodically in both directions, which is linked with strong perturbations of the tropopause [Appenzeller and Davies, 1992]. Experimental observations, both in-situ and remotely, show the existence of tropospheric air which originates in the midlatitude lowermost stratosphere [Hintsa et al., 1998], as well as stratospheric air intrusions into the troposphere [Danielsen, 1968; Stohl and Trickl, 1999]. Severe weather and peak ozone concentration at the surface of the Earth can be associated with fast deep descent of stratospheric air [Goering et al., 2001; Stohl et al., 2000]. However, Stohl et al.

[2003a] has indicated that most cross-tropopause exchange which takes place both ways is shallow and much of the air involved returns back from where it came within 24 hr across the tropopause (see Figure 1.3). Ozone concentration in the lower troposphere brought down by deep STT is maximum in late winter, while ozone concentrations in the lowermost stratosphere and upper troposphere have a spring maximum, suggesting that the observed ozone maximum in springtime in the lower troposphere may not be a result of STT. Danielsen [1968] pointed out that STT transport processes association with tropopause folding are major contributors to the tropospheric ozone budget in midlatitudes. Radioactive tracers and other constituents demonstrate maximum downward mass flux from the stratosphere into the troposphere in spring, while diabatic calculations show the peak downward mass flux in fall and winter [Schoeberl, 2004]. The seasonal variation of tropopause height solves the above discrepancy. The jumps of the tropopause height toward its climatological summer position results in springtime peak mass exchange. Similarly, less mass exchange is observed in fall and winter because of the lowering of tropopause height [Appenzeller et al., 1996b; Gettleman and Sobel, 2000; Seo and Bowman, 2002; Schoeberl, 2004]. Hence, one parameter that needs to be determined as precisely as possible in STE studies is the tropopause height. Moreover, tropopause height is a useful parameter for different applications such as synoptic weather analyses and forecasting, aircraft flight planning and forecasting as well as estimation of ozone concentration [Reed and Danielsen, 1959; Reiter et al., 1969].

The mean meridional circulation, large scale eddies and tropopause folding event, seasonal variation of the tropopause heights, turbulent diffusion across the tropopause and penetrating cumulonimbus towers in the tropics are among many different kinds of dynamical processes that results in STE, and have been discussed by various authors [e.g., Muramatsu et al., 1984]. The polar jet stream front is another important dynamical region which produces intrusion of stratospheric ozone into the troposphere, even if the relative importance of the process as compared to dynamical processes that lead to STE is not yet well understood [Muramatsu et al., 1984]. Turbulent mixing in the troposphere is also suggested to play a significant role in the STE processes.

One of the most encouraging instruments that is used remotely for measuring and monitoring tropopause height (besides wind velocity and turbulence) is VHF radar [Gage and Green, 1978; Rotteger and Liu, 1978; Rotteger and Vincent, 1978]. It employs the enhanced specular reflecting echoes from the upper troposphere and lower stratosphere observed with vertically pointing beams. However, due to contamination of data by a variety of unwanted targets such as aircraft that pass through the radar beam, there is difficulty in determining the height of the tropopause from the backscattered power. Moreover, there are also issues of distinguishing specular reflections from scatter caused by isotropic or anisotropic turbulence and also differentiating stable regions in the upper troposphere from the tropopause.

The tropopause height can be determined by analysing the profiles of the vertical backscattered radar power. Westwater et al. [1983] and Gage and Green [1982] have developed suitable algorithms for real-time computer calculation of the height of tropopause. The former method was developed for computer use while the latter one was adapted from machine computation [Sweezy et al. 1986]. The details of radar derived tropopause height, as well as measurements of wind velocity and turbulence strength, are discussed in the second chapter of this thesis.

1.5 Current understanding

Ozone in the extratropical upper troposphere varies noticeably with season. Photochemistry is the dominant source in summer while STT is dominant in winter and spring. Generally, the tropopause height in the extratropics has been observed to increase with time which results in ozone column changes in the troposphere. This long-term change is a possible signature of human effects on climate change. However, it is not clearly known yet how this change affects the STE processes on synoptic scales or the mesoscale.

Dry ozone-rich air (i.e., high ozone concentration and low relative humidity) is taken as partial indicator of air originated in the stratosphere. Hocking et al. [2007] have shown using windprofiler radars the detection of stratospheric ozone intrusions associated with sudden jumps of radar derived tropopause height. It has been determined by many studies

that the dynamical processes responsible for STT occurrence involves different mechanisms, and their contributions differ from event to event. Lamarque and Hess [1994] and Wirth [1995a] have indicated the existence of clouds in the upper troposphere and the latent heat linked release causes stratospheric air influx to the troposphere. Shapiro [1976] has singled out clear air turbulence at the jet stream while Shapiro [1980] has shown its importance for STE. Hartjenstein [2000] has pointed out tropopause folds and their irreversible vertical mixing is also a possible major contributor of the mass exchange. Moreover, Sorensen et al. [2001] suggested that diabatic processes are responsible for the exchange rather than the diffusive processes.

STE can be divided into two regimes, namely (i) shallow exchange events, when the air spends a brief time in either the lowermost stratosphere or upper troposphere, and (ii) deep exchange events, when air transports deep into the troposphere from the lowermost stratosphere [Stohl et al., 2003]. The same authors have suggested that shallow events accounted for the lion's share of the events, while deep exchange cases have a strong tendency of occurrence along the Pacific and Atlantic storm tracks, where tropopause folds are more common. These latter events occur preferentially in winter, but with high seasonal variability.

The cross-tropopause mass flux can be both diabatic, i.e., the mass flux across the 380 K isentropic surface, and adiabatic since the tropopause is not an isentropic surface (see Figure 1.3). The rate of mass exchange along the isentropes that cross the tropopause is fast and involves adiabatic flux, while gradual mass exchange occurs across the isentropic surfaces via diabatic flux. In the tropics, the diabatic mass flux is upward across the tropopause and the 380 K surface, while in the extratropics the diabatic mass flux is mostly downward. Air mass intrusion from the tropical upper troposphere into the midlatitude lowermost stratosphere or tropopause folds causes cross-tropopause adiabatic fluxes. These processes can transport mass in both directions. Adiabatic mass fluxes to the lowermost stratosphere mix with air coming from the stratosphere. The chemical composition of the lowermost stratosphere is thus determined by the mixture of these two source regions [Schoeberl, 2004].

In our own work, the analysis of the vertical distribution of ozone in midlatitudes and in the Arctic upper troposphere and lower stratosphere shows ozone rich dry stratospheric air in the middle and upper troposphere associated with the occurrence of at least one of the atmospheric dynamics parameters that we have diagnosed using radar measurements. These observations, together with GEM-FLEXPART numerical simulation emphasize the importance of variation of vertical wind velocity, vertical wind shear of horizontal wind speed and turbulence strengths for the stratosphere-troposphere exchange of ozone in the Arctic and midlatitude, as we will show in this thesis.

1.6   Motivation

Transport of stratospheric ozone across the tropopause is one naturally occurring atmospheric phenomenon that plays a significant role in determining the tropospheric ozone budget. STE refers to atmospheric dynamical processes through which air mass and chemical species are transported across the tropopause between the two atmospheric layers. Since this process transports species that are tropospheric in origin, such as chlorofluorocarbons, water vapor and hydrocarbons into the stratosphere, and also stratospheric origin such as ozone and nitric acid into the troposphere, it has impact on the chemistry of both regions. On a large-scale, these processes are driven by the Brewer-Dobson circulation that is largely forced by wave breaking in the upper troposphere, and acts to push air parcels up across isentropic surfaces in the tropics via adiabatic cooling and down across the isentropic surfaces in the extratropics via adiabatic heating. The net STE on an annual cycle is determined by the dynamics of this circulation. The circulation results in a net influx to the stratosphere in the tropics and to the troposphere in the extratropics. The dynamical small-scale processes affect the occurrence of where and when local STE of mass and chemical species occurs. These processes in particular affect the composition of the lowermost extratropical stratosphere, i.e., the part of the stratosphere that shares isentropic surfaces with the troposphere.

Small-scale atmospheric dynamical processes that cause STE in the tropics and extratropics are different. In the former case, STE occurs as a result of convection and the Brewer–Dobson circulation. The Brewer–Dobson circulation controls the subsequent uplift after the air parcels cross the tropopause via cumulus convection. In the latter case,

STE takes place between the lowermost stratosphere and the upper troposphere via transport across an isentropic surface. There are a number of dynamical processes including tropopause folds, cutoff lows, gravity waves, deep convection radiative processes in the vicinity of the tropopause; all are local dynamical instabilities that result in STE [Lamarque and Hess, 2003]. These processes often act simultaneously but with different magnitudes.

Therefore, a better understanding of the impact of STE on tropospheric ozone concentrations will play a major role in analysing the climate effects of perturbations of ozone due to anthropogenic activities. In studying the STE processes, the location of the tropopause, which is the boundary between the two regions, is an important process that helps in quantifying the amount of mass exchange between the two regions. Moreover, a clear description of the physics and dynamics of the atmosphere around the tropopause will assist in analysing stratosphere-troposphere interactions. One atmospheric instrument that is used to study the physical and dynamical processes of the atmosphere is the windprofiler radar. In my thesis, I mainly focus on identifying and describing small-scale processes that occur around the tropopause and cause STT.

1.7 Research objectives

Ozone intrusions from the stratosphere to the troposphere happen as part of the Brewer–Dobson circulation, but the details of the process is one unresolved issue in the scientific community. Small scale extratropical dynamical processes control the transport of masses from the lowermost stratosphere into the troposphere. My research mainly focuses on this region and examines the stratospheric ozone intrusion to the troposphere across the stable region tropopause. Therefore, my research objective is to address the following scientific questions: what atmospheric dynamics causes the intrusions of stratospheric ozone into the troposphere, and what is the relative importance of these parameters from case to case. We perform multiple studies and attempt to identify special events.

To achieve our objective and address the above issue, our first task was to examine which of the following possible mechanisms best accounts for the observed high ozone concentration episodes.

    i.   Stratospheric ozone intrusion or

    ii.   Long-range transport of ozone and its precursors or

    iii.   Photochemistry or

    iv.   All or any combination of the above

To identify if the ozone was stratospheric in origin, we diagnose the response of the radar derived tropopause to the ozone intrusion events. Low relative humidity from ozonesonde data as well as theoretical numerical simulation via GEM-FLEXPART [Stohl et al., 2002, 2005] both in forward and backward modes complement our measurements. To ascertain the long-range transport of ozone originating in the stratosphere, we looked at the radar and ozonesonde data and computer simulation using GEM-FLEXPART. If the high ozone concentration episode was not a result of stratospheric ozone intrusion and long-range transport of ozone and its precursors, then we generally concluded that it was most likely the result of photochemistry.

Once we ascertained the possible mechanisms for the observed dry ozone-rich air, we analyzed the atmospheric dynamics responsible for the stratospheric ozone intrusions. Radar measurements of atmospheric dynamics such as the standard deviation of vertical velocity of wind, wind shear and turbulence strengths were analyzed near tropopause regions to see their association with the observed ozone rich dry air in the middle and upper troposphere. To figure out the relative importance of these parameters from event to event, we looked at all of three parameters for all stratospheric ozone intrusion events to see which one of these correlated most strongly with the intrusion events. Moreover, we demonstrated the occurrence of these parameters from case to case.

To study STE we have used both observational and modeling approaches. Important information includes large-scale meteorological fields, ozonesonde data and radar measurements. Continuous experimental campaigns have been performed at different sites and times to better ascertain and adequately describe STE. A combination of windprofiler radars with frequent ozonesonde launches has offered a means of detection of STE using the radar derived tropopause height. Our experimental observations are

supplemented by theoretical computer simulation GEM-FLEXPART so as to model the intrusions of ozone originating from the stratosphere.

Addressing the above issues ultimately leads us to better understand the processes associated with stratosphere-troposphere exchange for ozone transport. This in turn helps to better quantify the relative contributions of the stratosphere on the tropospheric ozone budget, tells us how frequently stratospheric ozone increases ozone concentrations near the surface and recognizes what regions are most likely affected by stratospheric ozone. Moreover, STE study assists us to keep the environment safe and more efficiently handle emissions, as it offers a good understanding of the sources and sinks of atmospheric species that have negative impact on air quality, change climate and ozone depletion related problems.

The approach involves the analysis of data obtained simultaneously from ozonesonde campaign measurements at Egbert (5 – 11 May 2009 and 12 July – 4 August 2010), Eureka (24 February – 18 April 2008 and 24 February - 12 March 2010), Montreal (29 April – 10 May 2005 and 12 July – 4 August 2010) and Walsingham (17 – 26 November 2005 and 23 April – 3 May 2007) and associated windprofiler radar data. Simultaneously, the windprofiler radars have been employed to measure wind velocity, turbulence strengths and backscattered radar powers (from which radar derived tropopause heights are determined) whereas ozonesondes equipped with GPS receivers have been used for ozone, temperature, humidity and winds in some cases measurements. This work has also been supported by theoretical computer simulation, the Lagrangian particle dispersion model FLEXPART, for modeling ozone movement in the atmosphere. The campaigns were based at the radar sites. The GPS locations of the sites Egbert, Eureka, Harrow, McGill-Montreal, and Walsingham are, respectively, (44.27°N, 79.73°W), (79.99°N, 85.94°W), (45.50°N, 73.57°W), and (42.64°N, 80.57°W).

1.8   Thesis outline

During the course of the research described in this thesis, simultaneous and co-located measurements of ozonesonde and windprofiler radar were made. The work has been supplemented by theoretical computer analyses using GEM-FLEXPART to simulate

ozone transport in the atmosphere. Over this period, more than 200 ozonesonde flights were made.

Chapter 2 describes the methodology and the instruments I used for my work. Ozonesonde preparation and measurement are described. Radar measurements of atmospheric information are discussed. Advantages and disadvantages of spaced antenna versus DBS (Doppler Beam Swinging) are discussed. Numerical simulation using the GEM-FLEXPART is discussed in this chapter. Chapter 3 focuses on the results of a unique combination of ozonesonde and radar measurements. The detection of stratospheric ozone intrusions using radar derived tropopause heights along with ozonesonde measurements of relative humidity is discussed. The observed atmospheric dynamics such as the standard deviation of vertical wind velocity, wind shear and turbulence strengths that are responsible for the intrusion of stratospheric ozone are discussed. Experimental observations were supported by application of the GEM-FLEXPART computer model, which permitted modelling of ozone transport. The result of numerical simulations using the GEM-FLEXPART model is presented in Chapter 4. In Chapter 5, we describe numerical simulations employing MATLAB to see the effects of turbulence on the diffusing atmospheric gases. Interesting results from this simulation are presented in this chapter. Conclusions and summary of the thesis with suggestions for future research are discussed in Chapter 6.

Chapter 2

2 Methodology and research instruments

In this chapter, the methodology and the equipments used to study ozone measurements and dynamics of the atmosphere will be discussed. Primary instruments used have been ozonesonde, windprofiler radar and GEM-FLEXPART. Ozonesondes have been utilized for measuring height profiles of ozone concentrations, temperature, humidity, pressure as well as winds from the ground up to height of approximately 35 km. Windprofiler radar is employed for observing atmospheric dynamics parameters such as wind velocity, turbulence, and backscattered radar power. Numerical computer modeling has also been performed using GEM-FLEXPART to simulate ozone transport in the atmosphere.

2.1 Ozone Measurements

A complex interaction of atmospheric dynamics and photochemistry are the determinant factors producing the geographical and vertical distributions of ozone in the atmosphere. Ozone measurement in the atmosphere has received strong attention in recent years; it is important to understand its geographical and vertical distribution as it is an indicator and driver of climate change and air quality. The concentration of ozone in the atmosphere has been measured since the 1920s using instruments from ground-based spectrometers to balloons, aircraft, rockets, and satellites. Developments in ozone instrumentation have enabled measurements to expand from the atmosphere above an isolated ground station to daily global coverage and profiles of ozone in the atmosphere. Atmospheric ozone is measured both by remote sensing and by in situ techniques. For in-situ measurements, a sample of air is taken from the atmosphere and analyzed to determine its ozone content using optical, chemical, or electrochemical techniques. Remote sensing measurements are made by remote instruments using backscatter and differential absorption techniques, and can be made both from space and the ground.

As noted, in-situ measurements involve direct sampling of the atmosphere. A sample of the atmosphere is introduced into the instrument and analyzed to determine its properties, or its relative amount of various chemical components including ozone content. Optical,

chemical, or electrochemical techniques are among the methods used. An example of an in-situ measurement technique used to measure ozone vertical profiles involves an ozonesonde, which is an instrument carried on a weather balloon. Ozonesondes are composed of an ozone sensor, a battery, a small gas pump, and some electronic circuitry, connected to a meteorological radiosonde and GPS. This radiosonde transmits values of air temperature, air pressure, relative humidity, detector current, detector temperature, and pump speed to a ground receiving station. The air containing the ozone sample is pumped through a solution, which is oxidized by the ozone producing an electrical current. The electrical current is proportional to the flow of ozone. By knowing the flow rate (pump speed), the ozone concentration can be deduced. The result is an ozone partial pressure vertical profile.

In remote sensing measurements, the observation platform does not directly sample the atmospheric parameter of interest (such as ozone content). Instead it measures using some sort of remote sensing mechanism, often involves radio, optical or sound wave. As an example, we might measure the change in thermal or shortwave radiation that is due to the presence of the parameter. Total ozone is measured by remote-sensing techniques using ground-based and space (satellite) instruments which measure irradiances in the UV absorption spectrum of ozone between 300 - 340 nm. For ground-based total ozone the radiation source is the direct Sun, direct Moon, and zenith sky irradiances. For measurements from space, the solar UV radiation scattered back to space by the Earth's atmosphere is utilized. Furthermore, remote sensing measurement can be either passive or active. Active remote sensing involves sending out electromagnetic radiation and analyzing the change in returned signal due to the presence of our atmospheric quantity of interest (an example is radar). In the passive case the sources of electromagnetic radiation can be the Sun, stars and moon, i.e., natural sources of light or other electromagnetic radiation.

LIDAR (LIght Detection And Ranging) is a ground-based active remote sensing instrument which infers temperature, density, and trace constituent concentration profiles from measurements of backscattered laser light. The Dobson spectrophotometer is a ground-based passive remote sensing instrument that measures the amount of ozone

present in the atmosphere. The Dobson spectrometer is a passive remote sensing instrument which only measures the amount of radiation that it intercepts. It does not actually measure the amount of ozone itself like an ozonesonde in-situ measurement would. Nor does it send out any electromagnetic radiation, such as the laser beam of a LIDAR to make active remote sensing measurements.

For the Dobson technique, we note that ozone absorbs selected bands of the electromagnetic spectrum and at these wavelengths the amount of light that reaches the ground depends on the abundance of overhead ozone. Thus, measurement of the light intensity at a wavelength, where light is partially absorbed by ozone, allows us to quantify the abundance of overhead ozone. The Dobson spectrophotometer can be used to determine ozone by measuring light from either direct Sunlight, diffuse light from clear or cloudy skies, and even from reflected Sunlight from the Moon. The direct Sun measurements are preferred because the uncertainties of ozone measurements get larger as the amount of light entering the instrument decreases. The Brewer spectrophotometer measures ozone based using the same technique as the Dobson instrument. However, the Brewer spectrophotometer is completely automated and can be programmed by a laptop computer to make measurements at any given time during the day. Global measurements of ozone can be made from satellite platforms using passive remote sensing techniques based on different viewing geometry concepts. The four techniques for satellite passive remote sensing are the backscatter ultraviolet (BUV), the occultation, the limb emission, and the limb scattering techniques (see Fig. 2.1). Each technique involves a different viewing geometry. The viewing geometry affects the measurements of atmospheric radiation.
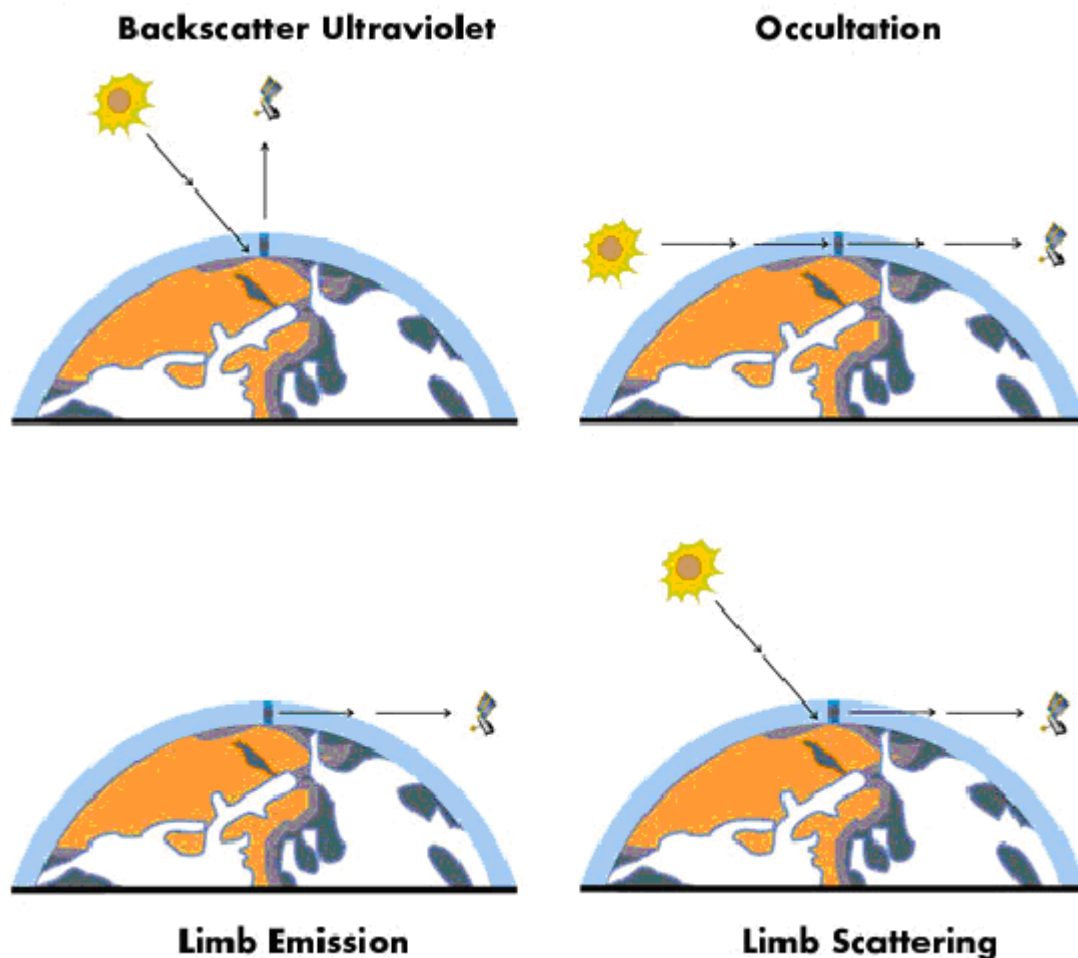
Figure 2.1. Satellite platforms based on different viewing geometry concepts adapted from Hilsenrath [2003] Figure 7.01.

Atmospheric ozone, which is routinely measured and recorded both by ground and satellite monitoring systems, is expressed as either surface ozone, or vertical profile of ozone, or total ozone. Surface ozone is the concentration of ozone from the surface of the Earth up to a few meters above the ground at a particular site. The vertical profile of ozone is the ozone concentration as a function of height. Total ozone is the total amount of ozone contained in a vertical column in the atmosphere above the ground. It is usually expressed in Dobson units. One Dobson unit defines the amount of ozone in the vertical column which, when reduced to a temperature of 0°C and a pressure of 101325 Pa will occupy a depth of 0.01mm.

Ozonesondes, LIDAR, ground-based spectrometers and various satellite-borne instruments are used to measure the vertical profile of ozone. The Brewer-Mast (BM) and electrochemical concentration cell (ECC) are ozonesondes in regular use. Balloon-borne ozonesondes are important for both campaign based intensive measurements as well as long term observations with high vertical height resolution [e.g., Thompson et al., 2003].

2.2 Ozonesonde

Ozonesondes, flown with large weather balloons, measure vertical height profiles of atmospheric ozone from the surface up to altitudes of typically 35 km. They function regularly under severe weather and conditions in all climatic regions. Since the late 1960s they have been the backbone of ozone height-profile measuring devices. Wet-chemical in-situ ozonesondes are based on the electrochemical oxidation of potassium iodide by ozone in an aqueous solution. Theoretically, the chemical reaction forms two electrons per ozone molecule entered in the solution and these produce a current flow. It is this current that quantitatively measure the number of ozone molecules pumped through the reaction chamber. The major components of the sonde are two reaction chambers, where ozone molecules react with the chemical solution, an air pump, a power supply and an electronic interface that digitizes the raw current signal and then transfers relevant information to the radiosonde. The information from the ozonesonde is telemetered to the ground receiver through the radiosonde transmitter. All components of the ozonesonde are placed in a Styrofoam box used to protect the sensitive parts from mechanical damage and from the impact of low temperature. Moreover, GPS is also used for the detection of the position of the sonde. Ozone concentration, ambient air pressure, temperature, humidity, and, wind speed and direction are the parameters normally measured by the sonde.

The two most common kinds of ozonesondes are the BM and the ECC. The BM as well as the ECC ozonesondes are still primary instruments for stratospheric ozone measurements and remain the major source of tropospheric ozone data [Lehmann and Easson, 2003], even though there are more sophisticated methods of measuring atmospheric ozone profiles such as satellite profilers [Frederick et al. 1986] and ground-based differential LIDAR [Carswell et al. 1991]. In these sondes, the aqueous chemical

sensing element is based on the redox reaction [see reaction 2.1] libration of free iodine, I_2. The method of detecting I_2 is an important characteristic of the two types of electrochemical cells. The pump which is driven by the battery is used for forcing the ambient air continuously into the sensing cell. An electrical current is produced proportional to the mass flow rate of ozone through the cell. The electrical current is converted to an ozone concentration under the assumption that the ozone reaction with potassium iodide is quantitatively known.

2.2.1 Brewer-Mast (BM)

The BM ozonesonde that derived from balloon-borne sondes was initially created by Brewer and Milford [1960] to determine the vertical atmospheric ozone profile [Angell and Korshover, 1983; Logan, 1994]. The BM ozone sensor is made up of a single electrochemical cell with a platinum cathode and silver anode submerged in an alkaline solution of potassium iodide. A 0.42 V polarizing potential is applied between the electrodes so that there will be no flow of current without the presence of free iodine. The sampled ambient air is forced through the sensing solution in the electrochemical cell (bubbler) to produce free iodine according to redox reaction (2.1). The bubbler's stirring action transports the iodine in to the platinum cathode and then the iodine is converted to iodide ions by up taking two electrons per molecule of iodine.

$$I_2 + 2e\text{-Pt} \rightarrow 2I^- \qquad \text{Cathode reaction}$$

At the anode two electrons are released through the ionization of two silver atoms, in the same way,

$$2Ag \rightarrow 2Ag^+ + 2e \qquad \text{Anode reaction}$$

so as to form nearly insoluble silver iodide, which prevents iodine from entering the solution. Theoretically, like ECC, each ozone molecule entering the sensor causes a current of two electrons to flow through the external circuit. A cylindrical platinum mesh cathode (~ 6 cm^2) and a thin silver wire as anode are contained in the reaction chamber (bubbler) which is made of Plexiglas. 2 ml of neutrally buffered aqueous solution of potassium iodide (0.1%) fills the bubbler. Ambient air is forced in to the bubbler by an

electrically driven gas sampling pump mounted at the side of the bubbler. Styrofoam is used to protect the sonde. In general, the measurement principle of the BM sonde is simpler than the ECC sensors, which consist of two chambers being separated by a diaphragm [Komhyr, 1986]. In the next section, details about the ECC will be mentioned since it was the primary sonde used in this research work.

2.2.2 Electrochemical Concentration Cell (ECC)

Of numerous kinds of balloon ozonesondes, the ECC ozonesonde is the most common as it is by far the most frequently used type of ozonesonde [Vomel et al., 2009]. ECC ozonesonde has been used extensively at different locations [Kley et al., 1996, Thompson et al., 2003, Schulz et al., 2001] for long period of time. The relative accuracy of ECC ozonesondes is generally 5% [Thompson et al., 2007]. The ECC ozonesonde, which was developed by Komhyr [1969], combines the basic principle of the reaction of ozone and iodide within a redox cell sensor coupled to a nonreactive air-sampling Teflon pump. The ECC sensors have a platinum electrode in each chamber (unlike the BM sensors that have a platinum cathode and a silver anode, both inside the single reaction chamber).
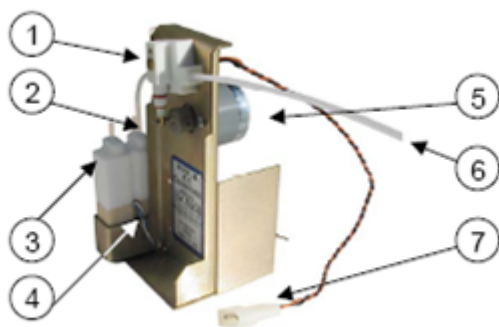
Figure 2.2. ECC Ozonesonde Sensor, showing the principal parts of the instrument adapted from Analog Ozonesonde RS92 [2004] Figure 2.

The following numbers refer to Figure 2.2 above.

1. Gas sampling pump

2. Ozone sensor cathode

3. Ozone sensor anode

4. Wires for interface

5. Motor

6. Air intake tube

7. Connector for pump battery

2.2.3 Operational Principle of ECC

The ECC ozonesonde consists of a small Teflon pump, an electrochemical cell and an electronic interface. It was originally built by Komhyr [1969]. It uses a platinum electrochemical cell sensor. The electrochemical cell consists of two small chambers containing potassium iodide (KI) of different concentrations. Each chamber has a Pt electrode at its base and is connected by an ion bridge that provides an ion pathway between the chambers while preventing the mixing of the cathode and anode electrolytes. A nonreactive gas sampling pump is used to supply ambient air through the cathode of the ECC. Ozone in the air reacts with KI in an aqueous solution to form iodine molecule (I_2), according to the following reaction.

$$2KI + O_3 + H_2O \rightarrow 2KOH + I_2 + O_2 \qquad\qquad 2.1$$
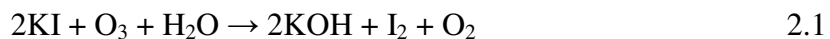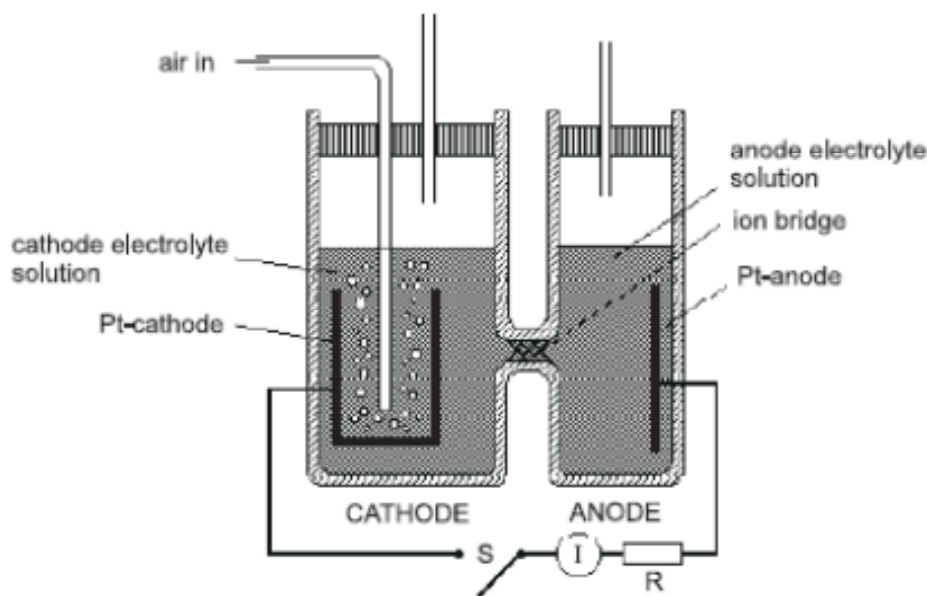
Figure 2.3. Electrochemical concentration cell adapted from Science Pump Corporation [1999] Figure 2.

The iodine molecule that is converted to iodide (I^-) through the uptake of two electrons in the Pt cathode chamber moves to the anode chamber via the ion bridge. At the anode chamber it is converted to I_2 through the release of two electrons. When the iodide changes to iodine [in the anode chamber] the two cells are no longer in electrical equilibrium and as a result the two electrons flow through the cell's external circuit in order to re-establish equilibrium. This means that the change in iodine concentration leads to a change in electrochemical equilibrium between the two half cells and causes two electrons to flow in the cells external circuit when the iodine is reconverted to iodide by the cell:

$$I_2 + 2e^- \rightarrow 2I^- \qquad\qquad 2.2$$

This flow of electrons, i.e., the sensor's output current, through the cells external circuit can be measured and is directly proportional to the partial pressure of ozone in the sampled air [Komhyr, 1969; Johnson et al., 2002].

Thus the sensor's output current is proportional to the rate at which ozone enters the sensor. Ozone partial pressure can then be computed from equation (2.2) if the flow rate and cell current (typically $0 - 6$ microamperes) are known [Johnson et al., 2002].

$$P_{O_3} = c * T * t_{100} * \gamma \left(I - I_{bg} \right)$$ 2.3

where P_{O_3} is ozone partial pressure, mPa (millipascals), I is the measured cell output current in μA, I_{bg} is the background current generated by the cell in the absence of ozone, typically 0-0.1 μA, and $c = \dfrac{R}{\chi F} = 4.309 \times 10^{-4}$ is the ratio of ideal gas constant R and Faraday constant F (this is the amount of electric charge carried by one mole , or Avogadro's number of electrons= 9.65 x 10^4 C/mol) divided by the yield ratio χ electrons per ozone molecule. In addition, T in [K] is the air temperature at the entrance to the cell, approximated by the temperature of the pump; t_{100} in [s] is the flow rate time to pump 100 ml of air; and γ is the pressure dependent pump efficiency, which corrects the reduced pump efficiency at low pressure. For laboratory measurements under normal surface pressure, γ equals one, i.e. these measurements are performed with direct flow rate measurements and do not require a flow rate correction, which is otherwise essential in the stratospheric measurements.

From eq. (2.3) one can derive the volume mixing ratio of ozone as

$$O_3 (ppbv) = \dfrac{10000 P_{O_3}}{P}$$ 2.4

where $O_3 (ppbv)$ is the measured ozone density in parts per billion by volume and P is the ambient air pressure in milibar or hPa.

There is uncertainty in the ozone partial pressure derived from eq. (2.3) as a result of the measurements of the parameters involved in the equation. Even if two electrons per ozone molecule is assumed in eq. (2.3), this yield ratio may change slightly because of secondary reactions that are not described by the basic chemistry described in eq. (2.1)

and eq. (2.2). Moreover, this yield ratio may also be affected by the surface chemistry on the platinum and the ion bridge. A thermistor imbedded in the Teflon pump is utilized to measure the pump temperature T and this is used to estimate the temperature of the ambient air entering the cell. This means that the pump temperature is assumed to be identical with the temperature of the air entering the cell. The accuracy of measuring the flow rate t_{100} is thought be within the abilities of the observer. Vomel and Diaz [2009] suggested that for a standard flow rate of 28 s the uncertainty for good measurement to be ±0.10. The pump efficiency correction has also been under question. Various authors including Johnson et al. [2002] have designed different approaches to measure it even if the results are not necessarily consistent. The difference observed in the upper stratosphere was as big as 10% and this undoubtedly shows the largest uncertainty for measurements taken in the stratosphere. The measured current accuracy is dependent on the cell current reader accuracy. The last parameter that the calculation of the ozone partial pressure depends on is the background current measure during the ozonesonde preparation. Vomel and Diaz [2009] have demonstrated that a background current measured at definite time after being subjected to high ozone may frequently overestimate the real background current, which can cause false low ozone concentrations in the upper tropical troposphere. This may result in operator dependent uncertainties. The same authors have proposed an improved cell current measurement which eliminates background current variability based on an operator reading and takes out possible manmade errors in the measurement.

The ozonesonde equipped with a balloon-borne radiosonde and GPS provides good vertical height resolution and a relatively inexpensive way to take measurement of ozone concentrations from the surface up to altitudes of about 35 km [Johnson et al., 2002]. The response time of the ECC ozonesonde for the entire flight is within 20–30 seconds [Smit et al., 2007]. Since ECC ozonesonde began measuring ozone profiles in the late 1960s, it has become an essential instrument in monitoring tropospheric and lower stratospheric ozone. Moreover, it has been employed for both field experiments and routine networks to investigate the problems of ecology, ozone layer, physics of the atmosphere etc. A complete ozonesonde system consists of the ozone sensor, temperature, humidity sensors, data acquisition and conversion, transmitter and ground receiving system. An ozonesonde

is placed in a Styrofoam box which is used for protecting the instrument from mechanical damage and the impact of low temperature. The ozonesonde has to be connected to a suitable meteorological radiosonde in order to transfer the ozone signal to a ground receiver. At Walsingham this was the 401.5 MHz radiosonde Vaisala RS-80.

Therefore, the current, which is produced as result of the reaction of the ozone in the air supplied to one side of the ECC, is digitized on the circuit board along with ambient temperature, pressure, humidity measurements obtained from a radiosonde Vaisala RS-80 as well as position information of the sonde obtained from a GPS receiver. The RS-80 radiosondes are modified in such a way that the analogue signals from it (produced by temperature, pressure, sometimes wind velocity, and humidity sensors) are digitized on the ozonesonde circuit board. These digitized signals from the RS-80 radiosondes combined with signals from the ECC and the GPS receiver and are then sent to the ground receiver via the transmitter of the radiosonde. The ground station consists of an antenna, a receiver, a modem, a PC and Metagraph software (ozone-observation program start-up kit). The software monitors a serial port on the PC to determine the incoming data stream from the modem.

The following numbers refers to Figure 2.4

1. Ozone sensor Styrofoam casing
2. Radiosonde
3. Ozonesonde Interface Card OIF11
4. Ozone sensor
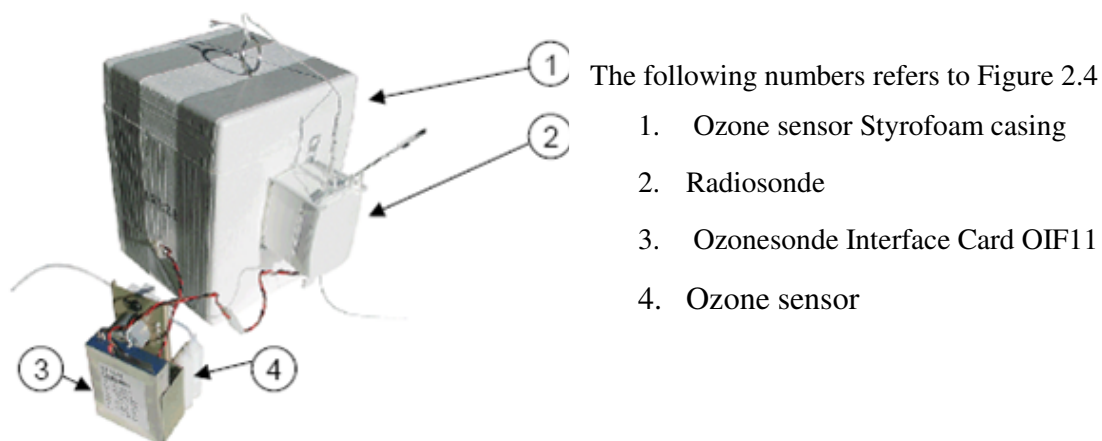
Figure 2.4. Radiosonde with ECC sonde adapted from Analog Ozonesonde RS92, [2004] Figure 1.

Among several types of balloon ozonesondes, the ECC ozonesonde is the most widespread ozone measuring instrument because of its advantages including yielding absolute ozone concentration with high accuracy in the 10-25 km region and the possibility for unskilled operator to achieve good results after short training. Moreover, unlike some ozonesondes, ECC sondes do not require an external electrical potential. The ECC gets its driving electromotive force from the difference in the concentration of the potassium iodide solutions in the instrument's cathode and anode chambers. When ozone enters the sensor, iodine is formed in the cathode half cell. The cell then converts the iodine to iodide, a process during which electrons flow in the cell's external circuit. By measuring the flow of current and the rate at which ozone enters the cell per unit time, ozone concentrations can be determined.

Even if ECC sondes have been used by a numerous ozone sounding stations for a long period of time, there are still unresolved issues regarding the sonde's response in laboratory conditions and during the flights in real atmosphere. In particular, the optimal KI solution concentration used in the ECC ozonesondes is significant because there is no consistency in the global network regarding this essential parameter. The real response of the sondes to ozone change and the influence of low pressure on the performance pumps at higher altitudes are also unresolved issues.

2.2.4 Ozonesonde preparation

The pre-launch preparation requires a special unit known as an Ozonizer/Test Unit. Using it, ozone in controlled concentrations can be generated for comparing the sensor response against that of a calibrator sensor within the Unit. Supplementary tools such as a vacuum/pressure measurement gauge, air flow meter, ozone destruction filter, thermometer, precise balance, stop watch, balloon, ozone-observation program start-up kit (Metagraph), data acquisition system and chemicals are also required during the preparation. The ECC sensor preparation has two parts: advance preparation and preparation on the day of sounding. The advance preparation should be prepared 3 days to 1 week prior to the flight date although on some cases a 1-day preparation is acceptable. This initial preparation is designed to clean the pump and air supply tubes to remove any contaminants that could destroy ozone, as well as it is to ensure that the

background current is low. Hence, this preparation includes pump performance checks and the flow rate measurement, conditioning the sonde with high ozone and charging the chambers with the solutions, testing background current and checking sensor response time. The purpose of performing initial charging of the sonde 3 days to 1 week in advance is to achieve a low sensor background current.

Preparation on the day of launch involves recharging by replacing the KI solutions in each chamber and checking the sonde to ensure it is working satisfactorily. The flow rate of air through the sonde, which is required for absolute calibration, is also measured at this stage. Sensor background current and sensor response time are also rechecked. At this point the assembly of payload follows and it is placed into the Styrofoam box. Sounding balloons of 1200 g were used to lift the sondes. The balloons were filled with helium gas until they were able to lift a mass of nearly 2.5 kg. To slow the descent of the sonde a parachute was connected to the balloon and a dropper was used to connect the payload to the parachute. The dropper was employed to permit a short length string between the balloon and payload during launch which makes launch easier, but also increases this distance between the balloon and sonde directly after launch to make sure that the measurements are not affected by the disturbed air passing close to the balloon. The final stage is to activate all the sensors and check out the output-numbers on the SPC DATA HANDLER window on the PC to ensure that data are being recorded and the sonde is operational. If they all are found to be reasonable, then the parachute-dropper is connected to the already inflated latex balloon and the payload to the dropper. The balloon is then launched after ensuring all systems are function properly. The ECC ozonesonde can also be prepared and flown on the same day, but in this case the background current may be slightly higher than the normal, which potentially may lessen the quality of the data.

2.2.4.1   Sensor solutions

Sensor solution requirements are very strict and the chemicals must be very pure in order to obtain the desired result. Syringes, balance, bottles and glassware etc are required for preparing and storing sensing solutions as well as for sensor cleaning. The ozonesonde's cathode and anode solutions are prepared in the following procedure and proportion. The

chemicals are not hazardous. To ensure good data quality, the procedures of preparation need to be followed carefully. The following is the preparation of 0.5% KI-b (buffered cathode solution).

A. Cathode solution

To 500ml distilled water add

5.00 g…………………KI (Potassium Iodide)

12.50 g………………KBr (Potassium Bromide)

0.63 g…………………$NaH_2PO4.H_2O$ (Sodium di-hydrogen orthophosphate 1-hydrate)

2.50 g…………………$Na_2HPO_4.12H_2O$ (Di-sodium hydrogen orthophosphate 12-hydrate)

> or

1.87 g……………….. $Na_2HPO_4.7H_2O$ (Di-sodium hydrogen orthophosphate 7-hydrate)

Shake vigorously to dissolve the chemicals and then add distilled water to make up 1000 ml of cathode sensing solution.

B. Anode solution

Fill a 100 ml plastic one-half with 50 ml cathode solution (prepared as described above). Add 70 g KI crystals to the solution, and shake vigorously to dissolve the crystals. Some crystals will remain undissolved, indicating that the solution is saturated.

C. Storage

Store the cathode and anode sensing solutions in a dark place at 20° to 25^oC until the day of sounding. If the solution is not used for a couple of months the old solution should be disposed of properly and a new solution prepared for use. In order to lengthen the life time of the solution one can store it in a refrigerator.

2.3 Radar

RAdio Detection And Ranging (RADAR), whose story dates back to Heinrich Hertz (1885-1888), refers to both a technique as well as a device. The radar transmits an electromagnetic wave (EM) in the radio and microwave regime and detects the reflections of these signals from objects in its line of sight. The radar technique uses the two-way travel time of the EM wave to determine the range to the detected object and its backscatter signal strength and character to deduce physical quantities such as size or surface roughness. Monostatic radar uses only one antenna both for transmitting and receiving signals, while bistatic radar employs transmitting and receiving antennas that are physically separated [Skolnik, 1980].

Radar has been used on the ground, in the air, on the sea, and in space. Ground-based radar has been utilized mainly for the detection, ranging, and tracing of aircraft or space targets. Shipboard radar is helpful for navigation and safety device to locate buoys, shore lines, and other ships as well as for detecting aircraft. Airborne radar is employed to detect other aircraft, ships, or land vehicles. In space, radar is used for guiding spacecraft and for remote sensing of the land and sea. The major areas of radar application include air traffic control, aircraft navigation, ship safety, military, ground penetrating radar (geology, gas pipe detection, archaeology, detection and location of mines), meteorology, study of atmosphere, etc.

The combination of radar observations with in situ, remote sensing and model simulations produce a most complete view of the atmosphere of Earth. EM waves of frequencies ranging from a few KHz up to some GHz are used for scientific studies of the Earth's atmosphere. Atmospheric radars are devised to transmit EM wave and to examine the consequences that the atmosphere has on the scattered wave. Bending of the radio wave path or reflection and scattering may be the outcome of these interactions. Generally, a transmit antenna and a receive antenna are needed that can be placed at separate locations. Usually in Mesosphere-Stratosphere-Troposphere (MST) study (as used in this thesis), the transmitter and receiver are co-located; in such cases, refraction of the ray paths is not generally important. Radar beams can be attenuated, reflected and bent by the atmosphere due to refractive index fluctuations. The strength of the received

echo can also be measured and it varies with the range, size, shape, speed, angle (azimuth and elevation), and composition of the target. In MST studies, reflection and scattering are the primary phenomena that need to be considered.

2.3.1 Radar Frequencies

No matter what its frequency, any device that detects and locates a target by transmitting radio wave and exploiting the echo scattered from a target can be classed as a radar [Skolnik, 1990]. Radars have been employed at frequencies from a few MHz to 3000 GHz [Skolnik, 1980; 1990]. Even though the practical implementation is extensively different, the basic principles are the same at any frequency.

Radar engineers and scientists apply letter designations to indicate the general frequency band at which a radar runs, as shown in Table 2.1. These letter bands have been officially accepted as a standard by the Institute of Electrical and Electronics Engineers (IEEE) and have been recognized by the U.S. Department of Defense. They are universally used in the world of radar.

Table 2.1. Standard radar-frequency letter band nomenclature.

Band Designation	Nominal Frequency Range
HF	3-30 MHz
VHF	30-300 MHz
UHF	300-1000 MHz
L	1-2 GHz
S	2-4GHz
C	4-8 GHz
X	8-12 GHz
K_u	12-18 GHz
K	18-27 GHz
K_a	27-40GHz
V	40-75 GHz
W	75-110 GHz
mm	110-300 GHz
sub mm	300-3000 GHz

From IEEE Standard 521-1984 taken from Peebles, 1998 and Skolnik, 1990.

2.3.2 Principles of Atmospheric radar measurement

The index of refraction, n, expresses the characteristics of the atmosphere seen by radio waves in the absence of liquid water [Fukao, 1989]. It is defined as

$$n = \frac{c}{v}$$ 2. 5

where c is the speed of light in vacuum and v is the speed of a radio wave in air.

Refraction or reflection is caused by macroscopic changes of n in space while scattering is caused by its small scale changes; the latter is the main subject in atmospheric radar. It is important to see what determines the background n even though the fluctuations of n from its background are of our interest. According to Balsley and Gage [1980], the main contributions to n at frequencies of HF up to UHF bands are approximately given by

$$n - 1 = \frac{3.75 \times 10^{-1} q}{T^2} + \frac{7.76 \times 10^{-5} P}{T} - \frac{N_e}{2N_c}$$ 2. 6

where $q(mb)$ is the partial pressure of water vapor, $P(mb)$ is the total atmospheric pressure, $T(K)$ is absolute temperature, N_e is the number density of electrons and N_c is the critical plasma density.

The first term in RHS of equation 2.6 is known as the wet term. It is more important in the lower troposphere because of the high water vapor content. The partial pressure of water vapor becomes very insignificant above the tropopause height. The second term, known to be the dry term, becomes dominant in the stratosphere. The third term is the main contributing factor due to free electrons. This term is negligible below 50 km but becomes dominant at ionospheric heights of above 80 km.

Reflection and scattering in the atmosphere arise from the EM wave interaction with changes in the refractive index. A variety of phenomena lead to refractive-index variations. Even if aircraft and missiles are the most common examples of radar targets, they are not the principal targets in the studies of atmosphere. Water droplets embedded

in the air are an example. Since the water droplets' refractive index is different from the surrounding air, each water droplet may scatter small amount of incident radiation. To produce a detectable scattered signal, scatter from a great deal of water droplets is required. Insects and birds can act as radio wave scatterers since they contain water.

Turbulence, which can mix the refractive index of the medium it exits, is also another example that causes change in refractive index in the lower and middle atmosphere. For example, the refractive index of the ionosphere is generally different from unity and events such as turbulence can mix an originally homogeneous region into one in which the refractive index differs both temporally and spatially. This phenomenon leads to radio wave scatter. The same type of events can happen to the neutral air. The air has a refractive index slightly different from one; the exact value depends on temperature, pressure, density, humidity and free electron density. The variations of refractive index from unity are a few parts to a few hundred parts per million. Even though quite small changes, the effects of this non-unity refractive index can be fairly intense. Turbulence and even small-scale atmospheric wave phenomenon can result in the variation of refraction index as a function of time and position and these small perturbations can also be a source of radio wave reflection and scattering. Radar with a suitable sensitivity can detect scatter from inhomogeneous regions in refractive index in spite of the very small refractive index perturbations. In fact, scatter as a result of turbulence induced refractive index perturbations in the air is usually one of the major processes exploited with high-gain atmospheric radars [Fukao, 1989; Hocking, 2009].

The backscattered radar power relates to the amplitude of the Bragg scale vector, which is one half of the radar wavelength for monostatic radar, aligned with wavefronts perpendicular to the line connecting the radar and the point of scatter. Therefore, generally turbulent scatter and scatter from atmospheric irregularities are referred to as Bragg scatter. Scatter from particulates such as water droplets is referred to as Rayleigh scatter and is often regarded as non-Bragg scatter. This definition seems to mislead. Even for scatter from particulates, the particulates can each be considered as small "delta function" scatterers and if we Fourier-analyze the entire field of delta functions, we will again obtain various Fourier components. Even in this case, the backscattered power

depends on the amplitude of the Bragg scale, so it is wrong to think of Rayleigh scatter as different to Bragg scatter. In spite of the similarities, each of these different kinds of scatter have unique characteristics associated with them, and it is important to understand the differences because it helps define the most suitable methods of radar design, data acquisition and data analysis. The main purpose of atmospheric radar is to employ radar techniques to examine the air and to interpret the signals received in order to better understand the motions and dynamics of the atmosphere. To do so, we need to understand the basic feature and principles of atmospheric radar [Hocking, 2009].

A simple bistatic radar consists of a radar controller, transmitter, transmit antenna, receiver antenna and receiver with some sort of recording device attached to it. Sometimes the same antenna is employed for transmission and reception using a special fast acting switch known as transmit-receive switch to interchange between the transmitter and receiver (e.g., Hocking [2009]).
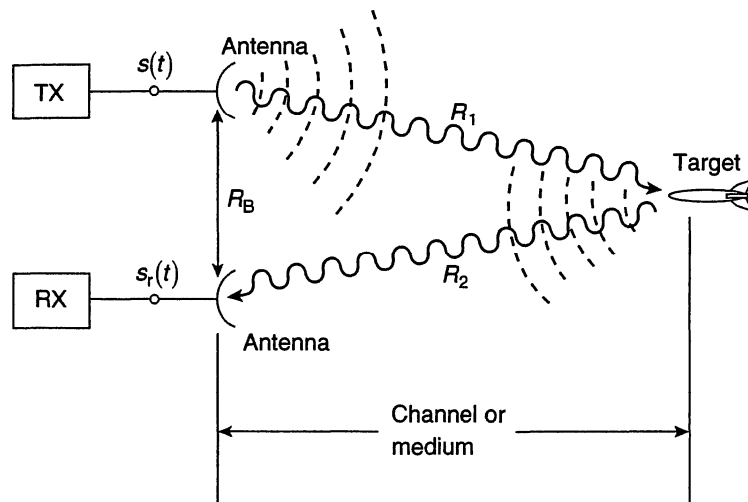
Figure 2.5. Basic form of radar taken from Peebles, 1998.

The most basic form of radar carries out all of the basic required functions shown in the block diagram in Figure 2.5. It comprises a transmitter (TX) connected to a transmitting antenna for sending out an EM wave from the transmitter, and a receiver (RX) connected to a receiving antenna for collecting any wave reflected from a target [Peebles, 1998]. In

Figure 2.5, *s(t)* is a waveform, and stands for the signal created at the output terminals of the transmitter. The signal *s(t)* will be radiated from the antenna. The signal will be converted to a radiating EM wave having the same shape as *s(t)* by the antenna. The target located at distance R_1 reflects/scatters some of the energy of the wave back toward the receiving antenna. The reflected wave is received by the receiving antenna after traveling a distance R_2 at the speed of light and the antenna converts the wave to a received waveform *s_r(t)* at its output terminals. The presence of a target can be detected by the radar via observing the existence of a signal *s_r(t)*.

In general, the transmit and receiving stations of Figure 2.5 can exist at the same location (where the distance R_B between stations is zero and it is called monostatic radar) or can have separate locations (where $R_B \neq 0$ and it is called a bistatic radar). Multistatic radar expands the bistatic radar notion by having more than one transmitter or receiver. Radars can also be classified based on their waveform *s(t)*. A continuous-wave (CW) radar is one that transmits continuously usually with constant amplitude [Peebles, 1998]. It can usually contain frequency modulation (FM) or can be constant-frequency. It often uses a single transmitter and receiver, and the transmit and receive antennas are usually co-located [Hocking, 2009]. However, when one wishes to use the same antennas for reception and transmission, a transmit-receive switch is required. A transmit-receive switch is a device used to connect/disconnect the antenna during the transmit and receive processes. It is not a continuous wave but rather a sequence of pulses that a pulsed radar transmits. The amplitude as well as phase of the received signal will vary from pulse to pulse and this is the information that is required and must be diagnosed. A pulsed radar is one that transmits pulsed waveform with or without FM [Peebles, 1998].

The most important functions that a radar can perform are resolution, detection and measurement [Peebles, 1998; Skolnik, 1990]. A radar's ability to separate one desired target signal from undesired target signals that may be noise and clutter is called resolution. Theoretically, we want to separate target signals from each other no matter how close the targets are in space and no matter how close the vector velocities are to each other. Actually there is a restriction in such separation that is dependent on the design of the signal and the characteristics of antenna. In regard to range separation,

larger bandwidths give better resolution in range while long transmitted pulses yield better resolution in frequency. In the case of angular resolutions, small spatial beamwidths offer better resolution of position. The perception of the presence of the reflected signal from some desired target in the receiver is called radar detection. Even if this looks like a simple task, the presence of unwanted reflected signals and receiver noise makes the task complicated. Better designing of receiver and transmitting larger energy per pulse signals can usually reduce noise effects. Proper signal design and appropriate signal-processing methods can often reduce unwanted reflected signals, including clutter. The word radar implicitly suggests the measurement of target range. Nevertheless, modern radars not only can measure radial range but also can measure position of a target in three dimension, its velocity in three dimension, angular direction, and angular velocity. In the presence of clutter and noise all these measurements can be simultaneously made on multiple desired targets. More advanced radars may even measure target size, shape, and classification (truck, tank, person, building, aircraft, etc.). Indeed, as technology proceeds, classification may eventually become accepted as another important radar function.

2.4   Radar Equation

The radar equation is perhaps the single most useful description of the factors influencing radar performance and a main ingredient for radar design [Skolnik, 1990; 1980]. It gives the desired target signal received power as a function of radar parameters (i.e., transmitter, receiver, antenna,), target, environment and geometry [Skolnik, 1990; 1980]. In this section, the radar equation in its simplest form is derived.

If P_t is the power of the radar transmitter and if the antenna radiates uniformly in all direction (isotropic antenna), the power density at a distance R from the radar is

$$p_{isotropic} = \frac{P_t}{4\pi R^2}$$

2.7

Where $p_{isotropic}$ is power density (power per unit area) from an isotropic antenna, and $4\pi R^2$ is the surface area of an imaginary sphere of radius R .

Radars utilize directive antennas to focus the radiated power P_t into some particular directions. The enhanced power radiated in the direction of the target as compared with the power that would have been radiated from an isotropic antenna is measured by the gain G of an antenna. It may be expressed as the ratio of the maximum radiation intensity from the subject antenna to the radiation from a lossless isotropic antenna with the same power input. The radiation intensity is the power radiated per unit solid angle in a given direction. The power density at the target from antenna with a transmitting gain G is

$$p_{directives} = \frac{P_t G}{4\pi R^2}$$
2.8

where $p_{directives}$ is power density (power per unit area) from directive antenna.

The target intercepts a fraction of the incident power and reradiates it in different directions. The measure of the amount of incident power intercepted by the target and reradiated back in the direction of the radar is designated as the radar cross section σ and is expressed by the relation

$$p_{echo} = \frac{P_t G}{4\pi R^2} \frac{\sigma}{4\pi R^2}$$
2.9

where p_{echo} is power density (power per unit area) of echo signal at the radar. Eq. (2.9) is true ONLY for hard targets.

The cross section of radar (i.e., the power backscatter per unit solid angle, per unit incident power density/4π radians) σ has units of area. It is a characteristic of the particular hard target and is a measure of its size as observed by the radar. A portion of the echo power is captured by the radar antenna. For soft targets eq. (2.9) would take a different form and the cross section of radar backscatter for a soft target becomes $\sigma = 0.00655\pi^{4/3} C_n^2 \lambda^{-1/3}$ as shown in Hocking [1985]. If the effective area of the receiving antenna is designated as A_e, the received signal power by the radar P_r is given by

$$P_r = \frac{P_t G}{4\pi R^2} \frac{\sigma}{4\pi R^2} A_e \qquad 2.10$$

For soft targets, the last equation would take a form

$P_R = \dfrac{P_T\, e_R\, e_T\, G_{Tm}\, A_{Rm}}{4\pi h^4}\, \sigma\, \dfrac{V}{\ln 2}$ as shown in Hocking [1985]. In the equation P_T refers to the

transmitter peak power, e_R is the efficiency of transfer of signal from the antenna to the

receiver (≤ 1), e_T refers to the efficiency of transfer of power from the transmitter to the

transmitting aerial (≤ 1), G_{Tm} refers to the gain for the transmitter, A_{Rm} is effective area of

the receiver antenna, h is height of scatter, $\sigma = 0.00655\,\pi^{4/3}\, C_n^2\, \lambda^{-1/3}$ and V is the volume

defined by the locus of the half power half width of the polar diagram at the height of

scatter, and the pulse length.

The right-hand side of eq. (2.10) is written as the product of three terms to point out the

physical processes going on. The first term indicates the power density at a distance R

from a radar that transmits a power of P_t from an antenna of gain G. The second term's

numerator is the target cross section σ while the denominator accounts for the

divergence on the return path of the EM radiation with range which is the same as the

denominator of the first term that accounts for the divergence on the outward path. The

power per unit area returned to the radar is represented by the product of the first two

terms. Effective aperture area of the antenna A_e, intercepts a fraction of this power to

produce an amount given by the product of the three terms.

The maximum radar range R_{max} beyond which the radar cannot detect targets take places

when the received power signal is the minimum detectable signal, S_{min}. Thus, using eq.

(2.10), we find

$$R_{max} = \left[\frac{P_t G A_e \sigma}{(4\pi)^2 S_{min}} \right]^{1/4} \qquad 2.11$$

This is the basic form of the radar equation. The transmitting gain and the receiving

effective area are the important parameters of the antenna.

When both the transmitting and receiving antennas are the same, the transmitting gain and the receiving effective aperture of the antenna A_e are related by

$$G = \frac{4\pi A_e}{\lambda^2}$$

2.12

where λ is the wavelength of the radar EM wave. Plugging back eq. (2.12) into eq. (2.11), one gets two other forms of the radar equation:

$$R_{max} = \left[\frac{P_t G^2 \lambda^2 \sigma}{(4\pi)^2 S_{min}} \right]^{\frac{1}{4}}$$

2.13

$$R_{max} = \left[\frac{P_t A_e^2 \sigma}{4\pi \lambda^2 S_{min}} \right]^{\frac{1}{4}}$$

2.14

The need to be careful in the interpretation of the radar equation is demonstrated in the three forms of eqns. (2.11, 2.13, and 2.14). For instance, eq. (2.13) indicates the range of a radar varies as $\lambda^{1/2}$ while eq. (2.14) reveals a $\lambda^{-1/2}$ relation and eq. (2.11) suggests the range to be independent of . The right relation relies on the assumption that either the gain is constant or the effective area is constant with wavelength. Moreover, other constraints introduction such as scanning a specified volume in a given time can yield different wavelength dependence [Skolnik, 1980].

These overly simplified forms of the radar equation do not sufficiently express the actual performance of a practical radar. The actual observed maximum radar ranges are often much smaller than what would be calculated using by the above equations. This is due to the fact that there are several essential elements that influence range which are not explicitly incorporated in the above equations. One of them is that various losses that can come about in a radar which are missing in the equations, and the other is the statistical nature of the target cross section and the minimum detectable signal. Determination of S_{min} depends on the signal processing procedure used (coherent integration, spectral analyses, filter design etc). Hence, the specification of the range has to be made in

statistical terms. Detail on the elaboration of the failure of the simple radar equation to correlate with actual performance is discussed in chapter 2 of Skolnik [1980] and the simple range equation to yield meaningful range predictions is explained in chapter 2 of Skolnik [1990].

2.4.1 Doppler radar

Doppler radars operate at several frequencies in the VHF (30-300 MHz) and UHF (300-3000 MHz) ranges to probe the atmosphere up to stratospheric altitudes. The Doppler effect is an increase or decrease (or shift) in the pitch or frequency of waves when a source of waves is moving toward or away relative to the observer. This situation is familiar to an observer who is listening to the blare of an auto horn as the source passes. The observer first hears a relatively high-frequency pitch as the source of the sound waves approaches, and then a noticeable decrease in frequency as the source of the sound waves recedes. In the same way, EM waves can also have Doppler shifts, for example when radiation is emitted from the Sun or other stars that recede from an observer. Spectral lines of emitted radiation are Doppler shifted to lower frequencies for receding targets. In this section, we explain how the Doppler effect is employed by radars to measure the velocity of atmospheric scatterers (e.g., turbulence, precipitation, insects, etc.).

In a pulsed radar the Doppler frequency shift produced by a moving target may be used to estimate the relative velocity of a target or to distinguish desired moving targets from undesired stationary objects. The application of Doppler frequency shift to separate small moving targets in the presence of large clutter is of particular interest. Atmospheric echoes detected by Doppler radars arise from scattering and partial specular reflections (at long wavelengths under special conditions) from irregularities in the radio refractive index with scale sizes comparable to one-half the radar wavelength [Gage and Balsley, 1978]. The Doppler power spectrum, i.e., relative echo power density as a function of frequency shift from the transmitter frequency, offers a variety of useful parameters from the signal returned at a given height. The mean radial component of motion of the scattering elements is obtained from Doppler shift. Moreover, information about turbulence intensity and wind shear can be inferred from the width and the amplitude of

the Doppler spectrum with appropriate assumptions. Other than the above parameters, at meter wavelengths, the intensity of strong echoes obtained at vertical incidence from stable regions of the atmosphere via partial specular reflections yields at least a qualitative measure of atmospheric stability. The radar's excellent time and height resolutions make them an outstanding tool for studying small-scale dynamics and these same characteristics are no less important for studies of larger scales.

A Doppler radar measures only a single radial component of velocity. Three or more Doppler radars could be used to obtain the full three dimensional air motion fields in precipitation by scanning together. This method led to the use of networks of Doppler radars for studies of individual clouds and larger-scale cloud systems.

2.4.2 MST Wind profiler radar

Wind profiler radars are another form of Doppler radar that have become popular in the atmospheric research community. Wind profilers operate at frequencies of VHF and UHF, and are fixed beam systems pointing vertically and off vertically. Wind profilers can make Doppler measurements throughout the range of altitudes from a few hundred meters from the surface of the Earth up to 16 km above the surface, depending upon the wavelength selected and the power-aperture product available [Skolnik, 1990 chap. 23]. Mesosphere-Stratosphere-Troposphere (MST) radars are very powerful radars because of their ability to make measurements throughout most of these atmospheric layers. MST radars have been running at many sites around the world. Outstanding facilities are located at Jicamarca, Peru; and at the University of Kyoto in Japan [Skolnik, 1990 chap. 23].

Wind profilers receive backscattered power from the inhomogeneities of refractive index due to atmospheric turbulence. The antenna systems often take the form of phased arrays. Generally, the transmitters are high powered, fully coherent transmitting tubes. Due to the ability of wind profiler radars to measure winds continuously under all atmospheric conditions, the radars show good promise in meteorology. This unique capability allows the study of smaller-scale temporal and spatial wind-field aspects than can be achieved from the global 12-hourly rawindsonde-balloon networks. Both for understanding local

as well as regional weather and for effective forecasting on these scales, smaller-scale measurements are essential. A two beam system can measure horizontal winds if the wind field is uniform and the vertical velocities are insignificant. Three beam systems can in principle measure all three components of velocity if the wind is uniform. A four and five beam systems allows one to determine the quality of the measurements by detecting the presence of heterogeneity. In the next section, we will discuss about wind measurements using wind profiler radars and associated errors with the measurement in detail.

It is well known that the stratospheric and tropospheric exchange of air at midlatitudes takes place mainly due to the tropopause folding that occurs around the cold-front surface and the troposphere. The measurements performed by radar have the desired time and height resolutions crucial to study this processes in detail, and offer the measurements of vertical wind that are required to better understand the atmospheric dynamics of mixing across the tropopause.

For studying dynamical processes of different temporal and spatial scales in the lower and middle atmosphere VHF radars have proven to be significant tools [e.g. Woodman et al., 1974; Miller et al., 1978; Balsley and Gage, 1980; Harper and Gordon, 1980; Czechowsky et al., 1984; Roster, 1984; Fukao et al., 1985]. Radars can continuously measure the three-dimensional velocity vector with good temporal and spatial resolution in the troposphere, and lower stratosphere. Wind profiler radars can continuously monitor physical parameters that include wind, vertical velocity, tropopause height, wave activity and turbulence intensity.

2.4.3 Radar Measurements of Wind

VHF and UHF Doppler radars are powerful tools for investigations of the dynamics and turbulence of the atmosphere at small scales. The radars measure the winds by detecting backscatter from turbulent fluctuations in the refractive index, i.e., the fluctuations of humidity, temperature and density. The description of the measurement techniques and numerous observational results are found in [Gage and Balsley, 1978; Balsley and Gage, 1980; Rottger, 1980; Harper and Gordon, 1980]. The great sensitivity of the radars to

obtain wind profiles with good height and time resolutions make the technique a natural candidate for investigations of relatively small-scale dynamics.

The high time resolution also implies a better estimate of wind over longer period times, as it is possible to average the data over suitable time scales. Moreover, measuring the vertical velocities with good time resolution on a routine basis is a unique capability of radars. Even if the measurements of vertical velocity can be made by other techniques, as far as measuring for a long period is concerned, the radars provide a useful alternative. This fact makes the radar a valuable asset in the field of synoptic meteorology, since so much of it involves the prediction of vertical velocities.

Using the DBS method the radial wind vector can be resolved into three dimensional wind velocity components, i.e., x-, y- and z-component. There is the possibility that the vertical velocity, z-component, determined this way can be affected due to the shape of the scatterers [Hocking, 1989]. For example, if the atmospheric scatterers are aligned with a small tilt from the horizontal, then the preferred direction of scatter will not be immediately abovehead but it will be off to one side. Consequently, small vertical velocities will be contaminated with a small component of the horizontal wind. To illustrate, assume an effective tilt of 1° and the beam half-power half-width is greater than 3°, then a 50 ms^{-1} horizontal wind causes a contribution to the vertical velocity of nearly 1 ms^{-1}. This is the reason that most analyses of vertical velocity are done using long term means, so that when averaged over long times, such tilts average out to zero. Even though, some caution must be taken. A bistatic radar with well separated transmitter and receiver is a better configuration for determination of vertical velocity. Other problems that occur relate to possible erroneous wind speeds and wind shears, which can result if the radar pulse-length is much greater than the thickness of the scattering layers [e.g., Hocking, 1983a; Fukao et a., 1988a, b; May et al., 1988]. Therefore, corrections should be applied for the vertical wind velocity as it is very useful in the application such as short range forecasting. Strauch et al. [1987] have demonstrated the importance of including the effects of large vertical motion, as a result of gravity waves or precipitation, in the horizontal wind component measurements since it raises the error noticeably.

Measuring the vertical wind velocities with high accuracy and good height and time resolutions continuously makes the radars' capability unique. Moreover, with regard to measuring continuously for long period of time, radars cannot be rivaled even though there are other techniques for vertical velocity measurements. Radars of meter-wavelength are sometimes capable of detecting inversions in the temperature profile. Just above the beginning of an inversion an enhanced reflections occur which offers helpful information about the tropopause height as well as an interesting view of the frontal systems' structure [Larsen and Rotteger, 1982].

2.5 Correction of vertical velocity

The capability of wind profiler radars for measuring vertical wind velocity over extended periods and over a large height range with high height resolution and excellent time resolution has been one of the most useful meteorological applications. In meteorology, vertical velocities have always had a special place for important reasons [Larsen, 1989]. Vertical velocity is important to predict using numerical models or better understand the vertical circulations that develop in the atmosphere. Upward vertical velocities yield clouds and precipitation. The large vertical gradients in atmospheric density cause heating or cooling during adiabatic ascents or descents that create significant temperature changes. The vertical gradients in atmospheric chemical constituent concentrations indicate that vertical circulation will have a large effect on trace concentrations.

Despite the clear need for, and many potential applications of, the radar measurements of vertical velocity, there are still many uncertainties that have to be addressed before the potential can be realized [Larsen, 1989]. The first problem is the accuracy of measurements of the vertical velocity. Even if horizontal velocities have been measured by several different techniques such as the Doppler method, the spaced antenna method and the interferometer method, it is by the Doppler method that all the various techniques measure vertical velocities. It appears to be that the signal received from the vertical direction is scattered by irregularities or sharp gradients in the refractive index, and that the Doppler shift of the received signal gives the line-sight, in this case, vertical velocity of the refractive index.

Comparing the measured vertical velocities with vertical velocities calculated from other data is a reasonable way to proceed in determining the accuracy of the measurements of the vertical velocity. A comparison of vertical velocities obtained from the SOUSY VHF radar located in the Harz Mountains in West Germany with the vertical velocities produced by the operational analysis procedure of the European Center Medium-range Weather Forecasting (ECMWF) was made by Larsen et al. [1988]. The result of the study was that the magnitudes of the calculated and measured values were approximately equal with the exception of poor agreement between specific features observed in connection with the passage of fronts as an example. Vertical velocities obtained from the Platteville radar located in Colorado compared well with precipitation data from the surrounding data by Gage and Nastrom [1985]. The authors inferred a general association of the type that would be expected between the times when precipitation happened downwind from the radar and the times when a pattern of upward motion showed by the radar.

The effect of aspect sensitivity on the effective look angle of the radar beam is another potential problem (see Figure C1 in Appendix C). These effects will only be noteworthy when longer wavelengths (for example 6 m) are utilized since the aspect sensitivity at 70 cm, for example, is insignificant in virtually all but the most exceptional circumstances. When the look direction is perpendicular to strong gradients in the refractive index associated with layers in the atmosphere aspect sensitivity causes the largest signal to be received. Generally the layers are tilted by a few degrees, i.e., it is within the beamwidth, except for the largest arrays. Thus, a vertically pointed beam may receive the strongest signal from a look direction that is a degree or a few degrees off vertical. Hence, the measurement comprises the projection of the true vertical velocity on the effective look direction (it is usually a minimal error) and the projection of the horizontal velocity along the look direction. Over 100 % error can be created by the latter case; this means that in some instance even the sign of the apparent velocity can be wrong. Rottger and Ierkic [1985] have described these problems and have shown that in order to make the necessary corrections to the measured velocities, data from a spaced antenna array can be used to calculate the tilt angle of the layers. Although very little of this type of error analysis has been accomplished so far, the effects have to be taken into consideration when VHF profilers are utilized. For some of the discrepancies found in the studies by

Nastrom et al. [1985] and Larsen et al. [1988] such effects may be responsible since both studies used data obtained with VHF radars.

Now, we will demonstrate how to correct the error of the Doppler radars measurement of vertical velocity that arises from the tilt of atmospheric scatterers. To start with we look at the vector representation of wind as show in the Figure 2.6 below.
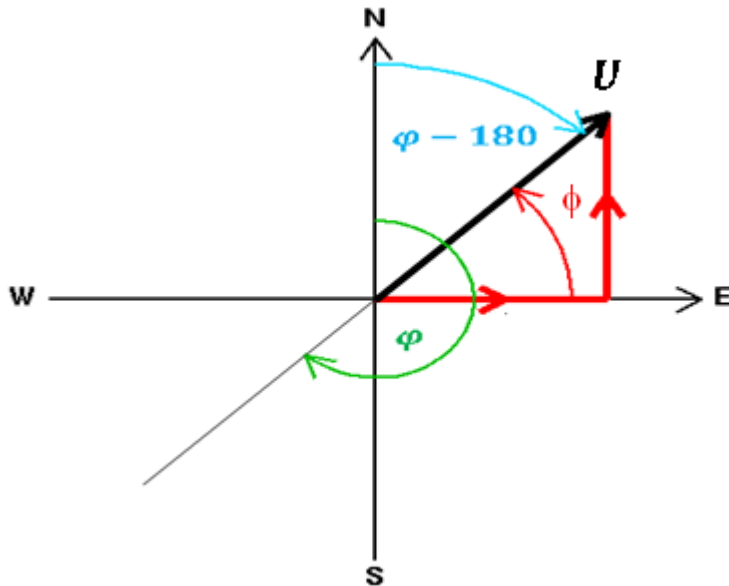
Figure 2.6. Representation of wind vector.

The wind vector can be expressed in terms of orthogonal velocity components. Let U_x be the zonal velocity, (i.e., east-west the component of the horizontal wind), U_y be meridional velocity, (i.e., the north-south component of the horizontal wind meridional velocity) and W be the vertical velocity, which is typically positive for an upward velocity. U is wind speed, φ is the meteorological wind direction, i.e. the direction from which the wind is blowing (it increases clockwise from North when viewed from above), and $\varphi - 180^o$ is the wind vector azimuth, i.e., the direction towards which the wind is blowing (it increases clockwise from North when viewed from above.) Terms such as northerly, easterly etc. represent meteorological wind directions while terms such as northward, eastward etc. mean wind vector azimuths. ϕ is the wind vector polar angle in two-dimensions. It increases anticlockwise from the positive x-axis, i.e. from East; this

in the opposite sense to the wind vector azimuth and the meteorological wind direction and has a different origin.

The relation between φ and ϕ can be written as

$$\varphi = \pi + \frac{\pi}{2} - \phi \qquad\qquad 2.15a$$

This implies

$$\phi = \frac{3\pi}{2} - \varphi \qquad\qquad 2.15b$$

Hence, the zonal and meridional velocities, respectively, become

$$U_x = U\cos\phi = U\cos\left(\frac{3\pi}{2} - \varphi\right) = -U\sin\varphi \qquad\qquad 2.16a$$

and

$$U_y = U\sin\phi = U\sin\left(\frac{3\pi}{2} - \varphi\right) = -U\cos\varphi \qquad\qquad 2.16b$$
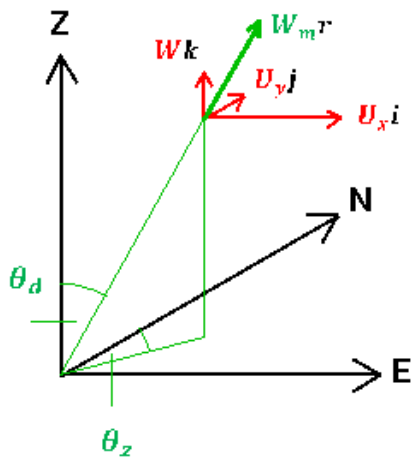
Figure 2.7. In this figure i, j, k and r represent unit vectors in the East, North, vertical and radial directions, respectively.

For a wind-profiler radar beam directed at a zenith angle of θ_d and at an azimuth angle of θ_z, the radial component of the wind vector, W_m, along the direction of the beam is expressed as

$$W_m = \left(U_x, U_y, W\right) \bullet \left(\sin\theta_d \cos\left(\frac{\pi}{2} - \theta_z\right), \sin\theta_d \sin\left(\frac{\pi}{2} - \theta_z\right), \cos\theta_d \right) \qquad 2.17$$

Where $\bullet$ means "scalar product".

We use the relationships

$$\cos\left(\frac{\pi}{2} - \theta_z\right) = \cos\frac{\pi}{2}\sin\theta_z + \sin\frac{\pi}{2}\sin\theta_z = \sin\theta_z \qquad 2.18a$$

and

$$\sin\left(\frac{\pi}{2} - \theta_z\right) = \sin\frac{\pi}{2}\cos\theta_z - \cos\frac{\pi}{2}\sin\theta_z = \cos\theta_z \qquad 2.18b$$

since $\cos\dfrac{\pi}{2} = 0$.

After simplification we find that

$$W_m = U_x \sin\theta_d \sin\theta_z + U_y \sin\theta_d \cos\theta_z + W\cos\theta_d \qquad 2.19a$$

Now solving for vertical component of the wind, W, and further simplifying, we arrive at

$$W = W_m \sec\theta_d + U \tan\theta_d \cos(\theta_z + \varphi) \qquad 2.19b$$

Since $U_x = -U\sin\varphi$ and $U_y = -U\cos\varphi$.

The corrected vertical velocities, due to the tilt of atmospheric scatterers, were calculated using the above expression. In the formula, θ_d is taken as the zenith angle at which we

find the maximum correlation between the vertical and horizontal velocities and θ_z is the corresponding azimuth angle at which the maximum correlation occurs. Even though we have derived and corrected the vertical wind velocity, we did not present any radar measurement of vertical wind (both corrected and uncorrected) since we did not see any positive correlation between the intrusion of stratospheric ozone and the vertical wind.

2.6 Tropopause detection by Radar

A simple but effective way to derive information about atmospheric scatterers is to record the backscattered radar power. It is possible to convert the carefully measured backscattered radar powers to effective reflection coefficients, backscatter cross sections, static stability, tropopause or estimate of the intensity of the turbulence [Hocking, 1989]. The backscattered radar power depends not only on turbulence intensity [e.g. Hocking, 1985] but also the mean potential refractive index gradient in which the turbulence exists. The latter term in the mesosphere is determined by the electron density, in the stratosphere by the gradient of the temperature and in the troposphere by the gradient of temperature and humidity.

The potential refractive index gradient for un-ionized atmosphere and for centimeter and meter radio waves is expressed as [Tatarski, 1961, pp 57; Hocking, 2009]

$$M = -77.6 \times 10^{-6} \frac{P}{T} \left(\frac{\partial \ln \theta}{\partial z} \right) \times \left[1 + \frac{15500q}{T} \left(1 - \frac{1}{2} \frac{\partial \ln q / \partial z}{\partial \ln \theta / \partial z} \right) \right] \qquad 2.20$$

where z is the range from radar, θ is the potential temperature in Kelvin, q is the specific humidity (mass of water vapor relative to the mass of air), T is the absolute temperature in Kelvin and P is the atmospheric pressure in millibars (hPa). The term q dominates in the troposphere and in the stratosphere, where q is small and the average value of $\dfrac{\partial \ln \theta}{\partial z}$ is large, so the term q is negligible. Hence terms involving q can be ignored in the stratosphere and mesosphere. Note that the term in the square bracket, which was first introduced in this form by Van Zandt et al. [1978], tends to unity as the humidity terms

go to zero. More on the corresponding potential refractive index gradient for the ionosphere region can be found in Hocking [1985].

Generally, the largest ratios of vertical-beam radar powers to off-vertical beam radar powers seem to occur in regions with highest stability. It has been observed that enhanced reflections of the vertical signal of VHF radars usually occurs at or above the height of the tropopause [Gage and Green, 1978; Röttger and Liu, 1978; Green and Gage, 1980; Balsley and Gage, 1981; Gage et al., 1981]. The characteristics of the vertical backscattered radar power peaks have been utilized to derive the tropopause height. Nevertheless, complexities exist in estimating the tropopause height from specular echoes, and these come from a number of sources. For instance, the data may be contaminated by radar returns from air craft passing through the radar beam. Moreover, there are issues of identifying specular reflections from scatter due to isotropic or anisotropic turbulence and of differentiating the tropopause from other stable regions in the upper troposphere. The methods utilized to estimate the tropopause are specular reflection method [Gage and Green, 1978; Röttger and Liu, 1978; Gage and Green, 1979], Zachs method [Westwater et al., 1983], maximum backscattered radar power method [Vaughan et al., 1995] and maximum backscattered radar power gradient method [Vaughan et al., 1995].

The beam radar return power from lower altitudes of the stratosphere for a vertically directed beam can be calculated from M^2/z^2 (where M is the vertical gradient of generalized potential refractive index (given above), and z is the range from the radar.), as shown by Hooper et al. [2004]; and hence sometimes backscattered radar power measurements permits the retrieval of profiles of static stability, i.e., Brunt-Vaisala frequency squared. The criteria to derive radar estimated tropopause altitude by Hooper and Arvelius [2000] is employed to determine the distribution of tropopause altitudes derived from the radar return signal power [Hooper et al., 2008]. Hocking et al. [2007] has used radar derived tropopause height to show the intrusion of stratospheric ozone. The same authors showed rapid vertical movements of the tropopause as seen by radar had association with high concentrations of stratospheric ozone in the upper troposphere.

The backscattered radar power provides a direct and simple technique for deriving the tropopause via the detection of stable atmospheric regions. When the well defined tropopause consists of a pronounced discontinuity in atmospheric stability, its height is defined in such a way that the height at which the intensity of backscattered radar power from the vertically directed beam begins to enhance noticeably. In this work, we have employed a superposition of the occurrences of maximum backscattered power and maximum echo power gradient methods in order to pick radar derive tropopause height. The result shows reasonable tracking of the lower edge of the secondary maxima of backscattered radar power, which is known as the radar derived tropopause height.

2.6.1 Determination of turbulence with MST radar

Turbulence remains an important unsolved problem in the realm of atmospheric physics. It has significant effects on atmospheric dynamics and chemistry as it mixes air of different composition. One remote sensing instrument that can be used to measure atmospheric turbulence is atmospheric radar. There are two major ways to measure atmospheric turbulence using radars. The first method involves measuring of the backscattered radar power. Since turbulence is the major cause of the radio wave scatterers, then it is possible to convert the returned signals to parameters which describe the turbulence, e.g., the turbulent energy dissipation rate, $\overline{\varepsilon}$ [Hocking, 1989]. The potential refractive index structure constant is one of the major parameters used to express the turbulence. The relation between the potential refractive index structure constant, C_n^2, and the turbulent energy dissipation rate, $\overline{\varepsilon}$, is give by Hocking [2009]

$$\overline{\varepsilon} = \left(\gamma \overline{C_n^2} \frac{\omega_B^2}{F^{\frac{1}{3}}} M^{-2} \right)^{\frac{3}{2}}$$ 2.21

where ω_B is the Vaisala-Brunt frequency. The parameter F represents the fraction of the radar volume that is filled by the turbulence, M is the potential refractive index gradient given above, γ was assumed constant in earlier work, but now it seems to be Richardson number dependent and also it depends on the Prandtl number [Hocking and Mu, 1997]. It

is not strange to see the dependence of $\overline{\varepsilon}$ on the Prandtl number, which expresses the relative diffusion rates of momentum and temperature, because turbulence intensity depends on momentum transport and the backscattered radar power depends on temperature and humidity transport. This method's simultaneous requirement of humidity and temperature data together with the radar data limits applicability of the technique.

The second method that is used for deducing turbulence strength is the radar signal, spectral width, which can be used to estimate the turbulence kinetic energy dissipation rate [e.g., Frisch and Clifford, 1974]. Doppler radars can sample a volume of air to derive spectral information about the motions of scatterers within it. The information includes the radial component of the mean velocity of the scatterers in the pulse volume which is determined from the Doppler shift of the mean frequency, i.e., first moment, as well as the variance of the velocity of the scatterers within the pulse volume which is determined from the width of the Doppler spectrum, i.e., second moment [Frisch and Strauch, 1976]. Information about turbulence is contained in the second moment of the radar signal spectra, i.e., spectral width. Hocking [1983a, 1985] has shown the extraction of turbulence intensities from each perspective and discussed the advantages and limitations of the methods. The turbulent kinetic energy dissipation rate $\overline{\varepsilon}$ is an essential parameter in the theory of turbulent mixing. Knowing the magnitude of $\overline{\varepsilon}$ helps in determining the rate of vertical mixing [Gregg 1977b; Ivey and Imberger 1991; Saggio and Imberger 2000]. Therefore, turbulence around the tropopause can be essential in the studies of stratosphere-troposphere exchange.

2.6.2 Analysis techniques of MST radars

The dynamics and the structure of the lower and middle atmosphere have been studied employing atmospheric radars in the modes of DBS (Doppler-Beam-Swinging) and the Spaced-Antenna (SA). In both techniques, information is gathered from radar echoes due to inhomogeneities of the refractive index of the atmosphere. In the troposphere, stratosphere and mesosphere, turbulence scattering as well as reflection and scatter from stratified structures can be involved in echoing mechanisms [Rottger and Liu, 1978; Rottger and Vincent, 1978; Gage and Green, 1978, 1979; Fukao et al., 1979; Vincent and Rottger, 1980; Harper and Gordon, 1980; Tsuda et al., 1986, 1988].

Doppler radars which sequentially switch one beam from one position to another are frequently called DBS systems. It is the major technique used at VHF. DBS engages measuring the mean Doppler shift of the returned signal using a narrow beam pointed in different directions. It is common to utilize a vertical and two or more noncolinear off vertical beam directions so as to resolve the three dimensional wind vector. The measured Doppler shift in each direction of the beam offers the corresponding radial velocity which is the background wind vector projected along the direction of beam of sight [Van Baelen et al., 1990]. The DBS method does have its limits even though it has been adopted by the majority of researchers. For instance, the method depends on measurements of components of wind at spatially different regions of the atmosphere; as a result the total wind is created by vector addition of two orthogonal components which are not collocated in either space or time [Hocking, 2011]. Moreover, especially for short term averages, the vertical components of velocity can more easily contaminate the Doppler winds [Hocking, 2011].

Initially Spaced antenna (SA) methods were utilized with MF radars [Briggs, 1984; Mitra, 1949; Vincent, 1984], and sometime later they were employed at VHF [Vincent and Rottger, 1980; Rottger, 1981] and more lately at UHF [Cohn et al., 1997]. It is well known that SA methods give dependable estimates of the mean horizontal velocities in the lower atmosphere [Praskovsky and Praskovskaya, 2003]. Moreover, parameters including turbulence intensity and spatial scales of the refractive index irregularities can also be measured, even though a caution is required in the interpretation of the results [Hocking et al., 1989]. The SA method, which uses multiple noncolinear receiving antennas to measure the atmospheric motion, is a generic term which involves different analysis techniques such as similar fades, full correlation analysis (FCA), and interferometry techniques. For deriving the motion of the atmosphere, the similar fades method utilizes the time series at the separate receiving antennas. The so-called apparent velocity is obtained from the time delays for maximum cross correlation between the received signals [Mitra, 1949]. FCA is usually preferred because the apparent velocity will bring about velocities that are too large if random changes associated with the motion of the atmospheric are not considered [Briggs, 1984].

FCA methods, which originated with Briggs et al. [1950] and were later improved by Phillips and Spencer [1955] and refined by Fedor [1967] and Gregory et al. [1979], take into consideration anisometric patterns and variations in the diffraction pattern structure, but assume that the spatial and temporal changes have the same functional form, mostly Gaussian. The FCA method obtains the so-called true velocity and information on the diffraction pattern from both the mean autocorrelation as well as the cross correlations and these do not have to be Gaussian. Briggs [1984] offers the most recent and straightforward FCA review to date. FCA was initially designed for studies of ionospheric E and F regions [Briggs, 1968], but it has also been utilized for the D region [Briggs, 1977] and intensively employed in the mesosphere at medium and high frequencies [Hocking, 1983c]. Moreover, the SA method has also been successfully implemented at VHF to detect tropospheric and stratospheric winds [Rottger and Vincent, 1978; Vincent and Rottger, 1980; Rottger, 1981; Vincent et al., 1987].

SA methods make all of their measurements at the one location of the atmosphere, but usually wider beam widths are involved, which can increase their uncertainty [Hocking, 2011]. SA methods also have a tendency to be dominated by specular reflectors if they are present which can cause errors in interpretation [Hocking, 2011]. These matters keep coming up, though many of the issues have been worked through in the 1980s and 1990s. SA studies will be readdressed shortly, particularly with respect to mesospheric measurements, as the desire for improved accuracy of wind measurements for incorporation in to numerical forecast models increases [Hocking, 2011].

Both the advantages and disadvantages of the SA and the DBS methods have been examined by Briggs [1980]. The same author has showed that both methods derive their information from the amplitudes and phases of the radar returns from different angles and provide similar information about scattering irregularities even if there is an apparent difference in processing the data. Comparisons of wind measurements using other means of instruments such as radiosondes, rockets, airplanes, and satellites have shown good agreements with the DBS method [Fukao et al., 1982; Larsen, 1983] and the SA method [Vincent et al., 1977; Meek and Manson, 1985; Labitzke et al., 1987; Vincent et al., 1987]. Vincent et al. [1987] also show that the balloon radiosonde measurements of

velocities usually lie between the averaged FCA true and apparent velocities and that the DBS measurements using an off-zenith angle of 4°, 7°, 11°, or 15° provide overall good agreement with SA results. The measurements are limited to the troposphere. Moreover, Van Baelen et al. [1990] perform a detailed comparison between colocated and almost simultaneous DBS and FCA determined wind profiles from the troposphere to the lower stratosphere so as to explore possible relationships of the differences between the two techniques with various parameters. The comparison shows that the DBS and FCA true and apparent velocity profiles generally agree. However, the DBS profile alternately agrees better with the true or the apparent velocity obtained by the FCA method at altitudes below and above the jet streams, and above 17.7 km. Even though the apparent direction displays more variability with altitude than do the true and DBS directions, the directions of all three wind estimations agree modestly well. It is also observed that a smaller true velocity estimation is made when a smaller spacing for the receiving array is utilized.

In this section, we describe the radar parameters used for the study. Except one which is located in the northern Canada, the rest are located in Ontario Canada [see Figure 2.10]. The windprofiler radars used for the ozonesonde campaigns were located at Egbert, Ontario (44.23°N, 79.78°W), Harrow, Ontario (42.03°N, 82.92°W), Montreal, Quebec (45.41°N, 73.94°W), Walsingham, Ontario (42.6°N, 80.6°W), and Eureka, Nunavut (79.98°N, 85.93°W). They had steerable beams with one-way beam half-power half-widths of 2.75^o (Egbert, Eureka, and Harrow), or 2.3^o (Montreal and Walsingham), which could be pointed vertically, or at 10.9^o off zenith, in various azimuthal directions. The operating frequencies of the radio wave used were 47.56 MHz (Egbert), 51.00 MHz (Eureka), 40.68 MHz (Harrow), 52.00 MHz (Montreal) and 44.50 MHz (Walsingham). In each case the vertical height resolution was 500 m.

2.6.3 Spectral and turbulence reflections

The mechanisms responsible for the radar reflections, when the radar beam points vertically, are one of the unsolved matters in the realm of atmospheric radar. The aspect sensitivity of VHF radar echoes refers to the feature of preferential scatter of radio signals from vertically pointed radar beams rather than from off-vertical angles. In the middle

and lower atmosphere this characteristic property is apparent. Gage and Green [1978] and Rottger and Liu [1978] first reported aspect sensitivity for the troposphere and stratosphere and then later Fukao et al. [1979] reported for the mesosphere.

There have been two major thoughts regarding the mechanisms responsible for the enhancement of VHF signals when the beam points vertically. One mechanism is specular reflections from horizontally stratified and extended layers, with sufficiently high vertical gradients in their index of refraction [Rottger and Liu, 1978] and the other is can be explained by anisotropic turbulence [Gage and Balsley, 1980; Doviak and Zrnic, 1984a]. Specular reflection has been observed by the occurrence of reflectors which strongly reflect signals vertically, but scatter very weakly when the radar beam is pointed off-vertical [Hocking, 2011]. Such reflectors also fade very slowly, that is, they have very narrow spectral widths. Turbulent reflection can also be anisotropic, with reflection being stronger when the radar beam points vertically, but weaker when the radar beam pointed off-vertical. However, the major problem remains is to determine what actually causes the anisotropy of the scatterers (i.e., turbulence or specular reflectors).

To explain the cause of specular reflections many models have been proposed, often involving sharp edges or anisotropic eddies near the edges of turbulent layers [e.g., Woodman and Chu, 1989; Lesicar et al., 1994]. Stretched irregularities at the edges of turbulent layers lead to specular reflections [e.g., see Woodman and Chu, 1989; Hocking, 1991]. Numerical modelling shows the production of Kelvin–Helmholtz waves as a consequence of the break-down of individual waves, and the end result of turbulence often shows elongated strata of refractive index layers that are very stretched at the edges of the turbulent layer [Hocking, 2011]. Gage et al. [1981] showed using VHF radars highly anisotropic echoes originating from hydrostatically stable regions of the troposphere and stratosphere. The enhanced echoes were seen due to in-phase (i.e., coherent) scattering from the half-wavelength Fourier component of the stratified irregularity structure parallel to the wave direction when the radar beam points vertically.

For the cases of strong turbulence, isotropic echoes result from layers of strong turbulence which are energetic enough to overcome buoyancy forces, and therefore have

no favored orientation. Turbulence generated in a region where there exists static stability will bring about isotropic fluctuations in index of refraction and thus isotropic radar reflectivity [Pepler et al., 1998]. Hocking and Hamza [1997] showed most isotropic turbulence when wind shears are weakest and the atmosphere is convectively unstable (conditions such as clouds, convection, and possibly precipitation). In a layer of less turbulence, buoyancy forces limit displacements in the vertical direction, and hence turbulence eventuates in anisotropic echoes.

2.6.4 Selection of radar spectral width

In this section we will not discuss in detail about the spectral width, but rather we will look at the selection of radar powers frequency range for analysis. Our standard analysis procedure with the radars is to form spectra for each range-gate and for each recording interval. Spectral information are stored in special files. Extra-large spikes (possibly due to spectral echoes) are removed. For routine analysis, a more compressed form of storage used. Rather than store all spectral points, we record total power under the spectrum in the frequency ranges -0.08 to 0.08 Hz, -0.8 to 0.8 Hz, -2.0 to 2.0 Hz and -4.0 to 4.0 Hz. This provides general information about the spectra but without the need for excessive storage. In addition to storage of the energy in these spectral bands, various type of fitting are employed to determine radial velocities and spectral widths, and this information is also stored to file. Figure 2.8 displays the approximate shape of the spectrum recorded with a vertically pointing beam with VHF radar.
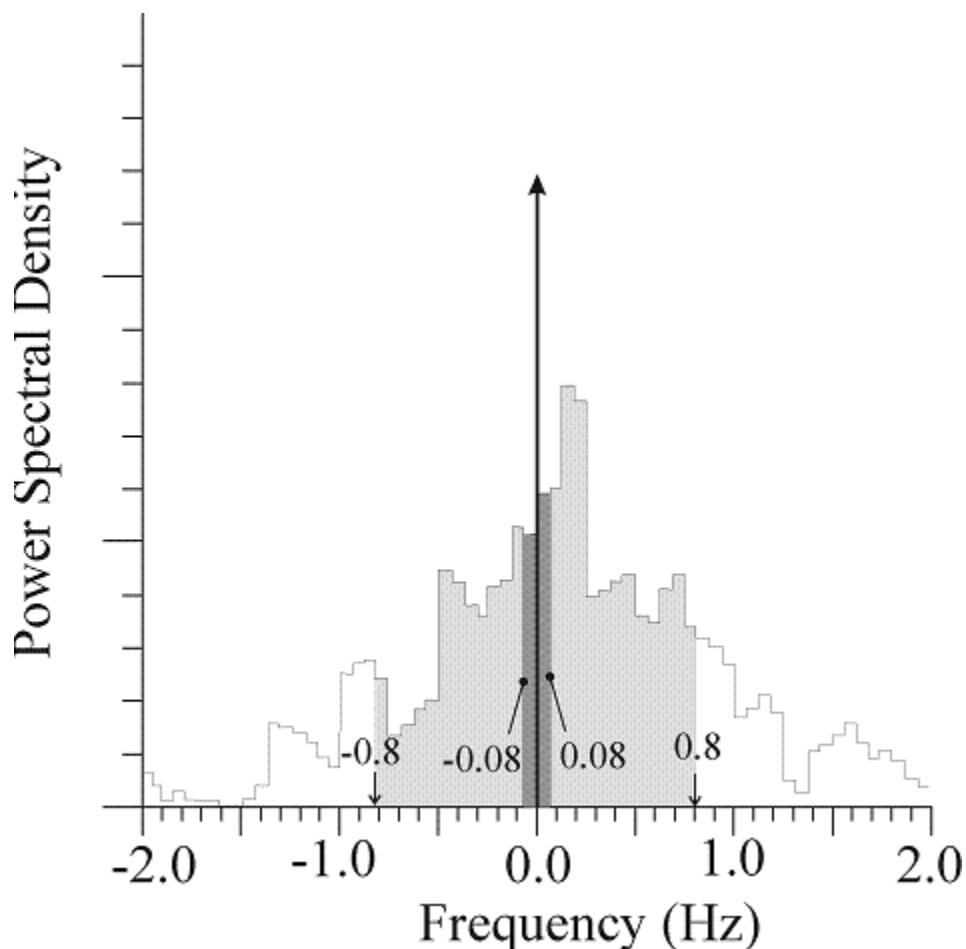
Figure 2.8. A schematic diagram of spectra recorded with VHF radar. The curve shows the approximate shape of the spectrum recorded with a vertically pointing beam.

The narrower the frequency band width the less contaminated the data is. Hence, in our backscatter radar power analysis to derive tropopause height we utilize the smallest frequency range so as to get rid of unwanted signals such as from aircraft. This results in exclusion of such signals from further process. Consequently, our selection the frequency range between -0.08 and 0.08 Hz (see the shaded region of Figure 2.8), effectively meets our target by successfully revealing tropopause heights. However, since larger spectra width values contain more spectral information, they are better to estimate wind speed.

2.6.5 Contamination of backscattered power by aircraft

In this section we illustrate how aircraft contaminates backscattered radar power, and the need to filter data. The situation shown in Figure 2.9 is an example of aircraft contaminated data (Figure 2.9a) and the filtered data (Figure 2.9b) at Harrow during the period 15 June – 10 July 2007.
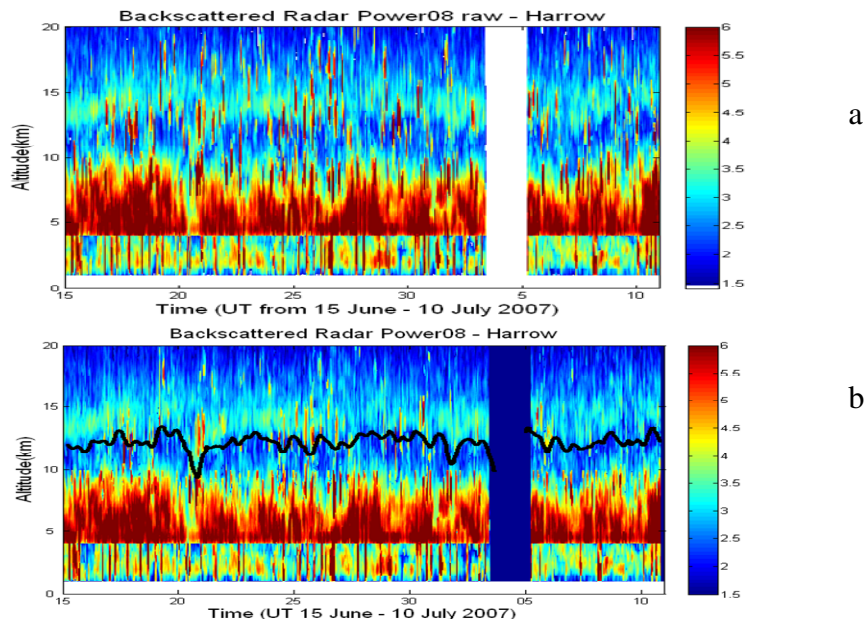
Figure 2.9. Comparison of contaminated data of backscattered radar power with the filtered data using multiple linear regression method.

Radar powers between -0.08 and 0.08 Hz observed with the radar vertical beam from 15 June – 10 July 2007 are shown in order to determine tropopause heights. Radar powers of more than 10^5 (expressed as digital units squared) above 5 km are removed and replaced using a multiple linear regression with a window of size 10 by 10 (i.e., a 10x10 matrix of radar data). Below 5 km, data with strengths more than 10^5 were kept. The purpose of the procedure was purely to disclose the tropopause as clearly as possible. Removals of these high powers effectively remove aircraft interference.

2.7 Lagrangian Particle Dispersion Models

In Lagrangian models (LMs) the movement of fluid parcels are tracked in their moving frame of reference. Scientists who use LMs are obliged to assume themselves moving with the parcel and encountering the effects of advection, turbulence and changes in the environment of the parcel. LMs have been improved in complexity over the last decades in order to increase their application for both scientific and social purposes. For example, nowadays, in order to diagnose a wide spectrum of geophysical phenomena, LMs are commonly used by researchers. Atmospheric chemists can track intercontinental transport of pollution plumes [Stohl et al., 2002] or airborne radioactivity [Wotawa et al., 2006]. By running LMs backward in time [Flesch et al., 1995; Lin et al., 2003], instrumentalists can trace back to the source of observed atmospheric species with high computational efficiency [Ryall et al., 2001]. Hence, LMs have been employed ever more to quantify sources and sinks of atmospheric species by joining theoretical simulations with experimental observations in an inverse modeling framework [Trusilova et al., 2010].

A recent indication of the tremendous societal importance of LMs was their role in predicting the spread of volcanic ash from the eruption of Eyjafjallajokull volcano in Iceland. It is essential to review the physical foundations and implementation aspects of LMs used today as Lagrangian modeling increases in complexity and popularity. From this point of view, scientists can define guidelines of further steps needed to improve Lagrangian modeling and to certify its successful application in the future.

As opposed to Eulerian models, which use grid cells that are fixed in place, LMs are known to generate minimal numerical diffusion, and as a result are able to preserve gradients in tracer concentrations. Lagrangian integration is numerically stable which means that models can take bigger time steps. Moreover, the Lagrangian simulation is a natural way to model turbulence since it is a nearer physical analog to the pathways traced by eddies.

These benefits helped as inspiration from which Lagrangian particle dispersion models (LPDM) have evolved, in which air parcels are simulated as infinitesimally small particles that are transported with random velocities representing turbulence. LPDMs are

more sophisticated than simple trajectory models since they often track up to millions of particles in three dimensions. Full three-dimensional LPDM simulations that were expensive to run just a decade ago are now routinely performed.

The development of LPDMs has mainly been the principle of "well-mixed criteria" (WMC), which is a consequence of the second law of thermodynamics [Thomson, 1987]. In accordance with WMC, particles that are distributed depending on atmospheric density must remain so in the LPDM simulation. However, due to physical inconsistencies in meteorological fields or model parameterizations LPDMs can violate the WMC. Running forward and backward in time is a way to disclose such inconsistencies, which in a perfect case should yield the same results [Lin et al., 2003]. Except in simple cases, introducing the WMC doesn't determine a formulation of a unique model [Wilson and Flesch, 1993].

Lagrangian simulations usually use observed meteorological data sets, or the output of meteorological fields from general circulation models (GCMs) or numerical weather prediction (NWP), or in our case global environmental multiscale (GEM). Variables may be eliminated, or the output resolution may be degraded, due to limited computational resources, which can lead to violation of basic conservation, e.g., such as mass, momentum and energy, with negative outcomes on the quality of the simulations [Nehrkorn et al., 2010].

Nowadays the least advanced aspect of Lagrangian modeling is probably parameterizing subgrid-scale processes. For instance, parameterizing the planetary boundary layer (PBL) height is essential, since transport of trace is strongly reliant on it; but methods to diagnose PBL height from NWP-output meteorological fields are still unsatisfactory [Seibert et al., 2000]. The second example is parameterization of moist convection. The role of convection in redistributing atmospheric tracers necessitates a description of updrafts/downdrafts that are consistent with the parent models such as GCM or NWP. While the corresponding mass fluxes can be used to describe the convective motion of Lagrangian particles [Forster et al., 2007], departures from WMC can arise if such mass fluxes are not correctly constructed [Nehrkorn et al., 2010]. Therefore, it is necessary for

LPDM developers to keep close connection with parent gridded models and to make better parameterizations of subgrid-scale processes.

Estimating uncertainty in LMs that are widely used in applications is required as they can be used in determining greenhouse gas emissions and preparing for emergencies associated with toxic releases. An example was the latest nuclear disaster at Japan's Fukushima I power plant. Due to this fact, it is crucial to construct methods that enable errors in LMs to be propagated into the resulting predictions, e.g., tracer concentrations or air parcel positions given with quantifiable uncertainties. Interpolation in space and time, numerical truncation, ill-defined starting position, wind fields and model formulation are sources of errors in LMs [Stohl, 1998].

To deal with such uncertainties, numerous methods have been proposed. Ensemble methods initially developed for NWP purposes and governed by the idea that a series of models or model runs can be used to signify uncertainty have inspired similar approaches in LPDMs [Galmarinia et al., 2004]. Kahl and Samson [1988] have calculated error trajectories that incorporate uncertainties within the motions of the Lagrangian air parcels. This can be implemented by simply increasing the diffusivity [Maryon and Best, 1995] or by modifying the trajectory traced by the air parcel with an error velocity that reflects quantified uncertainties in wind fields [Lin and Gerbig, 2005].

In the end LMs have to be verified using experimental observations and these comparisons can disclose the cumulative impact of errors from all five sources, helping to restrict model parameters. Laboratory experiments of dispersion in different media have assisted as good evaluations for LMs under perfect cases. But for tests in the real atmosphere over regional scales, tracer release experiments have helped as the "gold standard" for examining models. In these cases, specified amounts of tracers are released from specific locations into the atmosphere and measured at downwind locations. In spite of the significance of such experiment, it has been more than 15 years since the last major one was conducted. Furthermore, these experiments have been limited in temporal scope with a few exceptions, for example the Across North America Tracer Experiment

(ANATEX) over 3 months [Draxler and Heffter, 1989]. Hence, in the future more extensive tracer experiments will be needed.

Lagrangian modeling development and application has experienced explosive growth from time to time. For example, FLEXPART is among the most intensively utilized robust models for studying atmospheric dynamical processes around the globe, as a result of the growth in its computing power. Next we will discuss in detail about one of the Lagrangian dispersion models, FLEXPART and its meteorological wind fields input provider, the Environment Canada's Global Environmental Multiscale (GEM) model.

2.7.1 GEM-FLEXPART

Quantitative understanding of the sources and sinks of atmospheric gases is crucial in order to assess the anthropogenic and natural impacts on the environment. It is now recognized that atmospheric transport has a significant influence on the distribution of chemical species by moving them away from the location of their sources towards the location of their sinks, which requires integration over regional and continental scales. In coupling with analysis of observational data, accurate modeling of atmospheric transport is critical to quantitatively associate observed tracer distributions with sources and sinks, and then address issues of environmental concern. HYSPLIT [Draxler and Rolph, 2003 and Draxler, 2003], FLEXTRA [Stohl et al., 1995; Stohl and Seibert, 1998], LARGRANTO [Wernli and Davies, 1997], FLEXPART (Stohl et. al., 2002, 2005) and TRAJKS [Scheele et al., 1996] are among the many theoretical tools to study atmospheric chemical species. In such models, a small volume of air is advected using the mean horizontal and vertical winds from a meteorological model. FLEXPART, which can potentially address our environmental concerns, is the model that I have been using in my research work.

FLEXPART is a LPDM that simulates atmospheric air movement including ozone transport released from point, line, area or volume sources [Stohl et al., 2005]. It calculates the trajectories of the particles utilizing stochastically modeled turbulent fluctuations superposed on the grid scale winds provided by the Global Environmental Multiscale (GEM) in our case. It is one of the most popular numerical computer

simulation methods that helps better understand sources, sinks and transport of atmospheric air masses. The coupling of FLEXPART with atmospheric observation creates a unique opportunity to quantify the major sources and sinks of atmospheric gases including ozone and the pathways between them. FLEXPART can be run both forward and backward in time in order to simulate the dispersion of tracers from their sources and to determine potential source contributions for given receptors, respectively. FLEXPART uses meteorological wind fields obtained from the Environment Canada's Global Environmental Multiscale (GEM) Model as an input to describe the transport of air parcels in the atmosphere. In the next sections we discuss about Lagrangian Models in general and FLEXPART in particular, as well as the GEM model. Here after we use GEM-FLEXPART to refer to the integration of the models of GEM and FLEXPART.

FLEXPART is utilized in such a way that the entire atmosphere is represented by particles of equal mass, which is known as a domain-filling mode [Stohl et al., 2005]. FLEXTRA, which was developed by Stohl et al. [1995], was largely taken as the management of input data. Since FLEXPART was first developed, it has been improved and validated continuously until the version, 6.2, which I used in my work. Validation has been done extensively [Stohl and Trickl, 1999; Forster et al., 2001, 2004; Spichtinger et al., 2001; Stohl et al., 1998, 2002, 2003; Cooper et al., 2006].

The FLEXPART model is built based on the code from the Fortran 77 standard and checked with several compilers (e.g., gnu, Absoft, Portland Group) under numerous operating systems (e.g., Linux, Solaris,) [Stohl et al., 2005]. The code is carefully documented and optimized for run-time performance. The source code of FLEXPART and a manual are freely available from the internet [Stohl et al., 2008]. Even though FLEXPART 6.2 is described based on model level data of the numerical weather prediction model of the European Centre for Medium-Range Weather Forecasts (ECMWF), we have developed it using input data from the Environment Canada's GEM (Global Environmental Multiscale) model Cote et al. [1998a].

The Environment Canada's GEM model was developed at the Canadian Meteorological Centre and can be utilized to forecast the weather, address climate issues such as global

climate change, and deal with air quality issues such as smog, ozone depletion, and acid rain [Cote et al. 1998a]. A very wide range of space and time scales are covered in the modeled atmospheric phenomena. It varies temporally from a fraction of second scales of some chemical reactions to the centuries or even millennia of climate simulation, and spatially from fractions of a meter of chemical reaction and molecular diffusion, up to the global scale of tens of thousands of kilometers. The GEM model has been interfaced with the unified RPN (Recherche en Prevision Numerique) physics package, utilizing the RPN standardized interface. Since the interface allowed the immediate use of a tested set of parameterizations without any retuning, it greatly facilitated matters. Mailhot et al. [1997] discussed a recent description of the current operational parameterizations contained in it.

The following physical phenomena have parameterizations: turbulent fluxes of momentum, heat, and moisture over land, water, and ice, based on prognostic turbulent kinetic energy; surface-layer effects; gravity wave drag; prognostic clouds; solar and infrared radiation with or without cloud interaction; deep and shallow convection; condensation; and precipitation including evaporative effects [Cote et al., 1998a]. The space and time scales of the application and the resolution of the forecast or simulation determine the choice of parameterization [Bougeault, 1997]. For instance, for climate scale simulations a detailed and intensive radiation calculation is an essential ingredient, but much less so for short- and medium-range weather forecasting. Moreover, the suitable treatment of convection varies greatly [e.g., Weisman et al., 1997] between a large-scale application where it is parameterized, and a mesoscale where it may be parameterized in a different way or even represented explicitly. Experimenting with different parameterizations of a given process is also useful.

Table 2.2. Summary of the operational GEM regional forecast system.

Dynamics/numerics
hydrostatic primitive equations
global variable–resolution grid (horizontal and vertical)
cell-integrated finite-element discretization on Arakawa-C grid
terrain-following hydrostatic pressure vertical coordinate
two-time-level semi-implicit time scheme
3D semi-Lagrangian advection
Linear ∇^2 horizontal diffusion on all model variables, except specific humidity
periodic horizontal boundary conditions
no motion across the lower and upper boundaries
Physics
planetary boundary layer based on TKE
fully implicit vertical diffusion
stratified surface layer, distinct roughness lengths for momentum and heat/humidity
four types of surface represented: continent, water, sea ice, and glaciers
ISBA surface scheme for land surface processes
solar/infrared radiation schemes with cloud–radiation interactions based on predicted cloud radiative properties
Fritsch–Chappell convective scheme
Sundqvist scheme for grid-scale condensation

Regional data assimilation system
12-h data assimilation cycle with 6-h trial field from regional GEM
incremental 3DVAR algorithm
innovations computed with respect to background field at the full model resolution
analysis increments produced on a 240x120 (T108 spectral resolution) global Gaussian grid
analysis on model levels
initialization by a diabatic digital filter

Taken from Bélair et al. [2003].

2.7.2 GEM-FLEXPART Configuration

The integrated model, which we here call GEM-FLEXPART, assists as a platform for carrying out scientific studies on atmospheric processes and applications. FLEXPART is a LPDM that accounts for stirring and turbulence by calculating the trajectories of a large number of particles transported by the mean wind and by stochastically modeled turbulent fluctuations obtained from GEM. GEM has been a reasonable choice to be the host meteorological model for GEM-FLEXPART not only because it has already been employed successfully in Environment Canada's current operational air quality forecast system, but also because it has strong progress and maintenance support due to its role as Environment Canada's operational regional and global weather forecast model. The other advantage of utilizing GEM is that it supports three different grid configurations: a global uniform grid, a global variable grid and a nested regional limited-area grid. The GEM-FLEXPART model has been run for a number of scenarios ranging from a global uniform domain, global variable resolution for regional scenarios to high resolution studies. Here in my study, we used GEM-FLEXPART in a regional configuration covering North America, just as work found by, for example, Hocking et al. [2007] and He et al. [2011]. GEM-FLEXPART creates different output formats depending on what mode it is being

used. If it is run in the plume trajectory mode, then the output will be written to plain text files. In other modes, FLEXPART produces its output in binary files.

2.7.3 Model simulations

The domain defined for the model simulation is the region covering North America from 60.5^{o}W to 120°W and from 25°N to 84.5^{o}N with 432×565 (latitude by longitude) grid cells corresponding to a spatial resolution of 0.1375^{o}×0.1375^{o}, or nearly 15.3 km grid spacing in the core region, 450 s time step and 58 vertical levels up to 10 hPa (30 km). FLEXPART uses hourly meteorological wind fields obtained from a regional analysis model called GEM version 3.2.2 with physics version 4.5 as an input to describe the transport of ozone in the atmosphere.

GEM-FLEXPART was run for each campaign. The period of simulations were 29 April – 10 May 2005, 17 – 26 November 2005, 23 February – 4 March 2007, 24 February – 18 April 2008, 5 – 11 May 2009, 24 February - 12 March 2010, and 12 July – 4 August 2010.   In the forward mode of simulation, each FLEXPART run released 2,000,000 particles in the model domain, with those in the stratosphere initialized using an empirical relationship between potential vorticity and ozone concentration [Stohl et al., 2000]. These were then advected using wind fields from GEM and the resulting ozone field was output at 1°×1°×500 m resolution. In the model, chemistry is not included as the lifetime of stratospheric ozone in the troposphere is assumed to be infinite just as the work found by, for example, He et al. [2011]. This looks a reasonable assumption since we did not run our simulation for more than 15 days, and the lifetime of stratospheric ozone in the troposphere is 20-30 days [Stevenson et al., 2006]. Moreover, since the domain of simulation is limited it is unlikely that any particular particle to stay within the domain for such long period of time. Nevertheless, this tells us particles will have zero ozone concentration if they crossed from the stratosphere before entering the domain. This also means that the simulations are for only intrusions that occur within the domain. Since the domain of simulation is pretty large this may not be a major issue. The model was also run backward in time beginning from a given location (in our case where the measurements were made) in order to determine where ozone-rich air came from. Three-dimensional back-trajectories have been calculated corresponding to the observed ozone

peaks. 600,000 particles were released from a line in the height range between 5 and 7.5 km above the ground. FLEXPART back-trajectories of the previous 48 to 96 hours are generally calculated since the particles' release. More on FLEXPART is found in Appendix A.

2.8   Campaign Description

The ozonesonde-balloon campaigns were conducted during two periods: (29 April – 10 May 2005 and 12 July – 4 August 2010) at Montreal, Quebec (45.4^{o}N, 73.9^{o}W), two

campaigns (5 – 11 May 2009 and 12 July – 4 August 2010) at Egbert, Ontario (44.27°N, 79.73°W), two campaigns (17 – 26 November 2005 and 23 February – 4 March 2007) at Walsingham, Ontario (42.6^{o}N, 80.6^{o}W), and two campaigns (24 February – 18 April 2008 and 24 February - 12 March 2010) at Eureka, Nunavut (79.99^{o}N, 85.94^{o}W). The study involved mostly two launches per day for a total of 6 campaigns at midlatitude, southeastern Canada, and two at high latitude, northern Canada, intensive operational days.

Table 2.3. Campaign descriptions. On average there were two launches per day.

Campaign site	Location	Number of campaigns	Period of campaign
Montreal	45.4^{o}N, 73.9^{o}W	2	29 Apr – 10 May 2005 and 12 Jul – 4 Aug 2010
Egbert	44.27°N, 79.73°W	2	5 – 11 May 2009 and 12 Jul – 4 Aug 2010
Walsingham	42.6^{o}N, 80.6^{o}W	2	17 – 26 Nov 2005 and 23 Feb – 4 Mar 2007
Eureka	79.99^{o}N, 85.94^{o}W	2	24 Feb – 18 Apr 2008 and 24 Feb - 12 Mar 2010

1200 g balloons filled with helium gas used in the study carried EN-SCI model 2Z-ECC ozonesondes equipped with Global Positioning System (GPS) receivers and Vaisala RS80 radiosondes. In addition to ozone concentration from the sondes, ambient air pressure, temperature, sometimes wind speed, and humidity were collected by Vaisala RS-80 radiosondes and transmitted to the ground stations. The current, which is proportional to the partial pressure of ozone and produced as a result of the reaction of the ozone in the air supplied to one side of the ECC, is digitized along with ambient temperature, pressure, humidity measurements obtained from a Viasala RS-80 radiosonde as well as position information obtained from a GPS receiver before transmitting to ground. The RS-80 radiosondes are modified in order that the analogue signals obtained from it are digitized on the ozonesonde circuit board. These digitized signals are combined with signals from the ECC and the GPS receiver and then sent to the transmitter on the radiosonde. Data are transmitted using the Viasala RS-80 transmitter to the ground station. Signals are sent on average every 1.2 s to the receiver. The data are sent to a PC via modem through an RS-232 serial port. The ground station consists of an antenna, a receiver, a modem, a PC and METGRAPH software. The software monitors a serial port on the PC to capture the incoming data stream from the modem.

In a total of eight campaigns approximately 2o0 launches were carried out. Low relative humidity that was measured by the ozonesondes in the middle and upper troposphere and linked with ozone peaks was taken as partial evidence that the enhanced ozone was originated in the stratosphere. Accordingly, we observed stratospheric ozone intrusions into the troposphere in all campaigns. Windprofiler radars have been employed to measure the three components of wind velocity (zonal, meridional and vertical), turbulence intensity and backscattered radar power continuously with high temporal and height resolutions. Hence, they provide an opportunity to study the atmospheric dynamics in micro scale. Simultaneous and co-located measurements of ozonesonde and radar offer us a unique opportunity to identify and characterize the physical processes responsible for stratospheric ozone intrusion events.

2.9   Radar Observation and Ozonesonde Campaign Sites

The radar observations and ozonesonde campaigns were conducted at numerous field sites in order to obtain measurements of ozone and other atmospheric information. Sites used include Egbert, ON; Eureka, NU (not shown in the map); Harrow, ON; Montreal, QC; and Walsingham, ON. See figure below.
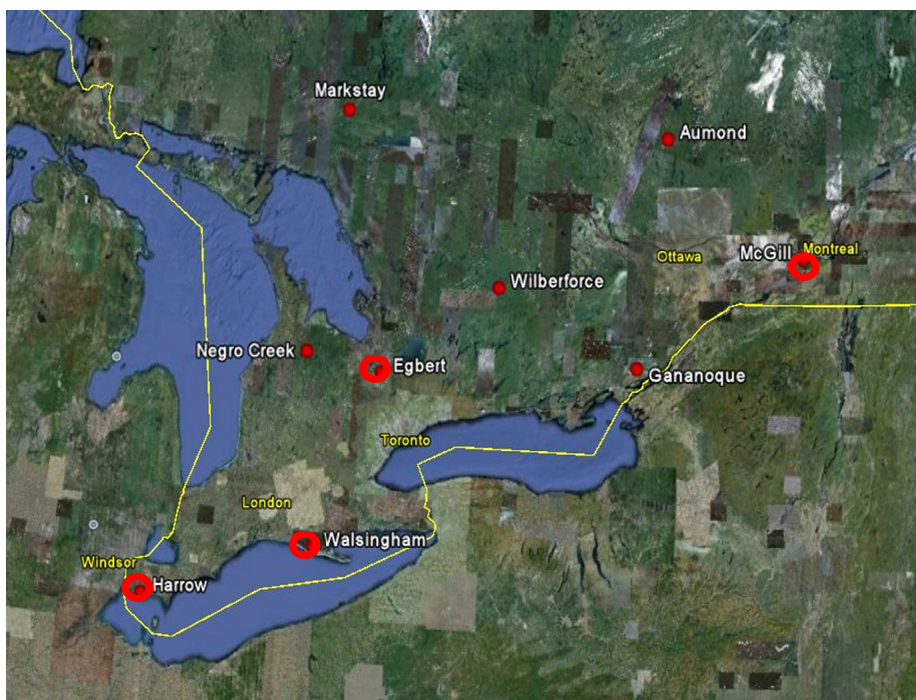
Figure 2.10. A map of radar sites. The red dots indicate the radar sites while the red circles show the radar sites where ozonesonde campaigns were carried out.

Chapter 3

3   Observational results and discussion

In this chapter, we examine the detection of stratospheric ozone intrusion events and diagnose the atmospheric dynamics responsible for the intrusions during seven ozonesonde measurement campaigns in Ontario, Nunavut and Quebec, Canada. The ozonesonde campaigns were made at Egbert (5 – 11 May 2009 and 12 July – 4 August 2010), Eureka (24 February – 18 April 2008 and 24 February - 12 March 2010), Montreal (29 April – 10 May 2005 and 12 Jul – 4 Aug 2010) and Walsingham (17 – 26 November 2005 and 23 February – 4 March 2007). Ozonesondes equipped with Global Positioning System (GPS) receivers were used for ozone, temperature and humidity measurements. Simultaneous measurements by windprofiler radars have been used to measure wind velocity, turbulence strengths and backscattered radar power, from which radar-derived tropopause heights were determined. In each campaign, we have observed at least one major event, i.e., high concentrations of ozone and low relative humidity in the lower and middle troposphere. Low relative humidity and sudden jumps of radar derived tropopause heights were taken as indicators of ozone originated from the stratosphere.

Ozone transport from the stratosphere to the troposphere in the midlatitudes is recognized to make a significant input to the global tropospheric ozone budget [Roelofs and Lelieveld, 1997; Davies and Schuepbach, 1994; Ladstatter-Weissenmayer et al., 2004; Stevenson et al., 2006]. It approximately contributes between 25% and 50% to the global tropospheric ozone concentrations, with the net photochemistry producing the balance. In such processes, air masses and accompanying traces gases are transported across the stable tropopause. An important mechanism for stratosphere-troposphere exchange of ozone in the extratropics is tropopause folding associated with planetary or synoptic scale Rossby wave breaking.

It is believed that on a global scale, troposphere-stratosphere exchange is driven primarily by the general atmospheric circulation that ascends in the equatorial region and descends

at middle and high latitudes [Holton et al., 1995]. However, the details of the process at small scale is not yet well understood.

While large scale motion and mean vertical downward velocities can transport ozone down from the tropopause once it has crossed the tropopause, difficulties still exist in explaining how the initial crossing occurs. The tropopause is generally a very stable region, and it is not necessarily obvious that movement down and across the tropopause should occur spontaneously. It is believed that some sort of extra small-scale mechanism is needed to trigger, or enhance this cross-tropopause transport. Examples might include enhanced diffusion, gravity wave activities and unusually strong downward motion. In this chapter, we will investigate possible small scale dynamics which may act as a trigger, or assist in, this initial cross-tropopause transport.

We have diagnosed parameters such as turbulence strengths, vertical wind shear of horizontal velocity, standard deviation of vertical velocity etc around the tropopause to determine the cause of the ozone transport from the stratosphere to troposphere. These physical quantities have been investigated carefully both before and during the intrusion events to see if there is any association between atmosphere dynamics and the observed enhanced ozone rich dry air. In general, we have found a good association of these dynamics with the intrusion of stratospheric ozone, but no one type of event dominates.

Gage and Green [1979] revealed that the enhanced echoes that are measured at vertical incidence by VHF radars are well associated with atmospheric stability. The capability for detection of atmospheric stable regions makes it possible to monitor inversions, specifically the tropopause and fronts. Nevertheless, the static stability of the atmosphere is altered locally by radiation, which may have significant consequences for the occurrence and strength of turbulence that happens on much shorter timescales than radiation. Turbulence is intermittent. Turbulence can be generated by convection, breaking gravity waves, wind shear and radiation. Wind shear, convection and turbulence act so as to enhance the area to volume ratio of a parcel of air and, thus, lead to a cascade down to ever smaller scales, on which air masses are eventually mixed by molecular diffusion.

In this chapter, we present ozonesonde campaign measurements in Egbert, Walsingham and Montreal. This chapter considers simultaneous ozonesonde and windprofiler radar observations so as to detect the intrusions of stratospheric ozone and determine the cause of the intrusions. The summary of the results that we have obtained for other campaigns, including the ones mentioned above, will be presented at later. The dynamical processes by which the transport of ozone from stratosphere to the troposphere takes place have been discussed thoroughly and are summarized. This study presents quantitative results of the cause of the intrusions, which is believed to contribute to a more comprehensive understanding of stratosphere-troposphere exchange. As a supplement to this work, we simulate the transport processes employing the Lagrangian particle dispersion model FLEXPART in chapter 4. It has been used to simulate intrusions of stratospheric air into the lower troposphere by running both in forward (to simulate the dispersion of tracers from their sources) and backward mode (to determine potential source contributions for given receptors).

3.1   Egbert 2009 Ozonesonde Campaign

The Egbert 2009 ozonesonde mini campaign was made at Egbert, Ontario (44.23°N, 79.78°W) from 5 – 11 May. Two launches were made per day except on 5th and 10th May when only one launch was made per day. The ozonesondes were released at around 11:00 and 23:00 UTC with a total of 12 launches. EN-SCI model 2Z-ECC ozonesondes equipped with GPS receivers and Vaisala RS80 radiosondes were the instruments used in the campaign. The instruments measured vertical profiles of ozone mixing ratio, temperature, pressure, humidity and sometimes wind speed and direction with a vertical resolution of approximately 100 - 150 m. The accuracy of ozone measurement was about 5% [Science Pump Corporation, 1999]. Simultaneous and co-located measurements of the windprofiler radars have been employed to measure wind velocity, turbulence strengths and backscattered radar power (from which radar derived tropopause heights can be determined). The radars had steerable beams with one-way beam half-power half-widths of 2.75^o which could be pointed vertically, or at 10.9^o off zenith in various azimuthal directions. The operating frequency of the radio wave used was 47.56 MHz. The vertical height resolution was 500 m.

The windprofiler radar measurement of backscattered radar power is taken as a means of quantitatively detecting and monitoring the tropopause heights. Sudden changes in tropopause heights are observed several times in the data collected during the campaigns. The height-time cross-section of the observed data during these campaigns will be highlighted here. Figure 3.1a represents time height series of the contour plots of backscattered radar power in logarithmic scale during the period 5 – 17 May 2009. The backscattered signal strength generally decreases with height in the troposphere but increases as a result of hydrostatically stable regions, mostly due to the specular reflection mechanism. The enhancement of turbulence also leads to an enhancement of the radar reflectivity [VanZandt and Fritts, 1989]. Generally, the lower stratosphere is characterized by large stability returns, and therefore the large secondary backscattered power at 7-14 km suggest that the location of the tropopause may be below 14 km. The lower edge of the secondary maximum quantitatively infers the location of the tropopause. The large positive vertical gradient in backscattered radar power has been used to develop a quantitative algorithm for detection and monitoring of tropopause heights by windprofiler VHF radar during the period 5 – 17 May 2009.

Figure 3.1b shows the contour plot of ozone mixing ratio in parts per billion by volume as a function of altitude and time for the period 5 – 11 May 2009. From the same figure, one can notice a descent of stratospheric ozone beginning on 7 May and an enhanced concentration of ozone in the middle and upper troposphere is seen afterwards. First, we need to diagnose whether the enhanced ozone is really originated from the stratosphere. If so, we then investigate the cause(s) of the intrusion by looking at radar measurement of the atmospheric dynamics. Here we closely inspect the events on 6th and 9th May. Both are cases where the tropopause heights suddenly jumps and which coincided with the intrusions of stratospheric ozone.

The balloon-borne ozonesonde measurement campaigns were made on radar observation days. We have selected some events of tropopause height jumps which demonstrate the signature of stratosphere-troposphere exchange of ozone. Moreover, we have also presented an event of tropopause weakening but with no corresponding jump of tropopause height, which does show an exchange of ozone. To verify the effect of

tropopause height jumps and tropopause weakening on the ozone concentration, only the main findings will be highlighted here.
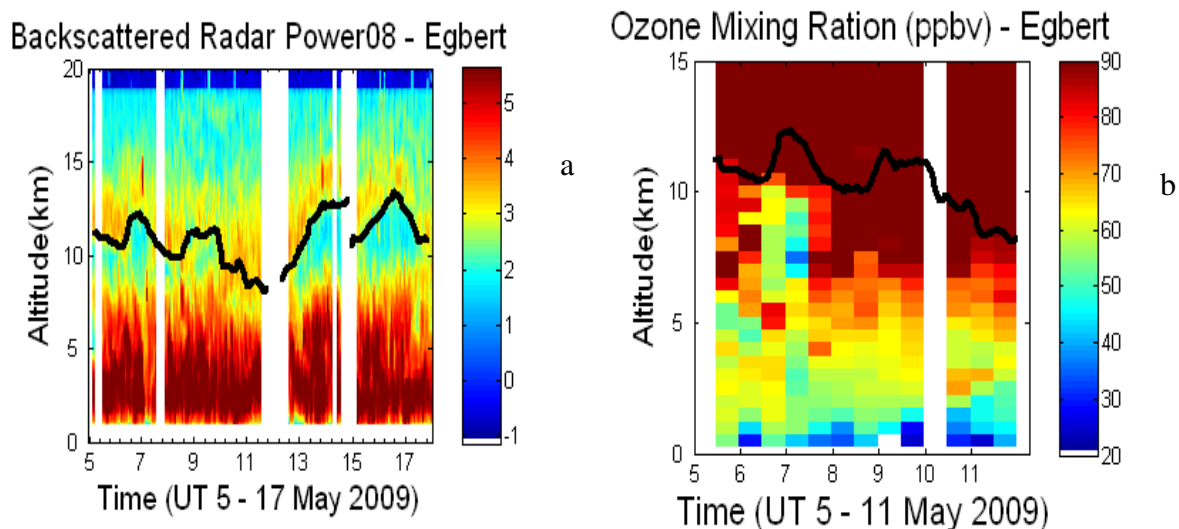
Figure 3.1. Egbert Ozonesonde Measurements Campaign May 2009. (a) Backscattered radar power plots as a function of altitude and time observed with the Egbert windprofiler radar, expressed in common logarithmic scale from 5 - 17 May 2009. In the lower troposphere, the occurrence of absolute maximum values of backscattered powers is noticed, whereas in the height range between 6 and 14 km a secondary maximum appeared. The lower edge of the secondary maximum, i.e., the height where local maximum gradient of power occurred, stands for the radar derived tropopause height, as has been revealed in Larsen et al. [1982], Hocking et al. [1986] and Gage et al. [1982]. The tropopause heights, are shown above as a black line, after smoothing using an 11 hour running mean filter. (b) The plot of ozone mixing ratio (measured in parts per billion by volume) as a function of altitude and time for the period 5 – 11 May 2009. Every launch is represented by a colored vertical column. The tropopause height as determined by the radar is marked as the solid black line at 6 – 14 km altitude. The two rapid tropopause height ascents on the 6th and 9th of May 2009 are associated with high stratospheric ozone in the middle and upper troposphere on 7 - 11 May.

Since the tropopause is a hydrostatically stable region, a large-scale instability in the atmosphere is required to destroy its stability. Earlier research [Fritts and Rastogi, 1985] suggests that there is a close correspondence between turbulence and/or gravity wave and instability. The detailed study of the effects of gravity wave activity on the tropopause height variation is beyond the scope of this thesis. The instability can result in a considerable amount of turbulence throughout the atmosphere [Fritts and Rostogi, 1985].

Figure 3.1a shows radar powers between -0.08 and 0.08 Hz observed with the radar vertical beam from 5 - 17 May and with radar powers more than 10^5 (expressed as digital units squared) above 5 km removed and replaced using multiple linear regression of a 10 by 10 window (i.e., 10x10 matrix of radar data). Such strong signals almost always correspond to aircraft echoes. Refer to Figure 2.8a to show what it looks like when aircraft contaminates the backscattered radar power and Figure 2.8b shows the same plot after removing such strong signals using the above techniques. The use of the narrow frequency band was required to remove interference including possible aircraft contamination. Below 5 km, data with strengths more than 10^5 were not removed. The purpose of the procedure was purely to reveal the tropopause as clearly as possible, which it has successfully done as shown in Figure 3.1a. The lower edge of a thin secondary layer is seen at 6 - 14 km, representing the radar tropopause, and rapid tropopause ascent is seen on 6th and 9th May. These were the only significant tropopause movements during the campaign.

The descent of stratospheric ozone begins on 7th May and continues afterwards to bring about a high ozone mixing ratio in the middle and upper troposphere subsequently. Due to the pre-existing ozone resulted from the first tropopause ascent, i.e. on 7th May, the effect of the second tropopause height ascent, i.e. on 9th of May, is not seen as clear as the first one. However, the high ozone concentration in the middle and upper troposphere is of stratospheric origin. This has been verified by examination of the relative humidity, which showed the low values as expected for stratospheric air. Relative humidity sensor measurements above about 8 km, (i.e., when temperature is less than $-30^{o}C$), are potentially unreliable. However, low relative humidity below about 8 km is still a good partial indicator of stratospheric ozone intrusion.
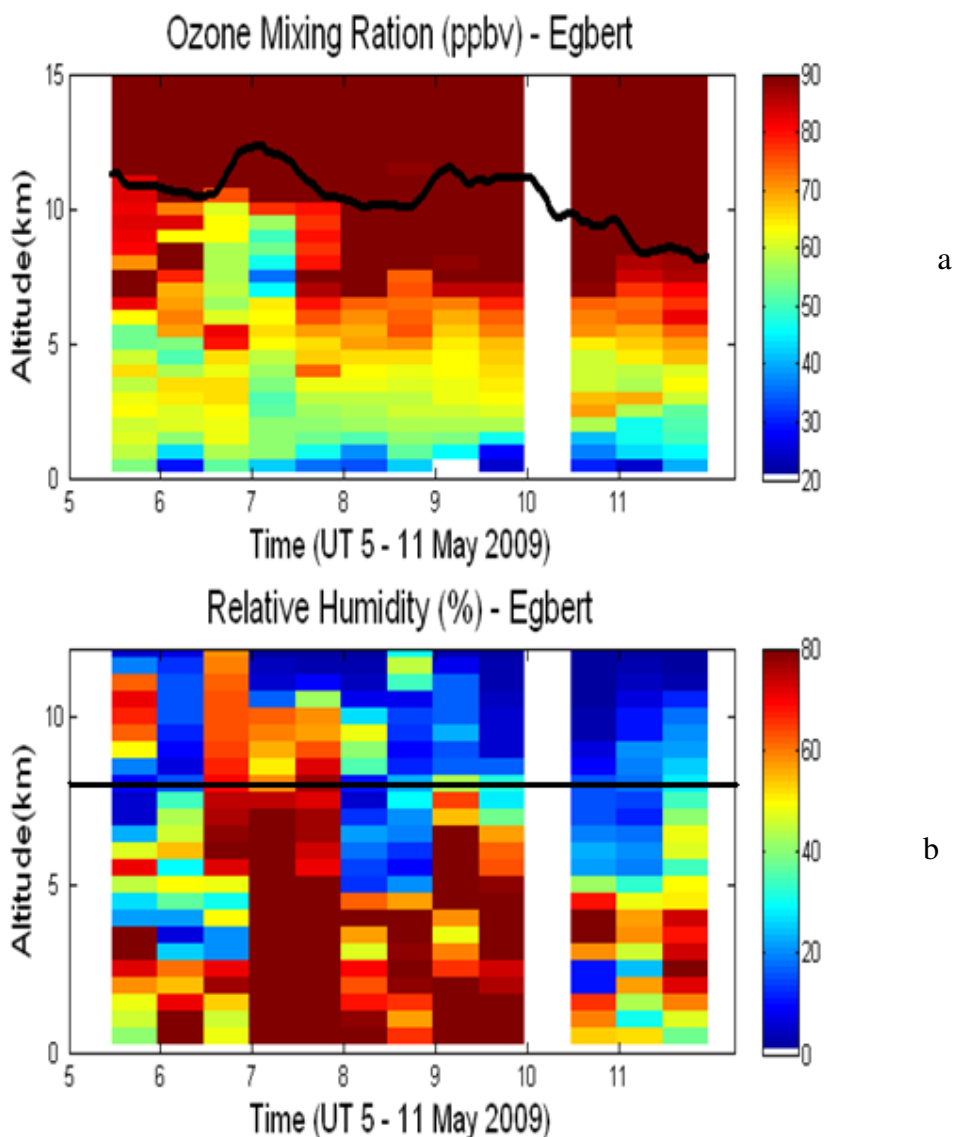
Figure 3.2. Egbert Ozonesonde Measurements Campaign May 2009. (a) Contour plot of ozone densities (expressed as parts per billion by volume) as a function of height and time for the period 5 - 11 May 2009. (b) Relative humidity (expressed as percentage) as a function of height and time for the same period. In both figures, each vertical column of colored boxes represents a different launch. The solid black lines in Figures 3.2a and b are the radar determined tropopause heights and height at about 8 km, respectively. Data above about 8 km (i.e., temperature less than -30°C) are potentially unreliable for many radiosonde measurements (R. J. Sica private communication 2012). However, low relative humidity below about 8 km is still a good indicator of stratospheric intrusion.

In Figure 3.2a, the black line on the contour plot of ozone mixing ratio is the radar derived tropopause heights determined from the plot of backscattered radar power (expressed as a common logarithmic scale) observed by windprofiler radar at Egbert as a function of height and time. The tropopause heights have been smoothed using an 11-hour running mean with triangular weighting. Figure 3.2b shows the contour plot of the ozonesonde measurement of relative humidity of the air sampled. As can be seen from Figure 3.2b the relative humidity is low on 8th, 10th and 11th of May, which attests that the ozone rich air originates from the stratosphere. Moreover, during these events the observed ozone concentration as low as 5 km is higher than the average volume mixing ratio of ozone in the troposphere, which normally ranges from 40 to 50 ppbv.

The radar derived tropopause height, the black line shown in Figure 3.2a, reveals large sudden jumps on 6th and 9th May. The association of sudden jumps of tropopause height with stratospheric ozone intrusion is clearly shown in the work of Hocking et al. [2007]. In both cases there can clearly be seen an apparent enhancement of ozone concentration as low as 5 km followed the tropopause jumps. The descent of stratospheric ozone begins following the tropopause events.

The next step is to make use of the capability of windprofilers to measure horizontal and vertical winds, the standard deviation of vertical wind, turbulence strengths and backscattered radar power, as they may have important implications for the stratospheric ozone intrusions. The capability of windprofiler radars in measuring vertical velocity has great importance in understanding many dynamical processes including stratosphere-troposphere exchange, vertical transport of heat, momentum and energy by waves. The windprofiler radar technique has the unique capability of directly measuring vertical winds with reasonable accuracy over a wide range of altitudes continuously with high temporal and height resolutions. The standard deviation of vertical velocity is the subject of the following discussion as it plays a vital role in mixing of air masses. The vertical resolution of the data was 500 m and the data was averaged over 2 hours. Nevertheless, as Rottger [1981] pointed out, the vertical velocity can have a small contribution from the horizontal velocity component, if the surface of reflection for the radar echoes is not exactly horizontal. This could happen during conditions of strong baroclinicity or in

connection with lee wave or strong gravity waves with significant amplitudes. Since tilted refractivity structure will lead to problems in vertical velocity, we have corrected the contamination of horizontal velocity to improve the result if required [see section 2.5 for the correction of vertical wind].
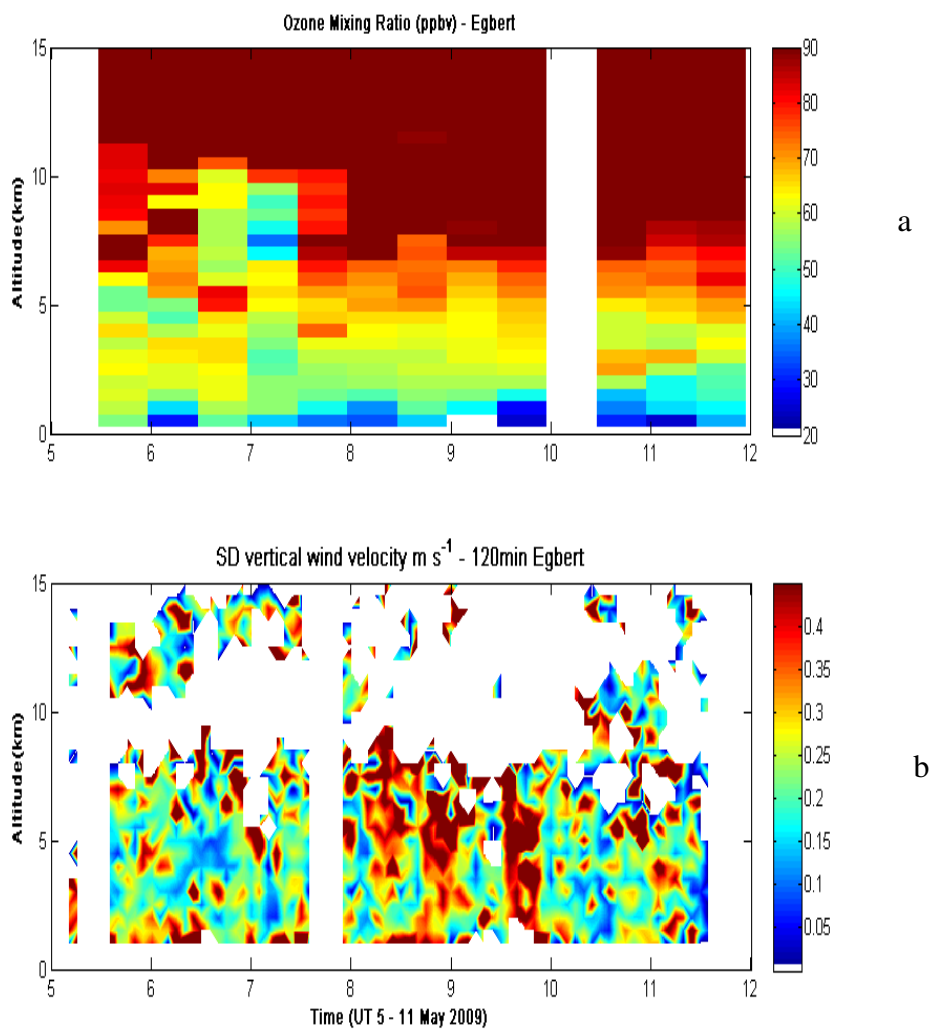
Figure 3.3. Egbert Ozonesonde Measurements Campaign May 2009. (a) Contour plots are ozone densities (expressed in parts per billion by volume) and (b) standard deviation of vertical component of wind velocity averaged over 2 hours (ms⁻¹) as a function of height and time for the period 5 - 11 May 2009 (this parameter is taken as an indicator of gravity wave activity). In Figure 3.3a, each vertical column of colored boxes represents a different launch. The ozonesondes were released at around 11:00 UTC and 23:00 UTC.

Figure 3.3b shows the height-time intensity plot of the standard deviation of vertical velocity for the period 5 - 11 May 2009 as indicator of gravity wave activity. It clearly shows a strong standard deviation of vertical wind velocity of more than 0.35 ms^{-1} on 8th and 9th May, initially at 6 – 7 km altitude (and possibly higher) and then spreading to cover a wider height range (down to 2 km) by late on May 9. This strong coincidence between standard deviation of vertical wind and high ozone mixing ratio suggests that the variance of vertical wind might be one of the small scale dynamical features that is responsible to bring down ozone rich dry air that was observed after the 7th of May. Nevertheless, we see missing radar measurement data of standard deviation of vertical wind above around 8 km. This might be either due to the dynamic was too weak or too strong to be detected by the radar. The large standard deviation of the vertical wind is taken as an indicator of enhanced gravity wave activity and may have been a mechanism to help the intrusion of stable stratospheric ozone into the upper and middle troposphere. Since there a is possibility that standard deviation of vertical velocity might act along with other parameters that can cause the descent of stratospheric air masses to the tropospheric, in the next sections we will examine the effect of vertical shear of the horizontal wind, and turbulence strengths. It is possible that all or any combination of these atmospheric dynamics could potentially have association with the observed enhanced ozone rich stratospheric air. On the other hand, one can find that only one of the parameters can act to cause to intrusions of stratospheric. This suggests that the atmospheric dynamics responsible for the event varies from case to case.

We have diagnosed vertical shear of horizontal wind to see if the intrusion of stratospheric ozone is caused by it. Radar measurement of wind shear will be presented in the next section. It is then followed by the measurement of turbulence strengths. Later a quantitative simulation of this transport phenomenon is performed using an atmospheric three-dimensional long-range dispersion model, GEM-FLEXPART and the result is shown in the next chapter.
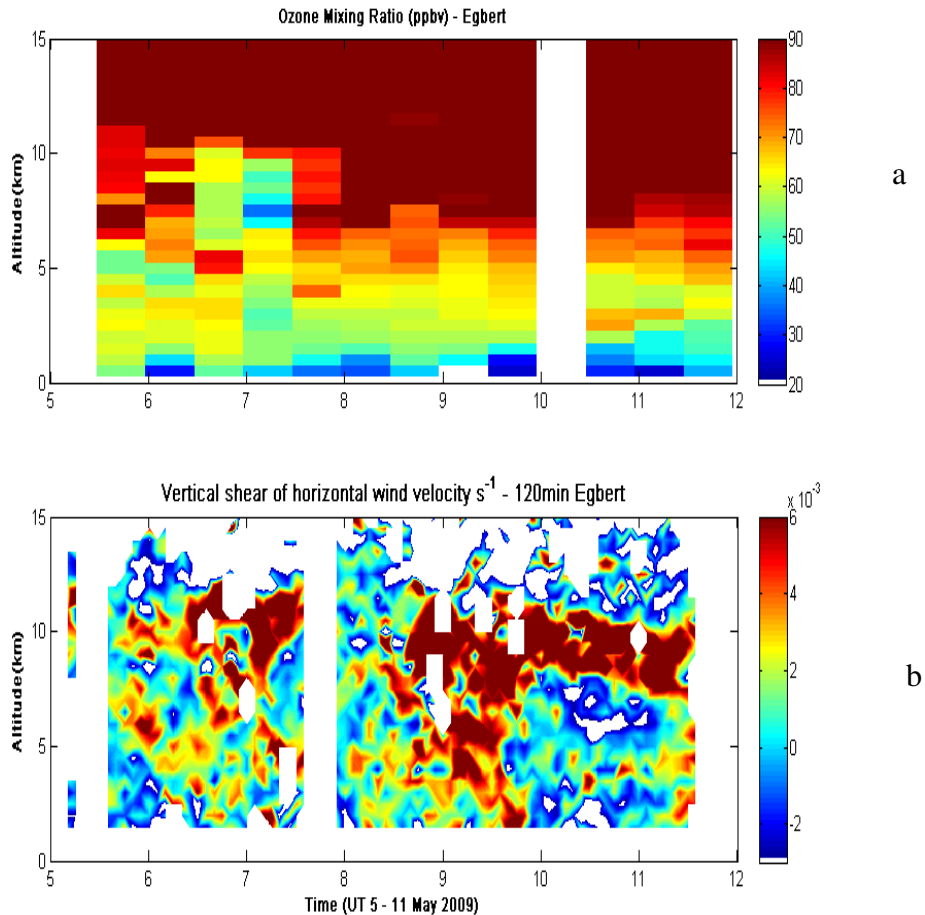
Figure 3.4. Egbert Ozonesonde Measurements Campaign May 2009. (a) Contour plots are ozone mixing ratios (expressed in parts per billion by volume) and (b) vertical wind shear of horizontal wind velocity averaged over 2 hours interval (expressed in s^{-1}) determined from radar as a function of height and time for the period 5 – 11 May 2009. In Figure 3.4a, each vertical column of colored boxes represents a different launch. The ozonesondes were released at around 11:00 UTC and 23:00 UTC.

Wind shear refers to a change in wind velocity with height in the atmosphere. Wind shear, a major source of turbulence, is one of atmospheric dynamics that the radar can measure, and can bring about mixing of atmospheric gases such as stratospheric ozone. It is a source of turbulent kinetic energy in the neutral and stably stratified boundary layers and can also be significant in the convective case.

Figure 3.4b reveals the windprofilers measurements wind shear averaged over 2 hours interval. As can be seen from Figure 3.4b, a fairly strong wind shear is observed from around noon of 6th May up to noon of the 7th May from about 7 km altitude which seems to have association with the observed enhanced stratospheric ozone following the event. Afternoon on 8th May and up until 11th May noon, where altitude range is small except on the 9th May which starts as low as 2 km, strong wind shear is noticeable between about 7.5 and 10.5 km which is accompanied with high stratospheric ozone observed in the middle and upper troposphere on 8th - 11th May. Hence, Figure 3.4 reveals that a correlation of the intensity of wind shear in the upper troposphere with enhanced stratospheric ozone intrusion events. This suggests that strong wind shear plays a vital role in mixing of air masses from the lowermost stratosphere into the upper and lower troposphere since stronger instability might be the cause for more effective STE.

By wind shear hereafter we mean vertical wind shear of the horizontal wind speed is the vertical gradient of horizontal wind which is expressed as

$$wind\ shear = \frac{\partial U}{\partial z}$$

where U is the radar measurement of horizontal component of wind speed and z is altitude.

It is noteworthy that the maximum values occurrence coincides with the enhanced stratospheric ozone intrusions. The vertical wind shear is much stronger during or before the event than that in the earlier case. This may be additional evidence for strong gravity wave activity. Stronger instability due to wind shear might be the cause for more effective STE. Establishing a qualitative relationship between the wind shear and stratospheric ozone influx is the purpose of this study, since wind shear causes strong mixing of air masses. The results are thought to be reliable, at least in a qualitative sense, because the largest downward transport of ozone across the tropopause occurrence is in regions with maximum wind shear. The correlation between strong wind shear and stratospheric ozone intrusions is fairly strong.

Therefore, at least from Figures 3.3 and 3.4 one can come to conclude that both standard deviation of vertical wind and wind shear have contributions to the observed enhanced ozone in the upper and lower troposphere of Egbert on $8^{th} - 11^{th}$ May 2009. In the next section, we will see whether or not atmospheric turbulence has a contribution on the downward transport of ozone and also results in the observed high ozone during the campaign.

It is believed that in a global scale the exchange of ozone between the stratosphere and troposphere to be occurred as a result of Brewer-Dobson circulation [Holton et al., 1995; Holton, 2003]. Small scale turbulence that causes local downward transport across the tropopause as well as mixing of atmospheric ozone may also be responsible for global scale ozone transport [Lamarque and Hess, 2003]. However, the detail of the role of turbulence is not clear yet and better understanding of it requires simultaneous observation of atmospheric turbulence and tracer gases such as ozone. Pavelin et al. [2002] and Whiteway et al. [2003] described aircraft and ozonesonde measurements of atmospheric dynamics and ozone transport. Measurements of surface ozone with the wind profiler data from Gadanki, India were also compared by Krishna Reddy et al. [2003].

In the past, atmospheric turbulence measurements have been made mainly with sensors on aircrafts [Sand et al., 1974]. However, the volume of air that can be sampled by an aircraft is small compared with the total volume of turbulent air, and a long time is demanded to collect even such a limited sample. In contrast, Doppler radars can sample a large volume of air in a very short time, gathering vast amounts of spectral information about the motions of scatterers within the sampled volume of air. The turbulent kinetic energy dissipation rate is an important atmospheric dynamic that plays a significant role in mixing air of different composition. Knowing the magnitude of turbulent kinetic energy dissipation rate allows the estimation of the rate of vertical mixing [Gregg et al. 1977; Ivey and Imberger 1991; and Saggio and Imberger 2001]. It is one of the atmospheric parameters that windprofiler radars can measure with high temporal and spatial resolutions from the ground up to an altitude of about 20 km depending on the output power.

The received radar power is a function of the inhomogeneity in refractive index, on the scale of half the radar wavelength (approximately 3 m in our case). In general, temperature and humidity variations affect the refractive index [Doviak and Zrnic, 1984b] but above about 5 - 6 km the impact of humidity weakens. As a result, refractive index inhomogeneities around the upper troposphere and lower stratosphere are mainly related to small-scale structure in the temperature field. Such structure is generally considered to come from the consequence of turbulence on a large-scale potential-temperature gradient [Gage and Balsley, 1980; Hocking 1985].

It is known that wind shear is an important cause of turbulence. Moreover, atmospheric radar shows that the breaking of internal gravity waves propagating upward from their source can generate turbulence many kilometers higher in the atmosphere. In this section, we discuss the role of turbulence around the tropopause in the stratosphere-troposphere exchange of air, specifically in constituents such as ozone. The measurement of turbulent kinetic energy dissipation rate (W/kg) shown in the figure below was made during the Egbert ozonesonde measurements campaign 5 - 17 May 2009.

Turbulent kinetic energy dissipation rate averaged over two hours is used in order to examine the impact of atmospheric turbulence on STE of ozone during the Egbert 2009 campaign. This averaging helps gain a better understanding of the average distribution and strength of turbulence over a longer period of time since turbulence is patchy and intermittent, and differs considerably from one measurement to the next. Radar measurements of turbulent kinetic energy dissipation rate in the range between 5 and 12 km are compared with the intrusion of stratospheric ozone obtained from ozonesonde at the same time. The simultaneous measurements of turbulence and ozone mixing ratio using radar and ozonesonde, respectively, is employed so as to correlate the cause (i.e., turbulence) and the effect (the observed enhanced ozone concentration in middle and upper troposphere) which as a result facilitates the study STE of ozone.
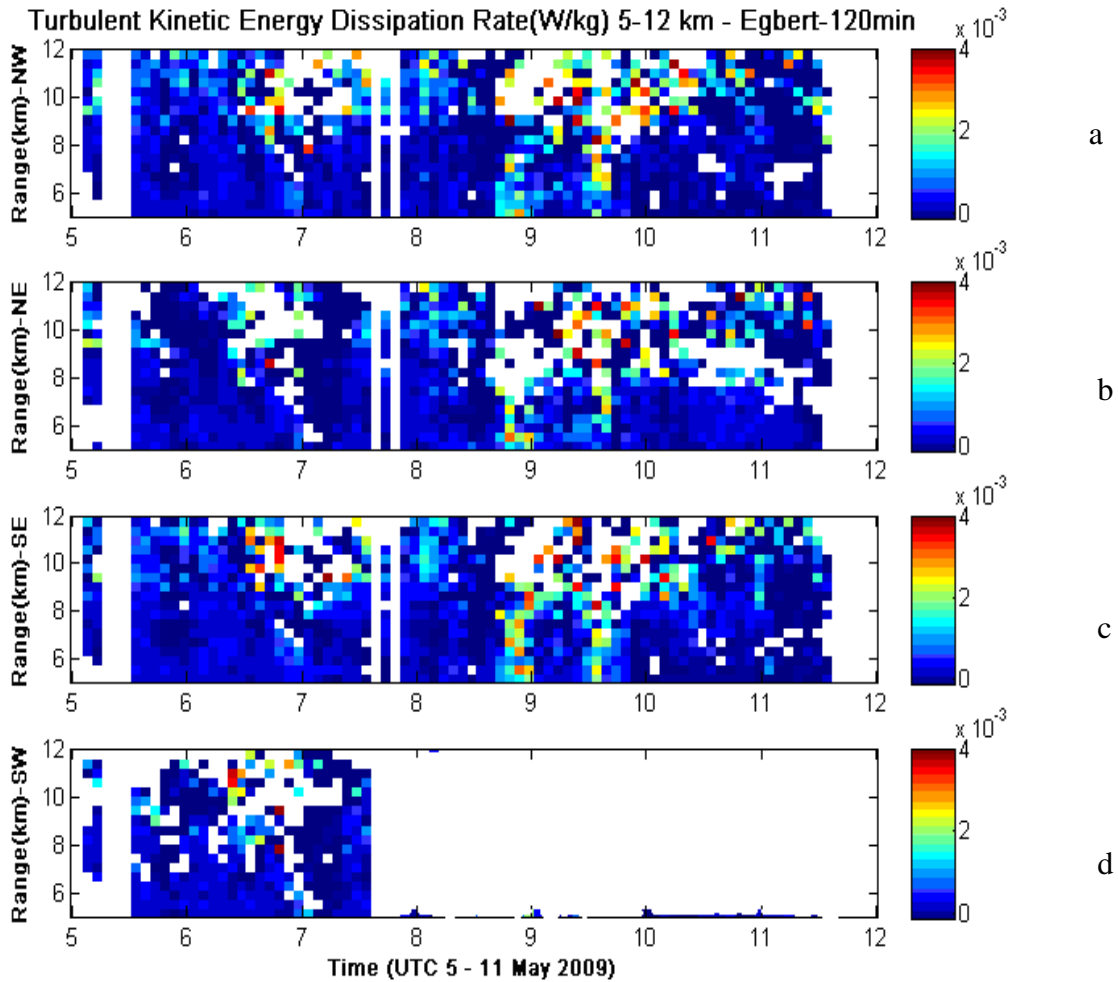
Figure 3.5. Egbert Ozonesonde Measurements Campaign May 2009. Contour plots of turbulence kinetic energy dissipation rate (Wkg^{-1}) averaged over 2 hours as a function of height and time for the period 5 - 11 May 2009 when the beam points northwest (a), northeast (b), southeast (c) and southwest (d). The missing data of the southwest (Figure 3.5d) is a beam failure due to high impedance.

Figure 3.5 depicts the mean values of turbulence kinetic energy dissipation rate for heights from 5 – 12 km for a time period of 5 – 11 May 2009. The four panels show the height-time cross section of the turbulent kinetic energy dissipation rate when the radar beam points in the direction of northwest, northeast, southeast and southwest, respectively. The red to blue colors indicate the highest to least strength of turbulence as observed by the radar, respectively. The missing data in Figure 3.5d after approximately at 16 UTC on 7th May might be due to the beam failure as a result of high impendance.

The most turbulent region on the four of the plots occurred on 9th May above 8 km altitude. Fairly strong turbulence strength can be seen at the end of 6th and beginning of 7th May above 10 km altitude. On the other hand, an enhanced ozone concentration at the middle and upper troposphere were observed on 8 – 11 May which suggests the strong turbulence observed during 6th – 7th May and 9th May might have made a contribution to the intrusion of stratospheric ozone in to the troposphere.

The height-time cross-section of turbulent kinetic energy dissipation rate, for example Figure 3.5, shows the occurrence of intensified turbulence which may make substantial impact on atmospheric dynamics and composition. This is clearly noticed on 9th May of Figure 3.5, where high ozone concentration are apparent on at least 9th May if not 10th – 11th May. This demonstrates that the turbulence may cause effective and irreversible transport of lower stratospheric air mass deeply into the troposphere. Therefore, in some cases and at some times turbulence enhanced around the tropopause may cause noticeable local transport of ozone from the stratosphere to the troposphere.

As can clearly be seen from Figures 3.3-3.5, the standard deviation of vertical wind, vertical shear of horizontal wind and turbulence strengths were simultaneously strong on 9th of May. It is, therefore, possible that the enhancement of the observed stratospheric ozone intrusion on 8 – 11 May is caused by simultaneous action of all of the atmospheric dynamics we have diagnosed. However, we evidently show in the next section that there is also a possibility that the enhancement of the observed stratospheric ozone intrusion may be related to one or any combination the parameters. On the other hand, there is possibility that the occurrence of enhanced stratospheric ozone may not to be associated with any of the parameters that have been analyzed. Hence, on such cases further studies would be necessary to ascertain the atmospheric dynamics responsible for the intrusions of stratospheric ozone, where the wind and turbulence effects are too weak to cause the intrusions of stratospheric ozone.

In the case when the atmospheric parameters are too weak to cause the intrusions stratospheric ozone, it is possible that the recorded stratospheric ozone peak in the troposphere might arise due to the long range transport of ozone. Such cases can be

further analyzed through numerical modeling utilizing GEM-FLEXPART, which among others, simulates the long range atmospheric transport and deposition of trace gases including ozone. Moreover, the radar measurement of wind, particularly horizontal wind velocity, can be used as further support regarding whether this stratospheric ozone was blown with the wind, resulting in ozone rich dry air being transported in the troposphere. The Eureka 2008 campaign is an example. In this campaign, we examined the detection of stratospheric ozone leakage from the stratosphere to the troposphere, as revealed by a continuous ozonesonde campaign made by Environment Canada at Eureka from February 24 up to April 18, 2008. Furthermore, we employed windprofiler radars simultaneously with the ozonesonde launches in order to investigate the ozone intrusion thoroughly. Stratospheric-Tropospheric Exchange of ozone was observed in April even though the ozone intrusion events occurred to the south of Eureka [Osman et al., 2010]. The authors have shown that the stratospheric ozone was steadily blown northward with the wind for approximately successive 13 days, resulting in ozone rich air with low relative humidity arriving in the middle and higher troposphere of Eureka. However, results of most of our analysis suggest that stratospheric ozone intrusion played an important role in the occurrence of this episode.

The dynamical processes of the atmosphere include different scales. Their strong nonlinear interaction may cause large-scale instability in the atmosphere and bring about turbulence. It is believed that the turbulence observed above the tropopause may break down the stability at the tropopause that normally restrains stratosphere-troposphere exchange of ozone and other trace gases. Therefore it can result in leakage of stratospheric ozone in to the troposphere across the tropopause. Moreover, strong turbulence can be responsible for enhanced backscatter power at the tropopause.

In some cases, turbulence above the tropopause brings about a weakening tropopause. Consequently, stratospheric air masses descend into the upper tropospheric via the weak tropopause if the magnitude of vertical velocity is low or direction is downward. Ozone is either carried along with this descending air mass or diffuses downward, driven by its own vertical gradient. These two mechanisms can also occur simultaneously. However, it is beyond the scope of this thesis to ascertain which of the two mechanisms prevails.

Both cases result in an increase in stratospheric ozone in the upper and middle troposphere. Hence, the exchange of ozone during tropopause weakening could have a noteworthy effect on the budget of atmospheric chemical composition, particularly for trace gases such as ozone.

3.2   The Walsingham 2005 Ozonesonde Campaign

The Walsingham 2005 ozonesonde campaign was made at Walsingham, Ontario (42.6^{o}N, 80.6^{o}W) site from 17 – 26 November 2005. The ozonesonde releases were at a temporal density of two per day (except on the 17th and 19th of November) at 00:00 and 12:00 UTC, with a total of 18 launches so as to achieve good ozone measurement continuity. Balloon-born ozonesondes equipped with GPS were released near to the windprofiler radars that have been utilized to measure atmospheric parameters. Detailed discussion about instruments, i.e., ozonesonde and windprofiler radar, is given in chapter 2. The radar at Walsingham had steerable beams with a one-way beam half-power half-widths of 2.3^o which could be pointed vertically, or at 10.9^o off zenith in various azimuthal directions. The operating frequency of the radio wave used was 44.50 MHz. The vertical height resolution was 500 m.

Figure 3.6 shows the height-time cross-section of ozone mixing ratio in parts per billion by volume from 17 – 26 November 2005. The black line in the figure represents the radar derived tropopause heights during the same period time. It is illuminated by the lower edge of the secondary maximum backscattered radar power, which ranges from approximately 7 to 10 km. The detail of the extraction procedure of radar derived tropopause height was mentioned in section 3.1 of the same chapter.

A sudden rapid and large ascent of the tropopause height is seen on 24th November, which was followed by a huge intrusion of stratospheric ozone. The balloon-borne ozonesonde measurement campaign was utilized simultaneously with radar observation. We have selected this event of tropopause heights jump as a good example which reveals the stratosphere-troposphere exchange of ozone. We have diagnosed atmospheric dynamics that may be responsible for the intrusion of stratospheric ozone.
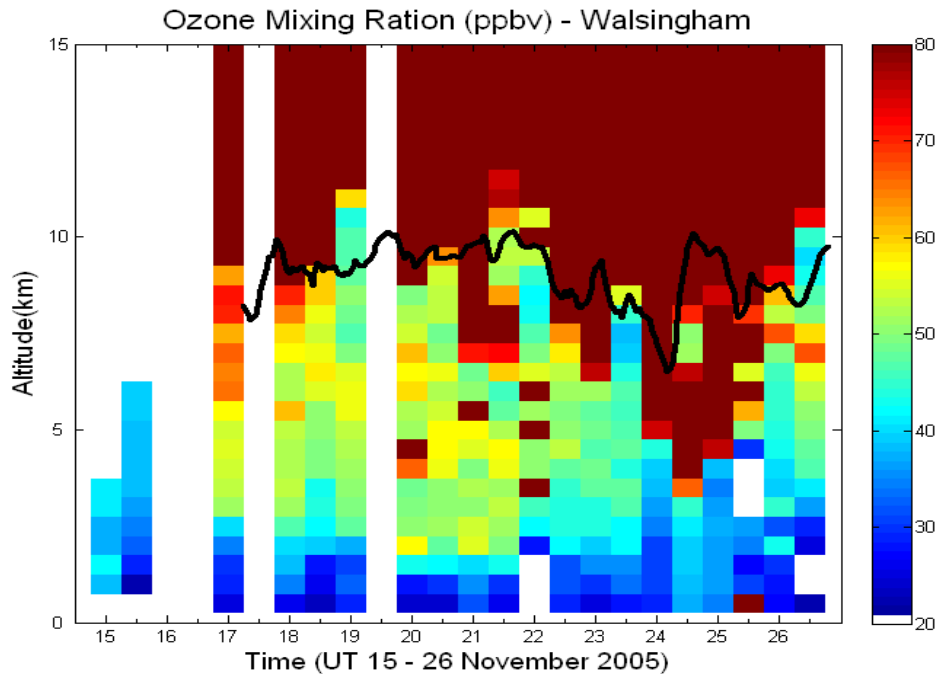
Figure 3.6. Walsingham Ozonesonde Measurements Campaign November 2005. Same as in Figure 3.1b except for time period 17 – 26 November 2005 at Walsingham. The tropopause height as determined by the radar is marked as the solid black line at 7 – 10 km altitude.

In order to determine tropopause heights, the vertical radar powers of the same frequency mentioned in previous section were used for the period 17 – 26 November 2005. We also applied the same producer as discussed earlier to disclose the tropopause height as clearly as possible. The lower edge of a secondary maximum, representing the radar tropopause, and rapid tropopause ascent is seen on 24th November. This was the only significant tropopause jump during the campaign.

In Figure 3.6, a descent of stratospheric ozone can be noticed to begin on 24 November, and as a result extremely high concentrations of ozone in the middle and upper troposphere are seen on 24 – 25 November. To confirm that the ozone really was stratospheric in origin, we have looked at the relative humidity, as it is considered as a partial indicator. As can be seen from Figure 3.7a, the relative humidity is noticeably low on 24 – 25 November which suggests the ozone is originated in the stratosphere. The observed ozone-rich stratospheric air at the middle and upper troposphere is much higher

than the average volume mixing ratio of ozone in the troposphere. As in the previous case, now we look at the windprofiler measurements of horizontal and vertical velocities, the variance of vertical velocities, and turbulence strengths.

a

b

Figure 3.7. Walsingham Ozonesonde Measurements Campaign November 2005. Same as in Figure 3.2 except for time period 17 – 26 November 2005 at Walsingham.
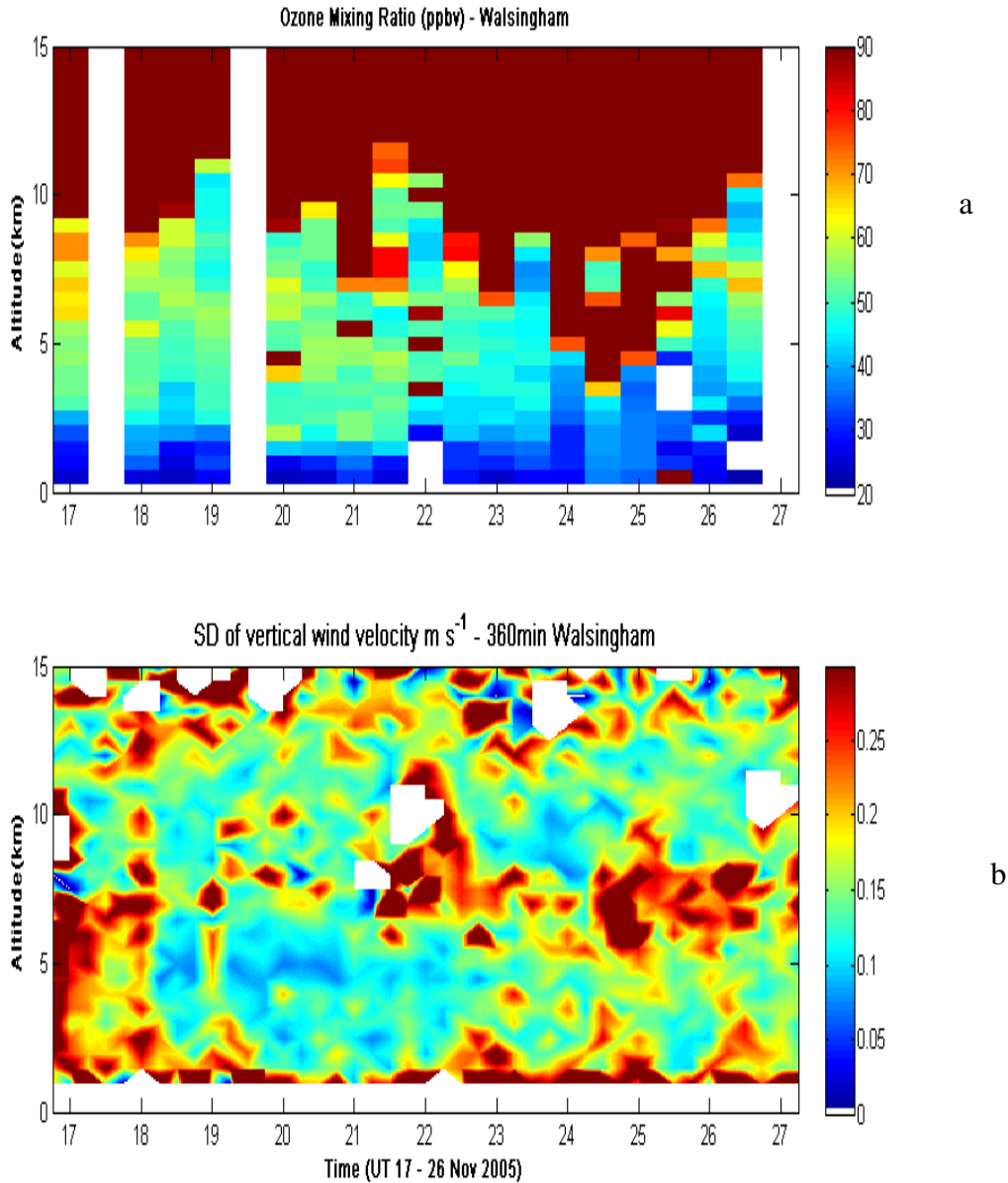
Figure 3.8. Walsingham Ozonesonde Measurements Campaign November 2005. Same as in Figure 3.3 except for time period 17 – 26 November 2005 at Walsingham and the standard deviation of wind averaged over 6 hours. The ozonesondes were released at around 00:00 UTC and 12:00 UTC

Now we will discuss about windprofilers measurement of standard deviation vertical wind as it is very useful in the study of STE of air masses including ozone. Figure 3.8b shows the height-time intensity plot of the standard deviation of vertical wind for the period 17 – 26 November 2005. That data were averaged over 6 hours. It evidently shows

a strong standard deviation of vertical wind to be more than 0.25 ms^{-1} on 24th – 25th November in the height range between about 6 and 9 km. Moreover, we can also see from Figure 3.8b strong variation of vertical wind velocity at the end of 22nd November and the beginning of 23rd November at the height 6 – 10 km that might cause ozone intrusion of the same day. It does seem that strong standard deviation of vertical wind activity appears to be one of the atmospheric dynamical features that is responsible for bringing down ozone rich dry air from the stratospheric ozone layer to the troposphere. Nevertheless, we do not assume that occurrence of a strong standard deviation of vertical wind forces an intrusion and other factors need to be also supportive of an intrusion before it becomes active, e.g., see November 16 – 17, where standard deviation is strong but no intrusion occurs. As we did in the previous case, in the next sections we will discuss the effect of vertical wind shear and turbulence strengths.

Figure 3.9b shows the windprofiler measurements of wind shear averaged over 6 hours interval. As can clearly be seen from the figure, strong wind shear is observed on 24th – 25th November from altitudes as low as about 2 km which seems to have association with the observed enhanced stratospheric ozone on the same day. One can also notice from Figure 3.9b that vertical wind shear at the end of 22nd and beginning of 23rd November at the height range about 6 – 9 km. Even though the altitude range is small, strong wind shear is noticed which is accompanied with high stratospheric ozone observed in the middle and upper troposphere on 22nd – 23rd November.
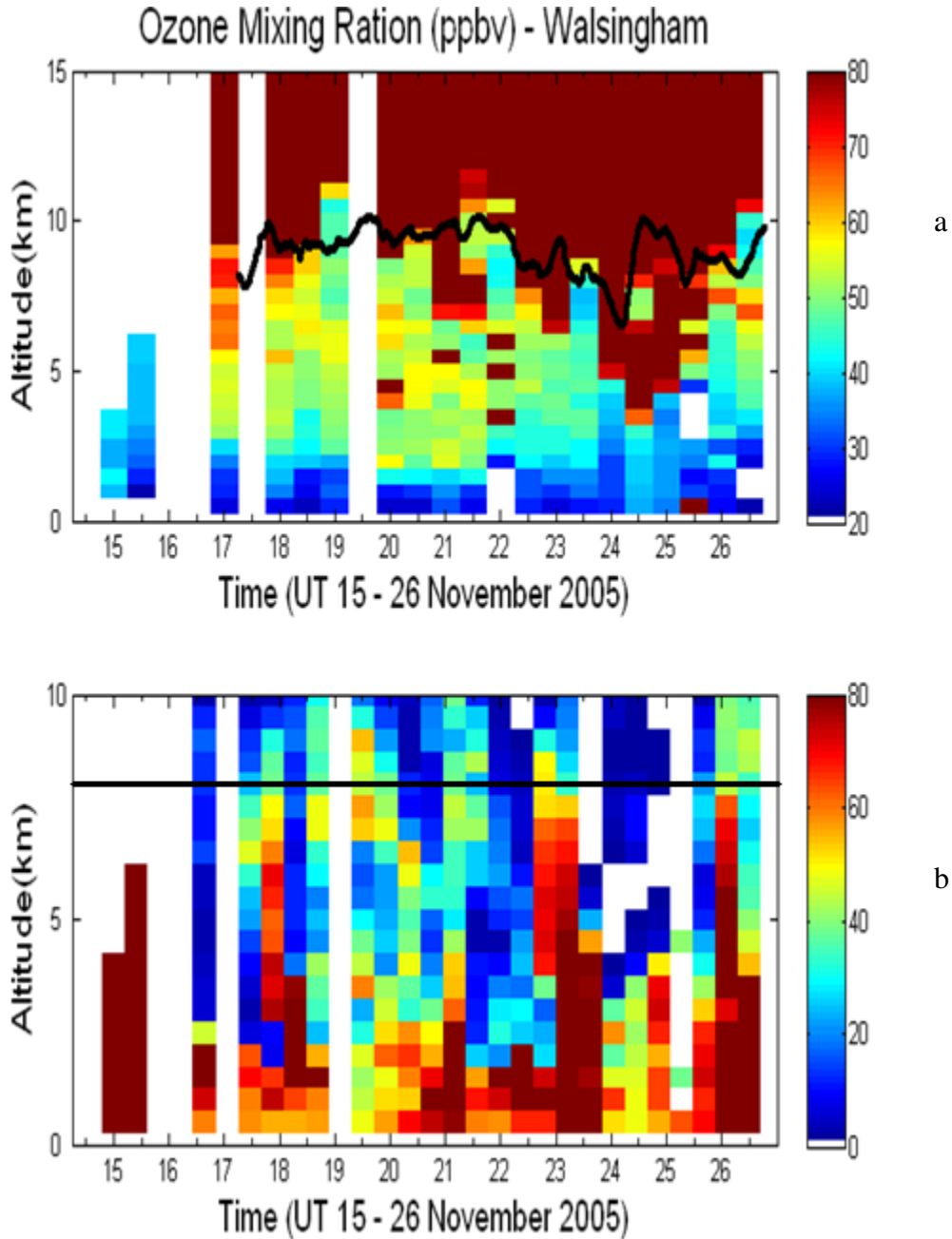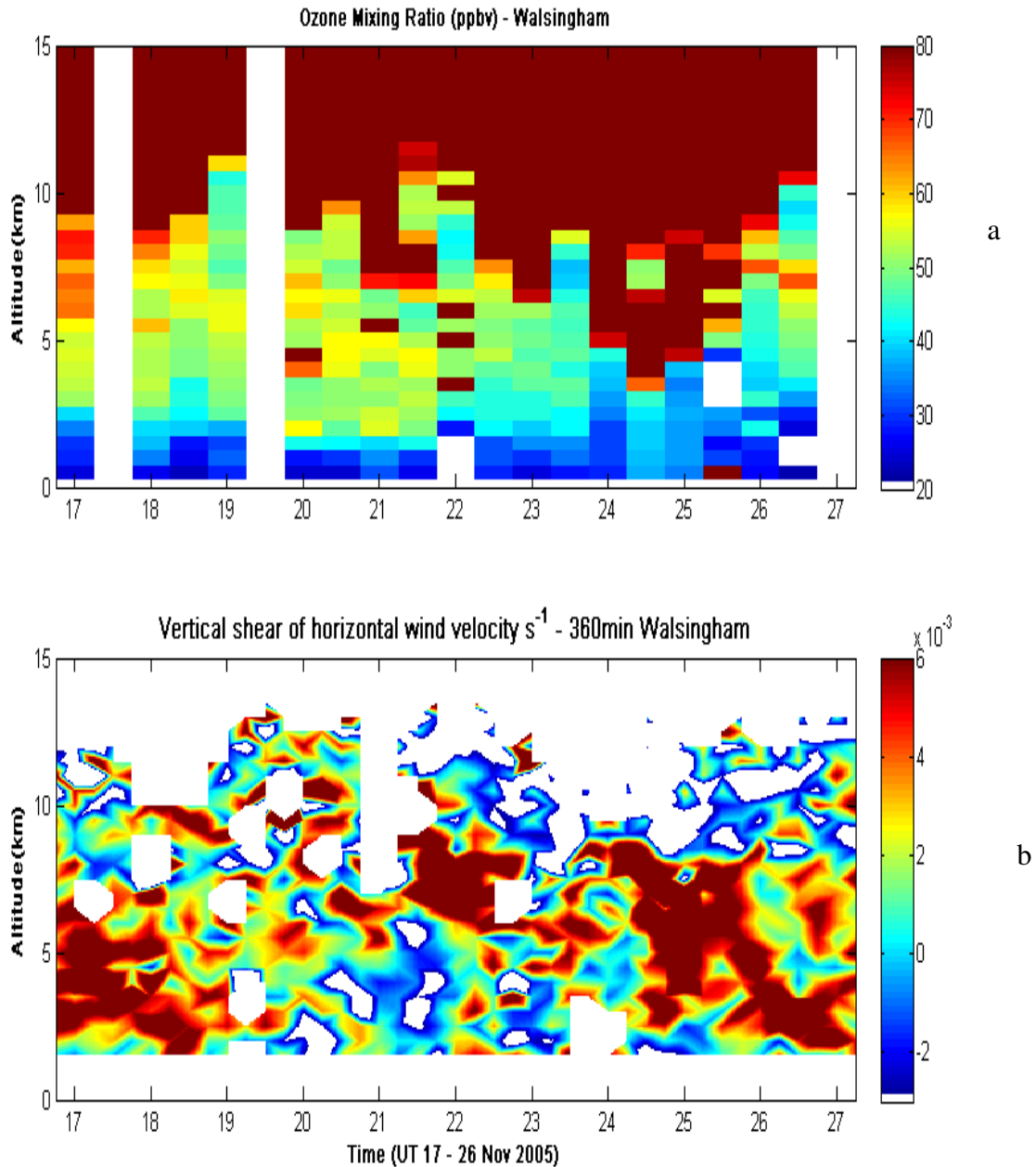
Figure 3.9. Walsingham Ozonesonde Measurements for the Campaign of November 2005. Same as in Figure 3.4 except for time period 17 – 26 November 2005 at Walsingham and the wind shear averaged over 6 hours. The ozonesondes were released at around 00:00 UTC and 12:00 UTC.

From the two cases (i.e., 22nd – 23rd and 24th – 25th November), the intensity of the wind shear in the upper troposphere appears to be positively correlated with the observed stratospheric ozone intrusion events. This reinforces the fact that strong wind shear plays

an important role in mixing of air mass from the lowermost stratosphere to the upper and lower troposphere, since stronger instability might be the cause for more effective STE. Strong wind shear may also be an indicator of enhanced gravity wave activity.

Another atmospheric dynamic that also plays a crucial role in stratosphere-troposphere exchange of ozone is the turbulent kinetic energy dissipation rate. It is one the parameter that windprofilers measure with good temporal and spatial resolutions. In this section, we also discuss the role of turbulence in the upper troposphere and lowermost stratosphere in the stratosphere-troposphere exchange of ozone. The measurement of turbulent kinetic energy dissipation rate (W/kg) shown in the Figure 3.10 was made during the Walsingham ozonesonde measurements campaign in November 2005.

In this thesis, we have analyzed turbulent kinetic energy dissipation rate data measured by windprofiler radar at Walsingham during the Walsingham ozonesonde measurements campaign from 17 – 26 November 2005. Turbulent kinetic energy dissipation rate averaged over 6 hours is used in order to study the impact of atmospheric turbulence on STE of ozone during the Walsingham 2005 campaign. Radar measurements of turbulent kinetic energy dissipation rate in the height range between 5 and 12 km are compared with the intrusion of the stratospheric ozone obtained from ozonesonde at the same time. The simultaneous measurements of turbulence and ozone mixing ratio using radar and ozonesonde, respectively, help correlate turbulence and the observed enhanced ozone concentration in middle and upper troposphere which as a result facilitates the study STE of ozone.
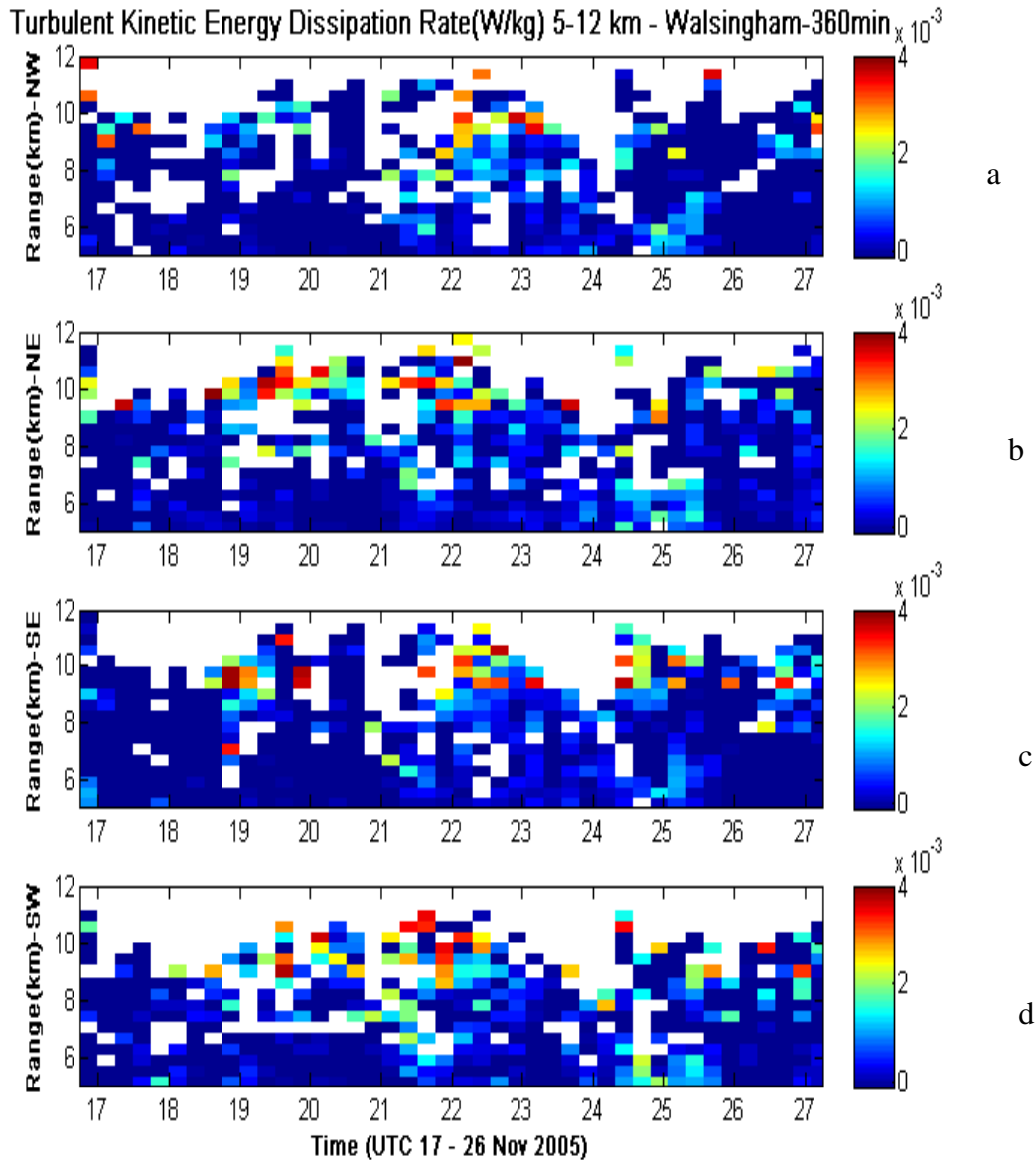
Figure 3.10. Walsingham Ozonesonde Measurements for the Campaign of November 2005. Same as in Figure 3.5 except for time period 17 – 26 November 2007 at Walsingham and the turbulence was averaged over 6 hours.

Figure 3.10 depicts the mean values of turbulence kinetic energy dissipation rate for heights from 5 – 12 km for a time period of 17 – 26 November 2007. The four panels (i.e., Figures 3.10 a - d) show the height-time cross section of the turbulent kinetic energy dissipation rate when the radar beam points in the direction of northwest, northeast, southeast and southwest, respectively. The most severe occurrence and the only turbulent

region that has to do with stratospheric ozone intrusion, occurred on 21st - 22nd November above 8 km altitude. On the other hand, an enhanced ozone concentration at the upper troposphere was observed in the middle and upper troposphere on 22nd – 23rd November which suggests the strong turbulence observed on the 21st - 22nd November may have made a contribution in the intrusion of stratospheric ozone in to the troposphere. Nevertheless, we do not see any outstanding turbulence activity that has to do with the extremely enhanced ozone concentration on the 24th – 25th November. This result suggests two possibilities. One the one hand it demonstrates that in order for stratosphere-troposphere exchange of ozone takes place strong turbulence is not necessarily required since other parameters can cause the intrusions. On the other hand, there is also possibility that radar missed to detect strong turbulence.

The absence of turbulence does not necessarily suggest a complete lack of turbulence because there is a possibility that the radar will not detect turbulence if strong turbulence mixes the air uniformly and the parcel of air is transported adiabatically to a new position [Hocking 2011]. This can be illustrated through Figure 3.9b. On 24th - 25th November, we can see a strong wind shear between about 2 km up to 10 km altitude which appears to have strong association with the enhanced ozone concentration seen by ozonesonde the same day while, we do not see strong turbulence detected by radar on the same date as shown in Figure 3.10. It is believed that wind shear causes turbulence but the strong wind shear observed in Figure 3.9b on 24th – 25th November did not result in turbulence. This might be either due to the fact that radar missed to detect strong turbulence as a result of mixing the air uniformly, or in fact there was no turbulence.

The height-time cross-section of turbulent kinetic energy dissipation rate, for example Figure 3.10, shows the occurrence of strong turbulence to be rare; however such turbulence may impact atmospheric composition. This might be noticed on 21st – 22nd November of Figure 3.10, where results in high ozone concentration occurred on 22nd – 23rd November in the upper troposphere. This suggests that the turbulence may cause effective and irreversible transport of lower stratospheric air mass deeply into the troposphere. Therefore, turbulence enhanced around the tropopause may cause noticeable stratospheric ozone intrusion to the troposphere.

Our findings show a unique combination of simultaneous measurement of radar and ozonesonde to study stratosphere-troposphere exchange of ozone. The radar estimation of tropopause heights detects the intrusion of stratospheric ozone measured by ozonesonde. Moreover, radar measurements of atmospheric dynamics such as variance of vertical wind, vertical wind shear and turbulence strengths help identify the cause of stratospheric ozone intrusion. Stratospheric air masses descend in to the upper tropospheric across the tropopause mostly as a result of these parameters. Moreover, this work shows that the transport of ozone across the tropopause could have a noteworthy effect on the budget of atmospheric chemical composition, particularly for trace gases such as ozone and this in turn will have impact both in air quality and climate change.

3.3   The Montreal 2005 Ozonesonde Campaign

The Montreal 2005 ozonesonde campaign was made at the Canadian Space Agency Head Office in St Hubert, Quebec about 45 km away from the location of the nearest windprofiler radar, which was situated at the MacDonald campus of McGill University (45.41^{o}N, 73.94^{o}W). The campaign was made from 29 April – 10 May 2005. Like other campaigns, the ozonesonde releases were at a temporal density of two per day except on the 10th May which had only one per day. The launches were made at 00:00 and 12:00 UTC with a total of 23 launches. Detailed technical specifications of the radar and the balloon-born ozonesondes equipped with GPS are mentioned in chapter 2.
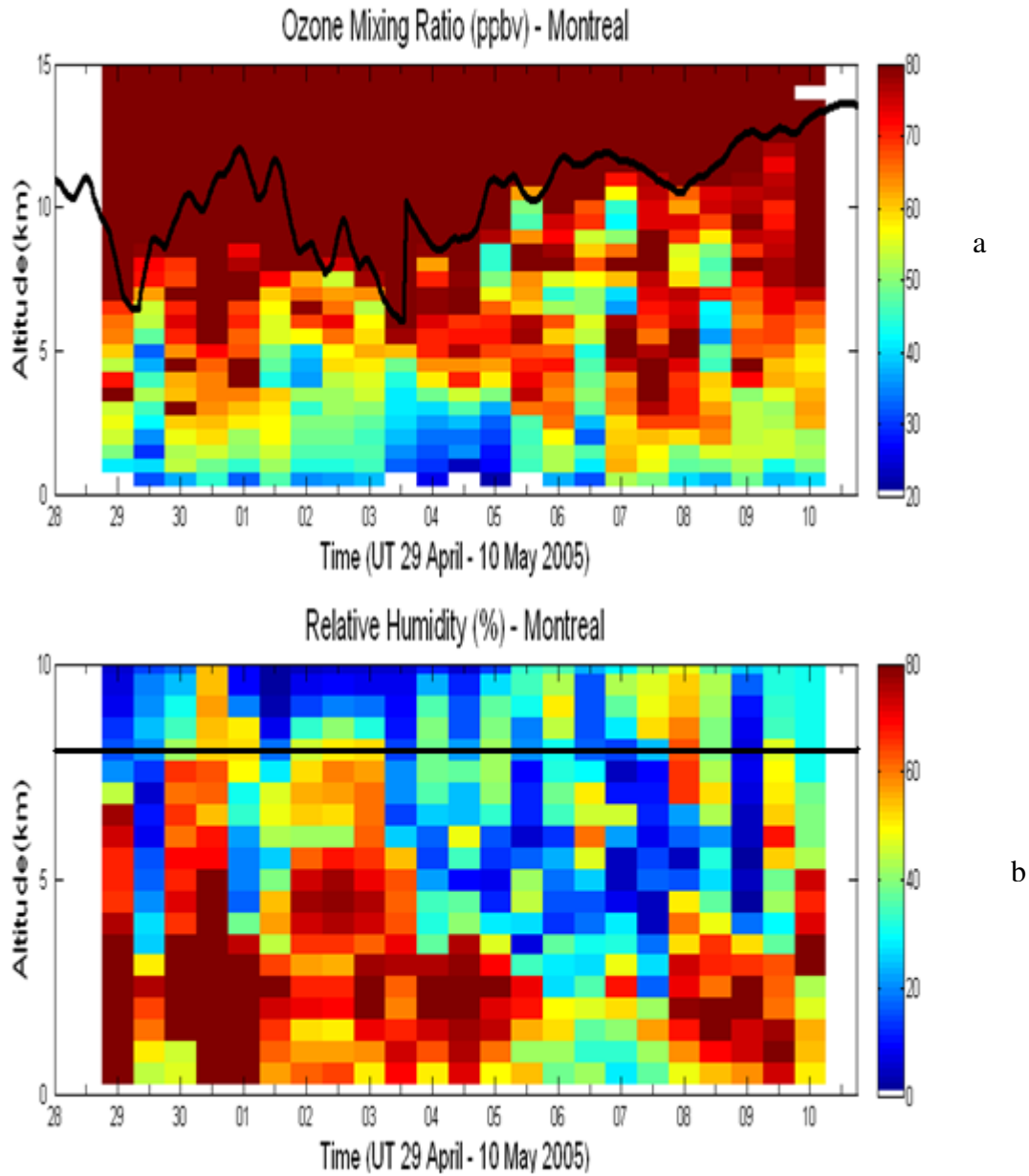
Figure 3.11. Montreal Ozonesonde Measurements for the Campaign of April – May 2005. This is the same as in Figure 3.2 except for the period 29 April – 10 May 2005 at Montreal.

To estimate the tropopause heights shown in black line (Figure 3.11a), the vertical beam of radar powers with same frequency range mentioned previously were used during the time period from 29 April to 10 May. The same procedure as we stated in the previous section was also applied so as to reveal the tropopause height. The result is shown in

Figure 3.11a above. The lower edge of a thin secondary layer is seen at 6 - 14 km, representing the radar tropopause, and rapid tropopause ascent is seen on 29th - 30th April, 3rd May and modest tropopause ascent on 5th and 8th May. These were the only significant tropopause movements during the campaign.

In Figure 3.11a, the black line on the contour plot of ozone mixing ratio is the radar derived tropopause heights determined from the plot of backscattered radar power (expressed in common logarithmic scale) observed by the windprofiler radar at McGill as a function of height and time. The tropopause heights have been smoothed using a 9 hour running mean filter. Enhanced concentrations of ozone at the middle and upper troposphere were observed during 30 April – 1 May, 4 - 6 May, 7 - 8 May and 9 - 10 May 2005. As can be seen from Figure 3.11b, the relative humidity is fairly low except in the first event which suggests that ozone-rich stratospheric air might have transported into the troposphere. During these events the observed ozone concentration at heights as low as 2 km altitude is higher than the average volume mixing ratio of ozone in the troposphere.

The radar derived tropopause height, the black line shown in Figure 3.11a, reveals big sudden jumps on 29 - 30 April, 3 May and modest jumps on 5 and 8 May. The correlation of sudden jumps of tropopause height with stratospheric ozone intrusion is clearly shown in the work of Hocking et al. [2007]. Even though modest jumps were observed on 5 and 8 May, in all the four cases there can clearly be seen an apparent enhancement of ozone concentration as low as 2 km followed the tropopause jumps. The descent of stratospheric ozone begins following the tropopause events.

The next step is to make use of the capability of windprofilers to measure horizontal and vertical velocities, the variance of vertical velocities and turbulence strengths as in the previous case. Figure 3.12 represents the contour plots of ozone mixing ratio in part per billion by volume and the standard deviation of vertical velocity of wind averaged over 6 hours in m/s.

Figure 3.12. Montreal Ozonesonde Measurements Campaign April – May 2005. This is the same as in Figure 3.3 except for the period 29 April – 10 May 2005 at Montreal and standard deviation of vertical wind averaged over 6 hours. The ozonesondes were released at around 00:00 UTC and 12:00 UTC.

Figure 3.12b shows the height-time intensity plot of the standard deviation of vertical wind for the period of 28 April – 10 May 2005. It was averaged over a time period of 6 hours. The purpose of taking the average over 6 hours was to see the effect of standard deviation vertical wind over a larger period of time so as to see the persistency of the vertical variation of the wind. Figure 3.12b clearly shows a strong standard deviation of vertical wind of more than 0.20 ms^{-1} on 29th April, 1st May and 6th – 7th May in the height range of 8 - 14 km. The strong standard deviation of vertical wind velocity of more than 0.25 ms^{-1} which was noticed on 29th April from altitudes as low as 2 km up to 14 km was

a strong activity which appears to be an atmospheric dynamical effect that may be responsible for bringing down ozone rich dry air as seen on 30 April – 1 May. The standard deviation of vertical wind velocity of approximately 0.20 ms^{-1} on 6th – 7th May from about 8 – 13 km seems to have contribution on the enhanced stratospheric ozone on 7th – 8th May. Nevertheless, we do not see the effect of the strong standard deviation of vertical wind observed on 1st May on stratospheric ozone intrusion. Moreover, there were enhanced ozone concentrations in the upper and middle troposphere on 4th - 5th May and 9th – 10th May despite weak standard deviation of vertical wind noticed during this times, which suggest that standard deviation of vertical wind velocity is not necessarily required in order to bring down dry ozone rich air from the stratosphere to the troposphere. The strong correlation between the standard deviation of vertical velocity and the mixing ratios of ozone in the troposphere implies that it may be the proxy for gravity waves that brings down ozone rich air from the stratosphere to the upper and lower troposphere.

As in previous sections, we now turn to considerations of the effect of vertical wind shear and turbulence strengths. We have diagnosed the vertical wind shear of horizontal velocity and turbulence and the results are shown below. We anticipate that all or any combinations these dynamics can cause the intrusion of stratospheric ozone.

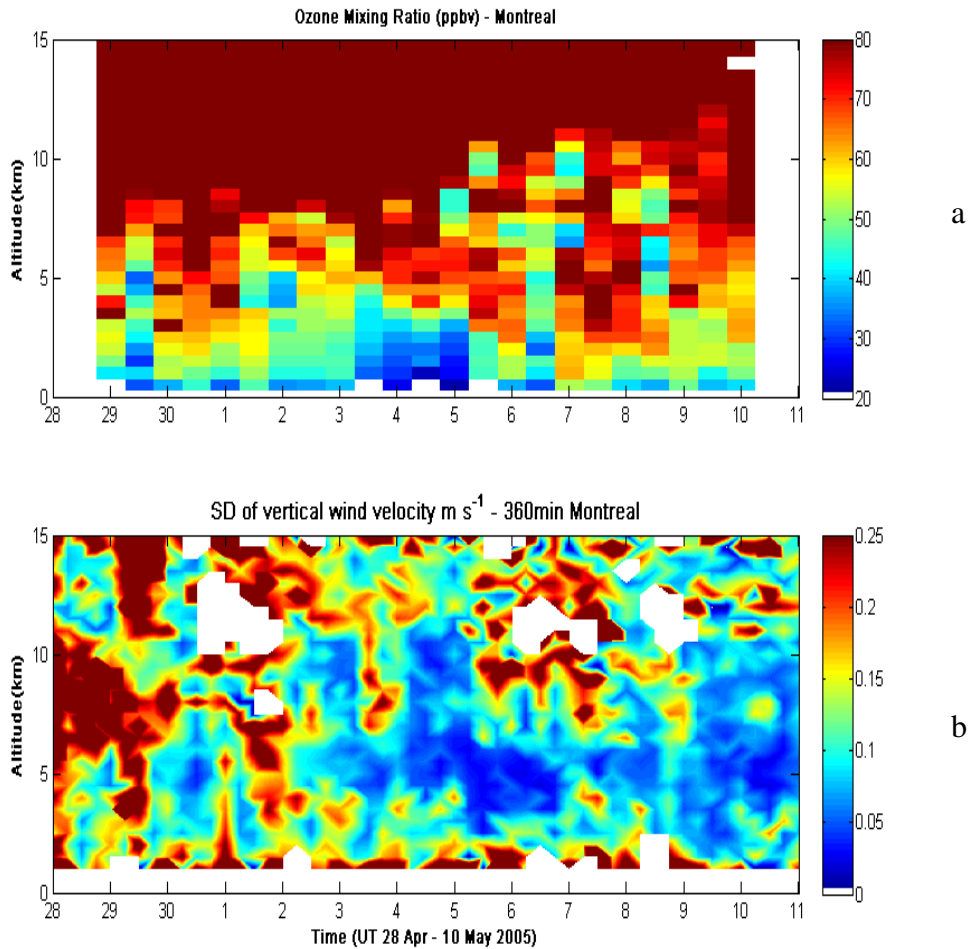**Figure 3.13. Montreal Ozonesonde Measurements Campaign April – May 2005. This is the same as in Figure 3.4 except for the period 29 April – 10 May 2005 at Montreal and the vertical wind shear is averaged over 6 hours. The ozonesondes were released at around 00:00 UTC and 12:00 UTC.**

Figure 3.13b demonstrates windprofiler measurements of wind shear averaged over a period of 6 hours. As can be seen from the figure, a fairly strong wind shear is observed on 30th April - 1st May from about 5 km up to 11 km which seems to have association with the observed enhanced stratospheric ozone on the same day. On 3rd May, although the altitude range is small, strong wind shear is noticed between about 5 and 9 km which was accompanied with high stratospheric ozone in the middle and upper troposphere on

4th - 6th May. Moreover, on 6th - 7th May one can see a strong wind shear between about 5 and 11 km which appears to have coincided with the observed enhanced high ozone concentration on 7 - 8 May. Nevertheless, we do not observe any strong wind shear that has to do with the enhanced ozone concentration on 9 - 10 May 2005 which suggests that we don't necessarily observe a large wind shear in order for stratospheric ozone intrusion to take place. From the three cases, the intensity of the wind shear in the upper troposphere appears to be correlated with the observed stratospheric ozone intrusion events. This means that strong wind shear plays a significant role in mixing of air mass from the lowermost stratosphere to the upper and lower troposphere since stronger instability might be the cause for STE of ozone.

Next, we again consider the role of turbulence strengths. We have analyzed turbulent kinetic energy dissipation rate measured by windprofiler radar at McGill during the Montreal ozonesonde measurements campaign from 29 April – 10 May 2005. Averaged over a period of 6 hours is used in order to examine the impact of atmospheric turbulence on STE of ozone on longer time. Radar measurements of turbulent kinetic energy dissipation rate in the range between 5 and 12 km are compared with the intrusion stratospheric ozone obtained from ozonesonde during the same time.

Figure 3.14 depicts the turbulence kinetic energy dissipation rate for heights from 5 – 12 km for the period of 28 April – 10 May 2005. The four panels (i.e., Figures 3.14 a - d) show the height-time cross section of the turbulent kinetic energy dissipation rate when the radar beam points in the direction of northwest, northeast, southeast and southwest, respectively.
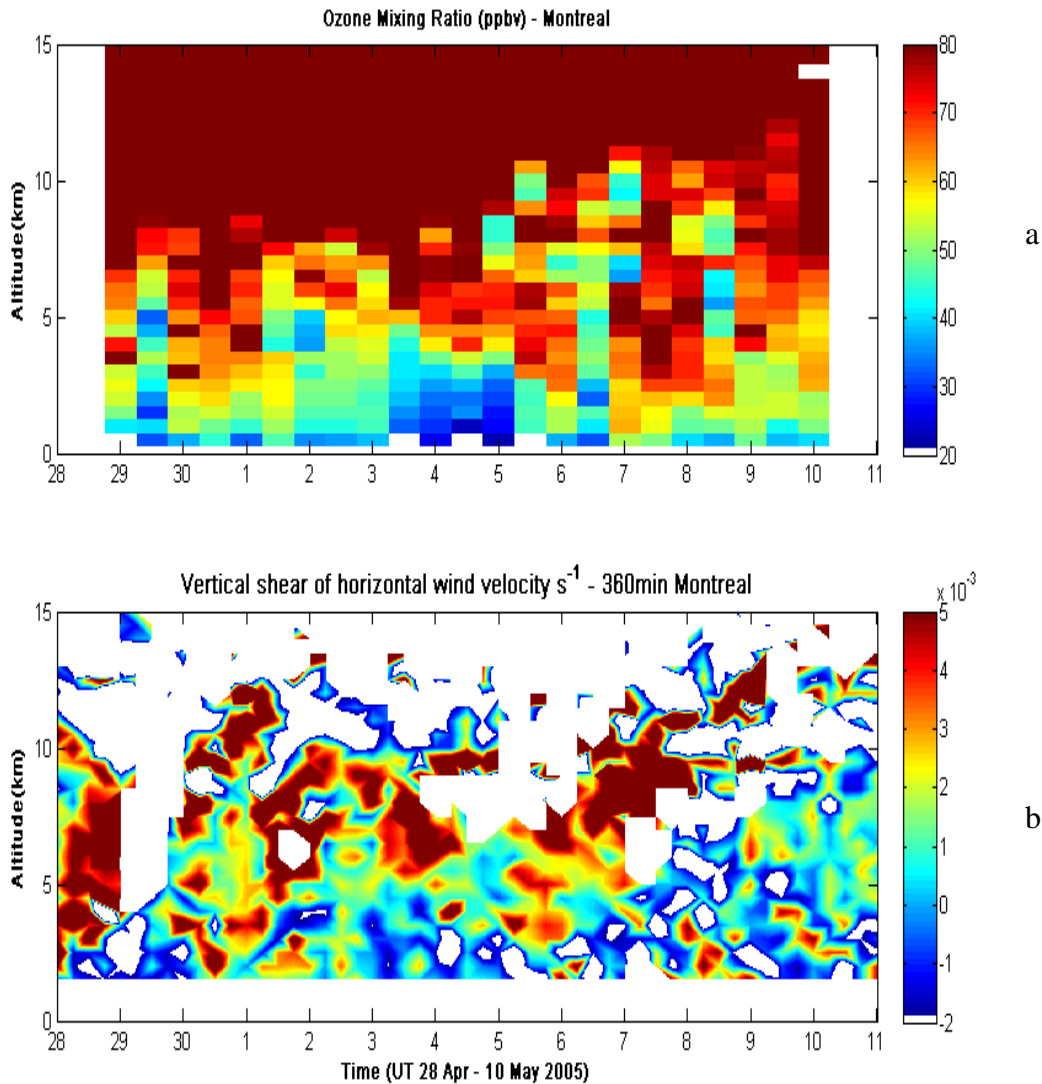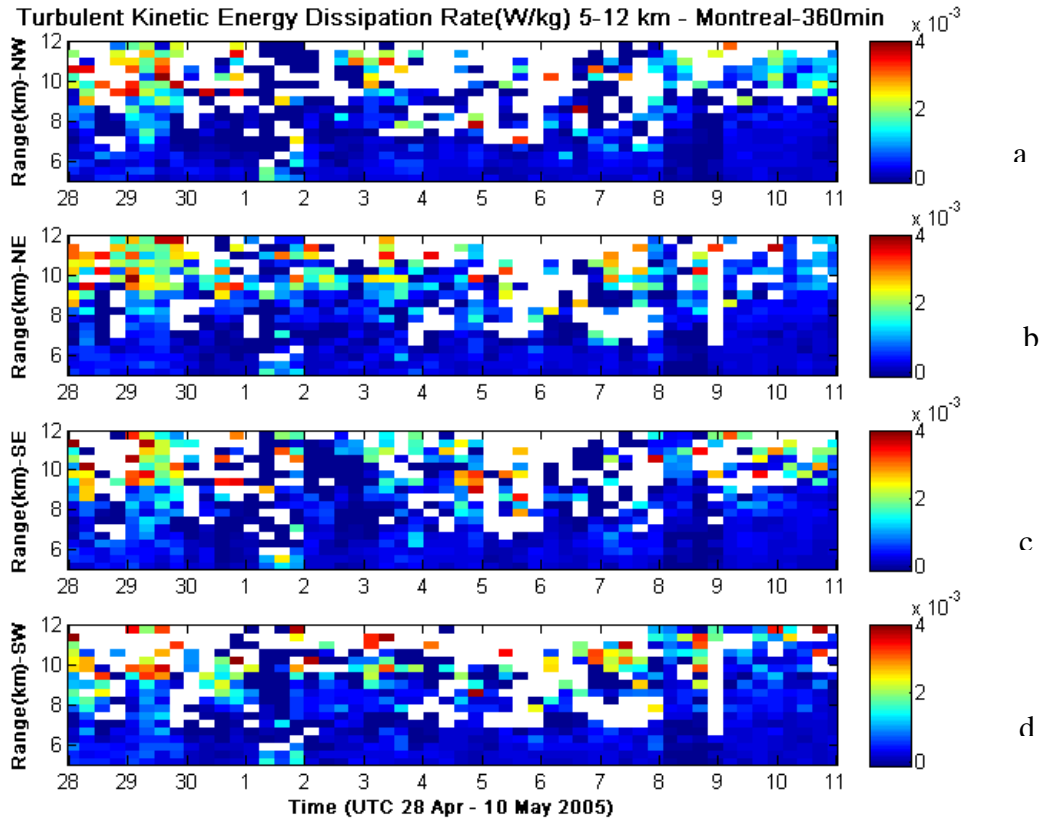
Figure 3.14. Montreal Radar Measurements of Turbulence April – May 2005. This is the same as in Figure 3.4 except for the period 29 April – 10 May 2005 at Montreal and the turbulence is averaged over 6 hours.

As can be seen from the figure, the most turbulent occurred on four of the plots on 29th April above 9 km altitude. On the other hand, an enhanced ozone concentration at the middle and upper troposphere were observed on 30 April – 1 May which suggests the strong turbulence observed on the 29th April may have contributed to the intrusion of stratospheric ozone in to the troposphere. Moreover, from Figure 3.14 one sees fairly strong turbulence on the 30th April, this can amplify the intrusion of stratospheric ozone that was seen on 30 April -1 May. Even though we notice in Figure 3.14 the association of strong turbulence with stratospheric ozone intrusion on 30 April -1 May, we do not see any outstanding positive correlation between turbulence and stratospheric ozone intrusion for the remaining events. Nevertheless, we notice fairly strong turbulence on the 3rd May above 9 km altitude which may be one of the causes for the enhanced ozone concentration on the 4th – 6th May. It is clear from the four panels of Figure 3.14 that

turbulence is persistently strong on 29 - 30 April above 8 km altitude while on 7th May strong turbulence is seen only on the second and forth panels (Figures 14a and d) above 9 km altitude.

As explained and showed in earlier sections, the absence of turbulence does not necessarily mean a complete lack of turbulence. This can again be illustrated through Figure 3.13b. On 6th - 7th May, we can see a strong wind shear between about 5 and 11 km altitude which appears to have association with the enhanced ozone concentration seen by ozonesonde on 7 - 8 May while the turbulence during this time doesn't seem to be persistently as strong as turbulence on 29 - 30 April. It is known that wind shear is one of the causes of turbulence but on 6th – 7th May (Figure 3.14) we do not see strong turbulence detected by radar which may be because this strong turbulence mixes the air uniformly so that the radar missed it.

High enhancements of ozone concentrations in the middle and upper troposphere on 9th – 10th May do not seem to coincide with any of the parameters that we have diagnosed above. As can clearly be seen from Figures 3.12 - 3.14, the standard deviation of vertical wind, vertical wind shear of horizontal wind and turbulence strengths were weak before or during the 9th – 10th of May. It is, therefore, possible that the enhancement of the observed stratospheric ozone intrusion may not be related to any of the atmospheric dynamics that have been diagnosed. On the other hand, there is a possibility that the occurrence of enhanced stratospheric ozone may be associated with all of the parameters that have been analyzed. For example, the observed high stratospheric ozone concentration on 30th April – 1st May coincides with strong standard deviation of vertical velocity, vertical wind shear and turbulence strengths during or before the intrusion. Hence, further studies would be necessary to ascertain the atmospheric dynamics responsible for the intrusions of stratospheric ozone in such cases where the atmospheric parameters are weak, yet intrusions still occur, for example on the 9th – 10th of May.

In the case when the atmospheric parameters are weak in relation to the intrusions of stratospheric ozone, it is possible that the observed stratospheric ozone peak in the troposphere might arise due to the long range transport of ozone. This further can be

examined through numerical modeling utilizing GEM-FLEXPART, which among other methods, simulates the long range atmospheric transport and deposition of trace gases including ozone. Moreover, the radar measurement of wind, particularly horizontal wind velocity, may be used to support this if the concept of dynamical transport when it occurs with the wind. Such results can be found for the Eureka 2008 campaign [Osman et al., 2010].

3.4   Summary of observational results

In this section, we summarize the observational results that we have obtained for other campaigns including the ones have been mentioned above. The association of stratospheric ozone intrusion with radar measurements of atmospheric dynamics is depicted in Table 3.1 below.

Table 3.1. Simultaneous measurements of ozonesonsonde and windprofiler radar for different ozonesonde campaigns.

Name of campaign	Number of Major Ozone Intrusion Events	Dates of Observation: High ozone and low relative humidity	Standard deviation of vertical wind		Vertical shear of horizontal wind		Turbulent Kinetic Energy Dissipation Rate	
Montreal 2005 29 Apr – 10 May	4	0430; 0504; 0507; 0509	SWSW	360min	SSSW	360min	SMWW	360min
Walsingham 2005 17 – 26 Nov	2	1121;1124	SS	360min	SS	360min	SM	360min
Walsingham 2007 23 Feb – 4 Mar	2	0226; 0302	SS	120min	SS	180min	SS	360min
Egbert 2009 5 - 11 May	2	0508; 0510	SS	120min	SS	120min	SS	120min
Eureka 2010 24 Feb - 12 Mar	3	0301; 0308; 0312	SSI	360min	SSI	120min	WWM	120min
Egbert 2010 12 Jul – 4 Aug	7	0714; 0716;0719; 0722; 0725; 0727; 0729	WWSSSSM	360min	MWSSSSM	360min	SSSSSWS	60min
Montreal 2010 12 Jul – 4 Aug	5	0714; 0722; 0724; 0729; 0803	MNSSS	360min	SNSMS	360min	SNSSS	60min

I, M, S, and W denote inconclusive, medium, strong and weak radar observed parameters during the campaign, respectively. N indicates absence of radar data. The period of time used for calculating the parameters are indicated by the time column.   Dates of observations indicated are read as MMDD.

The windprofiler radars measurements atmospheric dynamics we have diagnosed are standard deviation of vertical wind, vertical shear of horizontal wind and turbulence

strengths around the tropopause region, since these parameters are believed to be necessary for understanding and causing the cross-tropopause air mass exchange processes.

The Egbert 2010, the Walsingham 2007 and the Montreal 2010 ozonesonde campaigns were made at the sites described in sections 1, 2 and 3, respectively. The Montreal 2010 campaign was made during the period 10 July – 4 August 2010. There was one flight each day except some missing flights on July12[th], 19th, 23rd, 27th, and August 4th. In the Walsingham 2007 ozonesonde campaign, two launches per day (except on the 24th February and 4th March) were made during 23 February – 4 March 2007. The Egbert 2010 ozonesonde campaigns was made from10 July – 4 August 2010. Each day there was one flight except some missing flights on July13[th], 18th, 31st, August 1st, 3rd and 4th. The Eureka 2010 ozonesonde campaign was made at Eureka, Nunavut (79.99[o]N, 85.94[o]W) from 24 February - 12 March 2010. One launch per day was made except on the 27th of February.

The campaigns shown in Table 3.1 involved a total of 6 campaigns at midlatitudes, Southeastern Canada, and one at high latitude, Northern Canada, intensive operational days. The launching time was in general around 00:00 and 12:00 UTC. Table 3.1 reveals that there was a total of 25 major intrusion events in all the 7 campaigns. During the intrusion events the standard deviation of vertical wind was strong 68% of the time, vertical shear of the horizontal wind was strong 72% and turbulence strengths was 64%. This shows a strong relationship between enhanced ozone rich dry air in the upper and lower troposphere and strong atmospheric activity. This confirms our results found in sections 3.1 – 3.3, namely that stratospheric ozone transport and mixing in to the troposphere is arrived by atmospheric dynamics that the radar measured. These measurements provide confirming and exciting evidence of the relation between stratosphere-troposphere exchange of ozone and such dynamical events. This is important for the detection of stratospheric ozone intrusion, and deducing the atmospheric parameters that are probably responsible for the intrusion events.

As can be noticed from the table, during every event, at least one of the three atmospheric dynamical parameters were strong except

    i.   on 0509 (in the Montreal 2005 campaign case)

    ii.   Eureka 2008 (when transport was important from a source to the south of Eureka, not shown in the table)

Our intensive ozonesonde campaigns have revealed the association of stratospheric ozone intrusion and the role of atmospheric dynamics in the processes. From Table 3.1, one can clearly see that the atmospheric dynamics responsible for the intrusions varies from case to case. On the one hand, we see that all parameters can act simultaneously which clearly amplifies the intrusions. On the other hand, we see either any combination of the parameters or only any one of them to act and result in intrusions. This work demonstrates that the introduction of wind profilers has revolutionized in studying the dynamics of the lower atmosphere with their excellent height and temporal resolutions [Gage and Balsley, 1978; Balsley and Gage, 1982]. Moreover, windprofiler radars, in conjunction with frequent ozonesonde launches, have provided a way of detecting stratosphere-troposphere exchange utilizing radar derived tropopause heights and have provided a unique look at the dynamics that cause the stratospheric ozone intrusion. Hence, the combination of windprofiler and ozonesonde plays a significant role in better protecting the environment and more effectively regulating emissions, since the technique helps detect the sources and sinks of ozone-related atmospheric pollutants in the lower atmosphere.

Our experimental observations have also been supplemented using GEM-FLEXPART, a Lagrangian particle dispersion model. This model tracks stratospheric ozone particles as they cross the tropopause, and allows for an estimation of the quantity of ozone brought into the troposphere. It can also be run backward in time so as to determine the source. In the next chapter, we will discuss the numerical results we have obtained from GEM-FLEXPART, which further support our observational results.

Chapter 4

4 GEM-FLEXPART Numerical Simulation

In parallel with analysis of observational data, accurate modeling of atmospheric transport is critical to quantitatively associate observed tracer distributions with sources and sinks, and then to assess the anthropogenic and natural impacts on the environment. This ultimately addresses issues of environmental concern. FLEXPART [Stohl et. al., 2002, 2005] is among the many modeling tools to study atmospheric chemical species. In this model, a small volume of air is advected using the mean horizontal and vertical winds from a meteorological model. FLEXPART, which can potentially address our environmental concerns, is the model that I have been using in my studies.

We run FLEXPART both in the forward and backward modes in order to determine the stratospheric air intrusions. In this simulation, FLEXPART utilizes meteorological wind fields obtained from the Environment Canada's Global Environmental Multiscale (GEM) Model version 3.2.2 as an input to describe the transport of air parcels in the atmosphere. The model description is found in chapter 2 subsection 2.7.3. 2,000,000 (forward mode) and 600, 000 (backward mode) particles were released in each FLEXPART run.

All of our experimental observations are supplemented by computer simulation with GEM-FLEXPART. In the next sections, we discuss computer simulation results which can be obtained using FLEXPART and GEM models, so as to simulate the intrusions of ozone originated from the stratosphere, by running the combined models in both forward and backward mode. Afterwards, we use GEM-FLEXPART which refers to an integrated model using both GEM and FLEXPART.

4.1 Simulation of the Egbert 2009 Ozonesonde Campaign

To simulate transport processes, we employed the Lagrangian particle dispersion model FLEXPART, version 6.2. We ran GEM-FLEXPART in the forward mode during the period of 5 – 11 May 2009 in order to unambiguously confirm the stratospheric origin of high ozone concentration seen at the middle and upper troposphere on 8 – 11 May 2009.

We also ran GEM-FLEXPART in backward mode to further support the result and increase our level of certainty. The forward simulation describes where a particle will go and the backward simulation indicates where it came from. As a result, they are used to interpret measurements of atmospheric trace gases so as to set up relationships between their sources and their receptors [Stohl, 1998].

The results of GEM-FLEXPART are depicted in the next subsections. The numerical modeling indicates a significant downward motion that results in a deep stratospheric ozone influx over Egbert which evidently confirms to us that the enhanced ozone above Egbert originated in the stratosphere. Moreover, the GEM-FLEXPART simulation reveals that ozone rich dry air partially came from western Canada.

4.1.1 Forward Simulation

GEM-FLEXPART forward simulations are helpful for visualizing the dispersion of ozone originated in the stratosphere. We calculated the transport of ozone released in the stratosphere to see the effect an emission source has on downstream concentrations. The simulations started on 5 May and ended on 11 May 2009. During this period, particles were released across North America, [25.0^{o}N, 84.5^{o}N] x [60.5^{o}W, 120.0^{o}W] between altitudes of 10 and 28 km above ground. The total number of particles used was 2, 000, 000. In this model, the dynamic tropopause was used to separate the stratospheric and tropospheric air masses. The ozone tracer was initialized in the stratosphere, i.e., above the dynamic tropopause with potential vorticity greater than 2 pvu (1pvu=10^{-6} K kg^{-1} m^2 s^{-1}), using the relation $O_3(ppb) = S(ppb\ pvu^{-1}) \times PV(pvu)$, where S a parameter that depends on season. The monthly mean values of S used were 58, 63, 69, 65, 64, 60, 51, 42, 39, 35, 39 and 51 ppb pvu^{-1} from January through December, respectively [Stohl et al., 2000]. In the same manner, new particles were created and initialized at inflow boundaries. The figure below shows a three dimensional view of GEM-FLEXPART generated simulations.
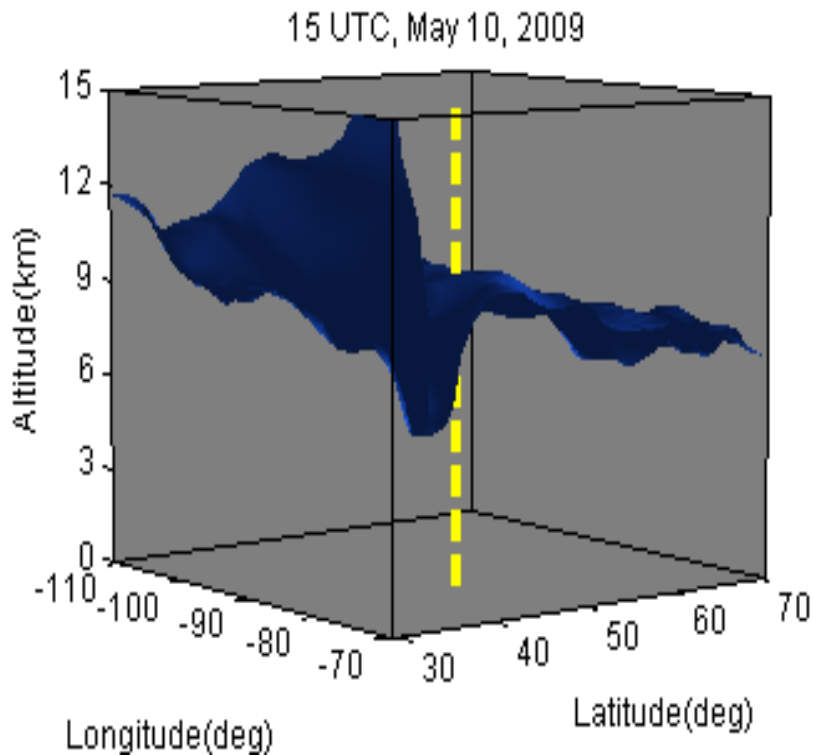
Figure 4.1. Three dimensional view of the selected instant of 2,000,000 particles released from the box [28ºN, 83ºN] X [62ºW, 119ºW] between altitudes 10 - 28 km from the ground. GEM-FLEXPART output showing the 80 ppbv ozone mixing ratio isosurface at 15 UTC on 10th May 2009. The vertical yellow dash line shows Egbert radar and ozonesonde launching site.

To visualize the stratospheric ozone intrusion in 3D, we started a 7-day forward simulation of ozone on 5 May and the result is shown in Figure 4.1. The figure reveals a snapshot of 80 ppbv ozone mixing ratio isosurface at 15 UTC on 10th May 2009 in 3D view which shows stratospheric ozone intrusions resulting in a tongue of ozone penetrating to lower troposphere over Egbert. The tongue of stratospheric air pointing down toward the radar results in sudden jumps of radar derived tropopause heights. This demonstrates a unique capability of windprofiler radar to detect the intrusion of stratospheric origin; otherwise this ozone tongue may have been missed without the use of radar. Indeed, we found the same result during the event of 9 – 11 May 2009, which is consistent with ozonesonde measurements at Egbert. The result reinforces that the dry

ozone rich air at Egbert came from stratosphere and hence the ozone mixing ratio enhancement is caused by stratosphere-troposphere exchange of ozone.

We have also looked at the two dimensional version of Figure 4.1. The average concentration of ozone in the height range between 3 and 10 km is displayed in Figure 4.2. As can be seen from the figure, ozone rich air seen at Egbert is come from the west of Egbert. The 2D view simulation (see Figure 4.2) reveals the variation of ozone mixing ratio and transport pattern of ozone as a function of latitude and longitude as time goes by.
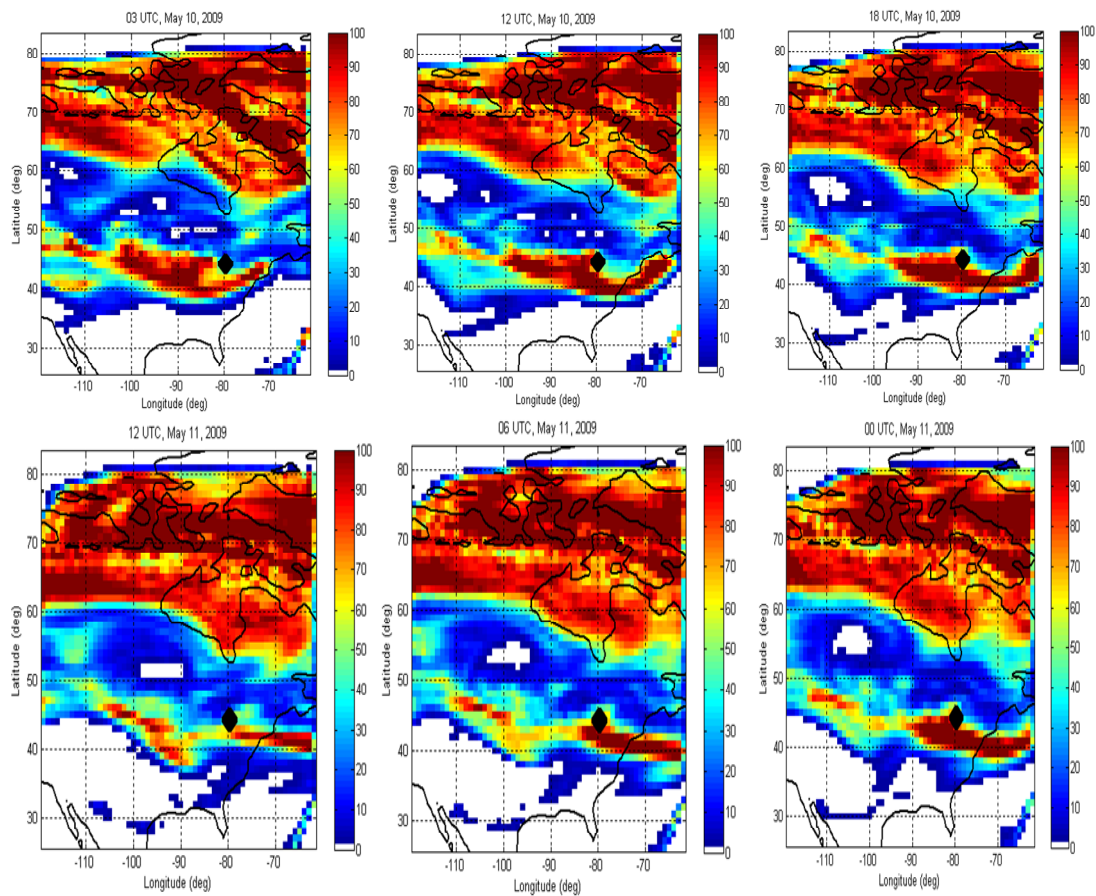
Figure 4.2. Ozone mixing ratios (expressed in parts per billion by volume, ppbv) from a GEM-FLEXPART simulation, averaged in the height range between 3 and 10 km, on 10th and 11th May 2009. The black dot represents Egbert radar and sonde launching site.

Figure 4.2 demonstrates the ozone mixing ratio (ppbv) from a GEM-FLEXPART simulation between height range 3 and 10 km over North America on 10th – 11th May 2009. Figure 4.2 reveals that stratospheric ozone intrusions take place in Egbert and areas close to Egbert. Even though we have displayed only data for 10th and 11th of May in Figure 4.2, generally a high stratospheric ozone intrusion was observed from 8 to 11 May at Egbert. As can be seen from Figure 4.2, the intrusion of stratospheric at Egbert and its neighboring area moves eastward, while its concentration decreases as it passes over Egbert and continues to move eastward.

Therefore, both the 2D and 3D views of the GEM-FLEXPART simulation suggest stratospheric influence on the ozone seen at Egbert in the upper troposphere (i.e., 7.2 – 7.3 km), which is partly confirmed by the ozonesonde measurements of low relative humidity and high ozone concentrations (see Figure 3.3). Moreover, the radar derived tropopause heights also suggest that the intrusions of stratospheric ozone followed the sudden jumps of the tropopause heights, which is consistent with the findings of Hocking et al. [2007]. As a supplement to our observational results found in chapter 3, the GEM-FLEXPART simulation of the ozone transport clearly indicates the downward influx of stratospheric ozone in to the troposphere in both 2D and 3D views. We also ran FLEXPART in backward mode to see the ozone movement as a reassurance for our result.

4.1.2   Backward Simulation

Backward time particle simulations enable the implementation of a source-receptor relationship that defines upstream influences on tracer observations at the receptor. It helps derive areas of influence that provide quantitative measures of the effects of different emissions on the air quality at receptor sites. Backward simulations with the particle model were introduced as an indispensable tool for a more detailed analysis of the source region of the observed enhanced ozone.

A total of 600,000 particles were released at the receptor, i.e., along a vertical line which spans the height range of enhanced ozone. As can be seen from Figure 4.3, low relative humidity and high ozone concentration is observed in the height range between 7.2 and

7.3 km so the receptor will be along a line between 7 and 7.5 km at Egbert (44.27°N, 79.73°W) on 10 May 2009 between 9 - 12 UTC) and it is transported backward in time for the previous 60 hours.
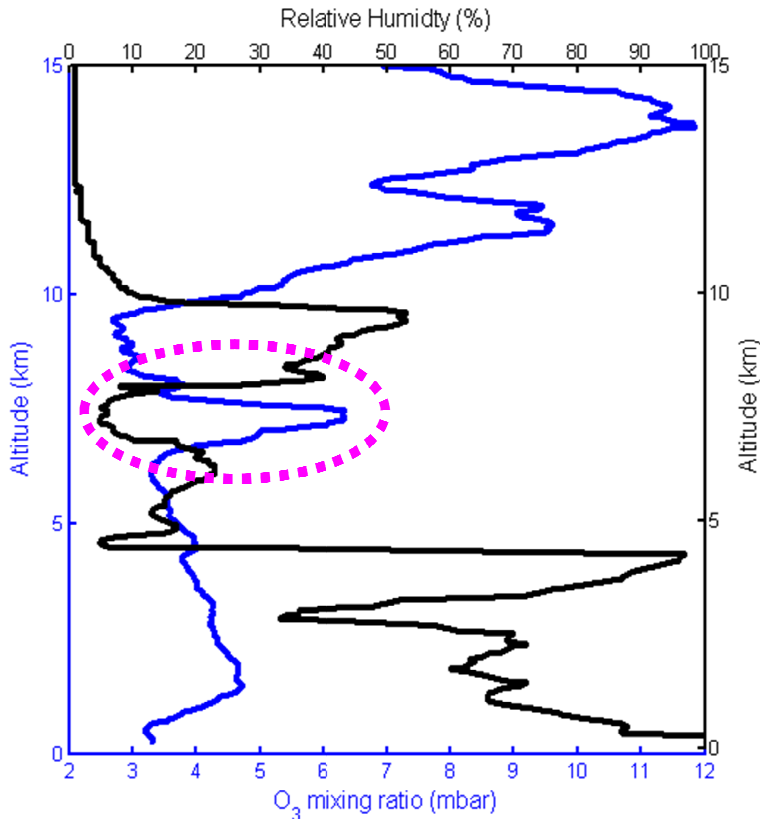
Figure 4.3. Ozonesonde measurement at Egbert on 10 May 2010 at around 11:00 UTC launch time. Particles release height and time was determined from launch time and the height where enhanced ozone concentration was observed. Accordingly, the particles were released on 10th May 2009 during 9 – 12 UTC, in the height range between 7200 – 7300 m and at Egbert (44.27°N, 79.73°W).

Signatures of the presence of stratospheric air in the lower troposphere are found for all profiles on 8 – 11 May. Figure 4.3 is one of the ozone height profiles which shows a distinct layer in the upper troposphere, i.e., in the height range between 7.2 and 7.3 km, with very low relative humidity and high-ozone mixing ratio at the Egbert station

(Ontario, Canada) on 10 May. This is a partial indicator that the ozone originated in the stratosphere. However, GEM-FLEXPART numerical modeling is required to clearly confirm its stratospheric origin. The back-trajectory numerical simulation was performed employing GEM-FLEXPART and the result is indicated in Figure 4.4.
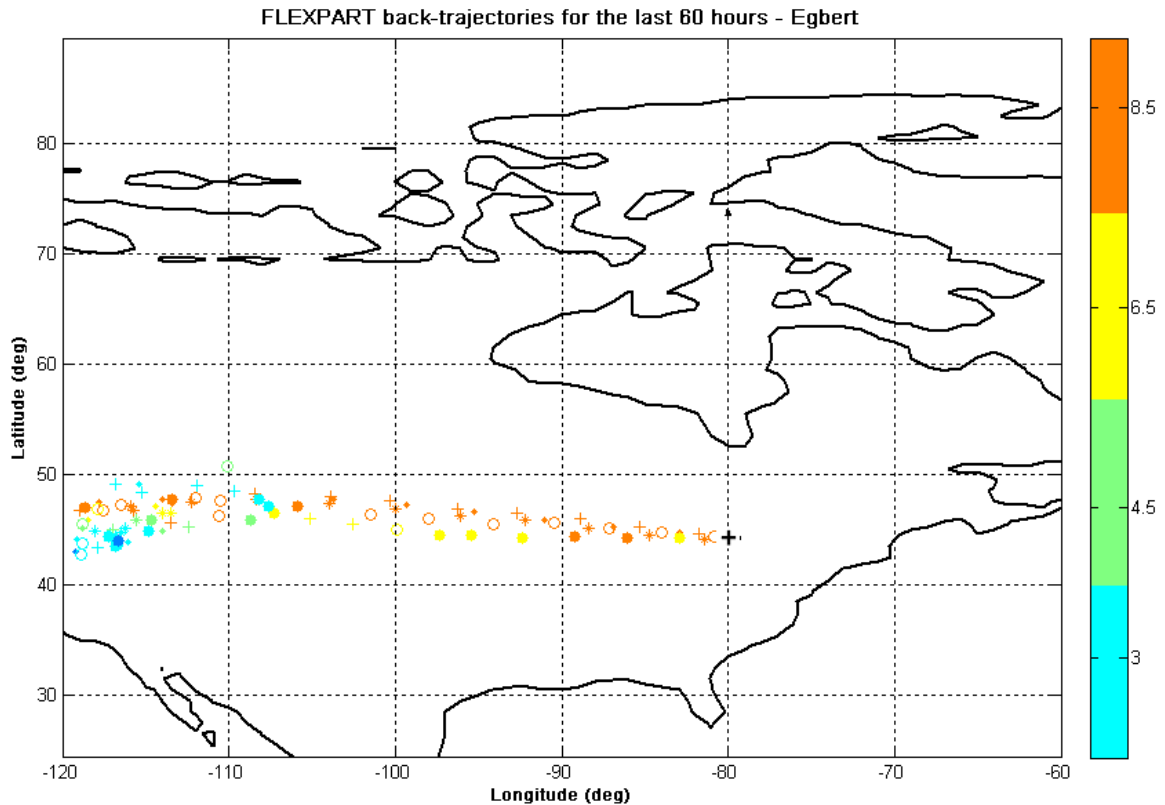
Figure 4.4. GEM-FLEXPART back-trajectories of the last 60 hours of 600,000 particles released from a line between 7 and 7.5 km at Egbert (44.27ºN, 79.73ºW) from 9 – 12 UTC. The black plus sign shows Egbert radar and ozonesonde launching site. The trajectories' colours, coded as in the label bar, refer to their actual altitude.

Figure 4.4 shows the origin and pathways of the air mass leading to the observed ozone enhancement in the upper troposphere (7.2 – 7.3 km above the ground) on 10th May 2009. The GEM-FLEXPART model, which was run in backward mode, takes into account both resolved motions and parameterized subgrid scale convection and

turbulence, using the same parameterizations as the forward model mentioned in chapter 2. The FLEXPART calculations of complex output can be compressed through clustering particles into a number of clustered positions during each output [Stohl et al., 2002]. Cluster is defined as grouping of similar trajectories during a specific time. Figure 4.4 shows the cluster back trajectories of the previous 60 hours preceding the release of the particles. In our case, the cluster parameter is 4. Variation of altitude along a given trajectory is shown by color coding, whose scale is displayed at right side of the plot.

From the backward GEM-FLEXPART simulations shown in Figure 4.4, one can clearly see that the ozone rich dry air in part came from west of Egbert. Hence, the high ozone concentration in the upper troposphere seen on 10th May 2009 at Egbert partially originated from transport from the stratosphere over the west of Egbert and blew with the wind horizontally. Our analysis of radar measurement of horizontal wind velocity (not shown in this thesis) indicates that the wind was dominantly blowing eastward, which reaffirms that the high ozone concentration at Egbert may have been in part the result of ozone which came from west of Egbert.

Even though it is believed that the long range ozone transport amplifies the amount of the observed ozone rich dry air in Figure 4.3, a considerable part of the observed enhanced dry ozone originated from the transport of ozone from the stratosphere to the troposphere. Figures 4.1 and 4.2 are clear evidence because both show the stratospheric ozone intrusion over Egbert. Furthermore, the apparent tropopause heights jump on 6th and 9th of May are also a partial indicator that the stratospheric ozone intrusion did indeed take place.

Ozonesonde measurements of low relative humidity and high ozone concentrations (see Figure 3.2) and GEM-FLEXPART numerical modeling (see Figures 4.1 – 4.4) and rapid radar derived tropopause height ascents (Figure 3.1), all suggest that stratospheric ozone intrusion events occurred on 8 – 11 May 2011. The atmospheric dynamics that cause the intrusions of stratospheric ozone at Egbert have been dealt with in depth in chapter 3 section 3.1. Indeed, determining the responsible dynamical factor that leads to stratospheric ozone intrusion is the main focus of this thesis and is mentioned there.

4.2 Simulation of the Walsingham 2005 Ozonesonde Campaign

As in the previous section, here we present another study of stratospheric ozone intrusion using GEM-FLEXPART models. Two significant ozone enhancements in the upper and middle troposphere were observed at Walsingham, Ontario during the Walsingham 2005 ozonesonde campaign shown in Figure 3.7. We ran GEM-FLEXPART in the forward mode during the period 17 – 26 November 2005 so as to clearly ascertain the stratospheric origin of high ozone concentrations observed at the middle and upper troposphere on 21, 24 and 25 November 2005. GEM-FLEXPART has also been run in the backward mode to further supplement our observational results.

The results of GEM-FLEXPART forward and backward simulations are shown in this section. As we can see shortly, the numerical modeling discloses a significant downward influx of stratospheric ozone over Walsingham, which clearly verifies that the enhanced ozone in Walsingham originated in the stratosphere. Moreover, the GEM-FLEXPART simulation shows that ozone rich dry air partly came from the high latitude northwest of Walsingham.

4.2.1 Forward Simulation

The forward simulation of GEM-FLEXPART is shown in the figure below. The following 3D view is generated in the same way as used in the previous section. The simulation shows the snapshots of the 80 ppbv ozone mixing ratio isosurface at 12 UTC on 24th November 2005. The ozone mixing ratio above the isosurface is more than 80 ppbv, while below the isosurface it is less than 80ppbv.
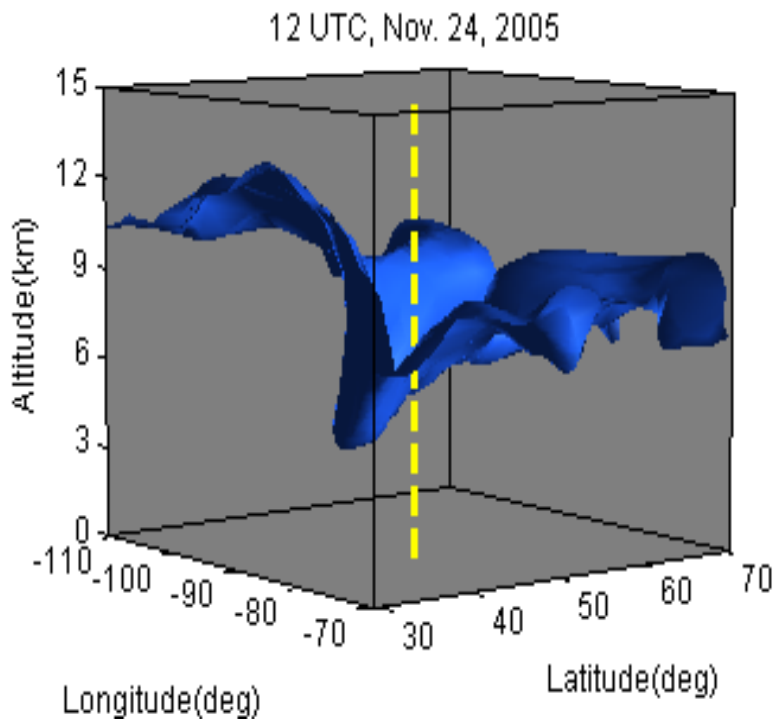
Figure 4.5. This three dimensional view is the same as in Figure 4.1 except for GEM-FLEXPART output is at 12 UTC on 24th November 2005 and the vertical yellow dash line represents Walsingham radar and ozonesonde launching site.

Figure 4.5 shows the result of a numerical simulation employing GEM-FLEXPART. The model evidently indicates an intrusion of stratospheric ozone from the stratosphere, resulting in a tongue of ozone penetrating to the lower troposphere, signifying noticeable descent of ozone. In both the Egbert 2009 (Figure 4.1) and the Walsingham 2005 (Figure 4.5) cases, the ozone seemed to mix with the surrounding air at 3-5 km altitude.
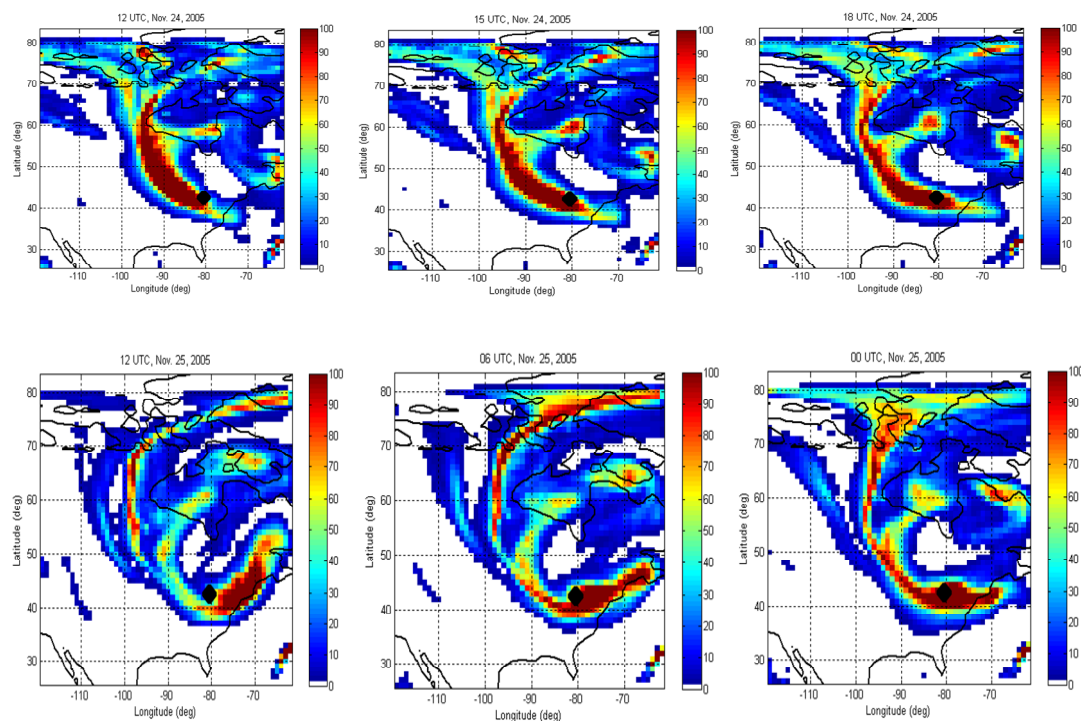
Figure 4.6. Ozone mixing ratios (ppbv) from GEM-FLEXPART, averaged in the height range between 3 and 8 km over the Walsingham site, on 24th and 25th November 2005. The black dot shows the location of the Walsingham site.

Figure 4.6 shows ozone mixing ratio expressed in ppbv obtained from a GEM-FLEXPART simulation between height range 3 and 8 km over North America on 24th – 25th November 2005. The intrusion of stratospheric ozone over Walsingham and nearby areas is revealed in the figure. The intrusion of stratospheric ozone seems to come from the northwest and to continue to move northeast as it passes over Walsingham. We also ran FLEXPART in backward mode to see where the ozone came from.

Both the 2D and 3D views of the GEM-FLEXPART simulations suggest stratospheric origin of the ozone seen at Walsingham at 5.5 - 6.5 km, which is in agreement with the ozonesonde measurements of low relative humidity and high ozone (see Figure 3.7). Unlike the Egbert case, which shows the intrusion pattern to be west to east, the 2D view of Walsingham evidently discloses the intrusion of stratospheric ozone to start in the northwest and to continue move northeast after passing over Walsingham.

4.2.2   Backward Simulation

Now we consider the backward trajectories, as in the previous section, by releasing tracers along a vertical line between 6 and 6.1 km at Walsingham (42.6^{o}N, 80.6^{o}W) on 24 – 25 November 2005. These are transported backward in time for the previous 48 hours. The vertical ozone concentration profiles obtained from ozonesondes were used to determine the releasing location and time of the simulation. The spatial variations in transport patterns are investigated in this section. It is found that the result is in good qualitative agreement with the 2D view of the forward simulation of GEM-FLEXPART (Figure 4.6).
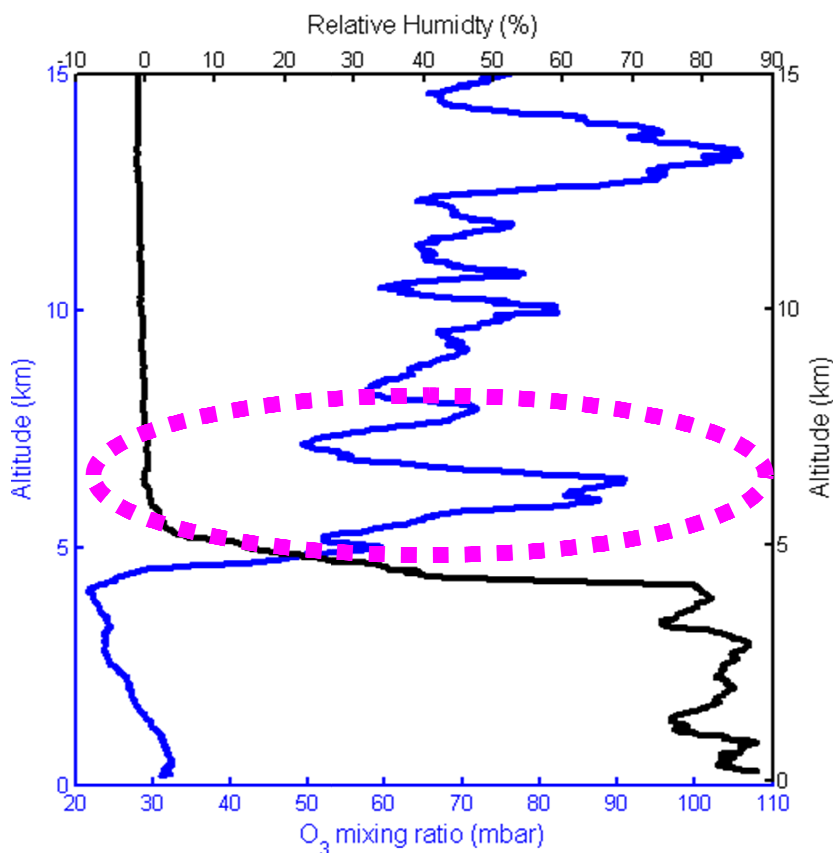
Figure 4.7. Ozonesonde measurement at Walsingham on 24 November 2005 at around 12:53 UTC.

Signatures of the presence of stratospheric air in the lower troposphere are found for all profiles on 8 – 11 May. Figure 4.7 shows the ozone height profile at Walsingham on 24 November 2005 that was launched at around 12:53 UTC. The plot clearly depicts the very low relative humidity and anomalously high-ozone mixing ratio measurement at Walsingham (Ontario, Canada) on 24 November. Even though we have displayed data only for the 24th November at 12:53 UTC, we also observed a very strong intrusion of stratospheric ozone on 25th November. The release of particles was determined from the time and the height of the observed enhanced ozone concentration as determined from the ozonesonde data. Accordingly, the particles were released during 24th - 25th November 2005 in the height range between 6000 – 6100 m and at Walsingham (42.6^{o}N, 80.6^{o}W). The back-trajectories numerical simulation was performed utilizing GEM-FLEXPART and the result is shown in Figure 4.8.

Figure 4.8. FLEXPART back-trajectories of the previous 48 hours of particles released from a line between 6 and 6.1 km at Walsingham (42.6ºN, 80.6ºW) from 24th – 25th November 2005 UTC. The black plus sign represents the location of the Walsingham site.

Figure 4.8 shows the back trajectories of particle transport which helps qualitatively link the source with the receptor. Variations of height along a given trajectory are indicated by color coding. The 48 hours cluster back trajectories using GEM-FLEXPART indicate that the origin and pathways of the high ozone concentration around 6 km on 24th of November was partially the result of horizontal ozone transport from the direction of generally northwest of Walsingham. Consistent with our 2D forward simulations shown in Figure 4.6, the stratospheric ozone intrusion also occurs to the northwest of Walsingham. This shows that the GEM-FLEXPART back trajectories in conjunction

with the forward simulation gives a clear picture of the possible sources of high ozone enhancement in the mid troposphere on 24th November 2005.

Therefore, from our observational and numerical modeling results, we conclude that the ozone enhancement in the middle troposphere over Walsingham on 24th November was mainly a result of stratosphere-troposphere exchange of ozone. Moreover, the occurrence of stratospheric ozone intrusion events to the northwest of Walsingham and the transport of this stratospheric ozone southeast with the wind (the radar measurements of horizontal wind is not shown here) may have partially contributed to ozone rich air with low relative humidity in the middle troposphere of Walsingham on 24th November.

4.3 Simulation of the Walsingham 2007 Ozonesonde Campaign

Like other campaigns, the Walsingham 2007 ozonesonde campaign was also supported by a theoretical computer simulation for modeling ozone movement using FLEXPART to verify if the observed high ozone concentration on 28th February 2007 at upper troposphere had leaked from stratosphere. We ran GEM-FLEXPART in the forward mode during the period of 23 February – 4 March 2007 and in the backward mode to further supplement our observational results. The results of GEM-FLEXPART forward and backward simulations are shown in this section.

As will be presented, the computer simulation undoubtedly reveals a significant descending movement that results in a stratospheric ozone leakage over Walsingham on 28th February 2008. Moreover, unlike the Walsingham 2005 back trajectories case, which suggests the ozone came mostly from northwest of Walsingham, the Walsingham 2007 backward simulation indicates the ozone rich dry air in part to come from west of the site.

4.3.1 Forward Simulation

The forward simulations started on 23 February and ended on 4 March 2007. The details of the particles releasing procedure are described in the previous section. The three dimensional view of the GEM-FLEXPART output is shown in Figure 4.9.
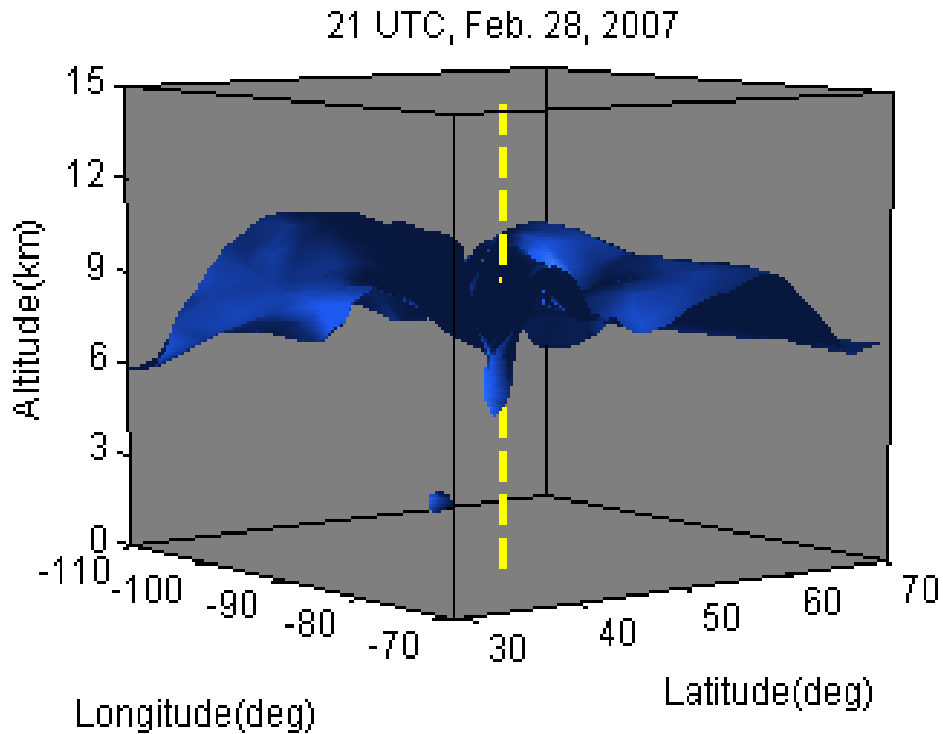
Figure 4.9. Three dimensional view of the GEM-FLEXPART output at 21 UTC on 28th February 2007. The vertical yellow dash line represents Walsingham radar and ozonesonde launching site.

Figure 4.9 shows a 3D snapshot view of the 80 ppbv ozone mixing ratio isosurface on 28th February 2007 at 21 UTC. It evidently shows the leakage of stratospheric ozone leading to a thin tongue of ozone penetrating to middle troposphere over Walsingham. Unlike the previous cases, in the Walsingham 2007 case the ozone seems to mix with the surrounding air at around 5 km. Moreover, our observational result also show the modest ascent of radar derived tropopause heights on 26th and 28th February, subsequent to which enhanced ozone is seen in the upper troposphere on 27 – 28 February. This confirms our experimental observations using ozonesonde and radar, as well numerical modeling, suggesting that the measured ozone rich dry air on 27 – 28 February in the upper troposphere is the consequence of leakage of stratospheric ozone into the troposphere.

Figure 4.10 is the two dimensional version of Figure 4.9 that demonstrates the pattern of ozone transport. The contour plot is the average ozone mixing ratio in the height range

between 4 and 9 km. Unlike the cases of Egbert 2009 and Walsingham 2005, which respectively show the ozone to come from the west and northwest, the Walsingham 2007 case shown in the figure below depicts a stream of ozone rich air moving northeastward and heading in the same direction after passing over Walsingham.
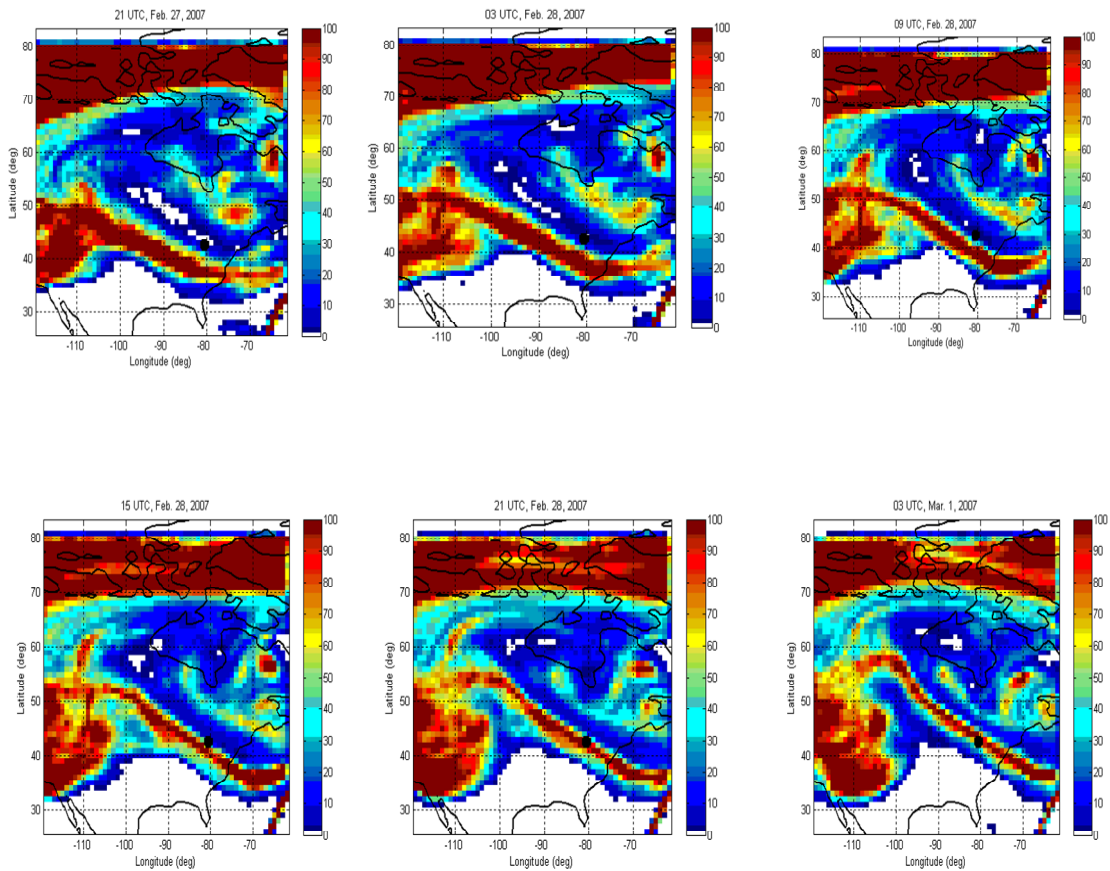
Figure 4.10. Ozone mixing ratios from GEM-FLEXPART, averaged in the height range between 4 and 9 km. The black dot shows Walsingham radar and sonde launching site.

Like the 3D view of the GEM-FLEXPART simulation, 2D view shown in Figure 4.10 also illustrates the stratospheric origin of the ozone seen at Walsingham at around 6 km, which is in agreement with the experimental observation. Now we consider the backward simulation of the GEM-FLEXPART to determine where the ozone came from.

4.3.2 Backward Simulation

The particles were released along a vertical line between 6 and 6.5 km over Walsingham (42.6°N, 80.6°W) on 28th February 2007 at 12 – 15 UTC and were transported backward in time for the previous 84 hours. The simulation starting time and location of particles are chosen to be the measurement time and height of enhanced ozone determined from the ozonesonde data.
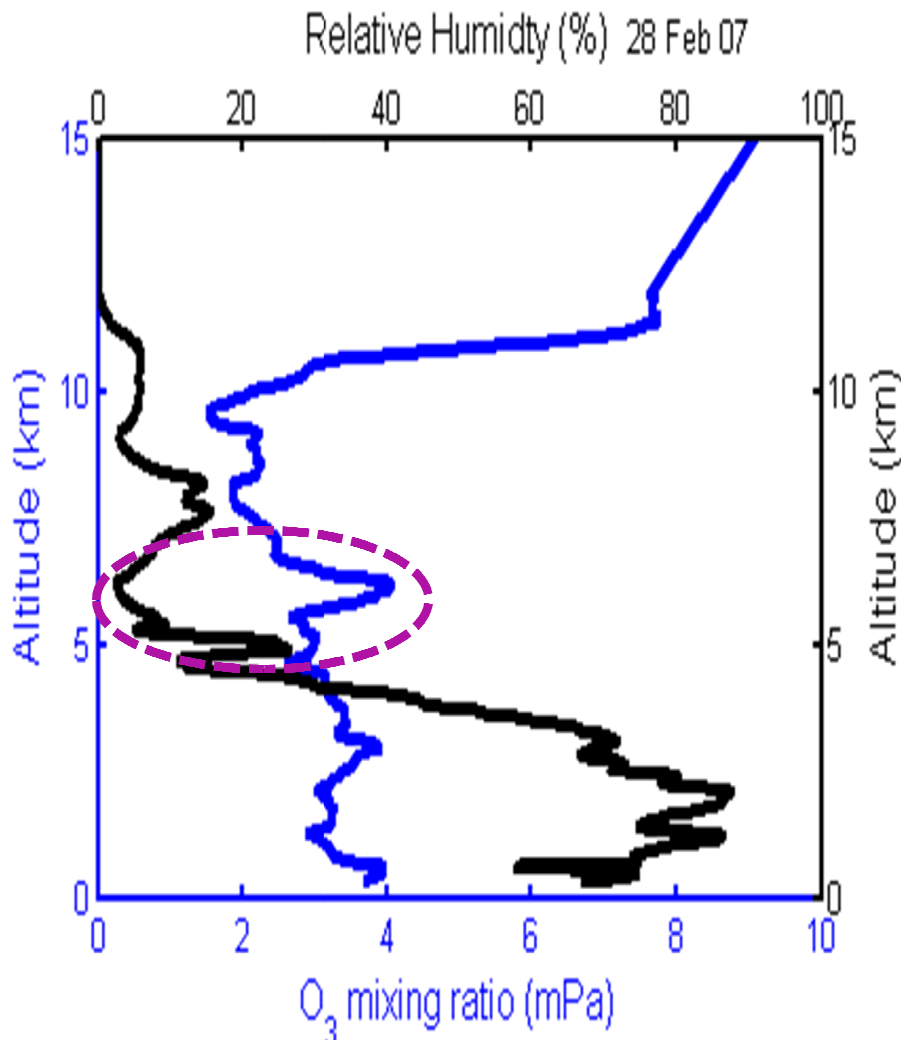
Figure 4.11. Ozonesonde launched on 28 February 2007 at 13:20 UTC. The purple dashed ellipse shows dry ozone rich air in the height range between 6000 – 6500 m.

The ozone height profiles shown in Figure 4.11 exhibits clear enhanced ozone concentrations at about 6 km on 28 February. As we did earlier, we ran GEM-FLEXPART to see if this situation can be explained numerically. The output of the simulation is indicated in Figure 4.12.
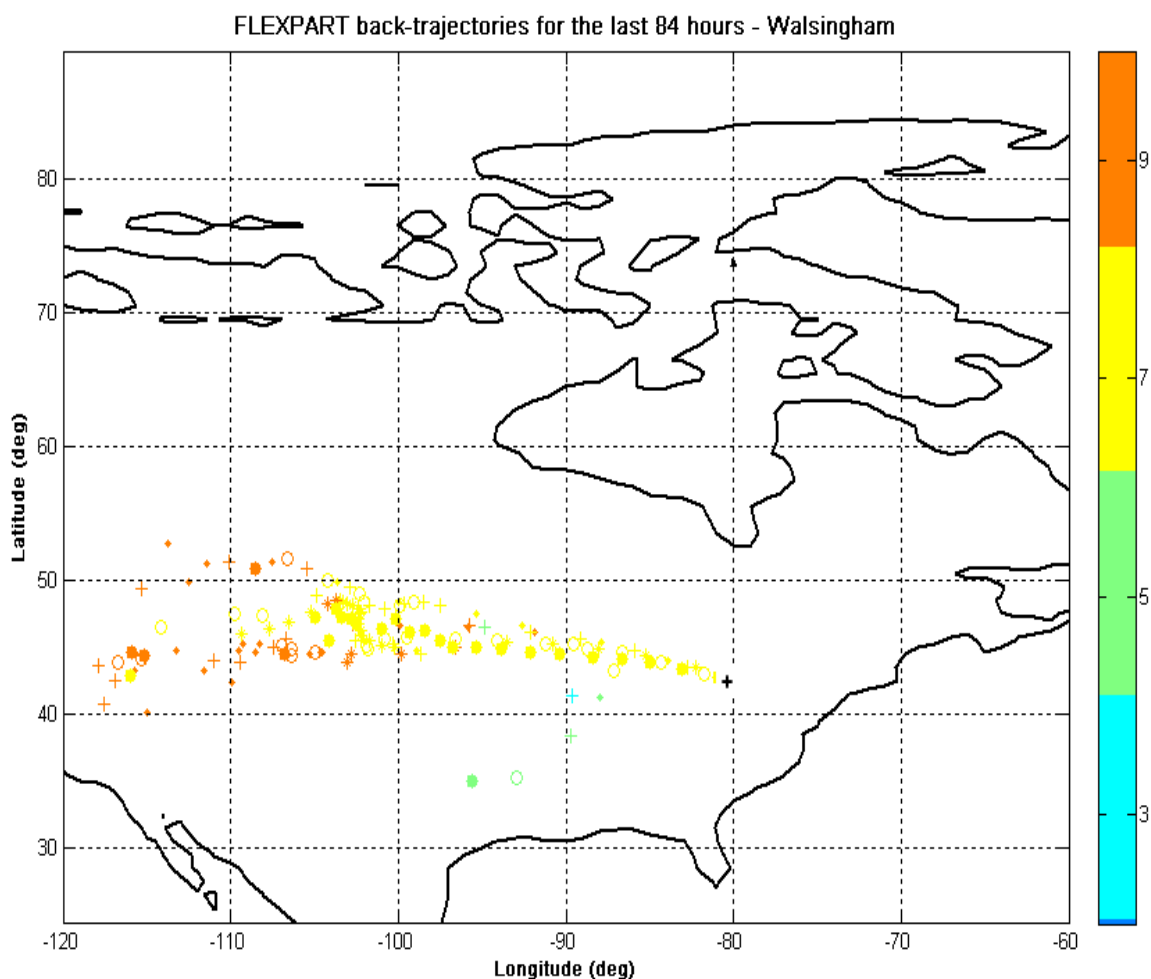
Figure 4.12. FLEXPART back-trajectories of the last 84 hours of particles released from a line between 6 and 6.5 km at Walsingham (42.6ᵒN, 80.6ᵒW) on 28ᵗʰ February 2007 at 12 – 15 UTC. The black plus sign represents Walsingham radar and ozonesonde launching site.

Figure 4.12 reveals the path of the air mass which resulted in the observed enhanced ozone in the middle troposphere (6 – 6.5 km above the ground) on 28ᵗʰ February 2009 at

around 13:30 UTC. It shows the cluster back trajectories of the previous 84 hours preceding the release of the particles along the line indicated above. As we said earlier, variation of height along a given trajectory is indicated by color coding.

One can clearly see from Figure 4.12 that the partial source of ozone rich dry air seems to come from the west of Walsingham, just like the case in the Egbert 2009 shown in Figure 4.4. This suggests the horizontal transport of stratospheric ozone from the west to have a contribution to the observed enhanced ozone in the upper troposphere on 28th February 2007 over Walsingham. Our analysis of radar measurement of horizontal wind velocity (not shown in this thesis) also shows that the wind was dominantly blowing eastward. This is consistent with our model results.

4.4 Summary of simulations

The GEM-FLEXPART simulations shown above confirm our observational results found in chapter 3. The above numerical simulations have shown successfully the leakage of stratospheric ozone in to the troposphere in all the three case studies. Summarizing, we make the following comments:

Figures (4.1, 4.5 and 4.9) show the 3D visualization of the results obtained from the GEM-FLEXPART. The 3D view shows the structure over the radars of ozone distribution according to the models. In all cases, there appears to be a noticeable stratospheric ozone intrusions resulting in a tongue of ozone penetrating to the lower troposphere over the campaign sites. From chapter 3 Figures (3.1 and 3.7), one can notice sudden jumps of radar derived tropopause heights that appear to have preceded the intrusion as shown in Hocking et al. [2007] findings. Moreover, the ozonesonde measurements also indicate low relative humidity and high ozone concentration which partially indicates the ozone to be originated in the stratosphere.

The contour plots of the average ozone mixing ratios are depicted in Figures (4.2, 4.6 and 4.10). They are the 2D representation of the 3D simulations. Such representation show the trend of ozone transport and reveals if there is stratospheric ozone leakage. Figures (4.2, 4.6 and 4.10) reassert the presence of high ozone concentration at the time of the

measurements. However, the approach path of ozone towards to the ozone measured area differs from campaign to campaign. For example, in the Walsingham 2005 case the intrusion seem to come from the northwest, while in the Egbert 2009 and Walsingham 2007 it appears to be from the west. In all the three cases, the pattern of ozone transport is in agreement with our radar measurements of horizontal winds (not shown in this thesis).

Back-trajectories, shown in Figures (4.4, 4.8 and 4.12), reveal the origins and paths of enhanced ozone seen in Figures (4.3, 4.7 and 4.11), respectively. It appears from the Figures (4.4, 4.8 and 4.12) that the air parcels come from the west in the Egbert 2009 and Walsingham 2007 cases, but for the Walsingham 2005 case, the air mass seems to come mostly from the northwest. These results coincide with 2D view of simulations of the corresponding sites which displays the pattern of the ozone transport in contour plots as time goes by.

Even though only three case studies have been presented, we have obtained the same result for other campaigns as well. Quantitative analysis needs to be done in order to determine whether the horizontal transport of ozone with the wind or stratosphere-troposphere exchange of ozone over the measured site is dominant. We believe that a considerable part of the observed enhanced dry ozone rich air originated as a result the latter case. The reasons are the following. There was an apparent ascent of radar derived tropopause heights as suggested in Hocking et al. [2007] associated with ozonesonde measurement of low relative humidity and high ozone concentration. The forward simulations of GEM-FLEXPART also show an unambiguously stratospheric ozone intrusions resulting in a tongue of ozone penetrating to lower troposphere. However, we assume that the horizontal transport of ozone amplifies the amount of the observed ozone rich dry air.

The conclusions of this chapter are as follows: GEM-FLEXPART numerical modelings suggest the leakage of stratospheric ozone in to the troposphere. The leakage can happen at the measurement site, or at some distance from the measurement site, and then reaches the radar site after being blown horizontally with the wind. Our numerical modeling results are consistent with the experimental observations shown in chapter 3. The

atmospheric parameters that lead to the stratospheric ozone leakage have also been analyzing in detail. The synoptic situation of the atmosphere is also examined to see the effects of synoptic dynamics on small-scale geographic regions that causes ozone enhancement in the middle and upper troposphere at the ozonesonde campaign sites. The result for selected cases is found in Appendix B.

Chapter 5

5   Simulation of Diffusion by Turbulence

The purpose of this chapter is to provide a numerical model for visualization of diffusion of atmospheric air due to turbulence using Matlab. The ideas presented are relevant to both large-scale and small-scale models. Numerical modeling is one means to study the atmosphere. It is particularly important for reinforcing the observational and theoretical studies. We especially wish to investigate the process of diffusion for the case that diffusion is not homogeneous and isotropic, but rather is assumed to occur in small, localized patches surrounded by more laminar layers [Dewan, 1981; Woodman and Rastogi, 1984; Hocking, 1991; Haynes and Anglade, 1997; Vanneste, 2004].

The model considers only atmospheric turbulence for the diffusion of gases. Moreover, we assumed both the turbulence and diffusion length exist in two dimensions, that is, in the vertical and horizontal dimensions. Particle displacements are assumed to obey a Rayleigh distribution. Our formulation of the model is not as complicated as most standard models that are formulated by starting from basic physical principles, such as conservation of mass, conservation of momentum, conservation of thermodynamic energy, and the radiative transfer equation. Even though such complicated models are relatively close to representing the real atmospheric conditions, we still choose to simplify the model and to see its output so as to demonstrate the diffusion of atmospheric trace gases such as ozone as a result of turbulence. In this simulation, we want to see the effect of atmospheric turbulence strengths on the diffusion. This approach may explain the limited dispersion of stratospheric ozone layers that descend into the troposphere. Furthermore, it may also clarify what atmospheric dynamics causes the diffusion of high concentrations of ozone in the upper troposphere.

We have built a very idealized model that is not intended to provide quantitatively accurate or physically complete descriptions of the natural phenomena, but rather is designed to encapsulate our physical understanding of a multifaceted phenomenon in the simplest possible form. Nevertheless, some quantitative results can be deduced.

There does not seem to be a single cause to the diffusion of air mass in the atmosphere. A great diversity of diffusion scenarios exist that are driven by quite different dynamical processes. One of these is turbulence-driven diffusion. In the next section, we describe our numerical model, which is designed solely based on turbulence. We would like to close this introduction with a caution. The model described in this chapter is designed as a conceptual tool to explain the dispersion of stratospheric ozone layers as well as the observed enhanced ozone measurements in the upper troposphere, and to see the relevance of turbulence in the stratosphere-troposphere exchange of trace gases. Although the output seems to enlighten us about the actual occurrence of dispersion of the air mass, the model does not consider all physical features that are involved in the process. Models using thorough, formal, and all-parameters-inclusive dynamics for turbulent diffusion representation is one active area of research and it is beyond the scope of this thesis.

Numerical modeling is one powerful tool for examining the atmosphere with the aid of observational as well as theoretical studies, and simulating the physical processes that occur in the atmosphere. There are different kinds of numerical models that are designed for different objectives. They are designed in such a way that they simulate the actual atmosphere as nearly as possible.

Our formulation of the numerical model is based on our understanding of the physics involved in the processes of diffusion of air mass. In designing the model, physical considerations play a major role.

5.1   Description of the simple model

The objective of our model is for simulating the dispersion of atmospheric trace gases including ozone as a result of turbulence. The motivation of this study is that the dispersion of stratospheric ozone layers descending into the troposphere seems less rapid than the expected dispersion for homogeneous turbulence. For example, if the diffusion coefficient $\kappa \approx 10 m^2 s^{-1}$, and a layer is 1 km deep, it should be largely destroyed in a time $t \approx \dfrac{(1000\,m)^2}{10\,m^2 s^{-1}} \approx 100,000\,s \approx 1\,day$. But 1 km thick layers often last much longer.

Above the tropopause, one of the main causes of turbulence is breaking of gravity waves. Gravity waves propagating upward, increase in amplitude (due to the decrease in density of air) resulting in breaking gravity waves (since the oscillation of the wave increases) and this in turn leads to turbulent layers just above the tropopause [Hocking 2009]. Turbulence affects its environment in at least two main ways: it may heat the fluid in which it exists and it causes diffusion of momentum, heat, particles and atmospheric constituents. In this chapter, we discuss the effect of turbulence on the diffusion of atmospheric constituents, in our case ozone.

Turbulence occurs over a wide range of length and time scales. By choosing the appropriate scale, we want to address the question of how turbulence contributes to the dispersion of air mass. Consequently, to address this matter, in this chapter we consider small scale turbulence that persists for short periods of time. Turbulent layers of thickness 1 km and width 5 km are assumed to persist for 5 min in our domain of simulation at randomly located positions. We assumed the turbulence within each layer to be uniform, and it is two-dimensional in form (i.e., vertical and horizontal). The entire domain of the simulation was 20 by 500 km (i.e., from the ground up until 20 km and a horizontal distance that covers 500 km).

5.1.1 Mathematical Equation of Turbulent diffusion

A variety of parameters are important in describing turbulence; however, from our point of view, the rate at which turbulence causes diffusion of atmospheric constituents, κ, is the only parameter that we have taken in to consideration. Nevertheless, for large scale diffusion rates, other processes such as stochastic diffusion and Stokes' diffusion need to be considered [Hocking 2009]. Here we shall consider perhaps the simplest situation, which still facilitates the exploration of complex mixing of atmospheric gases without resolving all the scales of the fluid dynamics equations.

The atmospheric diffusion length, L, is give by

$$L = (\kappa\, t)^{1/2} \qquad\qquad\qquad 5.1$$

Where κ is eddy diffusion coefficient and t is time of diffusion in sec. Early estimation of eddy diffusion coefficient in the lower stratosphere give values roughly in the range between 0.1 m^2s^{-1} and 10 m^2s^{-1} [Woodman and Rastogi, 1984; Fukao et al., 1994; Nastrom and Eaton, 1997; Patra and Lal, 1997]. Hence, in our simulation, we took κ≈10 m^2s^{-1} to calculate the diffusion length, and we also assumed homogeneous atmospheric turbulence to be the only important process in the transport of ozone both horizontally and vertically. Even though the assumption of 2D transport over simplifies the process of turbulent diffusion in the atmosphere, it gives a clue of the dispersion of air in a turbulent layer. Our modeling provides evidence for the decrease in ozone mixing ratio of stratospheric air as it descends into the troposphere. The dispersion of stratospheric air shows the relevance of turbulence in STE under this specific condition.

5.1.2 Matlab simulation

Atmospheric particles and turbulence regions were randomly generated with different resolutions using Matlab without any grid. The vertical and horizontal domain of simulation was from the ground up to 20 km altitude above the ground and covered a 500 km horizontal distance. Particles were randomly generated in the vertical domain of 10 to 12 km attitude above the ground and covering a horizontal distance of 500 km (see Figure 5.2). Then later, these particles were advected using the randomly generated isotropic turbulence in the domain from the ground up to 20 km altitude above the ground and covered a 500 km horizontal distance. Turbulence was the only input to describe the dispersion of particles in the atmosphere. It is further assumed that the duration of the simulation is long enough to allow a noticeable dispersion to take place in our region of interest in the atmosphere.

The turbulent patches were randomly generated as windows with scale 1 by 5 km, and are used to calculate the net transport of particles induced by such turbulent layers. If a particle exists within the window of the turbulent layer, we apply eq. (5.1) and a Rayleigh distribution, which is a continuous probability distribution, to calculate the distance travelled by the particle (i.e., diffusion length). Moreover, an angle between 0 and 2π radians was randomly generated as an angle of projection for every position of the particle and was used to calculate the horizontal and vertical displacements. The lifetime

of a given single event of turbulence is 5 min, which is a reasonable period for such layers to persist.

The total number of tracers involved in this simulation was 5000, which were initialized in the height between 10 and 12 km above the ground (see Figure 5.2). The resulting particles distribution after subjecting them to randomly generated turbulent layers is shown in the Figure 5.3. An example of randomly generated turbulence in the altitude between 10 and 12 km above the ground and covering a horizontal distance of 500 km is shown in Figure 5.1. Each turbulent patch has thickness (height) of 1 km and width (length) of 5 km.
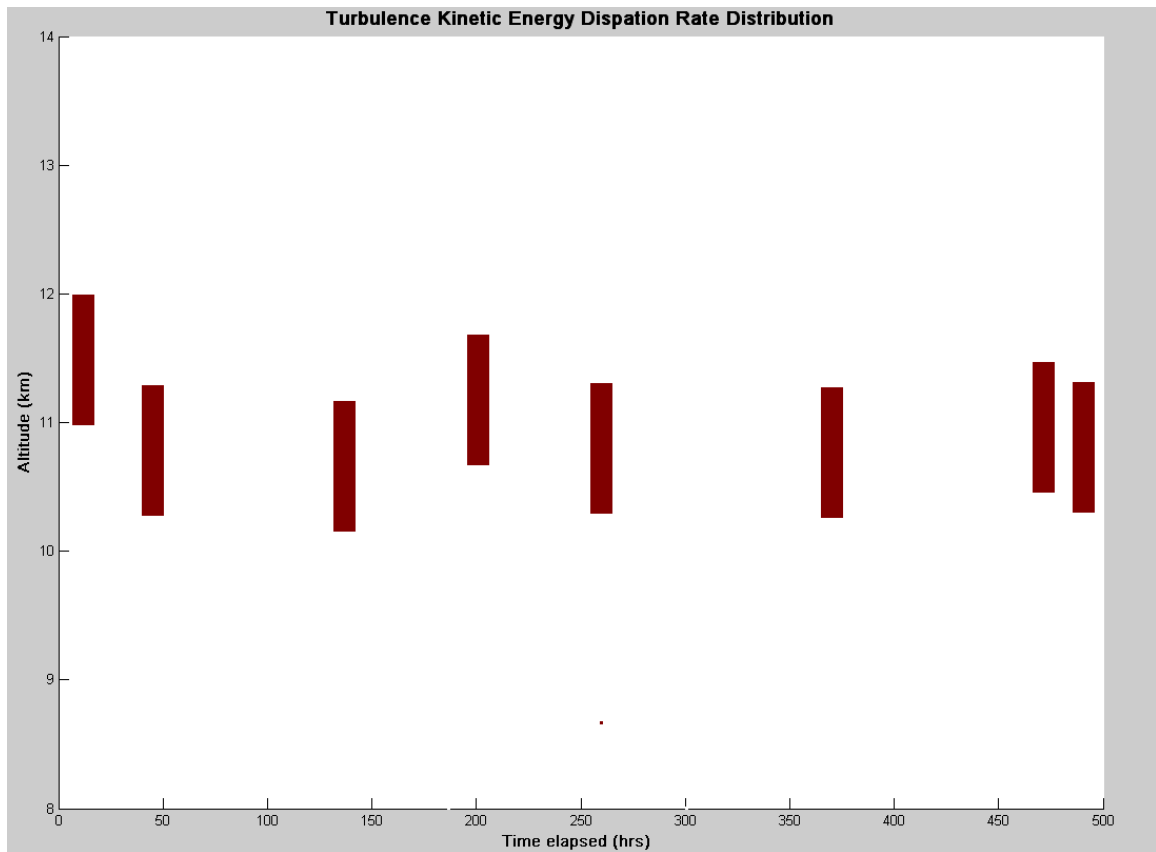
Figure 5.1. Random distribution of 8 turbulent patches of equal dimension (1 km thickness and 5 km width) in the altitude range between 10 and 12 km above the ground and covering a 500 km horizontal distance in one specific 5-min time period. After 5 min, a new set of patches is generated and the old ones are assumed to have dissipated.

Particles within turbulent layers are assumed to obey eq. (5.1) and a random displacement subject to the specified values of κ was assumed. Particles outside the turbulent layers were left stationary. After 5 min a new set of turbulent patches was introduced, and the process was repeated.

Our numerical modeling assumes that each of the released particles at sources (i.e., particles released in the height range between 10 and 12 km above the ground) to have exactly the same size, shape and chemical composition and remain the same throughout the course of the entire simulations. In the first results shown here (Figure 5.3), the simulations were run for 2000 min for comparison to the modeling with the observational results. A total of 100 turbulent layers were randomly generated within the simulation domain of [0, 20]x[0, 500] km^2 and were used to compute the diffusion length. Even though we have chosen 100 turbulent layers in this section, we compare the results of this simulation with different turbulent numbers of layers in the next section. The resulting particles distribution for different number of turbulent layers is shown in the next section.
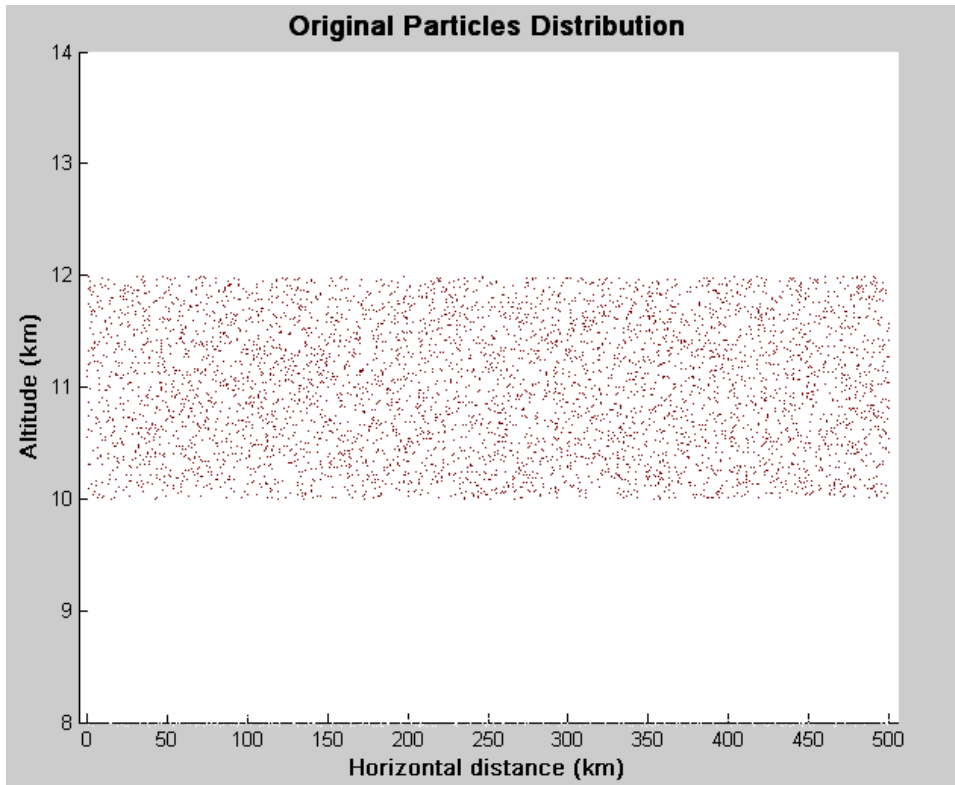
Figure 5.2. Random distribution of particle as a function of vertical height and horizontal distance. Particles were released in the height range between 10 and 12 km. The total number of particles was 5000.

Figure 5.2 shows the original particle distribution in two-dimensions. The release of a total of 5000 particles was chosen in the height range between 10 and 12 km because this is the region of our interest as it is close to tropopause. The purpose of releasing particles in the height range between 10 and 12 km was also to see the effect of turbulent diffusion on STE since it is an important region of our concern to better understand the chemical and dynamical processes involved in the stratosphere-troposphere transport. It is believed that the transport of atmospheric air and chemical trace constituents across the tropopause may result in major changes in the radiative as well as chemical budget of the atmosphere.

The simulation of turbulent diffusion and the prediction of the dispersion of particles is shown in the Figure 5.3. It displays the resulting particle distribution after subjecting our model to the original particle distribution shown in Figure 5.2. The number of turbulent

layers used in this simulation was 100. In Figure 5.3, as we go in the clockwise sense from the upper left corner, we notice that the particles are dispersed farther apart, which suggests that the turbulence causes particles to be permanently and increasingly displaced from where they were as time goes by.

Figure 5.3 shows vertical dispersion of particles, which indicates that turbulence plays an important role in the vertical transport of atmospheric trace gases and contaminants. Moreover, the figure shows the dispersion of particles vertically in both directions along concentration gradients, that is, from regions of higher concentrations to regions of lower concentrations. It is also noticeable from the upper left corner of the same figure that the thickness of the particle layer is doubled after 8 hours of exposing the particles to atmospheric turbulence. Furthermore, as time goes by the thickness of the particle-layer increases and ultimately reaches almost 7 times the original thickness at around 34 hours later.

Figure 5.3 can be considered as a reference as it shows the spreading expected due to a large number of turbulent layers. This will be similar to that expected for homogeneous turbulence. Our purpose is to explain why layers do NOT always spread this fast. And so in the next section we consider fewer turbulent patches.
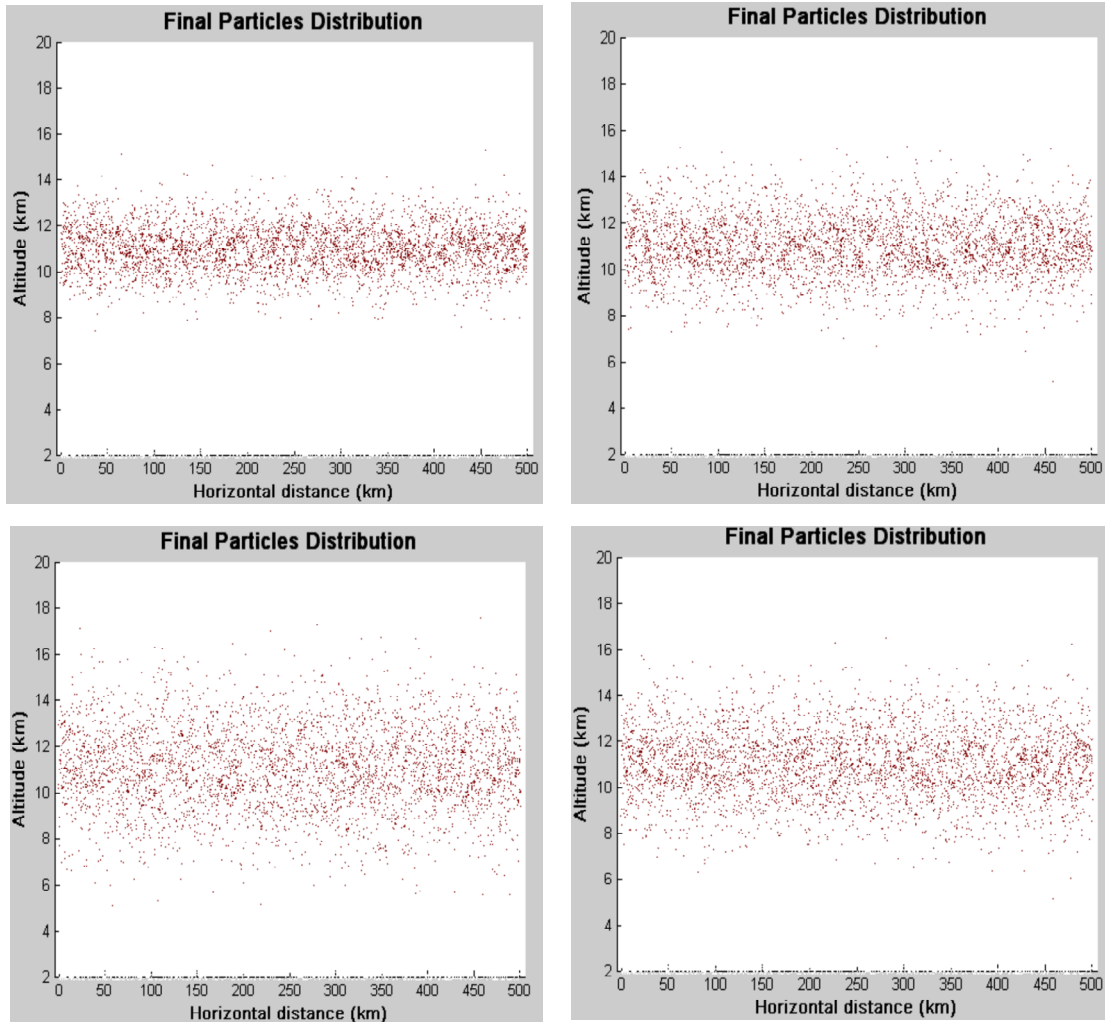
Figure 5.3. Random distribution of particle as a function of vertical height and horizontal distance. In the clockwise direction from the top left corner are the plots 8, 16, 24 and 34 hours after the release of the particles in the altitudes between 10 and 12 km.

We have looked at the net displacement of the center of mass of the system of particles to see if it changes with time. The variation of the mean altitude of the particles from the ground has also been studied. The result is displayed in Figure 5.4. As can clearly be seen from Figure 5.4a, the center mass of the system of particles remains pretty much where it was originally. Figure 5.2 demonstrates that the particles are initially distributed in the height range between 10 and 12 km, from which we find the mean altitude of the system of particles to be at approximately 11 km. This value remains nearly the same

thoughout the simulation (see Figure 5.4a). This indicates that the turbulence has no preferred direction to drift the particles. It pushes the particles evenly in the vertical direction. If we had included other physical parameter that involved in the processes, we would have seen a net transport of particles in the upward and/or downward direction. On the other hand, the standard deviation of the altitudes of the particles rises with time, which clearly proves that the particles are further spreading with time as one expects. This is revealed in Figure 5.4b.
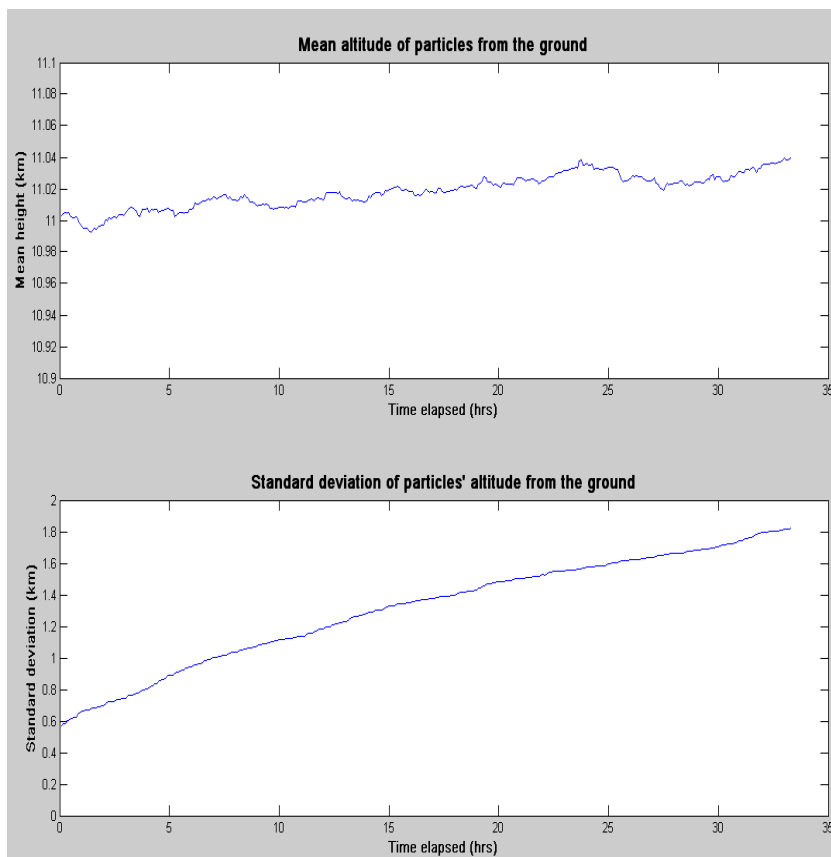
Figure 5.4. (a) The plot of the mean altitude of the particles from the ground (km) versus the time elapsed and (b) the time variation of the standard deviation of the altitude of particles above the ground (km).

In our numerical modeling, we showed that turbulent diffusion results in the downward and upward fluxes of atmospheric constituent gases. The spreading of particles make a physical sense as it can explain the dispersion of ozone (i.e., stratospheric ozone layers or high ozone concentration in the upper troposphere). This result is very fascinating since it

gives a clue behind the reason why stratospheric originated air will have less concentration of ozone as it descends into the troposphere. As measurements show, the ozone mixing ratio of a sample of the lowermost stratospheric air much higher than when the same sample of air descends into the troposphere. According to our model, the reason for the discrepancy in ozone mixing ratio for the same sample of air as it measured in the stratosphere and after descending in the troposphere is the atmospheric dispersion. This model clearly shows that the concentration of the tracers becomes less as it spreads away from the source.

Our analysis cannot give a complete picture of the turbulent diffusion since it is not consolidating the required physical parameters in the process. Moreover, we assumed uniformly distributed (isotropic) turbulence in the atmosphere, while the turbulence is often anisotropic. However, from the results shown in this chapter and chapter 3, it is clear that turbulence has association with the intrusion. Through assisting or triggering the vertical movement air mass, it facilitates STE.

5.2   Effects of turbulent layers on diffusion

Even though atmospheric diffusion for 100 turbulent layers has been presented, we have diagnosed the turbulent simulation for the turbulent layers from 5 up to 600. We have assumed the same atmospheric condition as described in the previous section. Accordingly, our numerical simulation results show that for smaller numbers of turbulent layers, the dispersion of the particles is very small. This is an important result. It demonstrates that even though radar and in-situ measurements may measure patches of turbulence with $\kappa \approx 10$ m^{2}s^{-1} or higher, the assumed mean turbulent diffusion can often be much less, because of the fact that turbulence does not fill the region of study [Hocking, 1991, Figures 1 and 2].
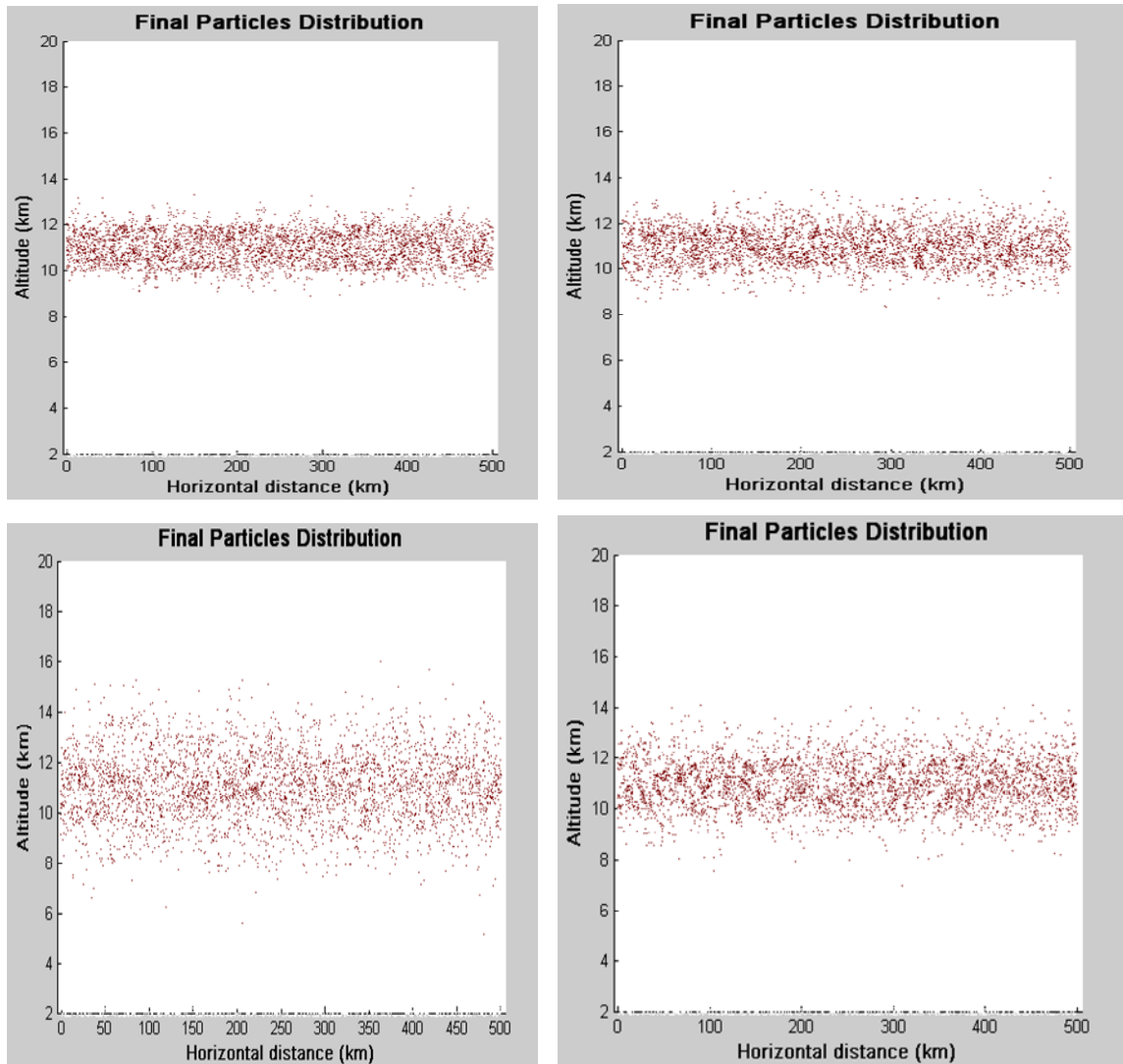
Figure 5.5. Final distribution of particles after 34 hours. In the clockwise sense from the top left corner are the plots for number of turbulent layers equal to 5, 10, 20 and 50, respectively. We used the same procedure and parameters described in the previous section except that the turbulent patches were between 6 and 14 km altitude above the ground.

The simulation results shown in Figure 5.5 are for number of turbulent layers equal to 5, 10, 20 and 50, as we go in the clockwise sense starting from the upper left corner, respectively. It can clearly be seen from the figure that as the number of turbulent layers increases the particles will be farther dispersed resulting in less concentration in the

height range between 10 and 12 km. We have also looked at the net displacement of the center of mass of the system of particles to see if there is any signifant variation among the different cases. Figure 5.6 shows the plot of the root mean square displacement of particles relative to their original positions as a function of time for different number of turbulent layers.
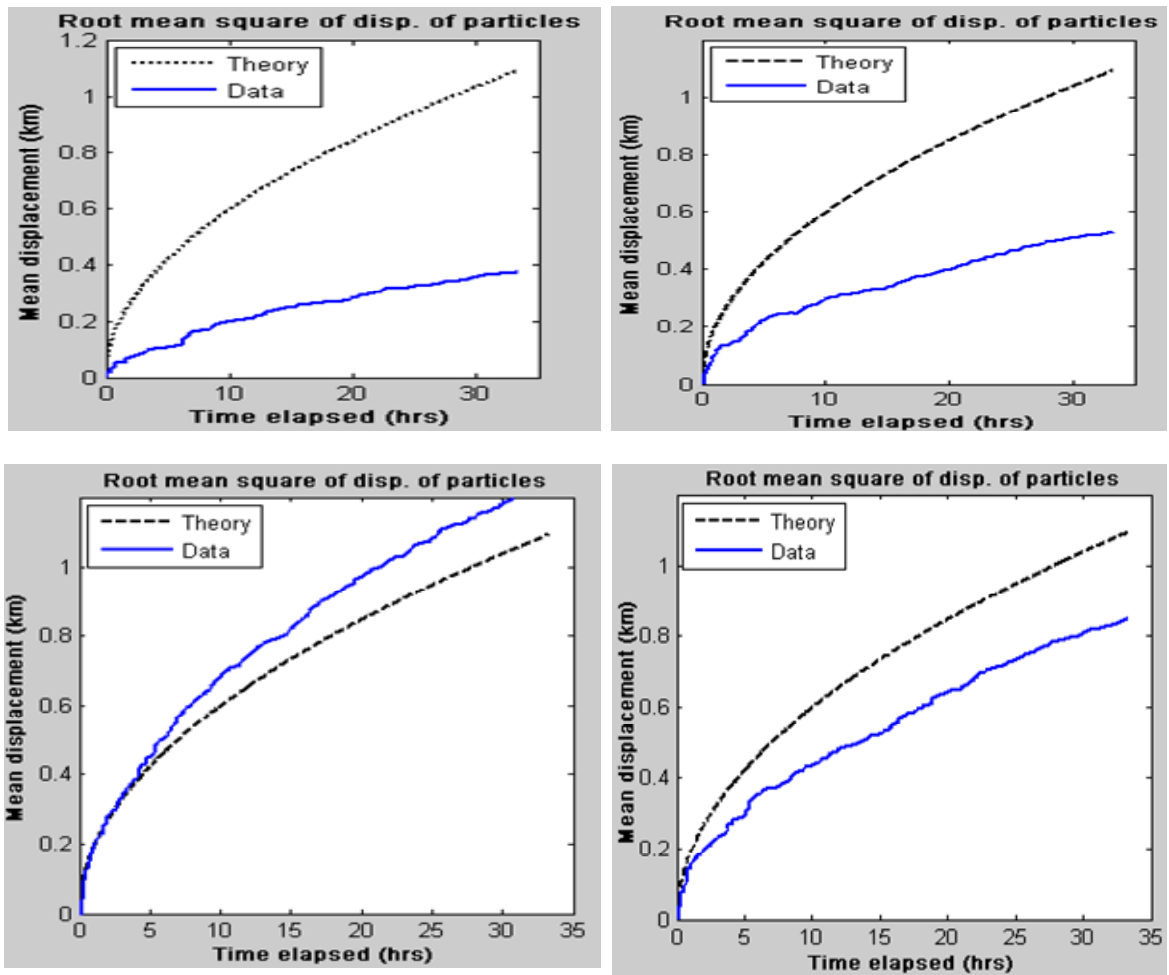
Figure 5.6. Plots of the time variation of the root mean square of particle displacement with respect to their original positions (km). In the clockwise sense from the top left corner, the number of turbulent layers is 5, 10, 20 and 50, respectively. The black dot line is for theoretical assuming $\kappa \approx 10$ m^{2}s^{-1}, while the blue line is for numerical output.

The slope of the numerical results becomes steeper as we go in the clockwise sense starting from the upper left corner of Figure 5.6. This indicates that the particles are spread further apart as the number of turbulent layers increases, which is consistent with our previous result. One can also notice from the same figure that the numerical outputs gets closer to the theoretical values as the number of turbulent layers increases. The theoretical value is obtained using eq. (5.1). Just as in Figure 5.4a, we have found the mean altitude of the particles from the ground to remain around 11 km, which implies the turbulence disperses the particles evenly in the vertical direction no matter how strong it is. The standard deviation of the altitudes of the particles was also observed to rise with time.

We calculated the percentage of the area filled by the turbulent patches as compared to the total area of simulations using
$(Total\ area\ of\ turbulent\ layers/turbulent\ layers\ generated\ area) \times 100\%$. The total area of turbulent patches is given by $number\ of\ turbulent\ patches \times area\ of\ each\ turbulent\ patch$. The area of each turbulent patch is obtained using the thickness and width of the patch. So it becomes $1 \times 5\ km^2 = 5\ km^2$. And the turbulent generated area is $(14 - 6) \times 500\ km^2 = 4000\ km^2$. Therefore, the percentages of the area filled by the turbulence for the number of turbulent patches equals to 5, 10, 20 and 50 are 0.625%, 1.25%, 2.5% and 6.25%, respectively. The result shows that as the percentage of the area filled by turbulence increases, the particles spread faster.

The above results show the requirement of the impact of number of turbulent layers on the degree of atmospheric diffusion. When the number of turbulent layers is small, we will not see any dispersion of particles even if the strength of turbulence within individual patches is strong. It also indicates that the number of turbulent layers is proportional to how far the particles are dispersed. This result is crucial to understanding of the dispersion of stratospheric ozone layers as they descend into the troposphere, since it highlights the importance of turbulence in order for diffusion to take place. Moreover, this vertical atmospheric diffusion results in mixing and modifying of air masses.

Our simple turbulent diffusion model, which is developed based on the assumption of uniformly distributed turbulence in the atmosphere, enables us to see interesting results by changing the number of turbulent layers. The interesting feature of these results is that the mean altitude of the particles from the ground remains the same for different values of turbulent layers, which shows the spreading out of particles to be even regardless of the strength of turbulence. According to our approaches, turbulent strength plays an important role in enhancing diffusion at greater depth, which increases the variance of the altitudes of particles from the ground. Clearly the impact of κ in producing diffusion is diminished for smaller number of turbulent patches.

Chapter 6

6 Summary and Conclusions

The transport of air mass and trace constituents between the stratosphere and troposphere has been a critical unresolved issue in the realm of atmospheric science. Stratospheric air has high potential vorticity, high ozone concentration, and low water vapor compared to the tropospheric air. Consequently, transport and mixing between the stratosphere and troposphere constituents can bring about changes in the chemical and dynamical characteristics of the atmosphere. Therefore, studying the atmospheric dynamics that trigger or assist or cause stratosphere-troposphere exchange is vital for a better understanding of the spatial distribution of trace constituents such as ozone and water vapor.

STE is an on-going process that takes place at different scales; from local scales, to synoptic scale events, up to the global scale Brewer-Dobson circulation. However, the details of the process is not well understood yet. Small scale extratropical dynamical processes control the transport of air mass from the lowermost stratosphere into the troposphere. The examination of the stratospheric ozone intrusion in to the troposphere across the stable region tropopause is the main focus of this work. Therefore, my research objective is to address what atmospheric dynamics triggers or causes the intrusions of stratospheric ozone into the troposphere, and how the relative importance of these parameters varies from case to case. Multiple studies and attempts have been performed to identify special events.

In order to meet our objective and address the above issue, our first task was to determine the source of the observed high ozone concentration episodes. To certify if the ozone was stratospheric in origin, we diagnose the response of the radar derived tropopause to the ozone intrusion events. Measurements of low relative humidity from ozonesondes as well as numerical simulation via GEM-FLEXPART complement our results. To ascertain the long-range transport of ozone originated in the stratosphere, we looked at the radar and ozonesonde data and computer simulation using GEM-FLEXPART. After identifying the

possible source for the observed dry ozone-rich air, we analyzed radar measurements of atmospheric parameters.

In our study of the atmospheric dynamics responsible for stratospheric ozone intrusion, we considered 8 intensive ozonesonde campaigns across Canada in high and mid latitudes. Windprofilers have been employed in conjunction with frequent ozonesonde launches to look at the dynamics of ozone intrusion. Stratospheric ozone intrusion was detected using sudden jumps of radar determined tropopause height. Moreover, ozonesonde measured low relative humidity was also taken as a partial indicator of ozone originated from the stratosphere. Our experimental observations have also been supplemented using GEM-FLEXPART, a Lagrangian particle dispersion model. We ran this model both in forward and backward modes to simulate the dispersion of stratospheric ozone particles from their sources and to determine potential source contributions for the measured enhanced ozone concentrations.

Small-scale atmospheric dynamics that have marked impact on the stratosphere-troposphere exchange of ozone have been examined exhaustively in this thesis. These parameters are the variance of vertical velocities, vertical shear of the horizontal velocities, turbulence strengths and backscattered radar power, as each may have important implications for the stratospheric ozone intrusions. The atmospheric conditions were observed and analyzed near the tropopause to see the association of the parameters with the observed ozone rich dry air in the middle and upper troposphere. Windprofiler measurements of these physical quantities were obtained with good spatial and temporal resolution continuously to allow the study of STE of ozone. The simultaneous measurements of the atmospheric dynamics and ozone mixing ratio using radar and ozonesonde, respectively, helped ascertain the cause of stratospheric ozone.

Atmospheric dynamical processes include various scales, and their interaction may result in small-scale instability in the atmosphere and bring about STE. It is believed that the strong atmospheric activity observed above the tropopause may break down the stability of the tropopause that normally restrains stratosphere-troposphere exchange of ozone and

other trace gases. Consequently, such strong activity might trigger the intrusion and result in leakage of stratospheric ozone in to the troposphere across the tropopause.

The estimation of tropopause height using radar was also required to detect the intrusion of stratospheric ozone, as shown in Hocking et al. [2007]. In order to determine tropopause heights, radar powers between frequency -0.08 and 0.08 Hz observed with the radar vertical beam during the ozonesonde campaigns were used. Radar powers of more than 10^5 (expressed as digital units squared) above 5 km were removed and replaced using multiple linear regression with a window of size 10 by 10. Below 5 km, data with strengths more than 10^5 were kept. The purpose of the procedure was purely to disclose the tropopause as clearly as possible. Removal of these high radar backscattered powers successfully eliminates aircraft interference.

We considered three case studies to illustrate the relationship between stratospheric ozone intrusion and radar measured atmospheric activities. The first case is the Egbert 2009 ozonesonde campaign, which was made at Egbert, Ontario from 5 – 11 May 2009. We have obtained an interesting result from this campaign. The backscattered radar power plot as a function of altitude and time observed with the Egbert windprofiler radar, revealed two rapid tropopause height ascents on the 6th and 9th of May 2009 (see Figure 3.1a). The ascents were found to be associated with high stratospheric ozone in the middle and upper troposphere on 7 - 11 May (see Figure 3.1b). As can clearly be seen from Figure 3.2, the ozonesonde measurement shows low relative humidity on 8, 10 – 11 May, while the observed ozone mixing ratio is high. This certifies that the enhanced ozone originated from the stratosphere, since low relative humidity is used as a partial indicator of ozone originated from the stratosphere.

The forward GEM-FLEXPART simulations both in 2- and 3-dimensions view also verify the downward influx stratospheric ozone to the troposphere over Egbert (see Figure 4.1 and 4.2), which is partly confirmed by the ozonesonde measurements of low relative humidity and high ozone concentrations (see Figure 3.2). As displayed in Figure 4.4, the backward GEM-FLEXPART simulation discloses that the ozone rich dry air in part came from west of Egbert. The analysis of radar measurement of horizontal wind (not shown in

this thesis) demonstrates that the prevailing wind was from west. This attests to the fact that the high ozone concentrations seen at Egbert on 10th May were in part the result of ozone which came from west of Egbert. The output of the back-trajectories of GEM-FLEXPART simulations is in agreement with the forward 2-dimension simulations, which shows the intrusion of stratospheric ozone at Egbert and nearby areas and continues to move eastward over Egbert. The mechanism by which stratospheric ozone intrusion takes place is explored through the analysis of radar measurements of standard deviation of vertical wind, vertical shear of the horizontal wind and turbulence strengths.

It is worth mentioning from Figures 3.3-3.5 that the standard deviation of the vertical wind, vertical shear of the horizontal wind and turbulence strengths were simultaneously strong on 9th of May. Evidence suggests that the enhancement of the observed stratospheric ozone intrusion on 8 – 11 May might have been caused by simultaneous action of all of the atmospheric dynamics we have diagnosed. We would like to point out that there is a possibility that the enhancement of the observed stratospheric ozone intrusion may be linked to one or any combination the atmospheric features. On the other hand, the occurrence of enhanced stratospheric ozone may not to be related to any of the parameters that have been analyzed. On such cases the wind and turbulence effects are too weak to cause the intrusions of stratospheric ozone. This kind of scenario requires further studies in order to ascertain the atmospheric dynamics responsible for the intrusions of stratospheric ozone.

The second case study we considered exemplifies the connection between stratospheric ozone intrusion and strong atmospheric activities was the Walsingham 2005 ozonesonde campaign. The campaign was made from 17 – 26 November 2005 at Walsingham, Ontario. A sudden rapid and large ascent of the tropopause height on 24th November and low relative humidity on (see Figure 3.7) effectively proves that the enhanced ozone concentration seen 24 – 25 November originated from the stratosphere. The GEM-FLEXPART output simulations in both 2- and 3-dimensions suggest stratospheric originated ozone is seen at Walsingham on 24th November, which is in agreement with the experimental observations.

Unlike the Egbert case, which shows the intrusion pattern to be west to east, the 2-dimension view of the GEM-FLEXPART output at Walsingham evidently discloses the intrusion of stratospheric ozone to start from northwest and to continue to move northeast after passing over Walsingham. Consistent with our 2-dimension forward simulations, the back-trajectories show the origin and pathways of the enhanced ozone concentration observed to be partially from northwest of Walsingham. Therefore, both experimental observation and numerical simulations certify the enhanced ozone concentrations in the mid troposphere on 24th – 25th November 2005 was as a result of the intrusion of stratospheric ozone. Hence, as in the previous case, the cause of intrusion of stratospheric ozone was studied by examining radar measurements of atmospheric parameters.

As radar measurements have shown in Figures 3.8b and 3.9b, the standard deviation of vertical wind and vertical shear of the horizontal wind seem to coincide with the enhancements of stratospheric ozone in the middle and upper troposphere on 22nd – 23rd November and 24th – 25th of November. Moreover, as can clearly be seen from Figure 10, the turbulence strength is strong on 21st - 22nd November, which might have assisted or caused the intrusion of stratospheric ozone, and resulted in the enhanced ozone on 22nd - 23rd November. However, we do not notice any strong turbulence that can be associated with the observed enhanced ozone on 24th – 25th November. The last result suggests that in order for stratosphere-troposphere exchange of ozone to take place, strong turbulence is not necessarily required since other parameters can play the intrusion role. The other is a possibility that radar missed detection of strong turbulence, which can happen if the turbulence is strong enough to produce complete adiabatic mixing.

In other words, the absence of radar detected turbulence does not necessarily suggest a complete lack of turbulence because there is a possibility that the radar will not detect turbulence if strong turbulence mixes the air uniformly and the parcel of air is transported adiabatically to a new position [Hocking 2011]. This can be illustrated through Figure 3.9b. On 24th - 25th November, we can see a strong wind shear, while the turbulence is weak. We know that wind shear causes turbulence but the strong wind shear observed on 24th – 25th November did not result in turbulence. This might be either due to the fact that

radar was not able to detect strong turbulence as a result of uniform mixing of the air, or in fact there was no turbulence.

The third case studied is the Montreal 2005 ozonesonde campaign. It was made from 29 April – 10 May 2005 at the Canadian Space Agency Head Office in St Hubert, Quebec about 45 km away from the location of the nearest windprofiler radar, which was situated at the MacDonald campus of McGill University. Figure 3.11 shows enhanced concentrations of ozone at the middle and upper troposphere were observed during 30 April – 1 May, 4 - 6 May, 7 - 8 May and 9 - 10 May 2005. The same figure reveals the relative humidity to be fairly low except in the first event. The latter event suggests that ozone-rich stratospheric air might have transported into the troposphere. The radar derived tropopause height discloses a big sudden jumps on 29 - 30 April, 3 May and modest jumps on 5 and 8 May. Even though modest jumps were observed on 5 and 8 May, in all the four cases there can clearly be seen an apparent enhancement of ozone concentration as low as 2 km followed the tropopause jumps.

The strong standard deviation of vertical wind velocity on 29th April, a fairly strong wind shear on 30th April – 1st May and strong turbulent strengths on 29th – 30th April all intensify atmospheric activity, and be responsible for bringing down ozone rich dry air as seen on 30 April – 1 May. On 3rd May, a strong wind shear is the only noticed dynamical feature which appears to be accompanied by high stratospheric ozone in the middle and upper troposphere on 4th - 6th May. Moreover, on 6th - 7th May one sees a strong standard deviation of vertical wind and wind shear that coincides with the observed enhanced high ozone concentration on 7 - 8 May.

We point out here that high enhancements of ozone concentrations in the middle and upper troposphere on 9th – 10th May do not always coincide with any of the parameters that we have diagnosed. As can be seen from Figures 3.12 - 3.14, the standard deviation of vertical wind, vertical shear of the horizontal wind and turbulence strengths were weak before or during the 9th – 10th of May. This is an indication of the possibility that the enhancement of the observed stratospheric ozone intrusion may not be related to any of the atmospheric dynamics that we have diagnosed. However, it is not always necessary

that the dynamical processes be evident directly over the radar, especially if intrusion occurred say 100 km upstream of the radar. On the other hand, there is a possibility that the occurrence of enhanced stratospheric ozone may be associated with all of the parameters that we have analyzed. For example, the observed high stratospheric ozone concentration on 30th April – 1st May coincides with strong standard deviation of vertical velocity, vertical wind shear and turbulence strengths during or before the intrusion. Hence, further studies would be necessary to ascertain the atmospheric dynamics responsible for the intrusions of stratospheric ozone in such cases where the atmospheric parameters are weak, yet intrusions still occur, for example on the 9th – 10th of May. Locally variable dynamics on scales of a few hundred km may be important.

Even though we have presented three case studies, there were a total of 8 ozonesonde campaigns across Canada at mid and high latitudes that we used for this thesis. A total of 25 major intrusion events were observed in all campaigns. As shown in the Table 3.1, we have seen positive correlation between enhanced ozone rich dry air in the upper and lower troposphere and strong radar measured atmospheric activity (i.e., standard deviation of vertical wind, vertical shear of horizontal wind and/or turbulence strengths). As can be noticed from the table, during every intrusion event, at least one of the three atmospheric dynamical parameters were strong except on 0509 (in the Montreal 2005 campaign case) and the Eureka 2008 campaign (when transport was important from a source to the south of Eureka as shown in Osman et al. [2010]). These measurements provide confirming and exciting evidence of the relation between stratosphere-troposphere exchange of ozone and such dynamical events. This is important for the detection of stratospheric ozone intrusion, and deducing the atmospheric parameters that may trigger or assist in the intrusion process.

Our findings demonstrate a unique combination of simultaneous measurement of radar and ozonesonde to study stratosphere-troposphere exchange of ozone. The radar estimation of tropopause heights detects the intrusion of stratospheric ozone measured by ozonesonde. Moreover, radar measurements of atmospheric dynamics such as variance of vertical wind, vertical wind shear and turbulence strengths help identify the cause of stratospheric ozone intrusion. Stratospheric air masses descend in to the upper

tropospheric across the tropopause mostly as a result of these parameters. Moreover, this work shows that the transport of ozone across the tropopause could have a noteworthy effect on the budget of atmospheric chemical composition, particularly for trace gases such as ozone which have impact both on air quality and climate change.

In this thesis, we have demonstrated frequent leakage of stratospheric ozone at the measurement site, or at some distance from the measurement site, and which then reaches the radar site after being blown horizontally with the wind. Likewise the transport path of ozone originated in the stratosphere differs from campaign to campaign; the atmospheric dynamics responsible for the intrusion of stratospheric ozone varies from case to case. On the one hand, we notice that all parameters can act simultaneously which clearly amplifies the intrusions. On the other hand, we observe either any combination of the parameters or only any one of them may act and bring about intrusions. Consequently, the dynamical features that lead to the stratospheric ozone leakage have been observed to be different for different campaigns. Therefore, one of the main achievements of this work is to clearly show the dynamical features that are responsible for the intrusion of stratospheric ozone and to identify the variation of the relative importance of the parameters from case to case.

This work demonstrates that the introduction of wind profilers has made an important impact on studying the dynamics of the lower atmosphere with good height and temporal resolution. Moreover, Windprofiler radars, in collaboration with frequent balloon-born ozonesonde launches, have been utilized to reveal stratosphere-troposphere exchange of ozone. It has also been used to study the atmospheric dynamics that cause the stratospheric ozone intrusion. Therefore, the simultaneous employment of windprofiler and ozonesonde plays a major role in better understanding as well as protecting the atmosphere and more effectively regulating emissions, since the technique helps detect the sources and sinks of ozone-related atmospheric pollutants in the lower atmosphere.

As an extra exercise we have also modeled the atmospheric diffusion, and examined the relative roles of homogeneous versus spatially intermittent turbulence on the dispersion of trace gases. In this modeling, we excluded the effects of any other physical parameters

in the process other than atmospheric turbulence. The particles, which were initially distributed in the height range between 10 and 12 km, were subjected to both spatially and temporally intermittent turbulence. The particles were subjected to different levels of turbulence intermittency. The mean altitude of the particles above the ground remains the same around 11 km throughout the simulations for any number of turbulent layers. However, the degree of spread of the particles was found to be dependent on the number of turbulent layers. The plots of both particles distribution and standard deviation of particles displacement confirm to us that when turbulence is intermittent, large scale spreading is reduced.

This approach, which differs from the classical view of homogeneous turbulence, provides a better understanding of the dispersion of stratospheric ozone layers as they come down in to the troposphere, and this in turn offers a clue on the consequent turbulence on stratosphere-troposphere exchange of ozone. Our model can also better explain the dispersion of enhanced ozone measurement in the upper troposphere and ultimately mixing with the surrounding air. Our approach can also provide a justification for the discrepancy in ozone mixing of the same sample of air when it is measured in the stratosphere compared to its value after descent into the troposphere. The model associates this discrepancy with the nature of dispersion of ozone layers as they descend in to the troposphere. Even though we have obtained a fascinating result from our simple turbulent diffusion model, incorporating more dynamical parameters that are involved in the process will give a comprehensive picture of the atmospheric diffusion. This is one research area that needs attention so as to step up the model and see the dispersion phenomena in detail.

Bibliography

Ahrens C. D., 2003. Meteorology today: an introduction to weather, climate, and the environment, 7th ed. Thomson Learning, Inc.

Alam, J. M, Lin, J. C., 2008. Toward a Fully Lagrangian Atmospheric Modeling System, Mon. Weather Rev., doi: 10.1175/2008MWR2515.1.

Allen, G., Vaughan, G., Bower, K. N., Williams, P. I., Crosier, J., Flynn, M., Connolly, P., Hamilton, J. F., Lee, J. D., Saxton, J. E., Watson, N. M., Gallagher, M., Coe, H., Allan, J., Choularton, T. W., Lewis, A. C., 2008. Aerosol and trace-gas measurements in the Darwin area during the wet season, J. Geophys. Res.-Atmos., 113(D6), D06306, doi:10.1029/2007JD008706.

Altshuller, A. P., Lefohn, A. S., 1996. Background ozone in the planetary boundary layer over the United States. J. Air Waste Manage. Assoc. 46, 134–141.

Analog Ozonesonde RS92, USER'S GUIDE, M210614EN-A, Helsinki, Vaisala 2004.

Andrews, D. G., Holton, J. R., Leovy, C. B., 1987. Middle Atmospheric Dynamics. New York: Academic Press.

Angell, J. K., Korshover, J., 1983. Global variation in total ozone and layer mean ozone: an update through 1981, J. Clim. appl. Meteorl., 22, 1611-1626.

Appenzeller, C., Davies, H. C., 1992. Structure of stratospheric intrusions into the troposphere. Nature, 358, 570–572.

Appenzeller, C., Davies, H. C., Norton, W. A., 1996. Fragmentation of stratospheric intrusions, J. Geophys. Res., 101, 1435– 1456.

Appenzeller, C., Holton, J. R., Rosenlof, K. H., 1996b. Seasonal variation of mass transport across the tropopause, J. Geophys. Res., 101, 15,071–15,078.

Austin, J. F., Follows, M. J., 1991. The ozone record at Payerne: An assessment of the cross tropopause flux, Atmos. Environ., Part A, 25, 1873–1880.

Balsley, B. B., Gage, K. S., 1980. The MST radar technique: Potential for middle atmospheric studies, Pure and Applied Geophys., 118(1), 452-493, doi: 10.1007/BF01586464.

Balsley, B. B., Gage, K. S., 1981. On the vertical incidence VHF backscattered power profile from the stratosphere, Geophys. Res. Lett., 8, 1173-1175.

Baumann, K., Stohl, A., 1997. Validation of a long-range trajectory model using gas balloon tracks from the Gordon Bennett Cup 95. J. Appl. Meteo., 36, 711-720.

Beekmann, M., Ancellet, G., Blonsky, S., De Muer, D., Ebel, A., Elbern, H., Hendricks, J., Kowol, J., Mancier, C., Sladkovic, R., Smit, H.G.J., Speth, P., Trickl, T., Van Haver, Ph., 1997. Regional and global tropopause fold occurrence and related ozone flux across the tropopause. J. Atmo. Chem., 28, 29-44.

Belair, S., Crevier, L.-P., Mailhot, J., Bilodeau, B., Delage, Y., 2003. Operational Implementation of the ISBA Land Surface Scheme in the Canadian Regional

Weather Forecast Model. Part I: Warm Season Results. J. Hydrometeor, 4, 352–370, doi: 10.1175/1525-7541(2003)4<352:OIOTIL>2.0.CO;2.

Bethan, S., G. Vaughan, S. J. Reid, 1996. A comparison of ozone and thermal tropopause heights and the impact of tropopause definition on quantifying the ozone content of the troposphere, Q. J. R. Meteorol. SOC. 122, pp. 929-944.

Bougeault, P., 1997. Physical parameterization for limited area models: some current problems and issues. Meteor. Atmos. Phys., 63, 71–88, doi: 10.1007/BF01025365.

Bourqui, M. S., 2004. Stratosphere-troposphere exchange from the Lagrangian perspective: a case study and method sensitivities; Atmos. Chem. Phys. Discuss., 4, 3249–3284.

Bourqui, M. S., 2006. Stratosphere-troposphere exchange from the Lagrangian perspective: a case study and method sensitivities, Atmos. Chem. Phys., 6, 2651–2670.

Bourqui, M. S., Trépanier, P.-Y., 2010. Descent of deep stratospheric intrusions during the IONS August 2006 campaign, J. Geophys. Res., 115, D18301, doi:10.1029/2009JD013183.

Brewer, A. M., 1949. Evidence for a world circulation provided by the measurements of helium and water vapor distribution in the stratosphere. Quart. J. Roy. Meteor. Soc., 75, 351–363.

Brewer, A. W., Milford, J. R. 1960. The Oxford-Kew ozone sonde, Proc. Roy. Soc. London, 256, 470-495.

Briggs, B. H., 1968. On the analysis of moving patterns in geophysics, I, Correlation analysis, J. Atmos. Terr. Phys., 30, 1777.

Briggs, B. H., 1977. Ionospheric drifts, J. Atmos. Terr. Phys., 39, 1023.

Briggs, B. H., 1980. Radar observations of atmospheric winds and turbulence: A comparison of techniques, J. Atmos. Terr. Phys., 42, 823.

Briggs, B. H., 1984. The analysis of spaced sensor records by correlation techniques, in Handbook for MAP, 13, 166-186, SCOSTEP Secr., Univ. of Ill., Urbana. IN: Van Baelen, J. S., Tsuda, T., Richmond, A. D., Avery, S. K., S. Kato, Fukao, S., Yamamoto, M., 1990. Comparison of VHF Doppler beam swinging and spaced antenna observations with the MU radar: First results, Radio Sci., 25(4), 629–640.

Briggs, B. H., Phillips, G. J., Shinn, D. H., 1950. The analysis of observations on spaced receivers of the fading of radio signals, Proc. Phys. Soc. London, Sect. B, 63, 106.

Brioude, J., Cammas, J.-P., Cooper, O. R., 2006. Stratosphere-troposphere exchange in a summertime extratropical low: analysis; Atmos. Chem. Phys., 6, 2337–2353.

Butchart, N., Scaife, A. A., 2001. Removal of chlorofluorocarbons by increased mass exchange between the stratosphere and troposphere in a changing climate. Nature, 410, 799–801.

Carswell, A. I., Pal, S. R., Steinbrecht, W., Whiteway, J. A., Ulitsky, A. Wang, T.Y., 1991. Lidar measurements in the middle atmosphere. Can. J. Phys., 69, 1076-1086.

Chen, P., 1995. Isentropic cross-tropopause mass exchange in the extratropics, J. Geophys. Res., 100, 16,661–16,673.

Cohn, S. A., Holloway, C. L., Oncley, S. P., Doviak, R. J., Lataitis, R. J., 1997. Validation of a UHF spaced antenna wind profiler for high-resolution boundary layer observations, Radio Sci., 32(3), 1279-1296.

Collins, W. J., Derwent, R. G., Garnier, B., Johnson, C. E., Sanderson, M. G., Stevenson, D. S., 2003. Effect of stratosphere-troposphere exchange on the future tropospheric ozone trend, J. Geophys. Res., 108, 8528, doi:10.1029/2002JD002617.

Cooper, O. R., Stohl, A., Trainer, M., Thompson, A. M., Witte, J. C., Oltmans, S. J., Morris, G., Pickering, K. E., Crawford, J. H., Chen, G., Cohen, R. C., Bertram, T. H., Wooldridge, P., Perring, A., Brune, W. H., Merrill, J., Moody, J. L., Tarasick, D., Nedelec, P., Forbes, G., Newchurch, M. J., Schmidlin, F. J., Johnson, B. J., Turquety, S., Baughcum, S. L., Ren, X., Fehsenfeld, F. C., Meagher, J. F., Spichtinger, N., Brown, C. C., McKeen, S. A., McDermid, Leblanc, I. S. T., 2006. Large upper tropospheric ozone enhancements above midlatitude North America during summer: In situ evidence from the IONS and MOZAIC ozone monitoring network, J. Geophys. Res. 111, D24S05, doi:10.1029/2006JD007306 (2006).

Cote, J., Desmarais, J.-G., Gravel, S., Méthot, A., Patoine, A., Roch, M., Staniforth, A., 1998b. The Operational CMC–MRB Global Environmental Multiscale (GEM) Model. Part II: Results. Mon. Wea. Rev., 126(6), 1397–1418. doi: 10.1175/1520-0493(1998)126<1397:TOCMGE>2.0.CO;2

Cote, J., Gravel, S., Methot, A., Patoine, A., Roch, M., 1998a. The operational CMC-MRB Global Environmental Multiscale (GEM) model, part I: Design considerations and formulation, Mon. Weather Rev., 126(6), 1373–1395.

Crutzen, P. J., Lawrence, M., 1999. On the background photochemistry of tropospheric ozone, Tellus, 51, 123– 146.

Czechowsky, P., Schmidt, G., Roster, R., 1984. The mobile SOUSY Doppler radar: Technical design and first results, Radio Sci., 19(1), 441-450.

Danielson, E., 1968. Stratospheric-tropospheric exchange based on radioactivity, ozone, and potential vorticity, J. Atmos. Sci., 25, 502–518.

Davies, J., Tarasick, D. W., McElroy, C. T., Kerr, J. B., Fogal, P. F., Savastiouk, V., 2000. Evaluation of ECC Ozonesonde Preparation Methods from Laboratory Tests and Field Comparisons during MANTRA, Proceedings of the Quadrennial Ozone Symposium Sapporo, Japan, 2000, edited by: Bojkov, R. D. and Kazuo, S., pp. 137–138, 2000.

Davies, T. D., Schuepbach, E., 1994. Episode of high ozone concentrations at the Earth's surface resulting from transport down from the upper troposphere/lower stratosphere: A review and case studies, Atmospheric Environment, 28, 53-68.

Davies, T. D., Schuepbach, E., 1994. Episodes of high ozone concentrations at the surface resulting from transport down the upper troposphere/lower stratosphere: A review and case studies, Atmos. Environ., 28, 53– 68.

Derwent, R. G., Simmonds, P. G., Seuring, S., Dimmer, C., 1998.Observation and interpretation of the seasonal cycles in the surface concentrations of ozone and carbon monoxide at Mace Head, Ireland from 1990 to 1994, Atmos. Environ., 32, 145– 157.

Dessler, A. E., Sherwood, S. C., 2004. Effect of convection on the summertime extratropical lower stratosphere, J. Geophys. Res., 109, D23 301, doi:10.1029/2004JD005209.

Dewan, E. M., 1981. Turbulent vertical transport due to thin intermittent mixing layers in the stratosphere and other stable fluids, Sci., 211, 1041, 1042, doi: 10.1126/science.211.4486.1041.

Dorling, S. R., Davies, T. D., Pierce, C. E., 1992. Cluster analysis: a technique for estimating the synoptic meteorological controls on air and precipitation chemistry – method and applications, Atmos. Environ., 26A, 2575–2581.

Doviak, R. J., Doviak, M. E. F., 2003 in Encyclopaedia of Atmospheric Sciences, vol. 5, edited by J. R. Holton, J. A. Curry, and J. A. Pyle, pp. 1802– 1812, Elsevier, New York.

Doviak, R. J., Zrnic, D. S., 1984a Reflection and scatter formula for an isotropically turbulent air, Radio Sci., 19, 325-336,.

Doviak, R. J., Zrnic, D. S., 1984b. Doppler radar and weather observations, Academic Press, Orlando, Fla.; Toronto.

Draxler, R. R., 2003. Evaluation of an ensemble dispersion calculation, J. Appl. Meteorol., 42, 308–317.

Draxler, R. R., Heffter, J. L., 1989. Across North America Tracer Experiment (ANATEX), vol. I, Description, Ground-Level Sampling at Primary Sites, and Meteorology, NOAA Tech. Memo., ERL ARL-167, 83pp.

Draxler, R. R., Rolph, G. D., 2003. HYSPLIT (HYbrid Single-Particle Lagrangian Integrated Trajectory), Model access via NOAA ARL READY Website NOAA Air Resources Laboratory, Silver Spring, MD, http://www.arl.noaa.gov/ready/hysplit4.html.

Egger, J., 1995. Tropopause height in baroclinic channel flow, J. Atmos. Sci., 52, 2232–2241.

Emanuel, K. A., Zivkovic-Rothman, M., 1999. Development and evaluation of a convection scheme for use in climate models. Journal of Atmospheric Science 56, 1766–1782.

EN-SCI Corporation, Instruction Manual, Model 1Z ECC-O3-Sondes, Boulder, Colo., 1994.

EN-SCI Corporation, Instruction Manual, Model 1Z ECC-O3-Sondes, Boulder, Colo., 1996.

Esler, J. G., Tan, D. G. H., Haynes, P. H., Evans, M. J., Law, K. S., Plantevin, P. H., Pyle, J. A., 2001. Stratosphere-troposphere exchange: Chemical sensitivity to mixing, J. Geophys. Res., 106, 4717– 4731.

ESPERE Climate Encyclopaedia, 2004 – 2006. http://espere.mpch-mainz.mpg.de/documents/pdf.

Fabian, P., Pruchniewicz, P. G., 1977. Meridional distribution of ozone in the troposphere and its seasonal variation, J. Geophys. Res., 82, 2063– 2073.

Fedor, L. S., 1967. A statistical approach to the determination of three-dimensional ionospheric drifts, J. Geophys. Res., 72, 5401.

Fishman, J., Solomon, S., Crutzen, P. J., 1979. Observational and theoretical evidence in support of a significant in-situ photochemical source of tropospheric ozone, Tellus 31, 432-446.

Flesch, T. K., Wilson, J. D., Yee, E., 1995. Backward-time Lagrangian stochastic dispersion models, and their application to estimate gaseous emissions. J. Appl. Meteorol., 34:1320-1332.

Follows, M. J., Austin, J. F., 1992. A zonal average model of the stratospheric contributions to the tropospheric ozone budget, J. Geophys. Res., 97, 18,047– 18,060.

Forster, C., Cooper, O. R., Stohl, A., Eckhardt, S., James, P., Dunlea, E. J., Nicks, D. K., Holloway, J. S., Hubler, G., Parrish, D. D., Ryerson, T. B., Trainer, M., 2004. Lagrangian transport model forecasts and a transport climatology for the Intercontinental Transport and Chemical Transformation 2002 (ITCT 2K2) measurement campaign, J. Geophys. Res. 109, D07S92, doi:10.1029/2003JD003589.

Forster, C., Stohl, A., Seibert, P., 2007: Parameterization of Convective Transport in a Lagrangian Particle Dispersion Model and Its Evaluation. J. Appl. Meteor. Climatol., 46, 403–422, doi: 10.1175/JAM2470.1.

Forster, C., Wandinger, U., Wotawa, G., James, P., Mattis, I., Althausen, D., Simmonds, P., O'Doherty, S., Kleefeld, C., Jennings, S. G., Schneider, J., Trickl, T., Kreipl, S., Jager, H., Stohl, A., 2001. Transport of boreal forest fire emissions from Canada to Europe, J. Geophys. Res., 106, 22887–22906, doi:10.1029/2001JD900115.

Frederick, J. E., 2003. Ozone as a UV Filter, in Encyclopaedia of Atmospheric Sciences, vol. 5, edited by J. R. Holton, J. A. Curry, and J. A. Pyle, pp. 1621– 1627, Elsevier, New York.

Frederick, J. E., Cebula, R. P., Heath, D. F., 1986. Instrument characterization for the detection of long-term changes in stratospheric ozone: an analysis of the SBUV/2 radiometer, J. Atmos. Oceanic Tech., 3, 472-480.

Frisch, A. S., Clifford, S. F., 1974. A Study of Convection Capped by a Stable Layer Using Doppler Radar and Acoustic Echo Sounders. J. Atmos. Sci., 31, 1622–1628. doi: 10.1175/1520-0469(1974)031<1622:ASOCCB>2.0.CO;2.

Frisch, A. S., Strauch, R. G., 1976. Doppler Radar Measurements of Turbulent Kinetic Energy Dissipation Rates in a Northeastern Colorado Convective Storm, J Appl. Meteor., 15(9), 1012-1017, doi: 10.1175/1520-0450(1976)015<1012:DRMOTK>2.0.CO;2.

Fritts, D., Rastogi, P., 1985. Convective and dynamical instabilities due to gravity wave motions in the lower and middle atmosphere: Theory and observations, Radio Sci., 20(6), 1247-1277.

Fukao, S., 1989. Middle Atmosphere Program, Handbook for MAP, Volume 30: International School on Atmospheric Radar, SCOSTEP Secr., Univ. of ill., Urbana.

Fukao, S., Inaba, M., Kimura, I., May, P., Sato, T., Tsuda, T., Kato, S., 1988b. A systematic error in MST/ST radar wind measurement induced by a finite range volume effect 2. Numerical considerations, Radio Sci., 23(1), 74-82.

Fukao, S., Sato, T., Kato, S., Harper, R. M., Woodman, R. F., Gordon, W. E., 1979. Mesospheric winds and waves over Jicamarca on May 23-24, 1974, J. Geophys. Res., 84, 4379.

Fukao, S., Sato, T., May, P., Tsuda, T., Kato, S., Inaba, M., Kimura, I., 1988a. A systematic error in MST/ST radar wind measurement induced by a finite range volume effect 1. Observational results, Radio Sci., 23(1), 59-73.

Fukao, S., Sato, T., Tsuda, T., Kato, S., Wakasugi, K., Makihira, T., 1985. The MU radar with an active phased array system-1. Antenna and power amplifiers, 2. In-house equipment, Radio Sci., 20(6), 1155-1176.

Fukao, S., Sato, T., Yamasuki, N., Harper, R. M., Kato, S., 1982. Winds measured by a UHF Doppler radar and rawindsondes Comparison made on 26 days (Aug.- Sept. 1977) at Arecibo, Puerto Rico, J. Appl. Meteorol., 21, 1357.

Fukao, S., Yamanaka, M., Ao, N., Hocking, W., Sato, T., Yamamoto, M., Nakamura, T., T. T., Kato, S., 1994. Seasonal variability of vertical eddy diffusivity in the middle atmosphere. Three-year observations by the middle and upper atmosphere radar, J. Geophys. Res., 99, 18,973–18,987.

Gage, K. S., B. B. Balsley, 1978: Doppler Radar Probing of the Clear Atmosphere. Bull. Amer. Meteor. Soc., 59, 1074–1093, doi: 10.1175/1520-0477(1978)059<1074:DRPOTC>2.0.CO;2.

Gage, K. S., B. B. Balsley, 1984. MST radar studies of wind and turbulence in the middle atmosphere. J. Atmos. Terr. Phys., 46, 739–753, doi: 10.1175/2008JTECHA1113.1.

Gage, K. S., Balsley, B. B., 1980. On the scattering and reflection mechanisms contributing to clear-air radar echoes from the troposphere, stratosphere, and mesosphere, Radio Sci., 15, 293.

Gage, K. S., Balsley, B. B., Green, J. L., 1981. Fresnel scattering model for the specular echoes observed by VHF radar, Radio Sci., 16, 1447-1453.

Gage, K. S., Green, J. L., 1978. Evidence for specular reflection from monostatic VHF radar observations of the stratosphere. Radio Sci., 13, 991 – 1001.

Gage, K. S., Green, J. L., 1979. Tropopause detection by partial specular reflection using VHF radar, Science, 203, 1238-1240.

Gage, K. S., Green, J. L., 1982. An objective method for determination of tropopause height from VHF radar observations. J. Appl. Meteor., 21, 1159 – 1163.

Gage, K. S., Nastrom, G. D., 1985. Relationship of Precipitation to Vertical Motion Observed Directly by a VHF Wind Profiler During a Spring Upslope Storm Near Denver, Colorado, Bull. Amer. Meteor. Soc., 66, 394–397, doi: 10.1175/1520-0477(1985)066<0394:ROPTVM>2.0.CO;2.

Galani, E., Balis, D., Zanis, P., Zerefos, C., Papayannis, A., Wernli, H., Gerasopoulos, E., 2003. Observations of stratosphere-to-troposphere transport events over the eastern Mediterranean using a ground-based lidar system, J. Geophys. Res., 108(D12), 8527, doi:10.1029/2002JD002596.

Galmarinia, S., Bianconib, R., Klugc, W., Mikkelsend, T., Addise, R., Andronopoulosf, S., Astrupd, P., Baklanovg, A., Bartnikif, J., Bartzish, J. C., Bellasiob, R., Bompayi, F., Buckleye, R., Bouzomi, M., Championm, H., D'Amoursn, R., Davakisf, E., Eleveldj, H., Geertsemak, G. T., Glaabl, H., Kollaxo, M., Ilvonenu, M., Manningm, A., Pechingerp, U., Perssono, C., Polreichp, E., Potemskiq, S., Prodanovar, M., Saltbonesh, J., Slaperj, H., Sofievt, M. A., Syrakovr, D., Sørenseng, J. H., Van der Auweras, L., Valkamat, I., Zelaznyq, R., 2004. Ensemble dispersion forecasting—Part I: concept, approach and indicators, Atmos. Environ., 38(28), 4607-4617, doi:10.1016/j.atmosenv.2004.05.030.

Gettleman, A., Sobel, A. H., 2000. Direct diagnoses of stratosphere-troposphere exchange, J. Atmos. Sci., 57, 3 –16.

Goering, M. A., Gallus, W. A. Jr., Olsen, M. A., Stanford, J. L., 2001. Role of stratospheric air in a severe weather event: Analysis of potential vorticity and total ozone. J. Geophys. Res., 106, 11813–11823.

Gravel, S., Erfani, A., Graman, U., 2004. A comparison of an interactive and noninteractive approach to mesoscale forecasting using the IOP-2B of MAP. Preprint: 11th Conference on Mountain Meteorology and the Annual Mesoscale Alpine Program (MAP), Bartlet, NH., June 20-25.

Green, J. L., Gage, K. S., 1980. Observations of stable layers in the troposphere and stratosphere using VHF radar, Radio Sci., 15, 395-406.

Green, J. L., Gage, K. S., van Zandt, T. E., 1979. Atmospheric measurements by VHF pulsed Doppler radar," IEEE Trans. Geosci. Electron., GE-17, 262-280.

Gregg, M. C., 1977: Variations in the Intensity of Small-Scale Mixing in the Main Thermocline. J. Phys. Oceanogr., 7, 436–454. doi: 10.1175/1520-0485(1977)007<0436:VITIOS>2.0.CO;2.

Gregory, J. B., Meek, C. E., Manson, A. H., Stephenson, D. G., 1979. Developments in the radio wave drifts technique for measurement of high-altitude winds, J. Appl. Meteorol., 18, 682.

Hall, M. P. M., 1984. A review of the application of multiple-parameter radar measurement of precipitation, Radio Sci., 19(1), 37–43, doi:10.1029/RS019i001p00037.

Hanna, S. R., 1982. Applications in air pollution modeling. In: Atmospheric turbulence and Air Pollution Modelling, editors F. T. M. Nieuwstadt and van Dop, H. Reidel, Dordrecht, Holland.

Hanssen R. F., 2001. RADAR INTERFEROMETRY, Data Interpretation and Error Analysis, Kluwer Academic Publishers, eBook ISBN: 0-306-47633-9, Print ISBN: 0-7923-6945-9.

Harper, R. M., Gordon, W. E., 1980. A review of radar studies of the middle atmosphere, Radio Sci., 15, 195.

Harris, J. M., Oltmans, S. J., Dlugokencky, E. J., Novelli, P. C., Johnson, B. J., Mefford, T., 1998. An investigation into the source of the springtime tropospheric ozone maximum at Mauna Loa Observatory, Geophys. Res. Lett., 25, 1895–1898, doi:10.1029/98GL01410.

Harrison, R. M., 1999. Understanding our Environment: An Introduction to Environmental Chemistry and Pollution, The Royal Society of Chemistry, third Edition, ISBN 0-85404-584-8.

Hartjenstein, G., 2000. Diffusive decay of tropopause folds and the related cross-tropopause mass flux, Mon. Wea. Rev., 128, 2958–2966.

Hauglustaine, D. A., Brasseur, G. P., Walters, S., Rasch, P. J., Muller, J., Emmons, L., Carroll, M. A., 1998. MOZART, a global chemical transport model for ozone and related chemical species: Model results and evaluation, J. Geophys. Res., 103, 28, 291– 28, 335.

Haynes, P. H., McIntyre, M. E., Shepherd, T. G., Marks, C. J., Shine, K. P., 1991. On the "downward control" of extratropical diabatic circulations by eddy-induced mean zonal forces. J. Atmos. Sci., 48, 651–678.

Haynes, P., Anglade, J., 1997. The Vertical-Scale Cascade in Atmospheric Tracers due to Large-Scale Differential Advection. J. Atmos. Sci., 54, 1121–1136, doi: http://dx.doi.org/10.1175/1520-0469(1997)054<1121:TVSCIA>2.0.CO;2.

He, H., Tarasick, D. W., Hocking, W. K., Carey-Smith, T. K., Rochon, Y., Zhang, J., Makar, P. A., Osman, M., Brook, J., Moran, M. D., Jones, D. B. A., Mihele, C., Wei, J. C., Osterman, G., Argal, P. S., McConnel, J., Bourqui, M. S., 2011. Transport analysis of ozone enhancement in Southern Ontario during BAQS-Met, Atmos. Chem. Phys., 11, 2569–2583, doi:10.5194/acpd-10-15559-2010.

Hilsenrath, E., 2003. The Stratospheric Ozone Electronic Textbook, NASA's Goddard Space Flight Center Atmospheric Chemistry and Dynamics Branch (Code 916), http://www.ccpo.odu.edu/~lizsmith/SEES/ozone/class/Chap_7/index.htm.

Hintsa, E. J., Boering, K. A., Weinstoc, E. M., Anderson, J. G., Gary, B. L., Pfister, L., Daube, B. C., Wofsy, S. C., Loewenstein, C., Podolske, J. R., Margitan, J. J., Bui, T. P., 1998. Troposphere-to-stratosphere transport in the lowermost stratosphere from measurements of H2O, CO2, N2O and O3. Geophys. Res. Lett., 25, 2655–2658.

Hirsch, A. I., Munger, J. W., Jacob, D. J., Horowitz, L. W. Goldstein, A. H., 1996. Seasonal variation of the ozone production efficiency per unit NOx at Harvard Forest, Massachusetts. J. Geophys. Res. 101, 12659–12666.

Hocking, W. K, 1991. The effects of middle atmosphere turbulence on coupling between atmospheric regions. J. Geomag. Geoelectr.43 (Suppl), 621–636.

Hocking, W. K., 1983a. On the extraction of atmospheric turbulence parameters from radar backscatter Doppler spectra I, Theory, J. Atmos. Terr. Phys., 45, 89-102.

Hocking, W. K., 1983c. The spaced antenna drift method, in Handbook for MAP, Vol. 9, pp.171-186, SCOSTEP Secr., Univ. of ill., Urbana. IN: Van Baelen, J. S., Tsuda, T., Richmond, A. D., Avery, S. K., S. Kato, Fukao, S., Yamamoto, M., 1990. Comparison of VHF Doppler beam swinging and spaced antenna observations with the MU radar: First results, Radio Sci., 25(4), 629–640.

Hocking, W. K., 1985. Measurement of turbulent energy dissipation rates in the middle atmosphere by radar techniques: A review, Radio Sci., 20, 1403.

Hocking, W. K., 1989. Target Parameter Estimation, In: Fukao, S., editor. Middle Atmosphere Program, Handbook for MAP, Volume 30: International School on Atmospheric Radar, SCOSTEP Secr., Univ. of ill., Urbana.

Hocking, W. K., 2009. MST12, the Twelfth International Radar School, Lecture on Technical and Scientific Aspects of MST Radar, London, Ontario, Canada, 12 – 16 May.

Hocking, W. K., 2011. A review of Mesosphere–Stratosphere–Troposphere (MST) radar developments and studies, circa1997–2008, J. Atmos. Sol. Terr. Phys., 73, 848–882, doi:10.1016/j.jastp.2010.12.009.

Hocking, W. K., Carey-Smith, T., Tarasick, D. W., Argall, P. S., Strong, K., Rochon, Y., Zawadzki, I., Taylor, P. A., 2007. Detection of Stratospheric Ozone Intrusions by Windprofiler Radars, Nature, 450, 281-284.

Hocking, W. K., Hamza, A. M., 1997: A quantitative measure of the degree of anisotropy of turbulence in terms of atmospheric parameters, with particular relevance to radar studies. J. Atmos. Sol. Terr. Phys., 59, 1011–1020.

Hocking, W. K., Mu, P. K. L., 1997. Upper and middle tropospheric kinetic energy dissipation rates from measurements of $\overline{C_n^2}$ - Review of theories, in-situ investigations, and experimental studies using the Buckland Park atmospheric radar in Australia. J. Atmos. Terr. Phys., 59, 1779–1803.

Hogrefe, C., Lynn, B., Civerolo, K., Rosenthal, J., Rosenthal, J., Rosenzweig, C., Gaffin, S., Knowlton, K., Knowlton, K., Kinney, P. L., 2004. Simulating changes in regional air pollution over the eastern United States due to changes in global and

regional climate and emissions. J. Geophys. Res. 109, D22301, doi:10.1029/2004JD004690.

Holton, J. R., 2003. Stratosphere–Troposphere Exchange – Global scale, in Encyclopaedia of Atmospheric Sciences, vol. 5, edited by J. R. Holton, J. A. Curry, and J. A. Pyle, pp. 2137– 2143, Elsevier, New York.

Holton, J. R., 2004. An Introduction to Dynamic Meteorology, Fourth Edition, Elsevier Academic Press.

Holton, J. R., Haynes, P. T., Mclntyre, M. E., 1995. Stratosphere-troposphere exchange, Rev. Geophys., 33, 403–439.

Hooper, D. A., Arvelius, J., 2000. Monitoring of the arctic winter tropopause: a comparison of radiosonde, ozonesonde and MST radar observations. In: Edwards, B., editor, STEP Handbook, Proceedings of the ninth International Workshop on Technical and Scientific Aspects of MST Radar combined with COST76 Final Profiler Workshop, Toulouse, France, pp.385–388.

Hooper, D. A., Nash, J., Oakley, T., Turp, M., 2008. Validation of a new signal processing scheme for the MST radar at Aberystwyth. Ann. Geophys. 26(11), 3253–3268.

Hooper, D., Thomas, L., 1995. Aspect sensitivity of VHF scatterers in the troposphere and stratosphere from comparisons of powers in off-vertical beams, J. Atmos. Terre. Phys., 57(6), 655-663.

Hoskins, B. J., 1991. Towards a PV-theta view of the general circulation, Tellus, Ser. A, 43, 27– 35.

Ivey, G. N., Imberger, J., 1991. On the nature of turbulence in a stratified fluid. Part I: The energetics of mixing. J. Phys. Oceanogr., 21, 650–658.

Janach, W.E., 1989. Surface ozone: Trend details, seasonal variations, and interpretation. J. Geophys. Res. 94, (D15), 18289 - 18295.

Jenkins, G. S., Camara, M., Ndiaye, S. A., 2008. Observational evidence of enhanced middle/upper tropospheric ozone via convective processes over the equatorial tropical Atlantic during the summer of 2006, Geophys. Res. Lett., 35, L12806, doi:10.1029/2008GL033954.

Johnson, B. J., Oltmans, S. J., Vomel, H., Smit, H. G. J., Deshler, T., Kroger, C., 2002. Electrochemical concentration cell (ECC) ozonesonde pump efficiency measurements and tests on the sensitivity to ozone of buffered and unbuffered ECC sensor cathode solutions, J. Geophys. Res., 107(D19), 4393, doi:10.1029/2001JD000557.

Kahl, J. D., Samson, P. J., 1988. Uncertainty in Estimating Boundary-Layer Transport during Highly Convective Conditions, J. Appl. Meteorol., 27(9), 1024-1035, doi: 10.1175/1520-0450(1988)027<1024:UIEBLT>2.0.CO;2.

Karpechko, A., 2007. Stratosphere-Troposphere Exchange (Ste): Dynamical Processes In The Stratosphere And Upper Troposphere And Their Influence On The

Distribution Of Trace Gases In The Polar Atmosphere, Academic Dissertation In Meteorology, Finnish Meteorological Institute.

Kentarchos, A. S., Roelofs, G. J., 2003. A model study of stratospheric ozone in the troposphere and its contribution to tropospheric OH formation, J. Geophys. Res., 108(D12), 8517, doi:10.1029/2002JD002598.

Kentarchos, A. S., Roelofs, G. J., Lelieveld, J., 2001. Altitude distribution of tropospheric ozone over the Northern Hemisphere during 1996, simulated with a chemistry-general circulation model at two different horizontal resolutions, J. Geophys. Res., 106, 17,453–17,470.

Kley, D., Crutzen, P. J., Smit, H. G. J., Vomel, H., Oltmans, S. J., Grassl, H., Ramanathan, V., 1996. Observations of near-zero ozone concentrations over the convective pacific: effects on air chemistry, Science, 274, 230–233.

Komhyr, W. D., 1986. Operations handbook-Ozone measurements to 40-km altitude with model 4A electrochemical concentration cell (ECC) ozonesondes (used with 1680 MHz radiosondes), NOAA Tech. Memo. ERL ARL-149, 49 pp., Air Resour. Lab., Boulder, Co.

Komhyr, W. D., Barnes, R. A., Brothers, G. B., Lathrop, J. A., Opperman, D. P., 1995. Electrochemical concentration cell ozonesonde performance evaluation during STOIC 1989, J. Geophys. Res., 100, 9231 – 9244.

Krishna Reddy, K., Lal, S., Kozu, T., Nakamura, K., Ohno, Y., Naja, M., Rao, D. N., 2003. An investigation of ozone and planetary boundary layer dynamics over Gadanki, India, Proceedings of the 10th Workshop on Technical and Scientific Aspects of MST Radar, Piura, Peru, May 13–20, 2003, pp. 330– 333, Piura Univ. Press, Piura, Peru.

Kumar, K. K., 2006. VHF radar observations of convectively generated gravity waves: Some new insights, Geophys. Res. Lett., 33, L01815, doi:10.1029/2005GL024109.

Kumar, K. K., Uma, K. N., 2009. High temporal resolution VHF radar observations of stratospheric air intrusions in to the upper troposphere during the passage of a mesoscale convective system over Gadanki (13.5oN, 79.2o E), Atmos. Chem. Phys. Discuss., 9, 13843–13857.

Labitzke, K., Manson, A. H., Barnett, J. J., Corney, M., 1987. Comparison of geostrophic and observed winds in the upper mesosphere over Saskatoon, Canada, J. Atmos. Terr. Phys., 49, 987.

Ladstatter-Weissenmayer, A., Meyer-Arnek, J., Schlemm, A., Burrows, J. P., 2004. Influence of stratospheric air masses on tropospheric vertical o3 columns based on gome (global ozone monitoring experiment) measurements and back trajectory calculation over the pacific, Atmos. Chem. Phys., 4, 903–909.

Lamarque, J. F., Hess, P. G., 1994. Cross-tropopause mass exchange and potential vorticity budget in a simulated tropopause folding, J. Atmos. Sci., 51, 2246–2269.

Lamarque, J. F., Hess, P. G., 2003. Stratosphere–Troposphere Exchange , Local Processes, in Encyclopaedia of Atmospheric Sciences, vol. 5, edited by J. R. Holton, J. A. Curry, and J. A. Pyle, pp. 2143– 2150, Elsevier, New York.

Lamarque, J. F., Hess, P. G., Tie, X. X., 1999. Three-dimensional study of the influence of stratosphere– troposphere exchange and its distribution on tropospheric chemistry, J. Geophys. Res., 104, 26,363–26,372.

Larsen, M. F., 1983. Can a VHF Doppler radar provide synoptic wind data? A comparison of 30 days of radar and radiosonde data, Mon. Weather. Rev., 111, 2047.

Larsen, M. F., 1989. Application of MST Radars: Meteorological Applications, In: Fukao, S., editor. Middle Atmosphere Program, Handbook for MAP, Volume 30: International School on Atmospheric Radar, SCOSTEP Secr., Univ. of ill., Urbana.

Larsen, M. F., Rotteger, J., 1982. VHF and UHF Doppler radars as tools for synoptic research. Bull. Amer. Meteor. Soc., 63, 996-1008.

Larsen, M. F., Rottger, J., Dennis, T. S., 1988. A Comparison of Operational Analysis and VHF Wind Profiler Vertical Velocities, Mon. Wea. Rev., 116, 48–59, doi: 10.1175/1520-0493(1988)116<0048:ACOOAA>2.0.CO;2.

Legg, B. J., Raupach, M. R., 1982. Markov-chain simulation of particle dispersion in inhomogeneous flows: the mean drift velocity induced by a gradient in Eulerian velocity variance. Boundary-layer Meteorology 24, 3-13.

Lehmann, P., Easson, J. R., 2003. A comparison of pump efficiency corrections for the Australian Brewer-Mast ozonesonde data record, Aust. Meteorl. Mag., 52, 259-264.

Lelieveld, J., Dentener, F., 2000. What controls tropospheric ozone? J. Geophys. Res., 105, 3531– 3551.

Lesicar, D., Hocking, W., Vincent, R., 1994. Comparative studies of scatterers observed by MF radars in the Southern Hemisphere mesosphere. J. Atmos. Terr. Phys. 56, 581–591.

Levy, H., II, 1971. Normal atmosphere: Large radical and formaldehyde concentrations predicted, Sciences, 173, 141-143.

Levy, H., II, Mahlman, J. D., Moxim, W. J., 1980. A stratospheric source of reactive nitrogen in the unpolluted troposphere, Geophys. Res. Lett., 7, 441-444.

Lin, C.-Y. C., Jacob, D. J., Munger, J. W. Fiore, A. M., 2000. Increasing background ozone in surface air over the United States. Geophys. Res. Lett. 27, 3465–3468.

Lin, J. C., Gerbig, C., 2005. Accounting for the effect of transport errors on tracer inversions, Geophys. Res. Lett., 32, L01802, doi:10.1029/2004GL021127.

Lin, J. C., Gerbig, C., Wofsy, S. C., Andrews, A. E., Daube, B. C., Davis, K. J., Grainger, C. A., 2003. A near-field tool for simulating the upstream influence of

atmospheric observations: The Stochastic Time-Inverted Lagrangian Transport (STILT) model, J. Geophys. Res., 108(D16), 4493, doi:10.1029/2002JD003161.

Liu, S. C., Trainer, M., Fehsenfeld, F. C., Parrish, D. D., Williams, E. J., Fahey, D. W., Hobler, G., Murphy, P. C., 1987. Ozone production in the rural troposphere and the implications for regional and global ozone distributions, J. Geophys. Res., 92, 4191– 4207.

Logan, J. A., 1994. Trends in the vertical distribution of ozone: An analysis of ozonesonde data. J. Geophys Res., 99, p. 25553-25585.

Mailhot, J., Sarrazin, R., Bilodeau, B., Brunet, N., Pellerin, G., 1997. Development of the 35-km version of the regional finite element model. Atmos.–Ocean, 35, 1–28, doi:10.1080/07055900.1997.9649583.

Mandal, T. K., Cho, J. Y. N., Rao, P. B., Jain, A. R., Peshin, S. K., Srivastava, S. K., Bohra, A. K., Mitra, A. P., 1998. Stratosphere-troposphere ozone exchange observed with the Indian MST radar and a simultaneous balloon-borne ozonesonde, Radio Sci., 33(4), 861-893.

Marshall, J., Plumb, A., 2007. Circulation of the Atmosphere and Ocean: an introductory text, Massachusetts Institute of Technology, www-paoc.mit.edu.

Martin, R. V., Sauvage, B., Folkins, I., Sioris, C. E., Boone, C., Bernath, P., Ziemke, J., 2007. Space-based constraints on the production of nitric oxide by lightning, J. Geophys. Res., 112, D09309, doi:10.1029/2006JD007831.

Maryon, R. H., Best, M. J., 1995. Estimating the emissions from a nuclear accident using observations of radioactivity with dispersion model products, Atmos. Environ., 29(15), 1853-1869, doi:10.1016/1352-2310(95)00042-W.

May, P., Fukao, S., Tsuda, T., Sato, T., Kato, S., 1988. The effect of thin scattering layers on the determination of wind by Doppler radars, Radio Sci., 23(1), 83-94.

Meek, C. E., Manson, A. H., 1985. Combination of Primrose Lake (54oN, 110oW) ROCOB winds (20-60 km) and Saskatoon (52oN, 107oW) MF radar winds (60-110 km): 1978-1983, J. Atmos. Terr. Phys., 47, 477.

Meek, C. E., Manson, A. H., 1987b. Mesospheric motions observed by simultaneous medium-frequency interferometer and spaced antenna experiments, J. Geophys. Res., 92, 5627.

Miller, K. L., Bowhill, S. A., Gibbs, K. P., Countryman, I. D., 1978. First measurements of mesospheric vertical velocities by VHF radar at temperate latitudes, Geophys. Res. Lett., 5(11), 939-942.

Mitra, S. N., 1949. A radio method of measuring winds in the ionosphere, Proceedings of the Institute of electrical engineers 96, 441-446.

Mohanakumar, K., 2008. Stratosphere Troposphere Interactions, ISBN 978-1-4020-8216-0, Springer.

Monks, P. S., 2000. A review of the observations and origins of the spring ozone maximum, Atmos. Environ., 34, 3545– 3561.

Mote, P. W., Rosenlof, K. H., Mclntyre, M. E., Carr, E. S., Gille, J. C., Holton, J. R., Kinnersley, J. S., Pumphrey, H. C., Russell, J. M. III, Waters, J. W., 1996. An atmospheric tape recorder: The imprint of tropical tropopause temperatures on stratospheric water vapor. J. Geophys. Res., 101, 3989–4006.

Mullendore, G. L., Durran, D. R., Holton, J. R., 2005. Cross-tropopause tracer transport in midlatitude convection, J. Geophys. Res., 110, D06113, doi:10.1029/2004JD005059.

Muramatsu, H., Sasaki, T., Hirota, M., Makino Y., 1984. An aircraft observation of an intrusion process of stratospheric ozone into the troposphere, Pap. Meteorol. Geophys., 35, 1–10, doi:10.2467/mripapers.35.1.

Nastrom, G., Eaton, F., 1997. Turbulent eddy dissipation rates from radar observations at 5-20 km at White Sand missile range: New Mexico, J. Geophys. Res., 102, 19,495–19,505.

Nastrom, O. D., Ecklund, W. L., Gage, K. S., 1985: Direct Measurement of Large-Scale Vertical Velocities Using Clear-Air Doppler Radars. Mon. Wea. Rev., 113, 708–718, doi: 10.1175/1520-0493(1985)113<0708:DMOLVV>2.0.CO;2.

Nehrkorn, T., Eluszkiewicz, J., Wofsy, S. C., Lin, John, C.; Gerbig, C., Longo, M., Freitas, S., 2010. Coupled weather research and forecasting-stochastic time-inverted Lagrangian transport (WRF-STILT) model, Meteorol. Atmos. Phys., 107(1-2), 51-64, doi: 10.1007/s00703-010-0068-x.

Osman, M., Hocking, W., Tarasick, D., Drummond, J., 2010. Stratosphere-Troposphere Exchange of Ozone from 24 Feb – 18 April 2008 in Eureka, Canada", In: Swarnalingam, N. and Hocking, W. K., editors, MST12, Proceedings of the Twelfth International Workshop on Technical and Scientific Aspects of MST Radar, London, Ontario, Canada, Canadian Association of Physicists (CAD), ISBN: 978-9867285-0-1, pp. 291-294.

Parrish, D. D., Holloway, J. S., Jakoubek, R., Trainer, M., Ryerson, T. B., Hubler, G., Fehsenfeld, F. C., Moody, J. L., Cooper, O. R., 2000. Mixing of anthropogenic pollution with stratospheric ozone: A case study from the North Atlantic wintertime troposphere, J. Geophys. Res., 105, 24, 363– 24,374.

Patra, P. K., Lal, S., 1997. Variability of eddy diffusivity in the stratosphere deduced from vertical distributions of N2O and CFC-12, J. Atmos. Solar Terr. Phys., 5(10), 1149-1157.

Pavelin, E., Whiteway, J. A., Busen, R., Hacker, J., 2002. Airborne observations of turbulence, mixing, and gravity waves in the tropopause region, J. Geophys. Res., 107(D10), 4084, doi:10.1029/2001JD000775.

Pawson, S., Labitzke, K., Leder, S., 1998. Stepwise changes in stratospheric temperature, Geophys. Res. Lett., 25, 2157– 2160.

Peebles, P. Z., Jr., 1998. RADAR PRINCIPLES, ISBN 0-471-25205-0, John Wiley and Sons, Inc.

Penkett, S. A., Brice, K. A., 1986. The spring maximum in photo-oxidants in the Northern Hemisphere troposphere, Nature, 319, 655– 657.

Pepler, S. J., Vaughan, G. Hooper, D. A., 1998. Detection of turbulence around jet streams using a VHF radar, Q. J. R. Meteorol. SOC., 124, 447-462.

Phillips, G. J., Spencer, M., 1955. The effects of anisometric amplitude patterns on the measurement of ionospheric drifts, Proc. Phys. Soc. London, Sect. B, 68, 481.

Pierrehumbert, R. T., Yang, H., 1993.Global chaotic mixing on isentropic surfaces, J. Atmos. Sci., 50, 2462–2480.

Plumb, R. A., 1996. A "tropical pipe" model of stratospheric transport. J. Geophys. Res., 101, 3957–3972.

Plumb, R. A., Eluszkiewicz, J., 1999. The Brewer–Dobson Circulation: Dynamics of the Tropical Upwelling. J. Atmos. Sci., 56, 868–890.

Praskovsky, A. A., Praskovskaya, E. A., 2003. Structure-function-based approach to analyzing received signals for spaced antenna radars, Radio Sci., 38(4), 1068, doi:10.1029/2001RS002544.

Rao I. S., Anandan, V. K., Reddy, P. N., 2008. Evaluation of DBS wind measurement technique in different beam configurations for a VHF wind profiler, J. Atmos. Oceanic Technol. 25, 2304–2312, doi: 10.1175/2008JTECHA1113.1.

Rao, T. N., Arvelius, J., Kirkwood, S., 2008. Climatology of tropopause folds over a European Arctic station (Esrange), J. Geophys. Res., 113, D00B03, doi:10.1029/2007JD009638.

Reed, R. J., Danielsen, 1959. Fronts in the vicinity of the tropopause. Arch. Meteor. Geophys. Bioklim, A11, 1-11.

Reiter, E. R., 1975. Stratospheric-Tropospheric Exchange Processes, Rev. Geophys. Space Phys., 13,459.

Reiter, E. R., Glasser, M. E., Mahlman, J. D., 1969. The role of the tropopause in the stratosphere-troposphere exchange processes. Rev. Geophys. Space Phys., 13, 459 – 473.

Rind, D., Shindell, D., Lonergan, P., Balachandran, N. K., 1998. Climate change and the middle atmosphere. Part III: The doubled CO2 climate revisited, J. Clim., 11, 876–894.

Rodean, H., 1996. Stochastic Lagrangian Models of Turbulent Diffusion, Meteorological Monographs, Vol. 26 (48). American Meteorological Society, Boston, U.S.A.

Roelofs, G. J., Lelieveld, J., 1997. Model study of the influence of cross-tropopause ozone transport on tropospheric ozone levels, Tellus, Ser. B, 49, 38– 55.

Roelofs, G.-J., Lelieveld, J., 1997. Model study of the influence of cross-tropopause O3 transport on tropospheric O3 levels, Tellus, 49B, 38-55.

Rosenlof, K. H., 1995. The seasonal cycle of the residual mean meridional circulation in the stratosphere, J. Geophys. Res., 100, 5173– 5191.

Roster, R., 1984. Winds and waves in the middle atmosphere as observed by ground-based radars, Adv. Space Res., 4, 3-18.

Rotteger, J., 1980a. Reflection and scattering of VHF radar signals from atmospheric refractivity structures, Radio Sci., 15, 259.

Rotteger, J., 1980b. Structure and dynamics of the stratosphere and mesosphere revealed by VHF radar investigations. Pure Appl. Geophys., 118(1), 494-527.

Rotteger, J., Liu, C. H., 1978. Partial reflection and scattering of VHF radar signals from the clear atmosphere. Geophys. Res. Lett., 5, 357 – 360.

Rotteger, J., Vincent, R. A., 1978. VHF radar studies of troposphere velocities and irregularities using spaced antenna techniques. Geophys. Res. Lett., 5, 917 – 920.

Rottger, J. 1981. Investigations of lower and middle atmosphere dynamics with spaced antenna drifts radars, J. Atmo. Terr. Phys., 43(4), 277-292.

Rottger, J., Ierkic, H. M., 1985. Postset beam steering and interferometer applications of VHF radars to study winds, waves, and turbulence in the lower and middle, atmosphere, Radio Sci., 20, 1461–1480.

Rottger, J., Klostermeyer, J., Czechowsky, P., Roster, R., Schmidt, G., 1978. Remote sensing of the atmosphere by VHF radar experiments, Naturwiss., vol. 65, pp. 285-296,

Rottger, J., Larsen, M. F., 1990. UHF/VHF radar techniques for atmospheric research and wind profiler applications. Radar in Meteorology, D. Atlas, Ed., Amer. Meteor. Soc., 235–281.

Rottger, J., Liu, C. H., 1978. Partial reflection and scattering of VHF radar signals from the clear atmosphere, Geophys. Res. Left., 5, 357.

Rottger, J., Vincent, R. A., 1978. VHF radar studies of tropospheric velocities and irregularities using spaced antenna techniques, Geophys. Res. Left., 5, 917.

Ruster, R., Klostermeyer, J., Rottger, J., 1986. SOUSY VHF Radar Measurements in the Lower and Middle Atmosphere, IEEE Trans. Geosci. Rem. Sensing, GE-24, 6, 966 – 974.

Ryall, D. B., Derwent, R. G., Manning, A. J., Simmonds, P. G., O'Doherty, S., 2001. Estimating source regions of European emissions of trace gases from observations at Mace Head, Atmos. Environ., 35 (14) 2507 – 2523, doi: 10.1016/S1352-2310(00)00433-7.

Saggio, A., Imberger, J., 2001. Mixing and turbulent fluxes in the metalimnion of a stratified lake. Limnol. Oceanogr., 46(2), 392–409.

Saha, K., 2008. The Earth's Atmosphere: Its Physics and Dynamics, Springer, ISBN: 978-3-540-78426-5, e-ISBN: 978-3-540-78427-2.

Sand, W. R., Musil, D. J., Kyle, T. G., 1974. Observations of turbulence and icing inside thunderstorms. Preprints 6th Conf. Aerospace and Aeronautical Meteorology, El Paso, Amer. Meteor Soc., 299-304.

Sausen, R., Santer, B. D., 2003. Use of changes in tropopause height to detect influences on climate. Meteorol Z 12(3): 131–136, doi: 10.1127/0941-2948/2003/0012-0131.

Sauvage, B., Martin, R. V., Donkelaar, A. van, Ziemke, J. R., 2007a. Quantification of the factors controlling tropical tropospheric ozone and the South Atlantic maximum, J. Geophys. Res., 112, D11309, doi:10.1029/2006JD008008.

Sawford, B. L., 2006. Lagrangian Stochastic Modelling of Chemical Reaction in a Scalar Mixing Layer, Boundary-Layer Meteorol., 118(1), 1-23, doi: 10.1007/s10546-005-4737-0.

Scheele, M. P., Siegmund, P. C., Velthoven, P. F. J., 1996. Sensitivity of trajectories to data resolution and its dependence on the starting point: in or outside a tropopause fold, Meteorol. Appl., 3, 267–273, doi: 10.1002/met.5060030308.

Schmidt, G., Roster, R., Czechowsky, P., 1979. Complementary code and digital filtering for detection of weak VHF radar signals from the mesosphere," IEEE Trans. Geosci. Electron., GE-17, 154-161.

Schoeberl, M. R., 2004. Extratropical stratosphere-troposphere mass exchange, J. Geophys. Res., 109, D13303, doi:10.1029/2004JD004525.

Schuepbach, E., Davies, T., Massacand, A., 1999. An unusual spring time ozone episode at high elevation in the Swiss Alps: Contributions both from cross-tropopause exchange and from the boundary layer, Atmos. Environ., 33, 1735– 1744.

Schulz, A., Rex, M., Harris, N. R. P., Braathen, G. O., Reimer, E., Alfier, I., Kilbane-Dawe, R.,., Eckermann, S., Allaart, M., Alpers, M., Bojkov, B., Cisneros, J., Claude, H., Cuevas, E., Davies, J., De Backer, H., Dier, H., Dorokhov, V., Fast, H., Godin, S., Johnson, B., Kois, B., Kondo, Y., Kosmidis, E., Kyro, E., Litynska, Z.,. Mikkelsen, S., Molyneux, M. J., Murphy, G., Nagai, T., Nakane, H., O'Connor, F., Parrondo, C., Schmidlin, F. J., Skrivankova, P., Varotsos, C., Vialle, C., Viatte, P., Yushkov, V., Zerefos, C., Gathen, P. von der, 2001. Arctic ozone loss in threshold conditions: Match observations in 1997/98 and 1998/99, J. Geophys. Res., 106, 7495– 7504.

Science Pump Corporation, Electrochemical Concentration Cell Ozonesonde Model ECC-1A Instruction Manual, Camden, N. J., 1968.

Science Pump Corporation, Operator's Manual Model 6A ECC Ozonesonde, Camden, N. J., 1996.

Science Pump Corporation, Operator's Manual Model 6A ECC Ozonesonde, SPC, 1999.

Seibert, P., Beyrich, F., Gryning, S.-E., Joffre, S., Rasmussen, A., Tercier, P., 2000. Review and intercomparison of operational methods for the determination of the mixing height, Atmos. Environ., 34, 1001-1027.

Seibert, P., Kruger, B., Frank, A., 2001. Parametrisation of convective mixing in a Lagrangian particle dispersion model. Proceedings of the Fifth GLOREAM Workshop, Wengen, Switzerland, 24–26 September 2001.

Seo, K.-H., Bowmanm, K., 2002. Lagrangian estimate of global stratosphere-troposphere mass exchange, J. Geophys. Res., 107(D21), 4555, doi:10.1029/2002JD002441.

Shapiro, M. A., 1976. The role of turbulent heat flux in the generation of potential vorticity in the vicinity of upper-level jet stream systems, Mon. Wea. Rev., 104, 892–906.

Shapiro, M. A., 1980. Turbulent mixing within tropopause folds as a mechanism for the exchange of chemical constituents between the stratosphere and troposphere, J. Atmos. Sci., 37, 994–1004.

Sigmond, M., Meloen, J., Siegmund, P. C., 2000. Stratosphere-troposphere exchange in an extratropical cyclone, calculated with a Lagrangian method, Ann. Geophy.18, 573-582.

Skolnik, M. I., 1980. Introduction to Radar Systems, McGraw-Hill, Inc., ISBN 0-07-057909-1, 2nd Ed.

Skolnik, M. I., 1990. Radar handbook, McGraw-Hill, Inc., ISBN 0-07-057913-X, 2nd Ed.

Smit, H. G. J., Straeter, W., Johnson, B., Oltmans, S., Davies, J., Tarasick, D. W., Hoegger, B., Stubi, R., Schmidlin, F., Northam, T., Thompson, A., Witte, J., Boyd, I., Posny, F., 2007. Assessment of the performance of ECC-ozonesondes under quasi-flight conditions in the environmental simulation chamber: Insights from the Juelich Ozone Sonde Intercomparison Experiment (JOSIE), J. Geophys Res., 112, D19306, doi:10.1029/2006JD007308.

Sorensen, J. H., Nielsen, N. W., 2001. Intrusion of Stratospheric Ozone to the Free Troposphere Through Tropopause Folds -A Case Study, Phys. Chem. Earth (B), 26 (10), 801-806.

Spichtinger, N., Wenig, M., James, P., Wagner, T., Platt, U., and Stohl, A., 2001. Satellite detection of a continental-scale plume of nitrogen oxides from boreal forest fires, Geophys. Res. Lett., 28(24), 4579–4582, doi:10.1029/2001GL013484.

Steinbrecht, W., Claude, H., Kohler, U., Hoinka, K. P., 1998. Correlations between tropopause height and total ozone: Implications for long-term changes, J. Geophys. Res., 103, 19,183– 19,192.

Stevenson, D. S., Dentener, F. J., Schultz, M. G., Ellingsen, K., Noije, T. P. C. van, Wild O., Zeng, G., Amann, M., Atherton, C. S., Bell, N., Bergmann, D. J., Bey, I., T. Butler, J. Cofala, W. J. Collins, R. G. Derwent, R. M. Doherty, J. Drevet, Eskes, H. J., Fiore, A. M., Gauss, M., Hauglustaine D. A., Horowitz, L. W., Isaksen, I. S. A., Krol, M. C., Lamarque, J.-F., Lawrence, M. G., Montanaro, V., Muller, J.-F., Pitari, G., Prather, M. J., Pyle, J. A., Rast, S., Rodriguez, J. M., Sanderson, M. G., Savage, N. H., Shindell, D. T., Strahan, S. E., Sudo, K., Szopa, S., 2006. Multimodel ensemble simulations of present-day and near future tropospheric ozone. J. Geophys. Res. 111, doi:10.1029/2005JD006338.

Stohl et al., 2008. The FLEXTRA and FLEXPART homepage, http://zardoz.nilu.no/_andreas/flextra+flexpart.html

Stohl, A., 1998. Computation, accuracy and applications of trajectories - review and bibliography, Atmos. Environ., 32(6), 947 – 966, doi:10.1016/S1352-2310(97)00457-3.

Stohl, A., Baumann, K., Wotawa, G., Langer, M., Neininger, B., Piringer, M. and Formayer, H., 1997. Diagnostic downscaling of large scale wind fields to compute local scale trajectories. Journal of Applied Meteorology 36, 931-942.

Stohl, A., Bonasoni, P., Cristofanelli, P., Collins, W., Feichter, J., Frank, A., Forster, C., Gerasopoulos, E., Gaggeler, H., James, P., Kentarchos, T., Kromp-Kolb, H., Kruger, B., Land, C., Meloen, J., Papayannis, A., Priller, A., Seibert, P., Sprenger, M., Roelofs, G. J., Scheel, H. E., Schnabel, C., Siegmund, P., Tobler, L., Trick, T., Wernli, H., Wirth, V., Zanis, P., Zerefos, C., 2003b. Stratosphere-troposphere exchange: A review and what we have learned from STACCATO, J. Geophys. Res., 108(D12), 8516, doi:10.1029/2002JD002490.

Stohl, A., Eckhardt, S., Forster, C., James, P., Spichtinger, N., and Seibert, P., 2002. A replacement for simple back trajectory calculations in the interpretation of atmospheric trace substance measurements, Atmos. Environ., 36, 4635–4648, doi:10.1016/S1352-2310(02)00416-8.

Stohl, A., Forster, C., Eckhardt, S., Spichtinger, N., Huntrieser, H., Heland, J., Schlager, H., Wilhelm, S., Arnold, F., and Cooper, O., 2003. A backward modeling study of intercontinental pollution transport using aircraft measurements, J. Geophys. Res., 108, 4370, doi:10.1029/2002JD002862.

Stohl, A., Forster, C., Frank, A., Seibert, P., Wotawa, G., 2005. Technical note: The Lagrangian particle dispersion model FLEXPART version 6.2, Atmos. Chem. Phys. Discuss., 5, 4739–4799.

Stohl, A., Hittenberger, M., Wotawa, G. 1998. Validation of the Lagrangian particle dispersion model FLEXPART against large scale tracer experiment data. Atmos. Environ. 24, 4245–4264.

Stohl, A., Seibert, P., 1998. Accuracy of trajectories as determined from the conservation of meteorological tracers, Q. J. Roy. Met. Soc. 124, 1465-1484.

Stohl, A., Spichtinger-Rakowsky, N., Bonasoni, P., Feldmann, H., Memmesheimer, M., Scheel, H. E., Trickl, T., Hubener, S., Ringer, W., Mandl, M., 2000. The influence of stratospheric intrusions on alpine ozone concentrations, Atmos. Environ., 34, 1323–1354.

Stohl, A., Thomson, D. J., 1999. A density correction for Lagrangian particle dispersion models. Boundary-Layer Meteorology 90, 155–167.

Stohl, A., Trickl, T., 1999. A textbook example of long-range transport: Simultaneous observation of ozone maxima of stratospheric and North American origin in the free troposphere over Europe, J. Geophys. Res., 104(D23), 30445–30462, doi:10.1029/1999JD900803.

Stohl, A., Wernli, H., James, P., Bourqui, M., Forster, C., Liniger, M. A., Seibert, P., Sprenger, M., 2003a: A new perspective of stratosphere–troposphere exchange. Bull. Amer. Meteor. Soc., 84, 1565–1573.

Stohl, A., Wotawa, G., Seibert, P., Kromp-Kolb, H., 1995. Interpolation errors in wind fields as a function of spatial and temporal resolution and their impact on different types of kinematic trajectories, J. Appl. Meteor., 34 (10), 2149–2165.

Strauch, R. G., Weber, B. L., Frisch, A. S., Little, C. G., Merritt, D. A., Moran, K. P., Welsh, D. C., 1987. The Precision and Relative Accuracy of Profiler Wind Measurements, J. Atmos. Ocean. Technol., 4, 563-571.

Sudo, K., Takahashi, M., Akimoto, H., 2003. Future changes in stratosphere-troposphere exchange and their impacts on future tropospheric ozone simulations, Geophys. Res. Lett., 30, 2256, doi:10.1029/2003GL018526.

Sweezy, W. B., Westwater, E. R., 1986. A comparison of Methods for Determining Tropopause Height from VHF Radar Observations, Journal of Atmospheric and Ocean Technology, Vol. 3.

Tarasick, D. W., Fioletov, V. E., Wardle, D. I., Kerr, J. B., Davies, J., 2005. Changes in the vertical distribution of ozone over Canada from ozonesondes: 1980–2001. J. Geophys. Res. 110, doi:10.1029/2004JD004643.

Tatarski, V. I., 1961. Wave propagation in a turbulent medium, New York, McGraw-Hill.

Thompson, A. M., Tao, W., Pickering, K. E., Scala, J. R., Simpson, J., 1997. Tropical deep convection and ozone formation, B. Am. Meteorol. Soc., 78, 1043–1054.

Thompson, A. M., Witte, J. C., McPeters, R. D., Oltmans, S. J., Schmidlin, F. J., Logan, J. A., Fujiwara, M., Kirchhoff, V. W. J. H., Posny, F., Coetzee, G. J. R., Hoegger, B., Kawakami, S., Ogawa, T., Johnson, B. J., Vomel, H., Labow, G., 2003. The 1998–2000 SHADOZ (Southern Hemispheric Additional Ozonesondes) tropical ozone climatology: 30 Comparison with TOMS and ground-based measurements, J. Geophys. Res., 108(D2), 8238, doi:10.1029/2001JD000967.

Thompson, A. M., Witte, J. C., Smit, H. G. J., Oltmans, S. J., Johnson, B. J., Kirchhoff, V. W. J. H., Schmidlin, F. J., 2007. Southern Hemisphere Additional Ozonesondes (SHADOZ) 1998–2004 tropical ozone climatology: 3. Instrumentation, station-to-station variability, and evaluation with simulated flight profiles.

Thomson, D. J., 1987. Criteria for the selection of stochastic models of particle trajectories in turbulent flows, J. Fluid Mech., 180, 529-556, doi: 10.1017/S0022112087001940.

Thouret, V., Cammas, J.-P., Sauvage, B., Athier, G., Zbinden, R., N´ed´elec, P., Simon, P., Karcher, F., 2005. Tropopause referenced ozone climatology and inter-annual variability (1994–2003) from the MOZAIC programme, Atmos. Chem. Phys. Discuss., 5, 5441–5488.

Thuburn, J., Craig, G. C., 1997. GCM tests of theories for the height of the tropopause, J. Atmos. Sci., 54, 869– 882.

Trusilova, K., Rodenbeck, C., Gerbig, C., Heimann, M., 2010. Technical Note: A new coupled system for global-to-regional downscaling of CO2 concentration estimation, Atmos. Chem. Phys., 10, 3205–3213.

Tsuda, T., May, P. T., Sato, T., Kato, S., Fukao, S., 1988. Simultaneous observations of reflection echoes and refractive index gradient in the troposphere and lower stratosphere, Radio Sci., 23, 655.

Tsuda, T., Sato, T., Hirose, K., Fukao, S., Kato, S., 1986. MU radar observations of the aspect sensitivity of backscattered VHF echo power in the troposphere and lower stratosphere, Radio Sci., 21, 971.

UGAMP (The UK Universities Global Atmospheric Modelling Program), A new understanding of stratosphere troposphere exchange, NERC, http://www.ugamp.nerc.ac.uk/research/brochure/21.htm.

Uliasz, M., 1994. Lagrangian particle dispersion modeling in mesoscale applications. In: Zannetti, P. (editor): Environmental Modeling, Vol. II. Computational Mechanics Publications, Southampton, UK.

Van Baelen, J. S., Tsuda, T., Richmond, A. D., Avery, S. K., S. Kato, Fukao, S., Yamamoto, M., 1990. Comparison of VHF Doppler beam swinging and spaced antenna observations with the MU radar: First results, Radio Sci., 25(4), 629–640.

Van Zandt, T., Green, J., Gage, K., Clark, W., 1978. Vertical profiles of refractivity turbulence structure constant: comparison of observations by the Sun set radar with a new theoretical model, Radio Sci., 13, 819–829.

Vanneste, J., 2004. Small-Scale Mixing, Large-Scale Advection, and Stratospheric Tracer Distributions, J Atm. Sci., 61(22), 2749-2761, DOI: 10.1175/JAS3303.1.

VanZandt, T. E., Fritts, D. C.,1989. A theory of enhanced saturation of the gravity wave spectrum due to increases in atmospheric stability. Pure Appl. Geophys., 130, 399-420.

Varotsos, C., Efstathiou, M., Tzanis, C., 2008. Scaling behaviour of the global tropopause, Atmos. Chem. Phys. Discuss., 8, 17891–17905.

Vaughan, G., Howells, A., Price, J. D., 2995. Use of MST radars to probe the mesoscale structure of the tropopause, Tellus, 47A, 759–765, DOI: 10.1034/j.1600-0870.1995.00118.x.

Vincent, R. A., 1984. MF/HF Radar Measurements of the Dynamics of the Mesopause Region - A Review, J. Atmo. Terr. Phys., 46, 961-974.

Vincent, R. A., May, P. T., Hocking, W. K., Elford, W. G., Candy, B. H., Briggs, B. H., 1987. First results with the Adelaide VHF radar: Spaced antenna studies of tropospheric winds, J. Atmos. Terr. Phys., 49, 353.

Vincent, R. A., Rottger, J., 1980. Spaced antenna VHF radar observations of tropospheric velocities and irregularities, Radio Sci., 15, 319.

Vincent, R. A., Stubbs, T. J., Pearson, P. H. O., Loyd, K. H., Low, C. H., 1977. A comparison of partial reflection drifts with winds determined by rocket techniques, J. Atmos. Terr. Phys., 39, 813.

Vomel, H., Diaz, K., 2009. Ozone sonde cell current measurements and implications for observations of near-zero ozone concentrations in the tropical upper troposphere, Atmos. Meas. Tech. Discuss., 2, 3153–3181.

Wang, Y., Logan, J., Jacob, D. J., 1998. Global simulation of tropospheric O3 –NOx–hydrocarbon chemistry: Model evaluation, J. Geophys. Res., 103, 10,727– 10,756.

Waterman, A. T., Hu, T. Z., Czechowsky, P., Röttger, J., 1985. Measurement of anisotropic permittivity structure of upper troposphere with clear-air radar. Radio Sci., 20, 1580–1592.

Waugh, D. W., 1996. Seasonal variation of isentropic transport out of the tropical stratosphere. J. Geophys. Res., 101, 4007–4023.

Weil, J. C., Sullivan, P. P., Moeng, C-H., 2004. On the use of large-eddy simulations in Lagrangian particle dispersion models, J. Atmos. Sci., 61(23), 2877-2887, doi: 10.1175/JAS-3302.1.

Weisman, M. L., Skamarock, W. C., Klemp, J. B., 1997. The resolution dependence of explicitly modeled convective systems, Mon. Wea. Rev., 125, 527–548.

Wernli, H. Bourqui, M. 2002. A Lagrangian "1-year climatology" of (deep) cross-tropopause exchange in the extratropical Northern Hemisphere, J. Geophys. Res., 107(D2), 4021, doi:10.1029/2001JD000812.

Wernli, H., Davies, H. C., 1997. A Lagrangian-based analysis of extratropical cyclones. I: The method and some applications, Q. J. R. Meteorol. Soc., 123, 467–489, doi: 10.1002/qj.49712353811.

Westwater, E. R., Decker, M. T., Zachs, A., Gage, K. S., 1983. Ground based remote sensing of temperature profiles by a combination of microwave radiometry and radar. J. Climate Appl. Meteor., 22, 126 – 133.

Westwater, E. R., Decker, M. T., Zachs, A., Gage, K. S., 1983. Ground-based remote sensing of temperature profiles by a combination of microwave radiometry and radar, J. Climate Appl. Meteor., 22, 126-133.

Whiteway, J. A., Pavelin, E. G., Busen, R., Hacker, J., Vosper, S., 2003. Airborne measurements of gravity wave breaking at the tropopause, Geophys. Res. Lett., 30(20), 2070, doi:10.1029/2003GL018207.

Wilson, J. D., Flesch, T. K., 1993. Flow Boundaries in Random-Flight Dispersion Models: Enforcing the Well-Mixed Condition, J. Appl. Meteor., 32(11), 1695-1707, doi: 10.1175/1520-0450(1993)032<1695:FBIRFD>2.0.CO;2.

Wilson, J. D., Legg, B. J., Thomson, D. J., 1983. Calculation of particle trajectories in the presence of a gradient in turbulent-velocity scale. Boundary layer Meteorology 27, 163-169.

Wirth, V., 1995a. Diabatic heating in an axisymetric cut-off cyclone and related stratosphere-troposphere exchange, Quart. J. Roy. Meteorol. Soc., 121, 127–147.

Woodman, R. F., Guillen, A., 1974. Radar observations of winds and turbulence in the stratosphere and mesosphere, J. Atmos. Sci., 31, 493-505, , doi: 10.1175/1520-0469(1974)031<0493:ROOWAT>2.0.CO;2.

Woodman, R., Chu, Y.-H., 1989. Aspect sensitivity measurements of VHF backscatter made with the Chung-Liradar: plausible mechanisms. Radio Sci.24, 113–125.

Woodman, R., Rastogi, P. 1984. Evaluation of effective eddy diffusive coefficients using radar observations of turbulence in the stratosphere, Geophys. Res. Lett., 11, 243–246.

World Meteorological Organization (1957) Definition of the tropopause. WMO Bulletin 6. Geneva: World Meteorological Organisation.

World Meteorological Organization, Scientific Assessment of Ozone Depletion: 1994, WMO 37, Geneva, Switzerland, 1995.

World Meteorological Organization. Scientific Assessment of Ozone Depletion 1998. Global Ozone Research Monitoring Project Report 44 (WMO, Geneva, 1999).

Wotawa, G., De Geer, L.-E., Becker, A., D'Amours, R., Jean, M., Servranckx, R., Ungar, K., 2006. Inter- and intra-continental transport of radioactive cesium released by boreal forest fires, Geophys. Res. Lett., 33, L12806, doi:10.1029/2006GL026206.

Yienger, J. J., Klonecki, A. A., Levy II, H., Moxim, W. J., Carmichael, G. R., 1999. An evaluation of chemistry's role in the winter-spring ozone maximum found in the northern midlatitude free troposphere, J. Geophys. Res., 104, 3655– 3667.

Zannetti, P., 1992. Particle Modeling and Its Application for Simulating Air Pollution Phenomena. In: Melli P. and P. Zannetti (editors): Environmental Modelling. Computational Mechanics Publications, Southampton, UK.

Appendices

Appendix A

FLEXPART, a Lagrangian particle dispersion model, was described and validated by Stohl et al. [1995], Baumann and Stohl [1997], Stohl et al. [1997], Stohl and Seibert [1998] as well as Stohl et al. [2005]. FLEXPART expresses transport and dispersion of a large number of particles by calculating the three-dimensional trajectories. This Lagrangian transport, as opposed to the Eulerian, model has advantages. The three most important advantages over Eulerian models are the following. The first is, the transport is more exactly described due to the fact that there are no numerical inaccuracies due to the advection scheme (which is particularly important in regions with large spatial concentration gradients, e.g., close to tropopause folds). The second is, individual particles travel independently from each other and thus can provide supplementary information. The third is, in an Eulerian model a tracer released from a point source is instantaneously mixed within the entire grid box, while a Lagrangian model is independent of a computational grid.

FLEXPART treats advection as well as turbulent diffusion by computing the trajectories of a large number of particles. To simulate transport by turbulent eddies, stochastic fluctuations, obtained by solving Langevin equations [Stohl and Thomson, 1999], are superimposed on the grid-scale winds interpolated from the Environment Canada's Global Environmental Multiscale (GEM) data. FLEXPART is equipped with the convection scheme developed by Emanuel and Zivkovic-Rothman [1999] so as to represent convective transport. The implementation of this scheme is described in Seibert et al. [2001]. In this study, FLEXPART model was driven by hourly regional meteorological wind fields data obtained from the GEM version 3.2.2, with 432×565 grid points over North America, 0.1375^{o} grid spacing in the core region, 450 s time step and 58 vertical levels up to 10 hPa.

FLEXPART computes the trajectories of a large number of particles, each representing a parcel of tracer gases, so as to simulate the dispersion of tracer gases in the atmosphere. The trajectories of the particles are determined using the expression

$$\boldsymbol{X}(t + \Delta t) = \boldsymbol{X}(t) + \boldsymbol{v}(\boldsymbol{X}, t) * \Delta t \qquad \text{A1}$$

where t is time, Δt is the increment of time, $\mathbf{X}$ is the position vector, and $\boldsymbol{v} = \bar{\boldsymbol{v}} + \boldsymbol{v}_t' + \boldsymbol{v}_m'$ is the wind vector that consists of the grid-scale wind $\bar{\boldsymbol{v}}$, the turbulent wind fluctuations $\boldsymbol{v}_t'$ [Zannetti, 1992] and the mesoscale wind fluctuations $\boldsymbol{v}_m'$.

According to the Langevin equation [Thomson, 1987], the turbulent fluctuations are expressed as

$$dv_{ti} = a_i(x, v_t, t)dt + b_{ij}(x, v_t, t)dW_j \qquad \text{A2}$$

where the drift term a and the diffusion term b are functions of the position, the turbulent velocity and time. The dW_j are incremental components of a Wiener process with mean zero and variance dt, which are uncorrelated in time [Legg and Raupach, 1982]. Cross correlations between the different components of wind are also not considered, since their effect for long-range dispersion is insignificant [Uliasz, 1994]. As an alternative, the Langevin equation can be rewritten in terms of $v_{ti}/\sigma_{v_{ti}}$, where $\sigma_{v_{ti}}$ is the standard deviation of the turbulent wind, substituting v_{ti} [Wilson et al., 1983]. Thomson [1987] showed expression in such form in order to fulfill the well-mixed criterion which states that 'if a species of passive marked particles is initially mixed uniformly in position and velocity space in a turbulent flow, it will stay that way' [Rodean, 1996]. Although the method proposed by Legg and Raupach [1982] violates this criterion when turbulence is strongly inhomogeneous, their expression was observed to be practical, as numerical results have revealed it is robust against an increase in the time step of integration utilized by the model as shown in Stohl et al. [1998].

In FLEXPART, the standard deviations of wind velocity and the Lagrangian time scales are obtained though the parameterization of Hanna [1982]. Boundary conditions at the surface and at the top of the planetary boundary layer are specified using Wilson and

Flesch [1993]. By solving Langevin equations [Stohl and Thomson, 1999], FLEXPART parameterizes turbulence in the boundary layer and in the free troposphere.

For this study, FLEXPART was run both forward from the stratosphere and backward in time from ozone measurement sites. Forward simulations are useful for visualizing the dispersion of atmospheric tracers as well as for understanding its relation to the synoptic situation. Backward trajectories are usually employed to interpret atmospheric trace gases measurements so as to create connections between their sources and their receptors [Stohl, 1998]. FLEXPART also uses a domain-filling procedure where the model domain is represented by particles of equal mass. This option is used to simulate stratospheric ozone tracer. The particles are then distributed in the model domain proportionally to air density. The dynamic tropopause, defined based on potential vorticity (PV), is used in FLEXPART to separate the stratospheric and tropospheric air masses. During model initialization, the PV at the position of a particle is determined by interpolation from the GEM data. Ozone particles initially located in the troposphere (i.e., those having a potential vorticity less than 2 PVU, where $1PVU = 10^{-6}$ K m^2 kg^{-1} s^{-1}) are considered to have an ozone concentration of zero. On the contrary, stratospheric ozone (PV > 2 PVU) are tagged with an ozone concentration determined using the relation O_3(ppb) = S(ppb PVU^{-1})×PV(PVU) [Danielsen, 1968; Beekmann et al., 1994], where the monthly average S values from January through December are 58, 63, 69, 65, 64, 60, 51, 42, 39, 35, 39 and 51 ppb PVU^{-1}, respectively [Stohl et al., 2000]. Stratospheric ozone is then allowed to advect through the stratosphere into the troposphere according to the model wind fields obtained from the GEM. The stratospheric ozone is treated as a passive tracer, and the resulting ozone distribution in the troposphere is only due to stratospheric ozone intrusion. In the forward simulation, ozone concentration fields were output every 3-hour at a resolution of 1°x1^{o}x500 m.

Particles are initiated in FLEXPART with a certain mass. Hence, each trajectory has a certain mass at each position and time. FLEXPART calculates the concentration of tracer in each grid cell of the three–dimensional output grid by summing up the mass fractions of all the particles located in an output grid cell and dividing them by the grid cell volume. This process is made more efficient through the use of a uniform kernel method

where the mass of a particle is divided between the nearest grid cells that fall within a grid box resolution from the central location of the particle as described by Stohl et al. [1998], who found that on average it performs similar to other methods to determine the concentrations of tracer. In order to avoid artificial smoothing of concentration fields close to the source, the kernel method is not used until 3 hours after the particles are released [Forster et al., 2004].

FLEXPART simulates the transport only and ignores chemistry by assuming a lifetime of the simulated species, in our case, stratospheric ozone. This is due to the fact that the lifetime of stratospheric ozone in the troposphere is of the order of one to two months [Fishman et al., 1979; Liu et al., 1987; Stevenson et al., 2006], while the length of the simulation of our model is less than 15 days. Hence, ozone is represented by a passive ozone-like tracer in the model that does not undergo chemical reactions. Moreover, any particular particle is improbable to stay for such long period of time within the domain due to the limited model domain size. On the top of the above, particles that crossed the tropopause from the stratosphere before entering the simulation domain will have zero ozone concentration. This means that only stratospheric intrusions that take place within the domain are simulated.

While forward trajectories describe where a particle will go, backward trajectories indicate where it came from. Backward simulations are helpful to determine source–receptor associations describing the sensitivity of a receptor to a source [Seibert and Frank, 2004]. In order to identify the sources of the measured enhanced ozone concentration, backward simulations are more efficient than forward ones (if the number of receptors is fewer than the number of sources) since particles can be released exactly at the measurement location and time. If FLEXPART is run backward in time, all advective processes acting on the particles are required to be reversed. Thus, in the convection scheme, the particles must be redistributed from their destination level back to their source level.

In this thesis, for every backward simulation 600000 particles were released at measurement site where and when high ozone concentration were measured and followed

backward in time for 48 - 60 hours. Stohl et al. [2002] suggested a method to condense the complex and large output of FLEXPART utilizing a cluster analysis [Dorling et al., 1992]. This method is used to cluster the positions of all particles originating from a release point at every output time and write out only clustered particle positions, along with additional information such as the fraction of particles in the atmospheric boundary layer and in the stratosphere. Cluster analysis technique is used to split the particles released into groups or clusters with similar trajectories. It then outputs the mean path of each cluster. This is especially useful in atmospheric studies where strongly divergent air patterns could cause the mean of all particle movement to lie in a completely different direction to the paths actually taken by the air parcels. In FLEXPART, this option can be activated by setting the number of cluster parameter. In this thesis, we set the number of cluster parameter to be 4.

Appendix B

In this section, we look at the synoptic systems to identify the effects of synoptic dynamics on small-scale geographic regions that causes ozone enhancement in the middle and upper troposphere at the ozonesonde campaign sites. Since transport between the lowermost stratosphere and the upper troposphere requires consideration of the details of small-scale as well as synoptic-scale processes. Hence, we examine the synoptic dynamics utilizing synoptic meteorology diagnosis obtained from the US Analysis/Satellite Composite image [NOAA/National Weather Service National Centers for Environmental Prediction Hydrometeorological Prediction Center] to see if synoptic weather patterns affect the movement and overall location atmospheric trace gases including ozone. In chapters 3 and 4, we have shown both experimentally and numerically the intrusions of stratospheric ozone at Egbert on 8 May 2009, at Montreal on 22 July 2010 and at Walsingham on 26 February 2007. The synoptic situations across North America for the corresponding dates are shown in the figures below. Surface analysis of the synoptic-scale features include high- and low-pressure areas as well as cold and warm frontal systems as indicated by the contour plots shown below.

Figure B1 shows the synoptic map plot for North America on 8 May 2009 at 12:00 UTC. The Egbert 2009 ozonesonde campaign or radar site is within the black circle shown in the figure. The map shows the pressure contour plot and frontal system. On the date mentioned above, we observed enhanced ozone in the upper troposphere; however, the synoptic maps do not seem to show any special synoptic event that is related with the intrusion of ozone-rich stratospheric air at Egbert. Synoptic plot for North America on 22 July 2010 at 12:00 UTC is illustrated in Figure B2. Even though we observed enhanced tropospheric ozone at Montreal (i.e., it is located within the red circle shown in the same figure) on 22 July 2010, the synoptic plot does not reveal any development of the frontal system that is associated with the intrusion of ozone-rich stratospheric air at Montreal on 22 July 2010. Figure B3 also demonstrates the synoptic situation for North America on 26 February 2007 at 12:00 UTC. Like in Egbert and Montreal cases, on this date we observed intrusion of stratospheric air at Walsingham (i.e., it is located within the black circle shown in the figure); however, there is no any significant change in synoptic

meteorological pattern that is correlated with a remarkable intrusion of stratospheric air downward into the troposphere at Walsingham. Even if we displayed the synoptic plots of three intrusion events, we observed the same situation for other intrusions cases as well.
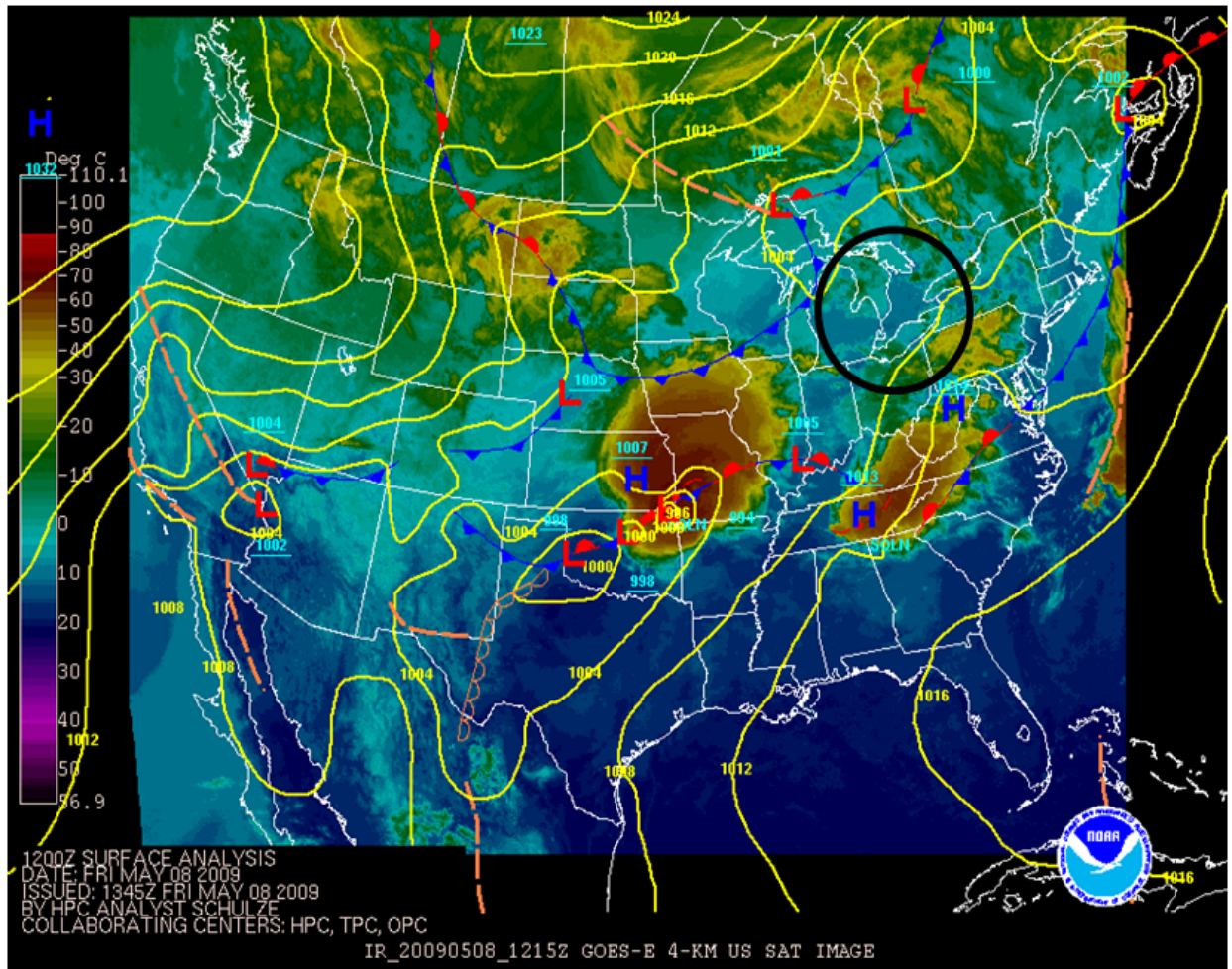
Figure B1. US Analysis/ Satellite Composite image. Selected an individual surface analysis map from the archive of NOAA/National Weather Service National Centers for Environmental Prediction Hydrometeorological Prediction Center on 8 May 2009 at 12:00 UTC. The yellow solid lines are isobars (hPa). H and L indicate high and low pressures, respectively. The cold and warm fronts are delineated by the triangular teeth and half-disk, respectively. Enhanced tropospheric ozone was observed at Egbert. The Egbert 2009 ozonesonde campaign was carried out within

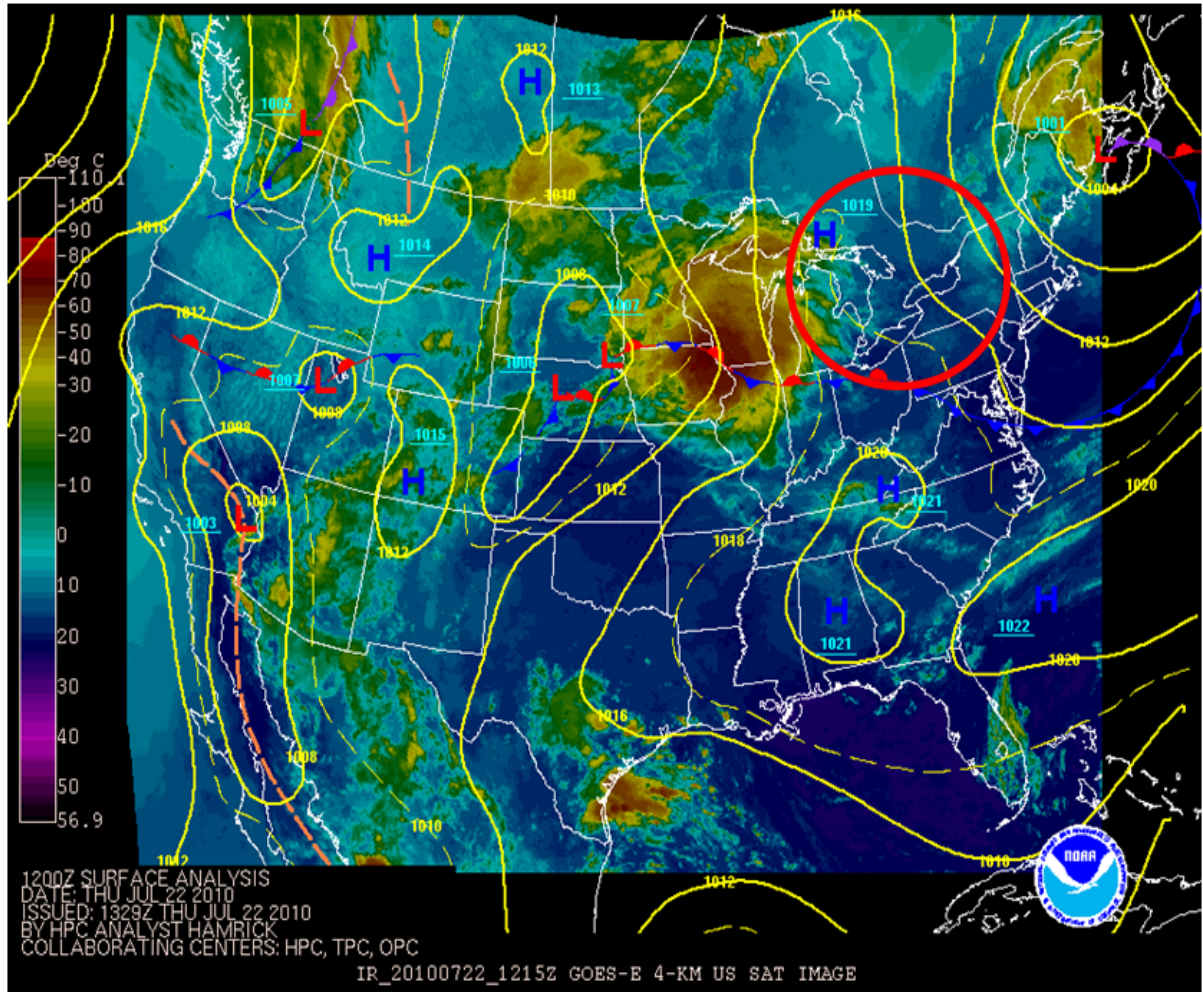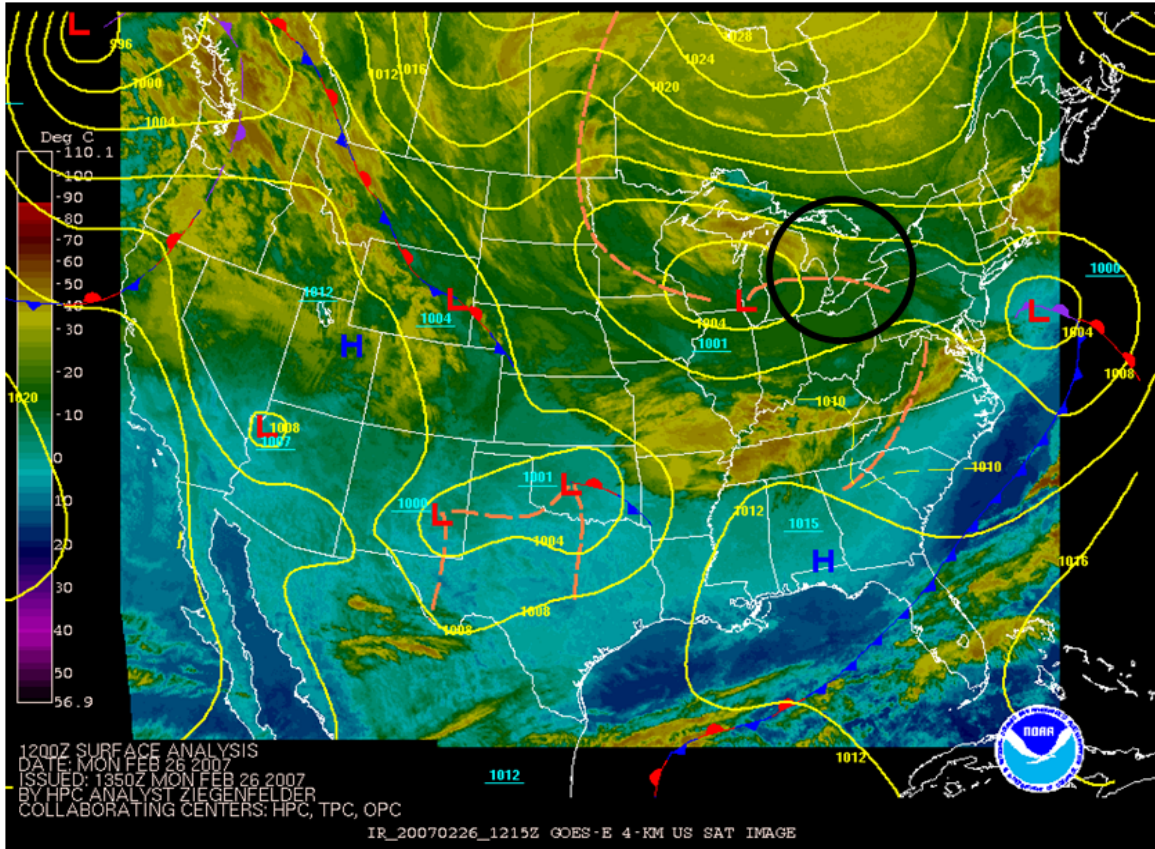the region of the black circle. The location of Egbert radar or ozonesonde campaign site is (44.27°N, 79.73°W).

Figure B2. This synoptic plot is the same as Figure B1 except that this is on 22 July 2010 at 12:00 UTC. The Montreal 2010 ozonesonde campaign was carried out within the region of the red circle. The location of Montreal radar or ozonesonde campaign site is (45.50°N, 73.57°W).

Figure B3. This synoptic plot is the same as Figure B1 except that this is on 26 February 20007 at 12:00 UTC. The Walsingham 2007 ozonesonde campaign was carried out within the region of the black circle. The location of Walsingham radar or ozonesonde campaign site is (42.6°N, 80.6°W).

Although we do not see any synoptic pattern developments (from Figures B1, B2 and B3) that can be associated with the stratospheric ozone intrusions, in chapter 3 we have shown that the radar measured small-scale atmospheric dynamics (i.e., variance of vertical wind, vertical wind shear of the horizontal wind and turbulence strengths) to be responsible for the downward transportation of ozone-rich stratospheric air into the middle and upper troposphere (see Table 3.1). However, detail consideration of synoptic system analysis is especially important for the horizontal transport of ozone in our case.

Appendix C

This section is to show the aspect sensitivity of the radar backscatter power in the troposphere and lower stratosphere. Figure C1 is adapted from Hocking [1989] to demonstrate the enhanced backscatter radar power at vertical incidence. The MU radar observation was near Kyoto of the backscatter for beams pointing vertically as well as off vertical at zenith angles of 1°, 2°, 3°, 4°, 6°, 7°, and 8°. Figure C1 indicates the ratio of power on each off vertical beam relative to that on the vertically pointing beam at each height.
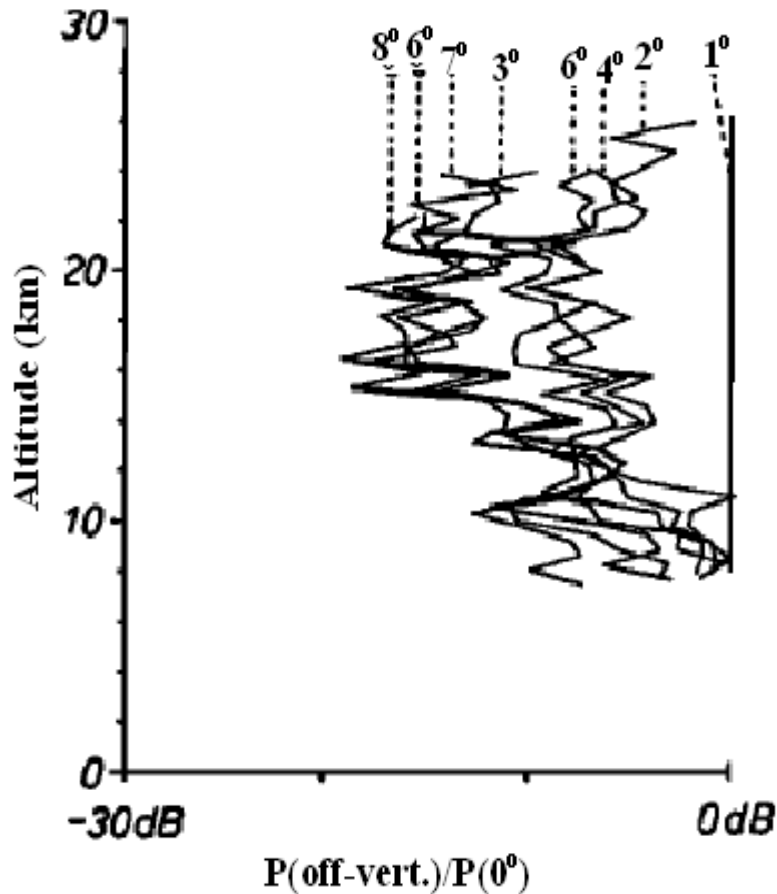

Figure C1. Ratios of mean power on the indicated beams relative to the power on the vertical beam at the same heights for 17-18 October 1988 using the MU radar near Kyoto in Japan operating at a frequency of 46.5 MHz, adapted from Hocking [1989].

Curriculum Vitae

Name: Mohammed Osman

Post-secondary Education and Degrees:
Addis Ababa University
Addis Ababa, Ethiopia
1996-2000 B.Sc.

Addis Ababa University
Addis Ababa, Ethiopia
2003-2005 M.Sc.

Ben-Gurion University of the Negev
Sede Boker, Israel
2005-2007 M.Sc.

The University of Western Ontario
London, Ontario, Canada
2007-2012 Ph.D.

Honours and

Awards:
Award of teaching and research assistantships from The University of Western Ontario
2007-2012

Scholarship from The Bona Terra Foundation for MSc studies in Solar Energy and Environmental Physics, Ben-Gurion University of the Negev
2005-2007

Related Work Experience
Teaching and Research Assistant
The University of Western Ontario
2007-2012

Physics lecturer
Addis Ababa University, Ethiopia
2004 - 2005

Physics Teacher
Derartu Tulu Senior Secondary, Addis Ababa, Ethiopia
2000 - 2003

Publications:
Osman, M., Hocking, W., Tarasick, D., Drummond, J., 2010. Stratosphere-Troposphere Exchange of Ozone from 24 Feb – 18 April 2008 in Eureka, Canada, In: Swarnalingam,

N. and Hocking, W. K., editors, MST12, Proceedings of the Twelfth International Workshop on Technical and Scientific Aspects of MST Radar, London, Ontario, Canada, Canadian Association of Physicists, 291-294.

Bourqui, M. S., Yamamoto, A., Tarasick, D., Moran, M. D., Beaudoin, L.-P., Beres, I., Davies, J., Elford, A., Hocking, W., Osman, M., Wilkinson, R., "A new real-time Lagrangian diagnostic system for stratosphere-troposphere exchange: Evaluation during a balloon sonde campaign in eastern Canada", Atmos. Chem. Phys., 12, 2661-2679, 2012.

He, H, Tarasick, D. W., Hocking, W. K., Carey-Smith, T. K., Rochon, Y., Zhang, J., Makar, P. A., Osman, M., Brook, J., Moran, M. D., Jones, D. B. A., Mihele, C., Wei, J. C., Osterman, G., Argall, P. S., McConnell, J., Bourqui, M. S., 2011. Transport analysis of ozone enhancement in Southern Ontario during BAQS-Met, Atmos. Chem. Phys., 11, 2569–2583.

Osman, M., Hocking, W., Tarasick, D., He, H. 2011. Stratosphere-troposphere exchange of ozone as observed from windprofiler radars, Environment Canada, Ontario Storm Prediction Center, Application of windprofiler radar in forecasting storm workshop, Toronto, Ontario, Canada, 22 – 23 February.

Osman, M., Hocking, W., Tarasick, D., He, H. 2010. Effects of Arctic ozone intrusions on high and mid latitudes, Canadian Network for the Detection of Atmospheric Change (CANDAC) Workshop 2010, Halifax, Nova Scotia, Canada, 1 – 3 November.

Hocking, W. K., Taylor, P. A., Swarnalingan, N., Argall, P. S., Sharma, S., Tarasick, D., Fabry, F., Barron, J., Mercer, R., Zhang, Y., Donaldson, N., Dehghan, A., Klaassen, G., Zawdazki, I., Campos, E., Osman, M., Sica, R., Hangan, H., McBean, G., 2009. The Canadian O-Qnet - a Relatively High-Density Windprofiler Network", paper S02 - O06, The 8th International Symposium on Tropospheric Profiling, Delft, The Netherlands, 19-23 October.

Osman, M., Hocking, W., Tarasick, D., Drummond, J., 2009. Stratosphere-Troposphere Exchange of Ozone from 24 Feb – 18 April 2008 in Eureka, Canada, the 12th International workshop on technical and scientific aspects of MST radar, London, Ontario, Canada, 17 – 23 May.